THE EFFECTS OF STRAIN AGEING AND GRAIN SIZE ON FATIGUE IN LOW CARBON STEELS

A Thesis presented for the Degree of Doctor of Philosophy in Mechanical Engineering in the University of Canterbury, Christchurch, New Zealand

by

CHONG CHON JIN, B.E. (Honours), M.Sc.

University of Canterbury,
Christchurch, NEW ZEALAND.

February 1980

SYNOPSIS

The traditional theory for the occurrence of a fatigue limit in low carbon steels is based on the suspected ability of these steels to strain age under dynamic stress conditions. A fatigue limit is thought to form when the damage process is outpaced by strain age hardening, resulting in the formation of a knee in the fatigue curve.

Experiments have also shown that the grain size of the steel has an effect on the actual fatigue process and the shape of the fatigue curve. It was found that only steels of coarse grained structures were affected by strain ageing, while fine grained steels were relatively insensitive to dynamic strain ageing. Therefore, whether strain ageing is solely responsible for the occurrence of a fatigue limit or not, is debatable.

Two types of steels of weak and strong propensity for strain ageing were chosen for investigation, the desired strain ageing properties being achieved by varying the active nitrogen content. For each type of steel, specimens of different grain sizes were produced. Complete reversed direct stress fatigue tests were carried out on each steel to determine its fatigue limit. Damping measurements were taken on four steels, two fine grained and two coarse grained steels of different strain ageing propensities. These tests were supplemented by temperature monitoring on specimens tested in fatigue, metallographic examination of fatigue specimens using optical and transmission electron microscopy, and tensile tests on cyclically pre-stressed specimens.

The results indicate that strain ageing occurs during fatigue but the degree of ageing is dependent on the grain size and the active nitrogen

content of the steel. Increasing the grain size and active nitrogen content promotes dynamic strain ageing. Consequently, the improvement in fatigue performance by strain ageing increases with increasing grain size.

A threshold stress, called the Critical Damping Stress, exists below the fatigue limit of steel, and is the minimum stress required for plastic deformation and strain hardening to occur during fatigue. Therefore, it can be regarded as the fatigue limit of a perfect plastic steel with no work hardening ability. The Critical Damping Stress is unaffected by the strain ageing propensity of the steel and is only slightly dependent on its grain size. Because all steels are capable of strain hardening, the fatigue limits are raised above their critical damping stress values, i.e., the difference between the fatigue limit and the critical damping stress is a result of cyclic strain hardening. This form of strengthening is more pronounced as the grain size is decreased.

Thus fatigue is a combination of three simultaneous dynamic processes, viz., fatigue damage, cyclic strain hardening and dynamic strain ageing. Basically, the fatigue limit is a result of the competitive process between damage and strain hardening, but if the steel contains sufficient active nitrogen, strain ageing may contribute to the total strengthening. In this case, the fatigue limit occurs when damage is outpaced by the total strengthening.

ACKNOWLEDGEMENTS

The support and guidance provided by my supervisor, Professor L. A. Erasmus, is gratefully acknowledged. His encouragement, suggestions and time spent in discussion have been much appreciated.

I am also indebted to Mr J. S. Smaill, my associate supervisor, for his valuable suggestions and the time he spent reading the manuscript. His encouragement is deeply appreciated.

Many members of the Department of Mechanical Engineering assisted with this research programme and with the preparation of the thesis. In particular, the assistance of Mr D. Somerville, Mr E. Retallick and Mr M. Flaws is acknowledged. My grateful thanks to Miss J. Shelton and Miss A. Scott for their help in preparing the diagrams and photographs, and to Mrs P. Dowell for her meticulous typing.

Materials for this research programme were kindly donated by Pacific Steel Ltd, Auckland, New Zealand.

Finally, I wish to extend my deepest gratitude to my family and Kiang for their continual sacrifice and encouragement which have enabled me to undertake and complete this study programme.

CONTENTS

LIST OF FIGURES

LIST OF TABLES

SOME NOTATION OF FREQUENT OCCURRENCE

SYMBOL	DEFINITION
N	Number of stress or strain cycles
PSB	Persistent slip band
k_y	Unpinning factor (Hall-Petch equation)
n	Strain hardening exponent (coefficient)
n	Dislocation mobility factor
t	Time
γ	Stacking fault energy
δ	Logarithmic decrement
ε	Strain
ε_L	Luders strain
ρ	Dislocation density
σ	True stress
σ_A	Anelastic limit
σ_E	Elastic limit
σ_ℓ	Fatigue limit
σ_i	Friction stress (Hall-Petch equation)
σ_Y	Lower yield stress
σ_{CD}	Critical damping stress
σ_{UTS}	Ultimate tensile stress
ΔY	Increase in yield stress
Δf	Increase in flow stress

CHAPTER ONE

INTRODUCTION

1.1 SCOPE OF THESIS

Fatigue failure can be defined as the progressive failure of a part or structure under a fluctuating load. These failures usually occur at stress levels which, under static loading conditions, should give infinite lives. Since only a limited number of mechanical components and structural elements are subjected to constant loads throughout their entire service lives, it is not surprising that fatigue failures constitute the most common source of service failures in machinery and structures. The characteristic "brittle appearance" of fatigue fractures had been noted as early as 1840 by Rankine[1] and despite the fact that a considerable amount of research has been done since then on a wide range of materials, fatigue failures remain a major problem to the present day.

When fatigue testing is carried out over a range of stress, low carbon steel exhibits a well-defined fatigue limit, and when stressed below this stress amplitude, these steels are able to withstand an infinite number of load cycles without fracture. By contrast, most non-ferrous metals do not show any fatigue limit and failures always occur at longer lives as the fatigue stress amplitude is lowered. For this reason many components manufactured from non-ferrous materials are designed to withstand only a specific number of stress cycles, and in applications where fracture would result in serious damage or loss of life, these components are then replaced at this life in anticipation of later failure, e.g., aircraft components and structures subjected to fatigue loads.

It is recognised that the materials that exhibit fatigue limits

also show an ability to strain age. The most popular theory on the existence of a fatigue limit is thus based on strain ageing. This theory argues that these materials dynamically strain age during the course of fatigue loading, so that the accumulation of fatigue damage and strain age hardening are envisaged as competitive processes, and the fatigue limit occurs when age hardening outpaces the damage process.

The effects of strain ageing on the fatigue strength of low carbon steels are well established[2,3]. However, experiments performed to establish the cause for the presence of a fatigue limit in steels showed varied results[4,5]. The absence of a single theory that satisfactorily explains the existence of fatigue limits in low carbon steels means that further investigation into this much-researched topic is still a worthy proposition.

Strain ageing at ambient temperatures is known to be a function of the free nitrogen content of the steel. In order to examine the contribution of strain ageing to fatigue strength, it seems necessary to compare the fatigue behaviours of steels with different nitrogen contents and consequential ageing propensities.

Fatigue properties of low carbon steels are also affected by the polycrystalline grain size [6,7,8]. Klesnil *et al*[8] presented metallographic evidence that grain boundaries hinder the growth of slip bands produced during the early stages of fatigue damage. They also showed that the dependence of fatigue limit on grain size follows a Hall-Petch type relationship. Hence, in order to compare fatigue behaviours of steels with different nitrogen contents, it is also necessary to take into consideration the grain size effect.

1.2 CHARACTERISTICS OF FATIGUE FRACTURES

The topography of fatigue fracture surfaces usually shows a number of common features. However, depending on the material, environment and loading conditions, some of these features may not be revealed clearly. The examination of a fracture surface produced by fatigue usually shows two distinct areas, a fatigue area which results from slow crack propagation, and an area of final failure which may be by microvoid coalescence or by cleavage fracture.

The fracture area reveals distinct fracture surface characteristics. This surface is generally flat, indicating an absence of any appreciable amount of gross plastic deformation. This surface also contains features which indicate the crack origin(s), rate and direction of crack growth at any particular stage in its history. In the case of service failures occurring over a long period of time, this fatigue surface area contains crack arrest lines, perpendicular to the direction of propagation, and usually referred to as "clam shell" markings, (see Figure 1.1). These marks are thought to occur by oxidation or corrosion of the crack surface during crack arrest periods, since by contrast, no such markings can be found on the fracture surface of laboratory specimens tested with a simple sinusoidal load. It is also sometimes possible to find radial marks which run from the crack origin in the general direction of crack propagation. These marks are ledges which result when cracks advancing at different levels, eventually meet. The final rupture area is rougher in texture and is produced by catastrophic separation of a part or a specimen during the last tensile quarter load cycle. Fracture may be by mocrovoid coalescence as indicated by tear dimples, or by cleavage.

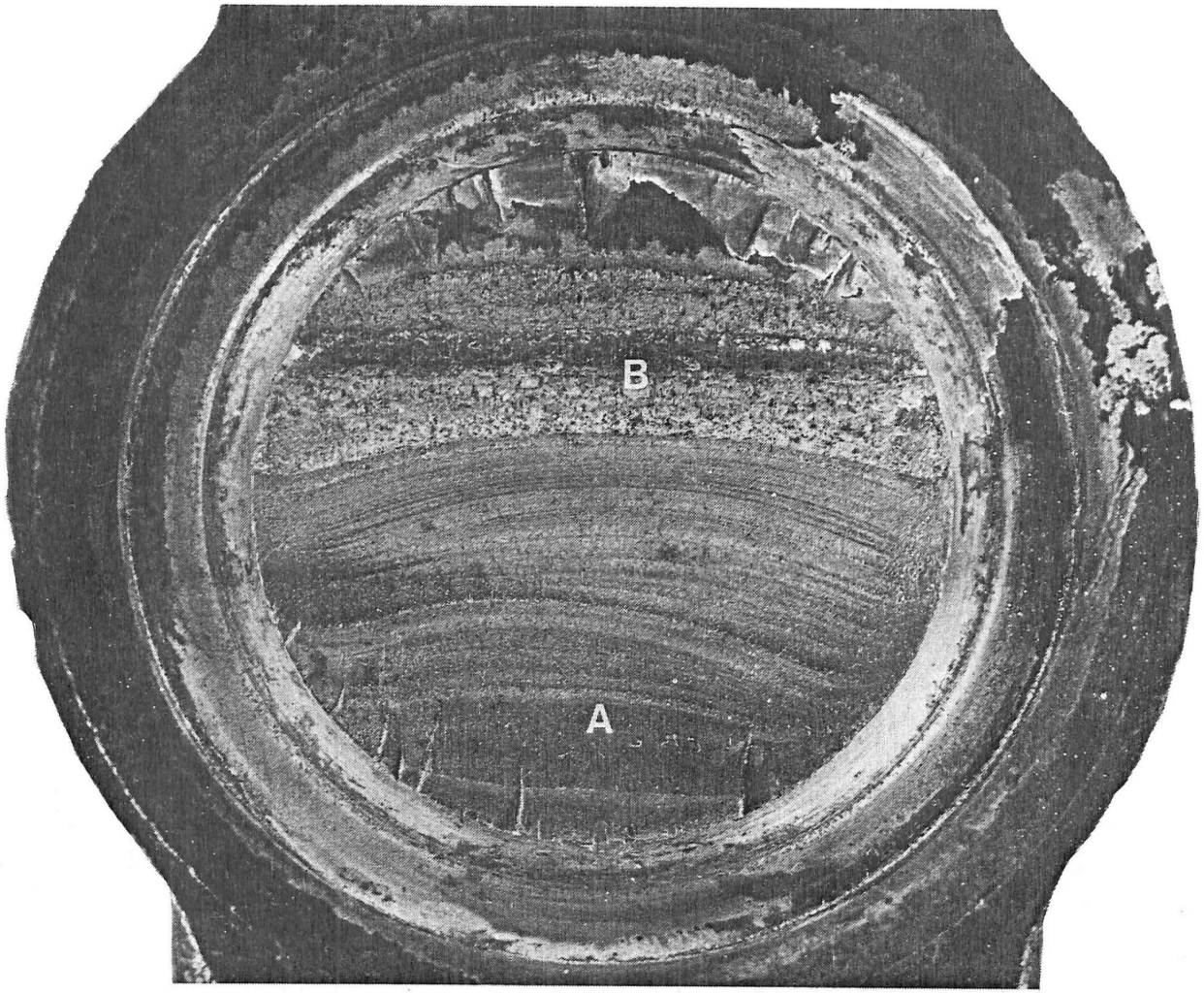

A = fatigue area B = final failure area

FIG. 1·1 FATIGUE FRACTURE SURFACE OF A VEHICLE STUB AXLE.

1.3 FATIGUE CRACK NUCLEATION AND PROPAGATION

The initiation of fatigue cracks is an important preliminary step to crack formation and crack propagation.

In engineering components, geometric effects such as notches or machining marks often determine the position of the initial crack. The feature of these sites is that they localise plastic deformation at a point on the free surface, and fatigue cracks are invariably nucleated at free surfaces. Thus, in order to determine the basic or intrinsic properties of a material, it is necessary to use longitudinally polished un-notched specimens carefully prepared and tested under standard laboratory atmospheric and temperature conditions.

The usual outcome of cyclic deformation is the production of changes in specimen surface topography in the form of persistent slip bands, intrusions and extrusions. The phenomenon of persistent slip bands and the importance of free surfaces in fatigue crack initiation were reported in the early work of Thompson *et al*[9]. They reported that the periodic removal of about 30μ from their direct stress specimen surfaces extended the lives of their copper crystals indefinitely.

It has long been appreciated that test atmospheres play an important role in fatigue. Fatigue tests at atmospheric and reduced pressures have shown that air profoundly reduces the lives of many metals and alloys. The beneficial effect of vacuum has been ascribed to the fact that newly produced steps or fracture surfaces remain free of absorbed gas, permitting slip reversal or crack rewelding on reversal of load[10]. Gates and Wood[11] found that copper specimens tested in argon had lives at least five times longer than those of specimens tested in air

while gold-plated specimens showed approximately 50% improvement.

The initiation of fatigue cracks in smooth specimens of ductile crystalline materials thus is a result of the formation of persistent slip bands, intrusions and extrusions and is very much dependent on the atmosphere.

It is now accepted[12] that fatigue crack extension after initiation occurs in either three or four stages, depending on the applied stress conditions, the specimen geometry, the test environment and metallurgical variables in the metal.

Stage I growth entails the deepening of a crack nucleated in a slip band or some other region of strain localisation. The precise point at which initiation changes over to propagation is a matter of contention and physical distinction is obviously difficult. It has, however, been shown that fatigue damage may be annealed out and the specimen restored to its original state, provided that the treatment is carried out before the onset of saturation hardening. Cracking can thus be considered to be coincidental with the exhaustion of work hardening capacity[13].

In single crystals, Stage I cracks propagate along crystallographic slip planes and in polycrystalline materials the cracks propagate into the material on a plane of maximum resolved shear stress. Such a Stage I crack may propagate across a few grains and its direction may change slightly due to different crystallographic orientation[14], but the general fracture plane remains one of maximum shear stress. In most engineering components and structures, Stage I crack cannot be seen on the fracture surface since this growth occurs over a very restricted distance (usually less than one grain). Certain conditions of stressing and environment favour this form of crack growth, for example, low stress amplitude, low mean tensile stress, smooth un-notched surfaces, and a corrosive

environment[14]. Thus this mode of propagation may be absent in acutely notched, highly stressed specimens, while in a corrosive environment, failure at stresses below the (air) fatigue limit may be entirely due to Stage I crack propagation[14]. The percentage of total life of Stage I crack propagation thus may vary from 0% to 90%[15], depending on these various factors.

As Stage I cracks propagate from the free surface into the interior of the specimen, the ratio of shear stress to tensile stress at the crack tip progressively decreases and propagation subsequently changes its plane from one of the maximum shear to one of maximum tensile stress. For polycrystalline materials, this transition usually occurs at a grain boundary and this mode of crack growth has been termed Stage II propagation by Forsyth[16]. Stage II crack growth generally produces by far the largest area of a fatigue fracture surface, although the process may occupy as little as 10% of the total fatigue life in un-notched specimens. It is promoted by high stress amplitudes in severely notched specimens. Stage II crack propagation may occupy between 10% to 100% of the specimen's total fatigue life.

It is during Stage II crack growth that the characteristic fatigue striations are formed. These are different from the macroscopic "clam shell" markings which may or may not be present. These striations are orientated perpendicular to the direction of crack growth and are usually several orders of magnitudes smaller than the crack arrest or "clam shell" markings. Two different types of fatigue striations have been reported by Forsyth *et. al.*[17] viz., type A or "ductile" striations, and type B or "brittle" striations. It has been shown there is a one-to-one correspondence between the formation of a striation and the crack advance during the application of a single stress cycle[13] and that the spacing of the striation is related to the cyclic stress level. The formation of these striations appears to occur

only under plain strain conditions and can apparently take many forms. They may be clearly or poorly delineated, adjacent pockets of striations are often at large angles to each other and there are often regions where no striations are observed, all apparently dependent on whether individual grains are favourably orientated with respect to the stress pattern at the tip of the crack.

Several mechanisms have been proposed for the formation of fatigue striations, these include the plastic blunting process proposed by Laird[15], the intersecting slip processes of Hertzberg[18], and the cleavage fracture-plastic deformation sequences of Forsyth and Ryder[19]. Laird[15] suggested that a striation is formed by crack tip extension during the tensile half cycle of stress which is followed by re-sharpening of the crack tip during the following compressive half cycle. Hertzberg[18] suggested that crack extension occurs in both tensile and compressive half cycles, while Forsyth[19] proposed that crack propagation takes place by cleavage fracture ahead of the crack tip and the elevation forming the striation occurs by ductile necking. The plastic blunting modes of crack propagation, as suggested by Laird[15] appear to be more acceptable in explaining the formation of fatigue striations. However, Meyn[20] has reported that fatigue striations are not formed when the fatigue crack propagates in vacuum. This observation casts some doubts over the validity of the plastic blunting process. Pelloux[21] also suggested that fatigue striations are the result of an environmental factor and not created by plastic blunting as suggested by Laird[15] (at least for low crack growth rates).

The fatigue striation patterns formed on low carbon steels fatigue fracture surfaces are generally of irregular appearance and are more jagged and unequally spaced. This is particularly true if the strain

amplitude is high. By contrast, fatigue striations formed on aluminium and aluminium alloys show well defined patterns. However, Koterazawa *et al*[22] showed that the striation spacing of a low carbon steel fracture surface covered mainly with these irregular "quasi-striations", generally agreed very well with the macroscopic crack growth rate in the same way as for the aluminium alloys, and they concluded that the "quasi-striations" in low carbon steels do not have a different role in the crack growth process, i.e. there is no significant difference between the crack growth process of these two materials.

At a later stage of fatigue crack propagation, the conditions of the crack tip sometimes change to plane stress or the Stage III propagation mode. Under these conditions the striations gradually give way to tear dimples[23], indicating successive steps of microvoid coalescence. The macro appearance of the fracture surface may not be greatly changed however, and the characteristic clam shell (crack arrest) marks may still be visible[24]. In this instance, Stage IV represents the final failure, and is also by microvoid coalescence. In certain cases, for example, a brittle material, the final failure stage may occur by cleavage.

1.4 THE METALLOGRAPHY OF FATIGUE

The most important factor that determines the fatigue life of a material is the magnitude of the externally applied stress or the cyclic strain amplitude. The most frequently used method of showing this dependence on stress or strain is to test a number of identical specimens at each load (stress) or strain level, and to plot the resultant lives on a graph of stress or strain amplitude against life to fracture, see Figure 1.2. Such graphs usually show considerable "scatter" in the resultant points, the scatter being usually broader at lower stress levels. The distribution of specimen lives tested at a particular stress level

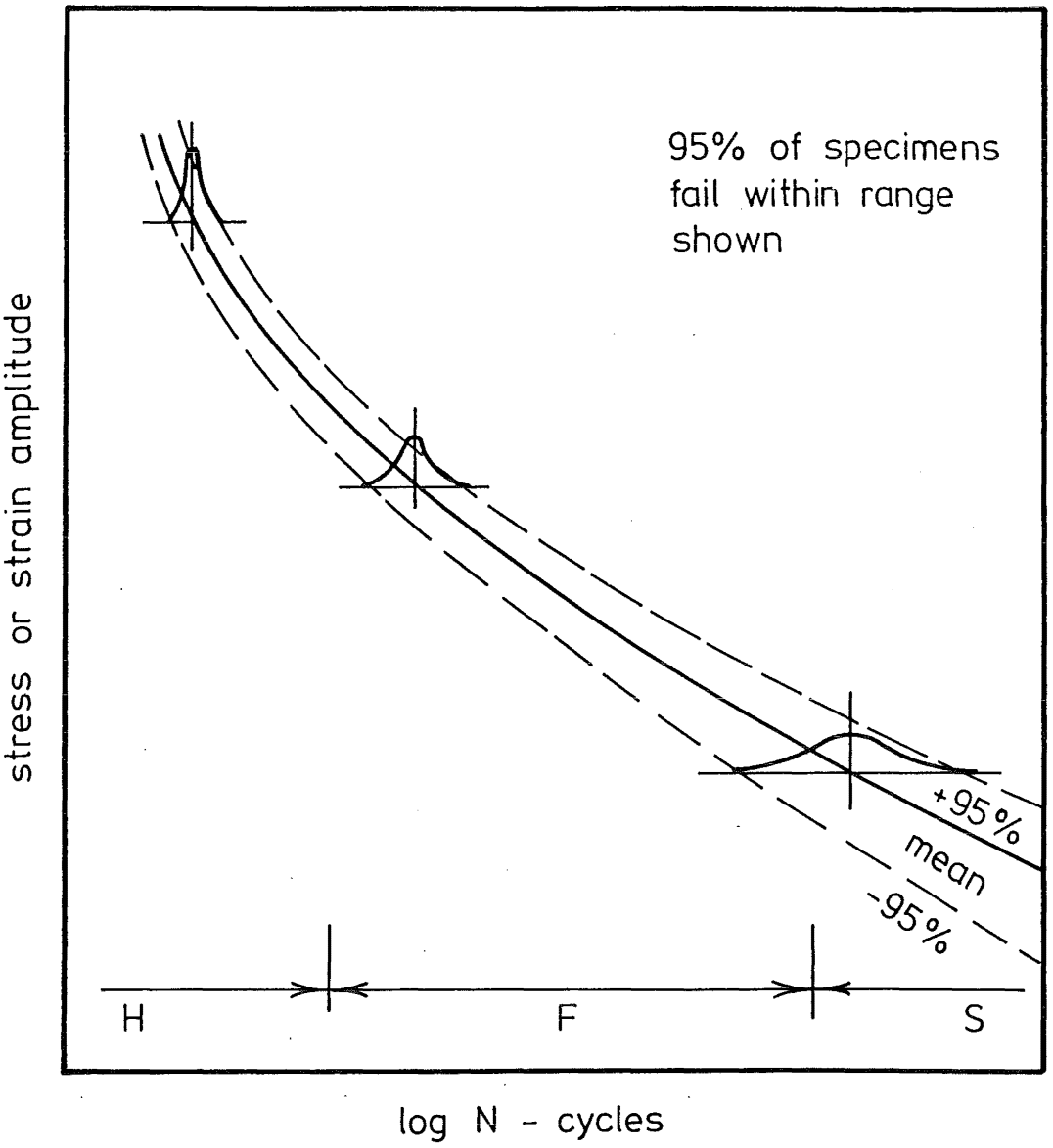

FIG. 1·2 FATIGUE CURVE SHOWING LOG-NORMAL DISTRIBUTION OF FAILURES.

gives a close approximation to a normal or Gaussian curve when the data is transformed to log N, i.e., a log-normal distribution[25]. It is now recognised that this scatter in fatigue life is inherent in the material and is thought to be due to the critical dependence of crack nucleation on the maximum local stress and the microscopic properties of the material. This is borne out by the fact that in the high strain (stress) low endurance region, where crack propagation takes place throughout most of the specimen's life, the amount of scatter is considerably reduced[25], i.e., nucleation and Stage I crack growth occupying only a small proportion of the specimen's total life, Stages II and III crack growth thus make up the largest proportions of the specimen's total life, and these stages not being markedly influenced by material properties[26].

The line which is drawn through all the points representing the mean lives of the material at various stress (strain) levels is called the S-N curve, see Figure 1.2. Although called an S-N curve, it is usually a plot of the stress (strain) amplitude against the log number of cycles to failure. A comprehensive study[27] of the structural changes produced on the free surface of lightly polished specimens has led to the now generally accepted division of the S-N curve into three basic regions, shown in Figure 1.2 as the H, F and S regions. This division is based on the slope of the curve and the type of damage produced at various load levels. In the H region the high strain reversals break down each grain into small regions of different lattice orientation and cell structures are formed. This is also the region where significant macroscopic deformation occurs and the Manson-Coffin relationship is found to apply[28]

$$(\Delta\varepsilon)\ N^{C} = \text{constant} \qquad \text{Equation (1.1)}$$

where $\Delta\varepsilon$ is the strain amplitude, N is the number of cycles, C is a constant.

Ideally, testing in the H region should be carried out using constant strain amplitude because of the occurrence of gross plastic deformation. However, it can be shown that provided the stress amplitude is well within the elastic limit, it is acceptable to use constant stress amplitude cycling.

The transition from H to F regions generally occurs at about 10^5 cycles. In the F region, the grains are able to accommodate the smaller strains without rumpling and disorientating significantly. Instead of each grain breaking up into several zones, slip bands are observed to run across the grain, which is without lattice discontinuity. It is believed that the reversed stressing causes dislocations to move to and fro along these 'active' slip bands[27] leading to large localized distortion and as a result, fatigue cracks are nucleated from these bands.

The transition from F to S mode behaviour occurs at about 10^7 cycles. This S region is thought to be the "pseudo-safe" region[27]. The slip movement is no longer concentrated in bands, but instead appears to be widely dispersed. Some 'active' slip bands may develop with prolonged cycling, however, they are usually few in number and are harmless as far as crack formation is concerned.

Electron microscope observations, using thin foil techniques, reveal that the type of dislocation arrangements depends on the strain (or stress) amplitude. Under high strain (low cycle $N < 10^5$) fatigue conditions, there is a tendency for a continuous cellular dislocation structure to be created, the cell walls consisting of clusters of dislocations surrounding areas of essentially dislocation-free material[29]. As cycling progresses, the cell walls sharpen and the cell volume decreases to a limiting value[30]. This observation of cellular structure is consistent with observations of specimen surfaces when tested

in the H region of the fatigue S-N curve.

Results from specimens tested under low strain amplitude (high cycle fatigue condition) are, however, complex and varied. Some observations suggest that a cell structure is not formed and that dislocations are dispersed in tangles[29]. Prismatic loops have also been observed and these are also heterogeneously dispersed[5,31]. However, in both copper and aluminium, a discontinuous dislocation arrangement has been seen to be superseded by a cellular structure on increasing the cyclic strain amplitude, which suggests that the former is simply a poorly developed case of the latter[13].

The above observations of dislocation distribution are regarded as typical of mechanical deformation, so that broad similarities in internal microstructure exist between cyclic and unidirectional straining. In both cases, three major factors influence the type of dislocation structure produced, these being the strain or strain amplitude, stacking fault energy of the material,and temperature[13]. High values of these terms promote cross-slip, and as the incidence of cross-slip increases, there is a tendency for a continuous cellular dislocation structure to be created[32].

The effect of strain amplitude has been mentioned and the following example illustrates the influence of stacking fault energy (S.F.E.), γ, on cell formation which is promoted by high γ values. Polycrystalline aluminium ($\gamma = 2\times10^{-5}$ J/cm^2) when subjected to cyclic strains giving fatigue lives of 2×10^6 cycles, will possess a subgrain structure[33]. Copper ($\gamma = 0.4\times10^{-5}$ J/cm^2) will do so at strains giving lifetimes of approximately 10^5 cycles, and in copper - 7½% aluminium, ($\gamma = 0.2\times10^{-5}$ J/cm^2) no cell structure is observed at cyclic strains which give lifetimes as short as 10^4 cycles. The effect of temperature on the type of dislocation

structure produced by cyclic loading is not as marked as that of strain amplitude or S.F.E. The net result is usually an alteration in the scale of the dislocation arrangement.

Since fatigue cracks are usually nucleated at a free surface, it is thought more important to relate changes in surface topography to the immediate sub-surface dislocation structure, rather than to the general dislocation structure within the specimen.

Attempts to correlate the sub-surface dislocation structure in the HCF (High Cycle Fatigue) range with changes in surface topography in the form of persistent slip bands, intrusions and extrusions, as observed in the F range of the fatigue curve shown in Figure 1.2, have been varied. For materials with medium and low S.F.E., e.g. copper, copper alloys, certain aluminium alloys, persistent slip bands appear to be associated with broad bands of dislocations. Lukas *et al*[34], who examined foils taken parallel and perpendicular to the surface found, however, that there was a three-dimensional arrangement associated with persistent slip bands. The alternate areas of high dislocation density seen when viewing planes parallel to the surface are linked below the surface, and the band is composed of regions of high dislocation density forming the walls of irregular cylinders, the axes of which are perpendicular to the primary slip plane.

Most of the above researchers have suggested that the sub-surface region between the persistent slip bands is essentially dislocation-free. Contrary to these observations are those of Wilson[35] who found that the persistent slip bands formed "channels" below the surface, these channels having a very low dislocation density by comparison with the grain matrix between channels. Klesnil[36] observed similar channels of low dislocation density within persistent slip bands in low carbon steels. However, in

this case, the channels were sandwiched between zones of very high dislocation density, the combined zones falling within one persistent slip band. These observations applied equally to both the LCF and HCF ranges, except that the persistent slip bands appeared to broaden in the LCF range. The persistent slip bands were separated by zones of relatively high dislocation density, these dislocations arranged in an ill-defined cell structure. The interior of these specimens tested under direct stress conditions showed the normal dislocation structure observed in cyclic or unidirectional deformation, i.e., a well-defined cell structure for high strain deformation and dislocations heterogeneously dispersed in tangles at low strains.

1.5 THE S-N CURVE

It is widely accepted that for metals, two distinct types of S-N curve exist, shown schematically in Figure 1.3. Certain metals such as cast and wrought iron, low and medium strength steels, aluminium-magnesium alloys and some titanium alloys, show a "knee" in their fatigue curves, type (a) in Figure 1.3. These metals, and chiefly low carbon steels, in a non-corrosive environment either fail in a few million cycles or never fail at all. The greatest stress amplitude these metals can withstand for an infinite number of cycles is defined as the fatigue limit, σ_ℓ, and since the curve is parallel to the log N axis at the fatigue limit, this also defines the "knee" stress, the knee usually occurring between 0.5×10^6 and 10×10^6 cycles.

By contrast, most non-ferrous metals such as gold, copper, brass, silver and most aluminium alloys do not show any fatigue limit. These metals have fatigue curves which do not become truly parallel to the log N axis, see curve (b) in Figure 1.3, and their fatigue strength is defined by an endurance limit, σ_e, which is defined as the stress amplitude

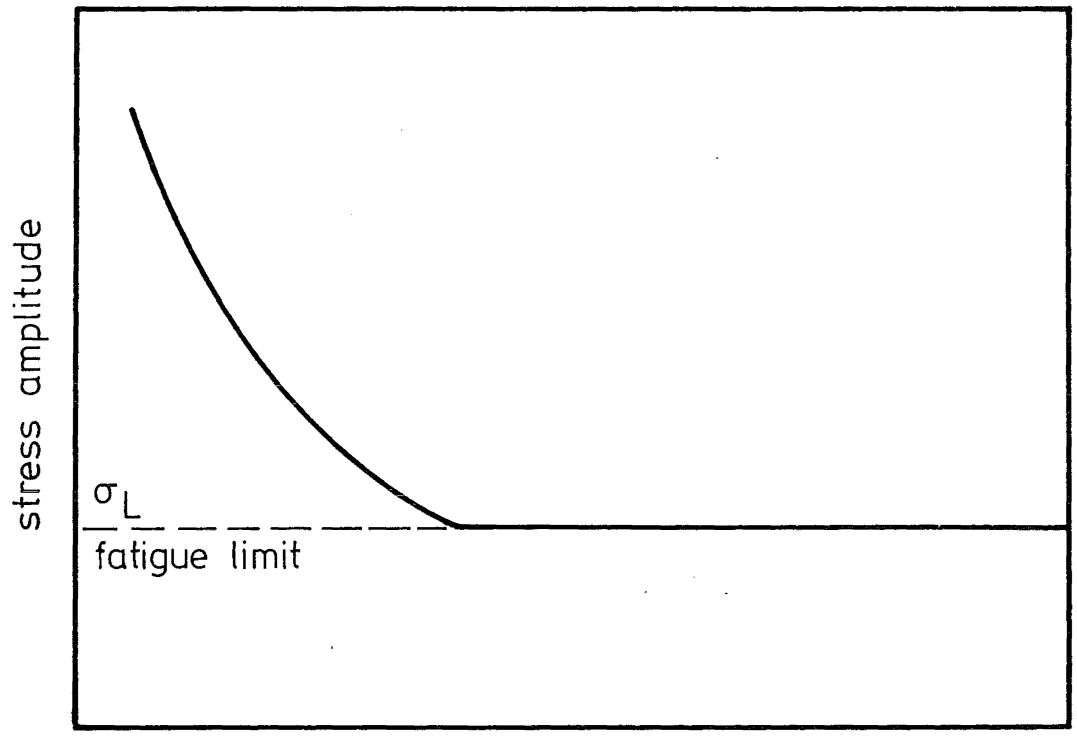

(a) ferrous materials

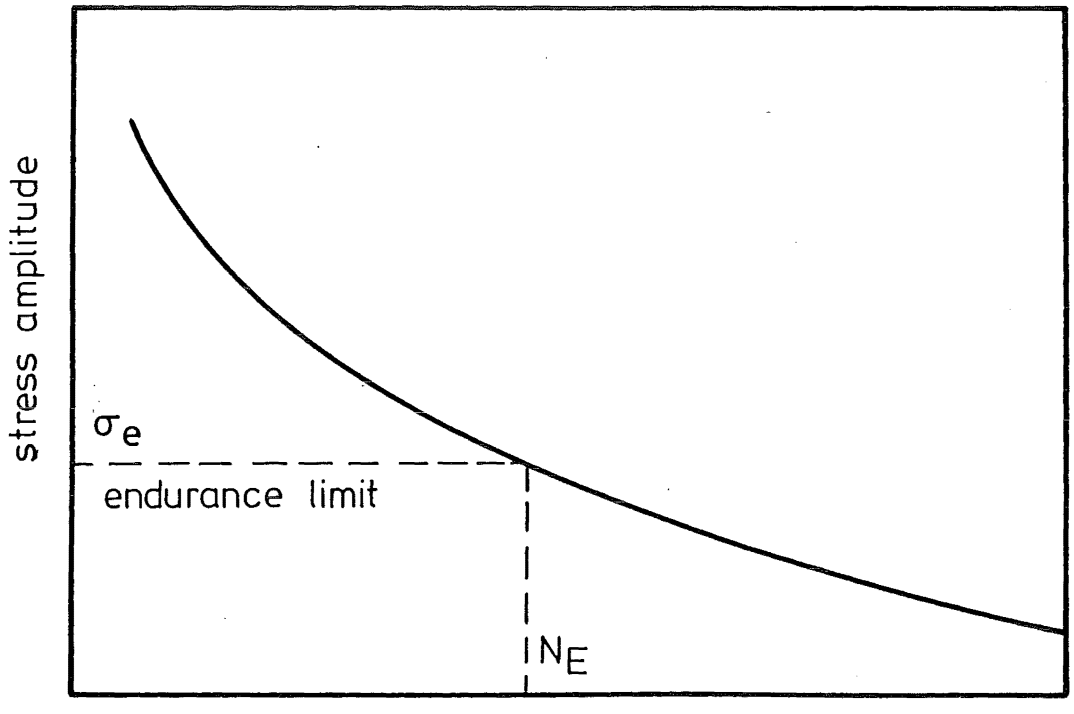

(b) non-ferrous materials

FIG. 1·3 SCHEMATIC FATIGUE CURVES (S-N DIAGRAMS)

required to cause fatigue failure in a stated number of cycles. The endurance limit is usually based on a life of 10^8 cycles. The "fatigue strength" is consequently an ambiguous term, referring in the case of metals showing a knee in the fatigue curve to the fatigue limit, and in the case of metals showing a continuous curve to an endurance limit usually based on a life of 10^8 cycles.

At first sight, the knee in the fatigue curve of low carbon steel gives the impression that there may be a fundamental difference in deformation behaviour above and below the fatigue limit. However, no such difference appears to exist, the same processes appearing to operate above and below the fatigue limit except that the deformation tends to reach a stable condition below the fatigue limit[37]. A similarity in fatigue processes between the two types of curve shown in Figure 1.3 has been suggested by Wood[38] except that the F region is absent from the fatigue curves of pure iron and low carbon steels.

Various theories have been put forward to explain the existence of fatigue limits in low carbon steels. There appears three main schools of thought[39], the first attributing the fatigue limit to the locking of dislocations by interstitials prior to testing; the second considering the fatigue limit to be due to dislocations-interstitial reactions during testing. A third group proposes that the fatigue limit results from a characteristic peculiar to the b.c.c. lattice and that this is an intrinsic property of the metal. This will be discussed in greater detail in a later chapter.

An interesting aspect of the fatigue limit in steels is its correlation with tensile strength (U.T.S.), and not the lower yield point as would be expected from Wilson's work[6]. A number of attempts have been made to correlate the fatigue strength with other commonly measured mechanical

properties such as yield stress, ductility, impact resistance and hardness. However, with the exception of the U.T.S., no relatively consistent relationship has been established[40]. This is more surprising when the basis for the definition of U.T.S. is considered.

CHAPTER TWO

THE PLASTIC FLOW OF LOW CARBON STEELS

2.1 INTRODUCTION

All metals exhibit an ability to strain or work harden when plastically deformed and this "non-ideal" behaviour of hardening under uniaxial tensile loading has been satisfactorily explained in terms of the dislocation theory[41]. Fatigue cycling of metals has also been shown to cause cyclic strain hardening[8] (or softening in some cases[8]) and studies using transmission electron microscope revealed that there is much resemblance between the dislocation structures produced by the two forms of stressing, i.e., tensile and fatigue[42].

One of the two factors affecting fatigue to be investigated in this research is the grain size of the steel. Since grain size has a considerable influence on hardening in uniaxial tension[43,44] and that cyclic strain hardening appears to be akin to this form of hardening, it seems relevant to discuss here the behaviour of low carbon steel during tensile loading. Also, this will provide some necessary background information for later discussion, even though it does not appear to have any direct influence on the design of the experimental programme.

2.2 THE LOAD-EXTENSION CURVE

As in the case for fatigue S-N curves, there are two distinct types of load-extension or stress-strain curves for metals tested in tension.

Most non-ferrous materials display a smooth and continuous stress-strain curve, see Figure 2.1(a). The initial part of the curve represents elastic extension, the slope being Young's modulus for the material. At some point just above the limit of proportionality the material deforms plastically. Plastic deformation is accompanied by strain-hardening and

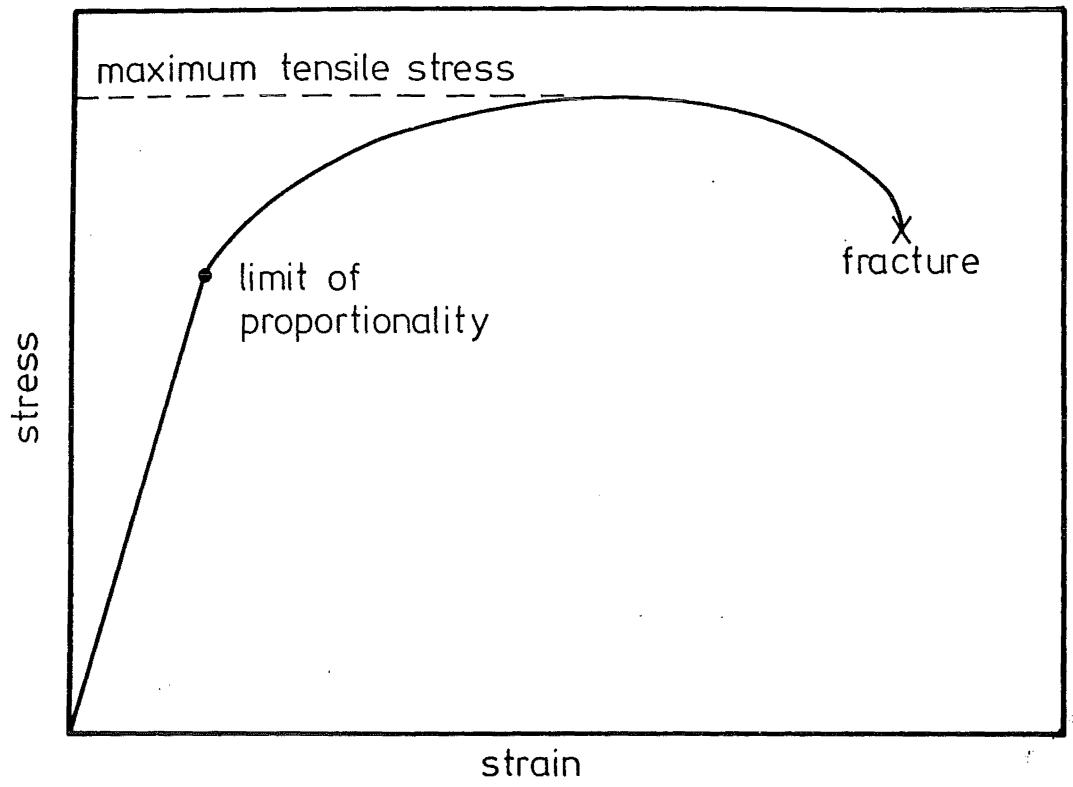

FIG 2·1(a) TYPICAL TENSILE CURVE OF A NON-FERROUS MATERIAL

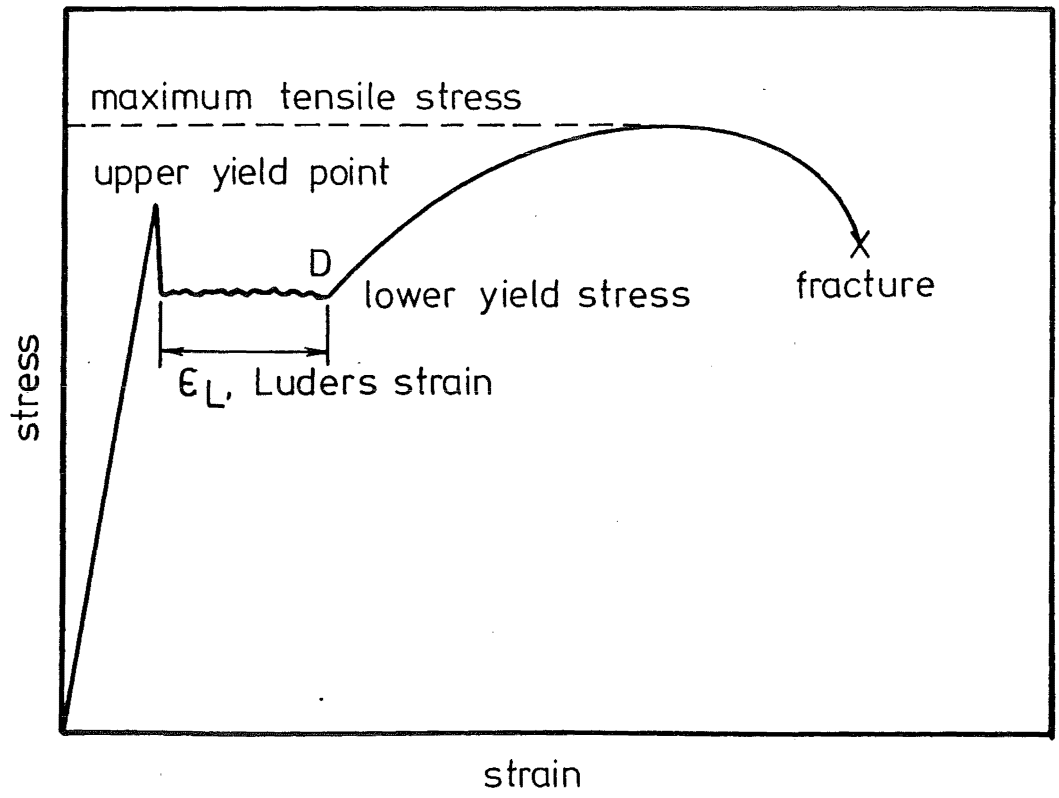

FIG 2·1 (b) TYPICAL TENSILE CURVE OF A LOW CARBON STEEL

this is indicated by the continued increase in flow stress until a point where plastic instability is reached. "Necking" of the specimen occurs at this point and the reduction in the cross-sectional area of the specimen results in a drop of load until fracture occurs. The point where plastic instability occurs is the peak of the stress-strain curve and the tensile stress is read from this point.

While the elastic limit for the above case is not easy to detect, the stress-strain curve of a low carbon steel specimen displays a distinct and characteristic discontinuous yield point, Figure 2.1(b). Up to the upper yield point the extension is purely elastic and at the upper yield point, there is a sudden drop in stress. Deformation now proceeds at a lower stress (almost constant) in an inhomogeneous manner due to the formation of discrete bands of plastically deformed metal. The bands are called Luders bands, and when they have spread along the entire specimen gauge length, uniform strain hardening starts. [Point D in Figure 2.1(b).] Due to this hardening, deformation is possible only through an increase in the applied stress. Ultimately, a maximum stress is attained and failure occurs in a manner similar to the previous case.

There are numerous variants on this stress-strain curve, dependent on material, temperature, grain size and other metallurgical variables[45]. At elevated temperatures, about 200°C, mild steel shows multiple yield points as plastic deformation begins. This is a result of interrupted motion of Luders band along the specimen. The movement of dislocations near the band front becomes locked (by interstitial atoms) - a phenomenon known as strain ageing (see Chapter 3) - and as a result, the stress has to rise to release the band front again. The ductility of the material is thereby reduced - a phenomenon known as blue brittleness - a result of simultaneous straining and ageing.

Finer grains give larger Luders strain and sharper Luders bands, increase the upper and lower stresses, and they also increase the rate of strain hardening.

Machine stiffness plays an important role in determining the yield points. In general, tensile machine may be divided into two types, the so-called "hard" and "soft" machines. For hard machines, the load is transmitted to the specimen by way of a load cell and very stiff members so that any slight variation in load can be rapidly and accurately determined. A soft machine on the other hand, is considered to transmit the load through a "soft spring" so that any minor load changes are absorbed by the spring and not recorded. The soft machine being less sensitive to load changes, cannot therefore give an accurate yield point.

2.3 THE UPPER YIELD POINT

The earliest theory put forward to explain the unusual feature of yield points in low carbon steels was the so-called "grain boundary" theory. This was suggested independently by Dalby[46] and Kuroda[47]. It was recognised that carbon content had an important effect on the yield point and since decarburised steels did not show such non-homogenous yielding, it was suggested that a thin film of iron carbide (Fe_3C) formed around each grain. This thin film inhibited plastic deformation during loading until the upper yield point was reached when it broke up and allowed Luders bands to spread across the specimen. This made plastic deformation possible.

This theory was, however, criticised by Cottrell[48], who pointed out that since only 0.02% by weight of carbon was sufficient to give a yield point, the carbide films had to be extremely thin and yet after the yield stress of the individual grain had been passed, this film would be called on to bear the load on the specimen which was impossible. Cottrell and

and Bilby[49] suggested instead the "Dislocation Locking Theory" which is now widely accepted. They assumed that carbon atoms in solution in the ferrite matrix diffuse to dislocations and remain there. Since the strain field of a dislocation may be reduced by having a carbon atom at the edge, the free energy of the crystal can be lowered. The relative atomic sizes of carbon and iron and the inter-atomic spacing of an iron crystal lattice favour such a process. The whole system, therefore, becomes more stable and the dislocation is said to be "locked" by the carbon atom. Also, since the migration of a carbon atom from the ferrite lattice to the tensile region of a dislocation represents a lowering of energy, this process is thermodynamically feasible and should be spontaneous. The diffusion and locking will obviously be more rapid at elevated temperatures.

The theory assumes that dislocations that are locked cannot move on the application of load until a critical stress, the upper yield point of the steel, is reached. At this point, the applied shear stress and thermal activation exceed the binding force between the solute atom and the dislocation. The dislocation breaks away and propagates along the specimen at a reduced stress, the lower yield stress. Cottrell and Bilby[49] estimated that as little as 10^{-6}% by weight of carbon was sufficient to place one carbon atom at each dislocation per atom plane, assuming the material has a dislocation density of 10^{8} lines/cm^{2} in the annealed state. The binding energy of a carbon locked dislocation was estimated to be about 0.5 eV per atom plane.

This theory proved to be an important step towards the understanding of the yield phenomenon. It was gradually expanded and modified. For example, it was proposed that instead of one carbon atom locking the dislocation, a group of carbon atoms could be present to cause "atmosphere locking". Precipitation may even occur between the carbon and iron atoms

so that in effect, precipitates as well as carbon atoms, lock the dislocations. Precipitates along dislocations have been observed in specimens using electron microscopes[50,51,52].

While the locking of dislocations in Cottrell and Bilby's theory successfully explains the presence of the upper yield point and other phenomena such as strain ageing, the unlocking of dislocations at the upper yield point cannot account satisfactorily for the sudden drop of yield stress at the upper yield point, the Luders strain, the Luders band velocity and the delay time phenomenon. A different concept developed by Gilman and Johnston[53] and later applied to b.c.c. iron by Hahn[54] suggests that instead of supplying mobile dislocations by unlocking, these could be generated from some other sources. By considering the dependence of the stress on the dislocation velocity, Hahn[54] derived an equation describing the flow stress in terms of the strain rate and initial dislocation density. This "dynamic model" will be discussed in greater detail in Chapter 5.

2.4 THE LOWER YIELD STRESS

Plastic deformation of a low carbon steel specimen in the initial stage occurs in a non-homogeneous nature. As soon as the yield drop has occurred, embryonic Luders bands are formed. These Luders bands represent areas that have been plastically deformed to a strain of ε_L, the Luders strain. Deformation of the specimen continues by macroscopic shear at the Luders band front. While the Luders band is being strain hardened, the rest of the material within the gauge length remains elastic. If the load is maintained, the Luders band will grow and the band spreads across the whole gauge length of the specimen at an almost constant stress, i.e., at the lower yield stress. Often, more than one Luders band is nucleated so that there are a number of fronts operating. When the whole gauge length of the specimen has yielded by an amount equal to ε_L,

uniform strain hardening occurs and deformation continues in a uniform and homogeneous manner.

The Luders strain is a function of the grain size of the specimen. Fine grains give a larger ε_L and produce sharper and more distinct bands. If the grains are coarse, ε_L is small and the bands become difficult to detect due to poor definition at the band front.

The lower yield stress may be considered as the growth stress of the Luders bands. The magnitude of the stress depends on the grain size, temperature and strain rate. The effect of grain size on the lower yield stress was first shown by Hall[55] in the form of an equation using Cottrell's 'breakaway' theory. The relation was later studied in greater detail by Petch and his co-workers[56,57]. Using the unpinning of dislocations as a basis, it was assumed that plastic deformation spread from grain to grain. Consider the case of two adjacent grains, one having yielded, A in Figure 2.2 and one still undeformed, grain B. Dislocations in A will pile up at the grain boundary that is common to both A and B when stress is applied. This pile-up causes an increase in stress in grain B and eventually, when the stress that is imparted on a locked dislocation at X in grain B reaches a critical value, the dislocation moves away from the pinned position, causing grain B to yield.

Let the applied stress in grain A be τ_y and the friction stress, which impedes the movement of dislocations, be τ_i. Therefore, the effective stress that is applied to the dislocations that are piled up at the grain boundary is $\tau_y - \tau_i$. This is also the stress that is being applied by the slip band to grain B. By analogy between a slip band and a crack, it can be shown from plastic theory that the applied stress at a distance r ahead of the blocked slip band is increased by a factor of about $(\frac{\ell}{4r})^{\frac{1}{2}}$. If r is taken as the average distance between the end of the blocked slip band and the nearest locked dislocation sources in the next grain, and assuming

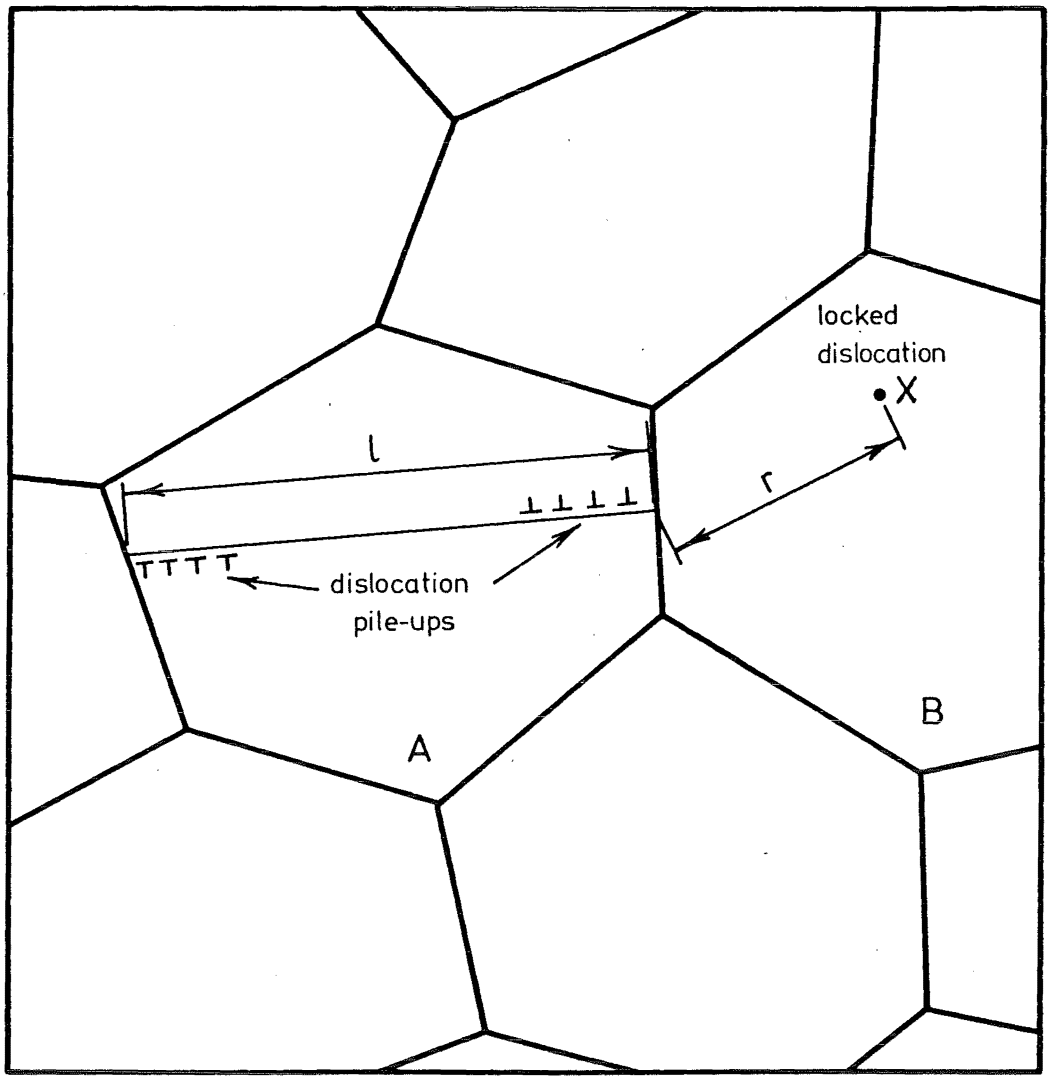

FIG. 2·2 THE HALL-PETCH MODEL OF LOWER YIELD STRESS. DISLOCATION PILE-UPS IN YIELDED GRAIN A CAUSE UNLOCKING OF A DISLOCATION IN GRAIN B.

that (a) ℓ is directly proportional to the grain diameter, d, so that

$\ell = R.d.$

(b) there is a critical shear stress value, τ_C, required to free locked dislocations,

then the pile-up stress in grain A can make grain B yield if

$$\tau_C = (\tau_y - \tau_i) \quad (\frac{\ell}{4r})^{\frac{1}{2}} \qquad \text{Equation (2.1)}$$

Assuming the applied shear stress is equal to the lower yield shear stress, and converting all shear stresses to their equivalent tensile stresses, Equation (2.1) becomes

$$\sigma_C = (\sigma_y - \sigma_i) \quad (\frac{Rd}{4r})^{\frac{1}{2}} \qquad \text{Equation (2.2)}$$

or

$$\sigma_y = \sigma_i + k_y d^{-\frac{1}{2}} \qquad \text{Equation (2.3)}$$

where $$k_y = 2\sigma_C \quad (\frac{r}{R})^{\frac{1}{2}} \qquad \text{Equation (2.3(a))}$$

Equation (2.3) is known as the Hall-Petch equation.

σ_i is called the friction stress and is very sensitive to the testing temperature. It has been shown that σ_i may be considered to comprise two components, one which is temperature independent representing the stress required to move free dislocations against the resistance of structure irregularities provided by dissolved solutes, fine precipitates, dislocations and sub-structures; and the other which is temperature dependent representing the Peierls-Nabarro force. Hence σ_i, besides being temperature dependent, also varies with the concentration of solute atoms and the degree of precipitation that has taken place.

From the derivation of the Hall-Petch equation, k_y is related to the "unpinning stress" σ_C and hence k_y is often known as the "unpinning factor". Since k_y is not concerned with moving dislocations across the lattice, it is independent of the solute atom concentration and strain rates, but rather it depends on how strongly the dislocations are anchored (i.e., the

locking mechanism). k_y should vary also with temperature and this has been shown to be true by Fisher[58] for steels that have been quenched and lightly aged. For annealed specimens, however, k_y has been found to be insensitive to temperature variation indicating that dislocation locking is strong, and mobile dislocations during plastic deformations come from nucleation and multiplication rather than from originally pinned sources.

2.5 THE FLOW STRESS

The Hall-Petch relationship which applies to the non-homogeneous yielding of low carbon steel has been found to apply to materials that do not exhibit the Luders strain. Instead of the lower yield stress, the flow stress was found to vary linearly with $d^{-\frac{1}{2}}$ [59], i.e.,

$$\sigma_f = \sigma_i' + k_f' \, d^{-\frac{1}{2}} \qquad \text{Equation (2.4)}$$

where σ_f is the flow stress, and σ_i' and k_f' are constants having the same definition as σ_i and k_f in the Hall-Petch equation.

Armstrong[59] hence argued that since there is no difference between the grain boundary effect on dislocation movement during non-homogeneous yielding (i.e. lower yield point) and the homogeneous plastic flow (the strain hardening part of stress-strain curve), the Hall-Petch relationship should equally apply to the flow stress of low carbon steel, i.e.

$$\sigma_f = \sigma_{of} + k_f \, d^{-\frac{1}{2}} \qquad \text{Equation (2.5)}$$

The friction stress in this case was found to be strain dependent and is made up of two parts with the following relationship

$$\sigma_{of} = \sigma_i + \alpha_o \varepsilon^{\frac{1}{2}} \qquad \text{Equation (2.6)}$$

where σ_i is the friction stress in the Hall-Petch equation, and α_o is a constant. $\alpha_o \varepsilon^{\frac{1}{2}}$ represents the additional resistance to dislocation motion produced by interactions with other dislocations.

k_f, initially thought to be constant, was found to vary with strain

as well, and Evans and Rawlings[60] made the following modification to relate k_f with strain,

$$k_f = k_f'' \varepsilon^n \qquad \text{Equation (2.7)}$$

where k_f'' is a constant and n is the strain hardening exponent.

Substituting Equation (2.6) and Equation (2.7) into Equation (2.5)

$$\sigma_f = \sigma_i + \alpha_o \varepsilon^{\frac{1}{2}} + k_f'' \varepsilon^n d^{-\frac{1}{2}} \qquad \text{Equation (2.8)}$$

Hence for a constant strain, $\sigma_f \propto d^{-\frac{1}{2}}$

Armstrong[59] showed this relationship holds for 70/30 brass, zinc, and 0.13%C steel. But Morrison[61] found that for his low carbon steel, the above linear relationship was not obeyed.

2.6 THE POWER LAW

During plastic deformation of a material after the yield point, if the material is perfectly plastic, then deformation should proceed at a constant stress. In practice, this is never the case because, as the material is strained, it hardens at the same time so that the stress required for further plastic deformation must increase all the time with strain. The relationship between the true stress, i.e. the true flow stress, and the true strain is described by the power function

$$\sigma = k\varepsilon^n \qquad \text{Equation (2.9)}$$

σ, the true stress, is calculated using the instantaneous true area, A_i of the specimen cross section. Thus, if the nominal stress is σ_f and the original cross-section area of the specimen is A_o, then

$$\sigma A_i = \sigma_f A_o$$

$$\sigma = \sigma_f \frac{A_o}{A_i} .$$

Assuming the volume of the gauge length material remains constant,

$A_o \ell_o = A_i \ell_i$ where ℓ_i is the magnitude of the instantaneous gauge length.

$$\therefore \quad \sigma = \sigma_f \frac{\ell_i}{\ell_o}$$

$$= \sigma_f (1 + \lambda) \qquad \text{Equation (2.10)}$$

where λ is the nominal strain

$$\lambda = \frac{\ell_i - \ell_o}{\ell_o}$$

The true strain, ε, is defined using the change in gauge length referred to the instantaneous gauge length rather than to the original gauge length, i.e.

$$\varepsilon = \frac{\ell_1 - \ell_o}{\ell_o} + \frac{\ell_2 - \ell_1}{\ell_1} + \ldots . \frac{\ell_i - \ell_{i-1}}{\ell_{i-1}}$$

$$= \sum_{n=1}^{i} \frac{\ell n - \ell n-1}{\ell n-1}$$

$$\text{As } \left| \ell n - \ell n-1 \right| \longrightarrow 0$$

$$\varepsilon = \int_{\ell_i}^{\ell_o} \frac{d\ell}{\ell}$$

$$= \ln \frac{\ell_i}{\ell_o}$$

$$= \ln (1 + \lambda) \qquad \text{Equation (2.11)}$$

k in Equation (2.9) is a constant called the strength coefficient and n is called the hardening exponent[62] or coefficient.

Equation (2.9) is an empirical formula chosen to best describe the actual stress-strain curve obtained experimentally. The difficulty involved in trying to describe the stress-strain curve accurately is

introduced by the fact that for a chosen value of n, the Power Function only describes accurately a portion of the actual curve. In other words, to describe the whole curve, n has to vary with strain.

2.7 STRAIN HARDENING

The explanation of strain hardening represents one of the most important contributions of the dislocation theory. There is no unified quantitative analysis that can describe exactly the phenomenon and various essentially different models have been developed, e.g., the "dislocation forest" theory of Kovács[63], the "Jog" theory developed by Hirsch[64,65], the "meshlength" theory of Kuhlmann-Wilsdorf[66], and the "long range stress" theory of Seeger[67,68]. However, the dislocation theory does offer a satisfactory qualitative account of the hardening process.

Most of the investigations on strain hardening have been carried out on f.c.c. materials and accordingly, the aforementioned theories have all been developed based on experimental observations of f.c.c. single crystal behaviour in tension. More recently, work by Sestak and Seeger[69] suggests that there is a close similarity between hardening in f.c.c. and b.c.c. crystals and they proposed a similar mechanism to account for strain hardening in b.c.c. crystals.

Single crystals of f.c.c. metals orientated for single slip show three stages of work hardening, Figure 2.3. For b.c.c. crystals, however, this three-stage hardening is observed only close to or above room temperature and disappears at low temperatures (below about 270k for iron)[70]. The reason for this transition is because of the dependence of screw dislocation mobility on temperatures. At room temperature or above, the thermal activation becomes sufficiently high to compensate for the large mobility difference between edge and screw dislocations.

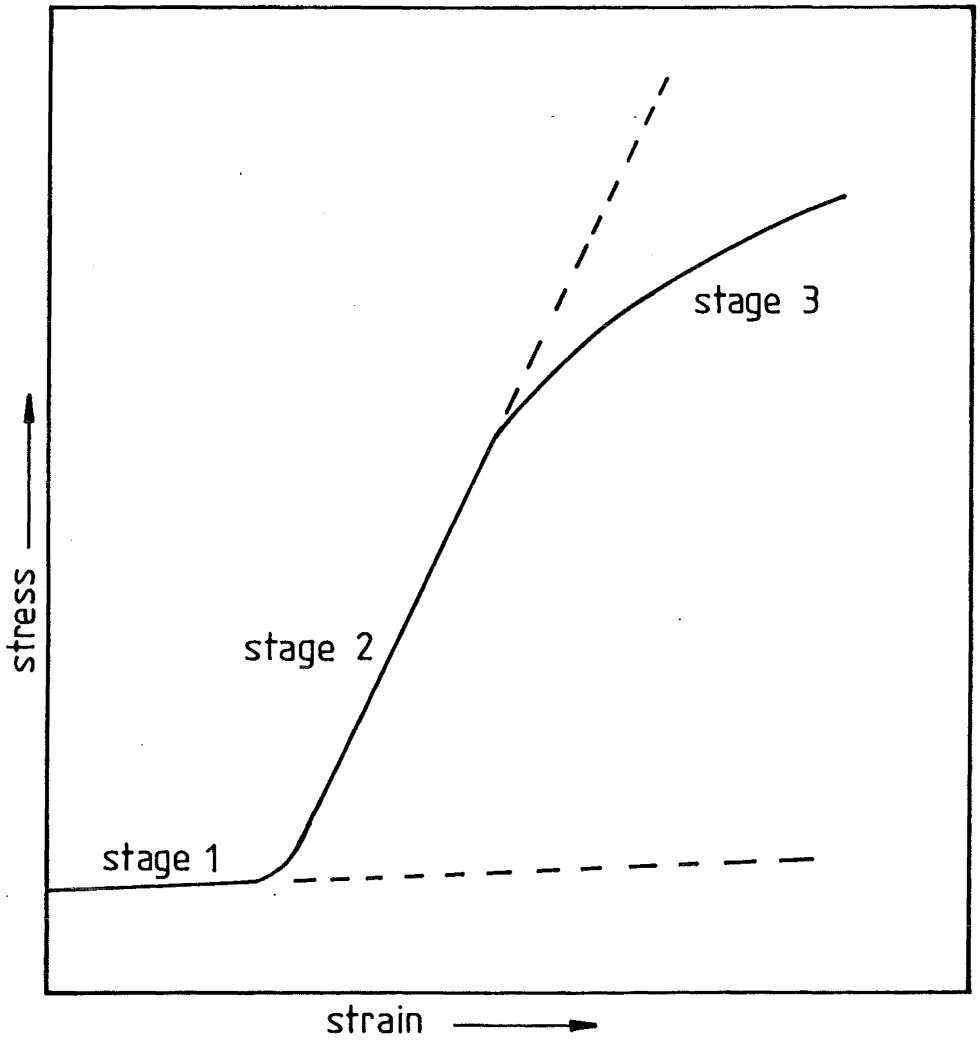

FIG. 2.3 3-STAGE DEFORMATION CURVE OF A F.C.C. CRYSTAL

Explained in terms of the dislocation theory, the three stages characterising the shape of the curve may be summarised as follows:

1) Stage I: This stage begins after elastic deformation and is also known as the "easy-glide" stage. Dislocations, particularly of the edge type, move relatively easily under stress with little intersection and they (edge dislocations) move out to the free surface to form long slip lines. The low strain hardening rate is due primarily to the elastic interaction of dislocations of opposite signs approaching each other on neighbouring planes. Hence, even though there is an increase in dislocation density, there is little change in the hardness.

2) Stage II: Strain hardening in this stage is attributed to the long-range stresses originating from dislocations in the primary system. These long-range stresses are set up when dislocations of the same sign pile up against some obstacles which may be immobile dislocations lying in an unfavourable slip plane. Although the resolved shear stress remains highest on one slip system, other secondary slip systems may eventually be operative to cause dislocation multiplication. The secondary dislocation density will increase but the secondary glide remains small since the displacement of secondary dislocations is insignificant. This stage is characterised by shorter, more closely but less regularly placed slip lines on the crystal surface[71].

3) Stage III: The beginning of this stage is marked by a decrease in the strain hardening rate (recovery). This is mainly due to the onset of thermally activated cross-slip when screw dislocations climb from one active slip plane to another parallel plane to avoid pinning by obstacles. Also, annihilation of primary screw dislocations of opposite signs begins to occur on a larger scale. The net result is that deformation of the crystal becomes easier. Traces of cross-slip

have been observed on glide bands on the surface of copper crystal in Stage III deformation[41]. Because cross-slip is facilitated by higher temperatures and stacking fault energies, the Stage III deformation stage is also a function of these factors.

The initial flow stress of b.c.c. crystal is usually larger. The major difference between yielding in b.c.c. and f.c.c. crystals is that cross-slip can take place more easily in b.c.c. crystals, and it frequently occurs even in Stage I deformation. The effects of this are that Stage I is less well-defined and hardening is smaller, but the resulting dislocation structure is similar to that in f.c.c. crystals[41].

Polycrystalline materials do not show the three-stage curve during deformation, the whole hardening process after elastic extension appears to be of the Stage II type. This may be explained by the observation that single crystal copper orientated for six slip systems to operate also exhibits only Stage III hardening. Thus it appears that widespread cross-slip takes place in a polycrystalline material due to the multiple active slip systems.

Dislocation structures resulting from tensile deformation have been studied on a variety of materials, notably copper[72], niobium[43] and low carbon steel[44]. A similar pattern is noted in each case,i.e., the type of dislocation structure formed is dependent on strain.

At small strains, the dislocation structure consists of long dislocations with "bow-outs". Edge-dislocation dipoles trailing behind moving screw dislocations and a large number of prismatic loops and dipole loops are also present. As the strain is increased, clusters of tangled dislocations are formed. These clusters are formed when a number of dislocations are immobilised by a common obstacle. Soh[44] found that such dislocation structure was observed at about 5% strain for low carbon

steel. Further straining causes the dislocations to rearrange into a cellular structure, the cell walls being regions of very high dislocation density and the interior being relatively free of dislocations. Conrad *et al*[43] found that cell size was proportional to the square root of grain size.

The dislocation density, ρ, of the material increases linearly with the amount of plastic strain and for a given strain, ρ is a function of the grain size, i.e., it increases with decreasing grain size. Thus, for a given strain, a fine grained material should strain harden more rapidly than a coarse grained material due to its higher dislocation density. This was confirmed by Soh's[44] results on low carbon steel and Conrad *et al*[43] results on niobium.

CHAPTER THREE

STRAIN AGEING OF LOW CARBON STEELS

3.1 INTRODUCTION

The exact contribution of strain ageing during fatigue is not known. However, its influence on the behaviour of some materials, particularly low carbon steels, under this mode of stressing is widely acknowledged. Strain ageing in fatigue should, strictly speaking, be considered in terms of dynamic strain ageing since it occurs simultaneously with the stressing process. However, because cyclic strain hardening also occurs during the stressing process, it is difficult, if not impossible, to isolate and study dynamic strain ageing on its own. Consequently, much of the explanation of this form of ageing has to be based on observations of static strain ageing.

The effects of strain ageing during fatigue is studied in this project by comparing steels with equivalent grain sizes but with different ageing propensities (defined in terms of static strain ageing). To discuss the results and effects of dynamic strain ageing, it is therefore necessary to first gain an understanding of strain ageing in the static case.

3.2 GENERAL FEATURES OF STRAIN AGEING

If a low carbon steel specimen (in annealed, normalised or as-rolled state) is strained to beyond the yield point elongation, it begins to strain harden and an increased load is required to continue plastic deformation. If the test is stopped at a point A on Figure 3.1(a), and the load removed and then reloaded within a short period of time, the steel will behave elastically until the previously applied load (or flow stress) is reached, A in figure 3.1(a), after which plastic deformation and strain hardening will occur as if the test had not been interrupted at A. The steel now behaves in the same way as any other metal where the

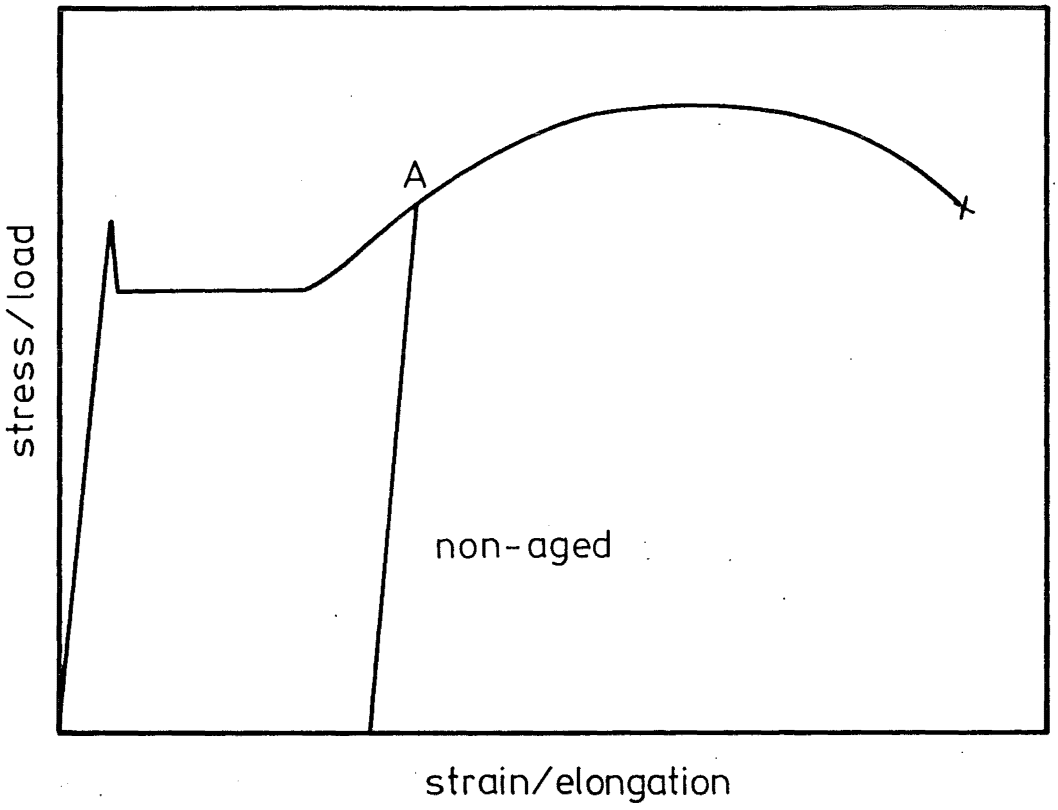

FIG 3·1 (a) TENSILE CURVE OF A NON-AGED STEEL SPECIMEN.

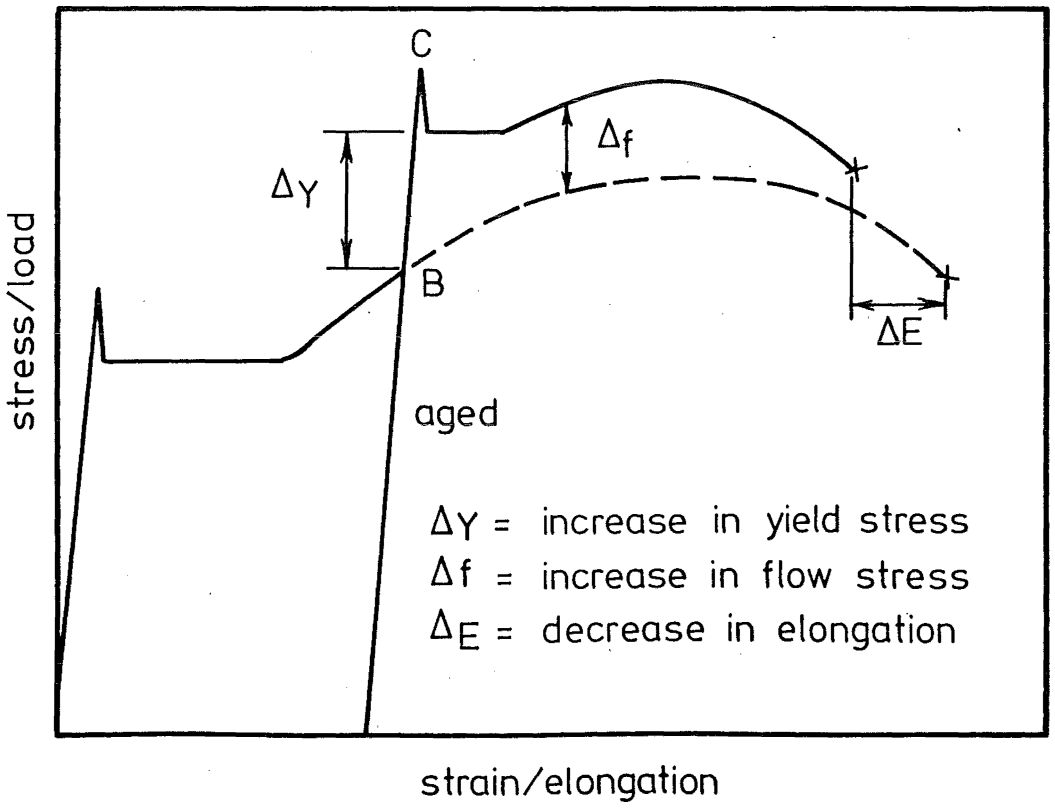

FIG. 3·1 (b) TENSILE CURVE OF AN AGED STEEL SPECIMEN

dislocations are not pinned by atmospheres or precipitates.

If a similar test is again interrupted, say at point B in Figure 3.1(b) but on this occasion the steel is allowed to age for a period, the yield point is found to have returned on retesting. This yield point returns at a higher stress, C in Figure 3.1(b), than the flow stress B of the non-aged steel, and the steel is now said to have "strain aged". The return of the yield point is usually accompanied by an increase in the tensile strength and a reduction in ductility (Figure 3.1(b)) called strain age hardening. The increase in yield stress, ΔY in Figure 3.1(b), is the universal indication of strain ageing.

Other properties of the steel affected by strain ageing include the ductile/brittle transition temperature, fatigue strength and electrical and magnetic properties[73,74].

3.3 MECHANISM OF STRAIN AGEING

Observations of the change in tensile properties with strain ageing have been explained on the basis of a two-stage ageing process[75]. In the first stage the interstitial solute atoms are assumed to migrate to the dislocations to form Cottrell atmospheres and that the magnitude of the discontinuous yield is directly related to the density of these atmospheres. Yielding at this stage appears to be by the unpinning of dislocations. This consequently affects only the upper and lower yield points and the Luders strain, i.e., the locking part of the tensile curve. The basic flow stress curve is not affected since on straining beyond the lower yield extension, the atmospheres are dispersed. With very low solute contents, only this first stage of strain ageing is obtained.

During the second stage of strain ageing, the interstitial solute atoms continue to segregate at the dislocations causing atmosphere formation to be exceeded. Precipitates are now formed along the dislocations. Since the dislocations are fully locked at the end of the first stage, the Luders

strain is little affected during this second stage. However, precipitate formation causes hardening, thus raising the flow stress and tensile stress of the steel (Figure 3.1(b)). The corresponding increase in the work hardening rate causes a reduction in the elongation at fracture. In most cases, this stage of ageing takes place unless the interstitial solute content is extremely low[75].

It is now universally accepted that interstitial carbon and nitrogen atoms are responsible for dislocation locking and strain ageing in low carbon steels. Since the relocking of dislocations by interstitial solute atoms is a process involving diffusion, it is therefore influenced by both time and temperature. Hundy[76] derived the following equation connecting strain ageing at ambient and elevated temperatures

$$\log \frac{t_r}{t} = H \left[\frac{1}{T_r} - \frac{1}{T}\right] - \log \frac{T}{T_r} \qquad \text{Equation (3.1)}$$

where t_r is the ageing time at ambient temperature T_r(k) and t is the ageing time at the elevated temperature T in Kelvin. The constant H, derived from diffusion coefficient, is equal to 4400 for the diffusion of carbon atoms and 4000 for the diffusion of nitrogen atoms. The small difference in H values for carbon atom diffusion and nitrogen atom diffusion means that at an elevated temperature the ageing times required for similar degree of carbon ageing and nitrogen ageing are approximately equal (Eqn 3.), i.e., the diffusion rates of carbon and nitrogen atoms to dislocations should be approximately equal. Hence at low temperatures, the degree of ageing produced by carbon and nitrogen should be about the same.

However, there is now considerable evidence to show that strain ageing in low carbon steels at temperatures below about 100°C - 150°C is different in character from ageing above this temperature[74] and that this low temperature ageing in slow cooled steels is predominantly due to nitrogen in the steel. Thus, if nitrogen atoms are combined with a strong nitride former, the steel shows negligible ageing below 100°C - 150°C.
The difference in effectiveness of carbon and nitrogen in producing

strain ageing at ambient temperatures can be explained if the solubility of these elements in ferrite is examined. The maximum solubility of nitrogen in ferrite is about 0.1% wt while that of carbon is about 0.022% wt and because the nitrides have lower equilibrium solubility temperature than carbides (see Figure 3.2), these nitrides have a lower stability than the iron carbides. The resolution of iron nitrides therefore takes place more rapidly giving a ready supply of interstitial nitrogen for dislocation locking.

Strain ageing begins to occur with interstitial content above 0.0002 - 0.0005% wt. In this range of interstitial content, partial first stage ageing can take place. When the interstitial content is about 0.0020% wt, ageing extends well into the second stage. From the solubility data on carbon (Figure 3.2), it may be said that interstitial carbon in solid solution at room temperature in normally cooled low carbon steels is insufficient to cause strain ageing and this has been confirmed by the experimental results of Butler[77].

3.4 THE EFFECTS OF STRAIN AGEING ON THE TENSILE PROPERTIES OF LOW CARBON STEELS

Qualitative studies of strain ageing have shown that the tensile properties are affected in two stages:

(a) In the first stage, due to 'atmosphere' formation on dislocations, only the yield point is affected, i.e., the upper and lower yield stresses, and the Luders strain.

(b) In the second stage, due to precipitation formation on dislocations, the lower yield stress, the tensile stress and the elongation at fracture are affected.

An attempt was made by Wilson and Russell[75] to show the effect of strain ageing on the Hall-Petch relationship, $\sigma_y = \sigma_i + k_y d^{-\frac{1}{2}}$. From Figure 3.3 it may be seen that pre-straining an annealed steel caused a

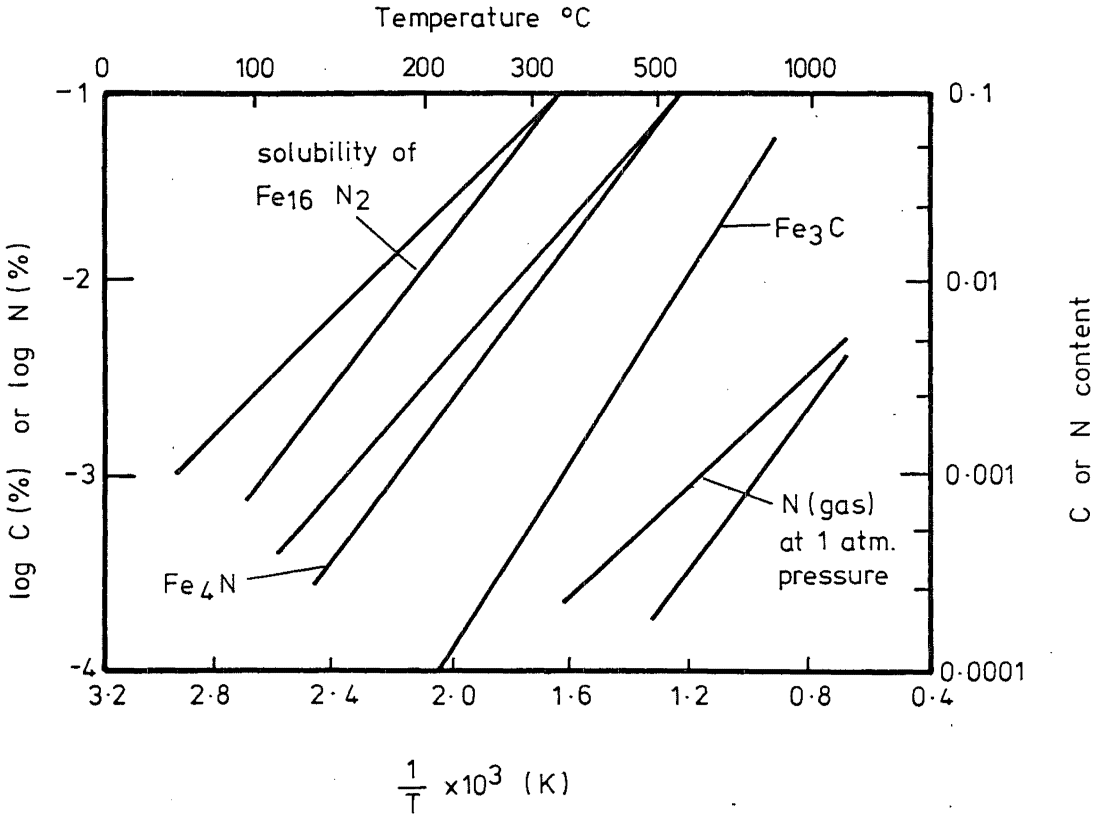

FIG. 3·2 SOLUBILITIES OF NITROGEN AND CARBON IN IRON (BAIRD[73])

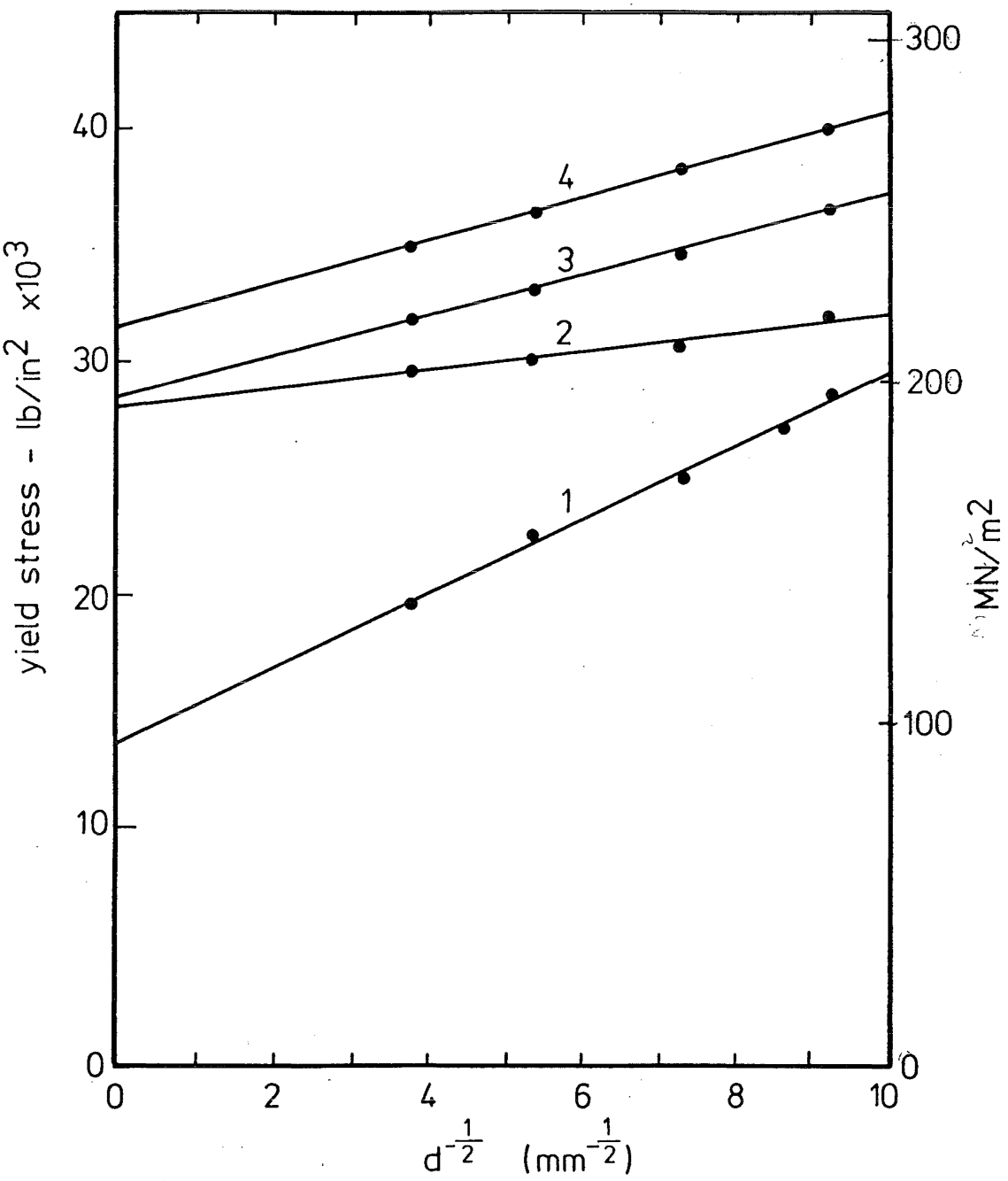

FIG 3·3 THE VARIATION OF THE LOWER YIELD (TENSILE) STRESS WITH $d^{-\frac{1}{2}}$ WHERE 2d IS THE GRAIN DIAMETER IN mms.

1. annealed specimen
2. prestrained 4%
3. prestrained 4%, aged to end of first stage
4. prestrained 4%, 'fully' aged (10^4 mins. at 60°C)

(Wilson & Russell [78])

pronounced increase in σ_i and a decrease in k_y. On subsequent ageing to the end of first stage, k_y increased while σ_i remained unaltered. Further ageing into the second stage produced no further change in k_y but σ_i increased. These results were expected on the basis of existing theory at that time, that yielding took place by the unpinning of locked dislocations and k_y in the strain aged specimen never reached the initial value of the annealed specimen. This is attributed to a decrease in r, see Equation (2.3(a)).

Since yielding in an annealed steel is now believed to take place at dislocation sources in grain boundaries[79], this leads to an unexplained reduction in k_y. This anomaly has been explained by Wilson[80] in his work on yielding of strain aged steels:

(a) the first stage of ageing is due to atmospheres locking of dislocations. The yield point behaviour during this state is consistent with Cottrell's original suggestion that mobile dislocations are nucleated by the unpinning process. Thus the yield stress will depend on k_y during this stage which will, in turn, depend on dislocation 'atmosphere' density.

(b) At the end of the first stage, continued segregation of the interstitial solute to dislocations has no further effect on k_y. Yielding by unpinning is very unlikely during this second stage of ageing. Mobile dislocations are probably nucleated at grain boundary sources as in the initial stage (annealed, normalised, as-rolled, etc.).

(c) The lower value of k_y during the second stage, as compared to its initial value k_{yo} ($k_y = 0.65 k_{yo}$) is explained by the assumption that pre-straining causes a reduction in stress σ_c required to nucleate dislocations from grain boundaries. Finally, a slow rise

in k_y to the original value k_{yo} may take place due to long range diffusion of solute atoms from grain interior to grain boundaries. This rate is clearly related to the interstitial content.

3.5 METHODS FOR PREVENTING STRAIN AGEING

As pointed out in Section 3.3, strain ageing is caused by the locking of mobile dislocations by carbon and nitrogen atoms during ageing. Thus if these two elements were either removed from the solid solution or prevented from existing in this free state in low carbon steels, strain ageing may be reduced, if not totally eliminated. The removal of nitrogen from steel is not an easy task since the atmosphere contains some 78% of free nitrogen. Consequently its presence in steel becomes inevitable. The removal of carbon from steel would defeat the purpose of strengthening iron by carbides.

Since the effect of carbon on ageing at temperatures below about 100°C is negligible and that all experiments in this project are to be carried out at ambient temperature, methods relating to the prevention of ageing by carbon will not be discussed further.

As far as nitrogen is concerned, several methods of retarding or preventing strain ageing are possible. For example, by retarding the cooling rate of steel from the austenite range, thus increasing the possibility of achieving equilibrium solubility and reducing the interstitial nitrogen content; by lowering the ageing temperature to well below the ambient temperature hence retarding the diffusion of interstitial nitrogen; by the addition of strong nitride forming elements to the steel, or by the addition of alloying elements such as manganese or silicon[81,82], which will interact with nitrogen atoms[74], and reduce their mobility in steel.

The addition of nitride formers is one of the more common methods used to render steels non-strain ageing and several elements have proved to be

successful. These elements include:

(i) Aluminium - Although aluminium is a strong nitride former, it has only a slight effect on strain ageing of as-rolled steels at all ageing temperatures up to 300°C[83]. However, strain ageing can be considerably reduced by normalising the steel, the reason being that AlN is slow to precipitate even during slow cooling and the precipitation is considerably quicker during the re-heating process. Thus commercially, aluminium may not be suitable for producing non-ageing steels in the as-rolled condition.

(ii) Boron - Boron has been used as a strain age inhibitor in Open Hearth steel sheet used for deep drawing and pressing in the automobile industry. The main advantage with boron stems from the fact that the small quantities that have to be added to reduce strain ageing do not significantly affect the rimming action of these steels. Morgan and Shyne[84] found that for their low carbon steel (0.06% C, 0.55% Mn, 0.004 - 0.006% N), there was an optimum boron content of 0.017 - 0.02%, if the boron content fell outside this range, ageing took place or affected the rimming action. Fountain and Chipman[85] found that the solubility of BN is lower than AlN in both ferrite and austenite, so that BN is more stable. It appears from literature, that boron, when added in suitable quantities, may be effective in precipitating most of the nitrogen as BN during the processing of hot rolled low carbon steels, and hence reduce the active nitrogen content. However, boron has been known to cause hot shortness which makes hot rolling difficult[86,87].

(iii) Titanium - Titanium is a strong and stable nitride former. Due to the extremely low solubility and high stability of TiN[88,89] when compared to other nitrides, precipitation of TiN may take place independent of the prior heat treatment given to the steel. Hence

it may be possible to precipitate nearly all the active nitrogen in low carbon steels as TiN by the addition of the necessary amount of Ti, regardless of the subsequent processing conditions. Titanium additions in excess of the Ti/N stoichiometric ratio can almost completely eliminate strain ageing in as-rolled C-Mn reinforcing steels[90] at ageing temperatures of 100°C or less. However, when the ageing temperature is increased to 205°C, commercial as-rolled high strength low-alloy steels with Ti contents well above the Ti/N stoichiometric ratio still show strain ageing due to the effect of carbon atoms.

(iv) Vanadium - Vanadium is also a strong nitride former[88,91]. Epstein *et al*[92] reported that sheet steels containing 0.03 - 0.05% V showed no sign of strain ageing. Frame and Schunk[93] recommended a vanadium content of 0.02 - 0.03% and an annealing temperature of 700°C for the prevention of strain ageing in low carbon steels. Jones and Coombs[94] found that the changes in yield stress (ΔY) and tensile stress (ΔU) after strain ageing (ageing temperature < 100°C) was negligible in low carbon steels having vanadium contents ranging from 0.03% to 0.1%. In this case, the steel had been treated at 680°C for 20 hours after hot rolling. However, when the annealing temperature was increased to 930°C, this material showed signs of strain ageing. When the ageing temperature was increased to well above 100°C, the steels were highly susceptible to strain ageing. Rashid[95] also reported strain ageing of a commercial as-rolled high strength low-alloy steel containing 0.11% V aged at 205°C. The susceptibility to strain ageing of vanadium-bearing steel as ageing temperature is raised to above 100°C may be due to the re-solution of Fe_3C[73] and hence carbon dislocation locking.

Nobium[83,88,96] and Zirconium[74,97,98] have also been tried as strain

age inhibitors with some success.

In addition to the elimination or reduction of strain ageing. these alloying elements have also been found to be effective in refining grain size in some steels. A more thorough review of the effects of these elements is given elsewhere[99].

Because aluminium's presence in steel may or may not prevent strain ageing from taking place (depending on the thermal history of the steel), it was decided to add aluminium to the experimental steel so that with appropriate heat treatments, two types of steel could be produced, one an ageing steel and the other a non-ageing steel.

Aluminium in the levels required for AlN also has little effect on other properties, i.e., yield stress, tensile stress etc.

CHAPTER FOUR

THE FATIGUE LIMIT OF LOW CARBON STEEL

4.1 INTRODUCTION

There is no one encompassing theory to explain why some metals possess a distinct fatigue limit while others do not. In general, materials that have fatigue limits also exhibit a discontinuous yield point during uniaxial tensile testing and may be strengthened by strain age hardening. Since the phenomena of yield points and strain age hardening are attributed to the locking of dislocations by interstitial atoms, atmospheres and precipitates, it is therefore not surprising that the effects of strain ageing have been studied in great detail in order to seek an explanation for the existence of a fatigue limit. The results obtained by various workers[2,3,4,5,6] on this topic have been equivocal and at times, contradictory. Some workers[2,3,6] believe that strain ageing is responsible for the presence of a fatigue limit, while others[4,5,7], in conceding that strain ageing has an effect on the fatigue limit, are of the opinion that strain ageing is not the prime source of the fatigue limit. They[4,5] proposed that the fatigue limit results from a characteristic peculiar to the body centre cubic (b.c.c.) lattice, so that the fatigue limit is an intrinsic property of the material. The group proposing a strain ageing mechanism may further be divided into two sub-groups, one[6,100] favouring the idea that initial dislocation locking, which occurs before fatigue testing, is important, and the other[2,3,101,102] believing that dynamic strain ageing, which occurs simultaneously with the fatigue test, plays the major role. The works and ideas of the various workers are grouped together according to their preferred hypothesis, and will be discussed here under the appropriate headings of Dynamic Strain Age Hardening Group, Initial Dislocation Locking Group, and B.C.C. Intrinsic Mechanism Group.

4.2 DYNAMIC STRAIN AGE HARDENING GROUP

The first experiments performed to attempt to relate strain ageing to the fatigue limit were those of Levy and Sinclair[3] and Rally and Sinclair[2]. Assuming that strain ageing would occur as predicted by Cottrell's strain ageing theory, they[3] predicted that the fatigue limit of a mild steel would increase with temperature to a peak at about 230°C, the argument being that the fatigue limit is dependent on strain ageing, and strain ageing is a function of temperature (diffusion rate). Their experimental results on SAE 1018 steel largely bore out their prediction. However, since they did not publish the carbon and nitrogen analyses for their heat-treated specimens, the strain ageing ability of the steels was not known. Thus, although the effect of strain ageing was apparent on the fatigue limit, the cause was not proved directly.

Rally and Sinclair assumed that the knee of a S-N curve for steel was caused by strain ageing. In other words, an elimination of strain ageing by complete removal of carbon and nitrogen as interstitials should give a smooth S-N curve. Thus the above hypothesis predicted that a reduction in carbon and nitrogen content would shift the knee to a longer life. Rally and Sinclair suggested that the major effect of reducing carbon and nitrogen was to increase the mean distance over which the interstitials must diffuse to achieve effective pinning of dislocations. The net effect predicted was a longer life at the knee because of the longer time needed to diffuse the extra distance. The results of Rally and Sinclair[2] on this agreed with their prediction and they also found that increasing the temperature up to about 225°C shifted the knee to the left. However, their results on the finite life portions of the S-N curves for helium-treated steel tested in fatigue at various temperatures, showed a maximum life at room temperature, in apparent contradiction to the results of Levy and Sinclair[3].

Lipsitt and Horne[101] compared the S-N curve for specimens of SAE 1008

steel in the as-received and as-decarburised states. Their results showed a marked decrease of the fatigue limit (stress) of 69 MN/m^2 (10,000 psi) when the carbon and nitrogen levels were reduced to insignificant amounts (carbon from 0.09% to 0.003 - 0.005%, nitrogen to 0.00018%). There was a simultaneous shift of the knee of the S-N curve to the right from 2.5×10^6 to 10^7 cycles. The results indicated that since reducing strain ageing lowered the fatigue limit and shifted the knee to the right, complete elimination of strain ageing might shift the knee to such a long life that the S-N curve became essentially smooth, i.e., the fatigue limit being eliminated. Lipsitt and Horne[101] gave an explanation of the S-N curve with a knee by assuming the effects of strain ageing. Starting from a smooth curve for pure iron, it was suggested that the curve would shift to the right with the addition of a small amount of carbon (or nitrogen). This shift was due to strengthening by solid solution and a precipitation effect if there was excess carbon. In addition, carbon (or nitrogen) gave rise to strain ageing so that there was a further shift of the curve to the right. Since strain ageing, unlike fatigue damage, was not expected to be a function of stress if the carbon (or nitrogen) content, temperature and speed of testing were kept constant, there would be some limiting stress at which the damage and strain ageing hardening occurred at the same pace. This limiting stress thus defined the fatigue limit of the steel.

Lipsitt and Horne[101] concluded that partial removal of carbon and nitrogen from an SAE 1008 steel would lower the fatigue limit and reduce the life of the steel at a given stress above its fatigue limit, while complete removal of these interstitials would suppress the fatigue limit. Their conclusion, however, seemed unjustified because there was a marked difference in grain size between the as-received and as-decarburised specimens (grain size of ASTM No.3-5 and ASTM No.7-9 respectively), so that a substantial reduction in the fatigue limit (stress) was, in fact, caused by variation in

grain size. Also their conclusion on the effect of interstitial content on the fatigue life of the steel was contradicted by their experimental results. (Their results showed that reducing the carbon and nitrogen contents actually shifted the knee of the S-N curve to the right, i.e., the life of the same steel at a given stress was increased). Lipsitt and Horne[101] also did some rotating-bending fatigue tests on the as-decarburised steel and found the fatigue limit of the rotating-bending test was lower than that of the direct stress tests. This suggests that their bars were case-decarburised so that the surface was considerably softer than the core and this non-homogeneity had a greater effect on the rotating-bending tests. The fact that a knee was still present in the S-N curve of the as-decarburised steel, which contained insufficient carbon and nitrogen (~0.004% and 0.00018% respectively) for ageing at room temperature also casts doubts on the role played by strain ageing in causing a fatigue limit in steel.

A completely different approach was taken by Levy and Kanitkar[102] to investigate the effect of dynamic strain ageing on the fatigue properties of mild steel. They proposed that if the fatigue limit was due to dynamic strain ageing, and if this property was eliminated before fatigue testing, the resultant S-N curve should be smooth and without the knee. The explanation proposed by Levy[103] to show how the knee could be formed as a direct result of strain age hardening is depicted in Figure 4.1. It was postulated that the fatigue curve for the material, were it by some means prevented from strain ageing during the test, would be the smooth curve A - A' shown in Figure 4.1. If, on the other hand, the material was fully strain aged before the commencement of the test, the resultant fatigue curve would be represented by another smooth curve X - X'. Both curves are smooth or continuous because no strain ageing is allowed to occur during the test.

However, since plastic straining is known to occur during fatigue tests, even at stresses below the fatigue limit in low carbon steels, and since

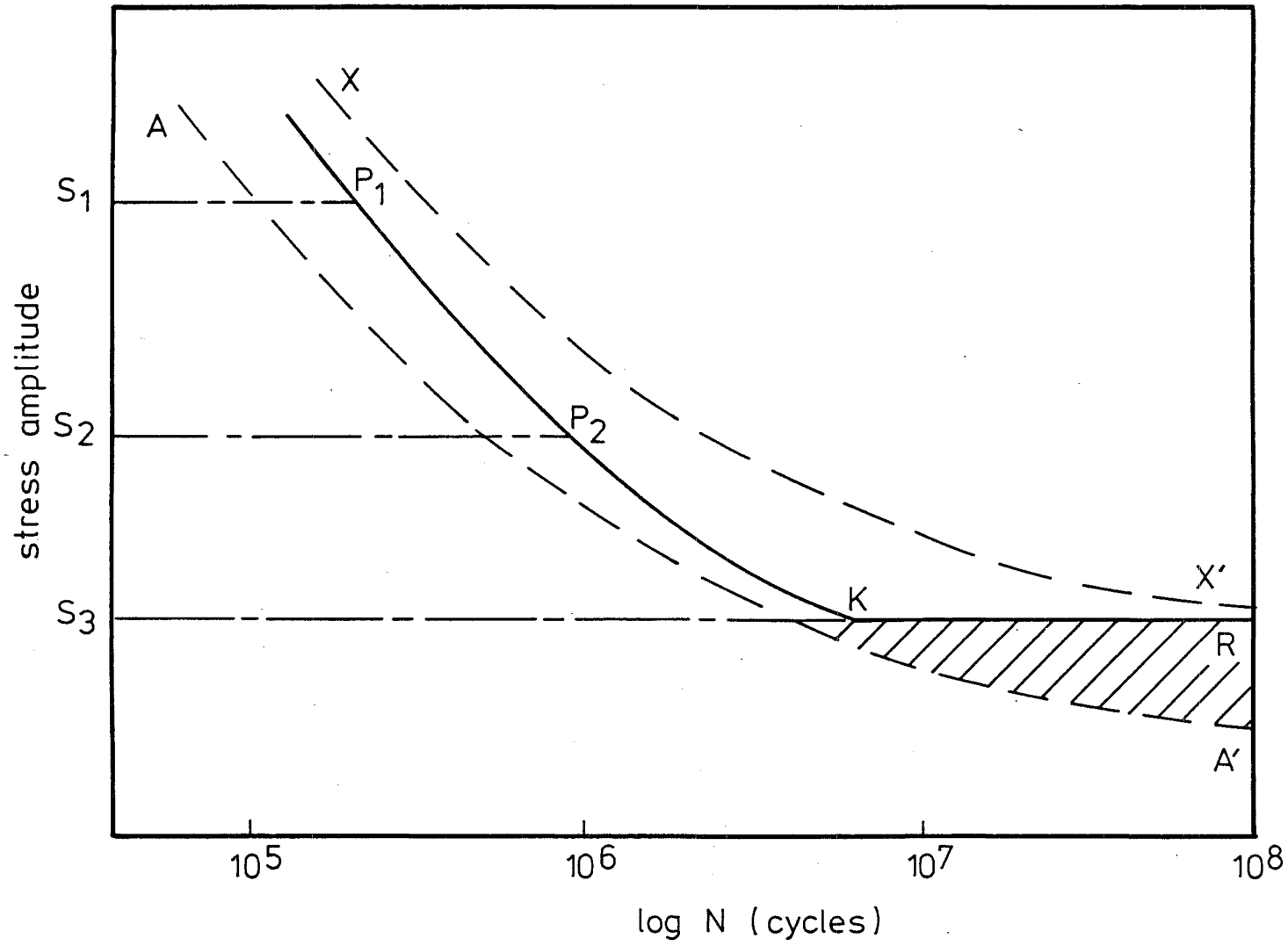

FIG. 4·1 EFFECT OF STRAIN AGEING OCCURRING DURING FATIGUE TEST. (Ref 103)

steels with dissolved interstitial solute age spontaneously after plastic straining, it was argued that there would be a consequent increase in fatigue strength during the test. In Figure 4.1, the actual fatigue curve therefore falls somewhere between the curves A - A' and X - X', say along P_1P_2 at stresses S_1 and S_2. However, at a lower stress, S_3, the conditions of stress, time and temperature are such that sufficient strain ageing takes place to convert the material to that represented by the curve X - X' before the specimen can fracture at K. If S_3K does not now intersect X - X', fracture cannot occur, and the observed fatigue curve will have the form P_1P_2 K R with a knee at K.

Levy and Kanitkar[102] sought to exhaust the strain ageing ability of their steel by prior 'coaxing' from a stress level below the original fatigue limit. ('Coaxing' is a form of progressive 'understressing' whereby a specimen is given a large number of cycles ($>2 \times 10^7$) at a stress level below the fatigue limit and the stress is then raised to a slightly higher value. A further 20 million cycles are then applied and the stress raised again. This process is stopped when either the specimen fails or when the chosen stress level has been attained without failure.) The specimens that survived the 'coaxing' treatment were then tested at different higher stress levels to give a new S-N curve. Levy and Kanitkar[102] found that the S-N curve of the coaxed material was smooth with continual failures up to 100 million cycles. They also found that for any given stress, the coaxed material had a longer life than the original material, i.e., the S-N curve was raised by coaxing.

The effect of artificial strain ageing was also studied. Here the specimens were not given the full 2×10^7 cycles at each stress level, but were coaxed to only 2 - 10 million cycles and then they were artificially aged at 100°C for one hour. The result of this was that all the specimens failed at stresses below the fatigue limit of the coaxed material. It was therefore concluded that, as far as the coaxing effect was concerned, part of the cycle

increment could not be replaced by static strain ageing.

The results of Levy and Kanitkar must be treated with caution because their conclusions were based on data from only twelve coaxed specimens. Moreover, four of the twelve did not survive the coaxing treatment, so that the S-N curve of the coaxed material was obtained from only eight specimens. The significance of the premature failures was not considered by the authors and only favourable results were discussed. They concluded that the S-N curve of the coaxed material was a smooth one without a knee because one long-life failure was observed, at 1.6×10^7 cycles. The wide scatter of fatigue test results especially at stresses near to the fatigue limit, is well known, and Yoshikawa and Sugeno[7] obtained S-N curves of steels with knees present showing failures up to 10^8 cycles, so the conclusion of Levy and Kanitkar[102] on a smooth S-N curve here must be considered doubtful.

The importance of strain hardening of steel during fatigue cycling was neglected by Levy and Kanitkar[102]. In their coaxing treatment, specimens were taken from 214 MN/m^2, (31,000 lb/in^2) to 262 Mn/m^2 (38,000 lb/in^2). The fatigue limit of the as-received material was about 235 MN/m^2 (34,000 lb/in^2) so that a large part of the coaxing run was done at stresses above the original fatigue limit. Cyclic stressing above the fatigue limit has been shown to work harden the material[8] and the degree of work hardening increases with increasing coaxing stress. Thus the eight surviving coaxed specimens were heavily cold worked and they, not surprisingly, showed improved fatigue endurance. Specimens that were partially coaxed (2 - 10 million cycles instead of 20 million cycles) and then artificially aged, showed inferior fatigue strength to the fully coaxed ones. This was possibly due to the ineffectiveness of dynamic strain age hardening compared to strain hardening.

The results of Oates and Wilson[6] on coarse grained steel (90 grains/mm^2) showed that strain ageing had a significant effect on its fatigue performance.

Pre-straining the annealed steel to 4½% was found to improve the fatigue limit/tensile strength ratio. Since pre-straining increased the number of mobile dislocations and hence ageing potential of the steel, the improved performance was attributed to the effect of strain age hardening. Oates and Wilson[6] also found that testing at -60°C, which was expected to reduce the strengthening effects of ordinary solute strain ageing to an insignificant level, yielded a smooth S-N curve with no apparent knee up to 2×10^7 cycles. Specimens quenched from 600°C to increase the ageing potential were found to have a markedly improved fatigue limit. However, specimens quenched and then artificially aged, were found to show an equal improvement.

It was also found that the yield point of the coarse-grained specimens could be eliminated by fatigue cycling at stresses below the fatigue limit. Metallographic examinations revealed widespread plastic deformation with groups of grains showing fatigue striation markings. Because of the ease of plastic yielding, Oates and Wilson[6] concluded that for a coarse grained steel, the emergence of a definite fatigue limit probably depended on the relocking of dislocations by strain ageing during fatigue. Their results on pre-strained and quenched specimens appeared to support this suggestion.

Yoshikawa and Sugeno[7] found that the S-N curve of a coarse grained steel (25 grains/mm^2) could be raised to a higher stress level by increasing the interstitial content. That is, increasing the ageing potential of the coarse grained steel apparently caused a corresponding increase in fatigue strength. Yoshikawa and Sugeno[7], in agreement with Oates and Wilson[6], found that testing at -67°C raised the S-N curve of a coarse-grained steel to higher stress. Since strain ageing is not expected to occur at -67°C, one would expect the fatigue limit of the steel to be lower at -67°C than at room temperature. Therefore, either strain ageing was not responsible for the presence of a fatigue limit, or the reduction in fatigue limit at -67°C due to lack of strain ageing, was off-set by the increase in strength of the material at a lower temperature[104]. It has been shown that increasing the yield stress of a material tends to increase its fatigue strength[6]. The

effects of strain age hardening or the lack of it, at low temperature, therefore, has not been conclusively established.

4.3 INITIAL DISLOCATION LOCKING GROUP

The data of Oates and Wilson[6] on fine grained low carbon steel (2500 grains/mm^2) indicated that strain age hardening was absent during fatigue testing. Specimens tested at -60°C still exhibited a definite fatigue limit and since strain ageing was not expected to occur at -60°C, the presence of a fatigue limit could not be attributed to strain ageing. The yield points of this steel could not be removed by fatigue cycling at stress levels below the fatigue limit, and Oates and Wilson[6] observed only isolated grains showing striation markings, i.e., there were no visible signs to indicate a spread of plastic deformation across grain boundaries. However, when the stress was above the fatigue limit, widespread yielding was observed, and Oates and Wilson[6] concluded that in this case, (i.e., fine grained steel), the important factor that governed the spread of plastic deformation and the fatigue limit was the initial dislocation locking.

Kettunen[100] found a systematic variation in the fatigue limit behaviour of Armco iron (0.027% C) as a function of the amount of pre-strain and ageing prior to fatigue. When slowly cooled in a step-wise manner from 700°C, the steel showed no definite fatigue limit. But if the steel was quenched from 700°C, a sharp fatigue limit was produced on the S-N curve. Pre-straining and ageing both groups produced a change in the S-N curves. For the slow-cooled specimens, a fatigue limit was introduced while for the quenched ones, the S-N curve was raised to higher stress, the increase being dependent on the amount of pre-strain.

Kettunen[100] suggested that the absence of a fatigue limit in the slowly cooled specimens was due to weak locking. During slow cooling, most of the carbon and nitrogen precipitated out into coarse carbo-nitride precipitates, which left the matrix relatively free of interstitials. Thus Cottrell

locking was minimal and since the potential trough of a Cottrell atmosphere is narrow, dislocations could easily escape. These dislocations would glide and multiply due to the alternating stress and when they were blocked and locked by precipitates, those following would change planes and continue to glide. However, with the reversal stress, these dislocations were not returned to the sources. Since most dislocations could move to and fro according to the alternating stress, and also bypass any obstacles, the slowly cooled material behaved in the same way as a pure metal and did not show a fatigue limit. In contrast, the water quenched specimens had a greater abundance of fine and well dispersed precipitates which effectively blocked and locked any mobile dislocations. To allow continuous deformation to take place, the stress had to be sufficiently high to release the dislocations from these precipitates and Snoek atmospheres. Hence the water quenched specimen had a sharp fatigue limit.

The observation that pre-straining and ageing introduced a fatigue limit to the slowly cooled specimens led Kettunen[100] to conclude that strain ageing before, and not during, fatigue was responsible for the fatigue limit, since the dynamic strain ageing theory could not explain why a material behaved differently before and after pre-strain ageing. It is not clear how this condition differs in kind from the concept of initial dislocation locking as proposed by Oates and Wilson[6] for fine grained steels. Yet Kettunen's results appeared to agree more with the coarse grained steels of Oates and Wilson. Indeed, Kettunen used a fairly coarse grained structure, (200 grains/mm^2 compared to 90 grains/mm^2 for coarse grained and 2500 grains/mm^2 for fine grained steels of Oates and Wilson). Pre-straining and ageing was found to improve the fatigue limit of Kettunen's water quenched specimen and Oates and Wilson found this to be true for only coarse grained material. Nevertheless, Kettunen's suggestion was similar to the initial dislocation locking concept in that both were not dependent on a dynamic strain ageing process during testing.

Yoshikawa and Sugeno[7] suggested that for fine grained steels, interstitial impurities strongly segregated at boundaries and the hindering of slip by grain boundaries was thus enhanced. This idea is again similar to that of Oates and Wilson[6] in the sense that both considered the fatigue limit to be the critical stress which determined whether plastic deformation was developed beyond grain boundaries or not. While Oates and Wilson[6] believed that the spread of plasticity was governed by the strength of initial dislocation lockings, Yoshikawa and Sugeno[7] considered the grain boundary effect to be the important factor.

4.4 BODY CENTRE CUBIC (B.C.C.) INTRINSIC MECHANISM GROUP

The best way to examine the effects of strain ageing on the fatigue limit of steels is to compare the results of tests using ageing and non-ageing steels. The difficulty involved in rendering steel non-ageing is that often side effects are introduced so that the properties of the steel are also modified, making comparison of results difficult. Nevertheless, such an exercise should still provide some qualitative evidence of the significance of strain ageing during fatigue.

Ferro and Montalenti[4] using Armco iron provided results that showed strain ageing was not the contributing factor for the presence of a sharp fatigue limit. They purified their samples so that there was less than 0.001% carbon and 0.0001% nitrogen. This very low level of interstitial content, particularly of nitrogen, ensured that ageing could not take place at any time. Yet a knee was formed on the S-N curve of the purified iron at about 10^6 cycles with both polycrystalline specimens and single crystals (d = 5 mm). They also found that the fatigue limit of Armco iron increased with the strength of the material provided the strengthening was achieved by precipitation of carbides or nitrides. However, if the hardening was obtained by dislocation locking, such as in quenched and strain aged specimens containing carbon, the fatigue curve became smooth with no apparent knee before 10^7 cycles, and the fatigue endurance was only slightly

increased. In this case, it was observed that softening occurred during fatigue, unlike the hardening obtained in annealed specimens. Ferro and Montalenti[4] hence suggested that dislocation locking due to interstitials was not stable under repeated stress, and dislocations were continually being "torn away" from their pinned positions. De Fouquet[105], in fact, directly showed by internal friction methods, that the free carbon content increased during fatigue, at least up to a certain number of cycles. Ferro and Montalenti concluded that ageing in the sense of progressive anchoring of dislocations by interstitial atoms, was unlikely to be the cause of the sharp fatigue limit.

It is interesting to note that Kettunen[100] and Ferro and Montalenti[4] obtained different results on quenched and strain aged specimens. Kettunen[100] found a fatigue limit at about 2×10^6 cycles, but Ferro and Montalenti[4] obtained a smooth curve up to 10^7 cycles. In tensile tests, the decarburised specimens of Ferro and Montalenti[4] still showed some traces of a yield point. This suggests that the interstitial level was still not sufficiently low to completely remove the yield point. Thus, whether this purified steel which still possessed a fatigue limit underwent strain ageing during the test, is open to question.

Bergström *et al*[5] stabilised their α-iron by adding titanium to form stable carbo-nitride precipitates. This stabilised material (0.009% carbon and 0.006% nitrogen with 0.3% titanium) was found to be non-ageing, and fatigue testing of this material indicated that a sharp knee was still present in the fatigue curve. Bergström *et al*[5] also found that the dislocation structures of specimens fatigued at stresses above and below the fatigue limit, were different. At stress amplitudes below the fatigue limit, rows of loops and elongated dislocation tangles were observed, whereas when the stress amplitudes were above the fatigue limit, dense dislocation clusters developed.

These observations agreed with those obtained by Wood *et al*[38] who reported different microstructural changes for Armco iron and a high purity iron, depending whether testing was above or below the fatigue limit. A cell structure was formed at stresses above the fatigue limit and a dispersed fine slip below the fatigue limit, with no transition structure of broad slip bands as found for f.c.c. metals. Since iron, unlike f.c.c. metals, apparently did not have to pass through this transition range into what they described as a pseudo-safe range of dispersed slip, they suggested that this was the reason for the basic difference between fatigue curves of b.c.c. and f.c.c. metals. They further suggested that the pseudo-safe range was an inherent property of a b.c.c. lattice.

Finally, Bishop *et al*[106] tested titanium alloys RC 130 - B and Ti 150 - A. These alloys which exhibited fatigue limit at room temperature, were found to retain well-defined knees in their S-N curves even when tested at -78°C and -196°C. Since strain ageing was not expected to occur at such low temperatures, they concluded that strain ageing was not the cause of the fatigue limits in these alloys.

4.5 SUMMARY

The evidence is strong and convincing that dynamic strain ageing plays a dominant role in positioning the knee of a S-N curve; it is less convincing as a mechanism responsible for the existence of the fatigue limit. Some of the conclusions made by previous workers were drawn from too few experimental data points, and often efforts to remove strain ageing or to induce complete ageing prior to fatigue testing caused a change in the material properties. The changes were often neglected. Levy's[102] method of coaxing his specimens to achieve complete ageing providing a good example. While the fatigue endurance of coaxed specimens was improved, the contribution of strain hardening was not considered.

Oates and Wilson[6] and Yoshikawa and Sugeno[7] obtained different results for fine and coarse grained steels and hence concluded that the controlling factor for the appearance of the sharp fatigue limit was not strain ageing during fatigue but grain size. Oates and Wilson[6] based their argument on the observations that fatigue cycling at a stress just below the fatigue limit caused widespread plastic deformation in a coarse grained steel, but not in a fine grained steel. However, this result is not unexpected if one considers the fact that for a coarse grained steel, the fatigue limit stress is higher than the static yield stress and the reverse is true for a fine grained steel. Therefore, fatigue cycling a fine grained steel at a stress below the fatigue limit and well below the static yield stress, cannot cause yielding to spread across the grain boundary according to the Hall-Petch yielding model. However, for a coarse grained steel, fatigue cycling at a stress below the fatigue limit may still be able to spread plastic deformation if the stress is higher than the static yield stress.

Yoshikawa and Sugeno[7] found that the sharpness of the knee was apparently dependent on the grain size. They considered that the sharp knee for a fine grained steel was a result of segregation of interstitial impurities at the grain boundaries. This segregation made grain boundaries effective barriers to the propagation of slip. Thus a coarse grained steel with less total grain boundary area was less effective in inhibiting the spread of plastic deformation and consequently had a lower fatigue limit and a less well defined knee.

Both groups of workers[6,7] pointed out that the important factor governing fatigue failure was the spread of plasticity across grain boundaries during fatigue testing. Thus the fatigue mechanism could be explained in terms of grain size rather than strain ageing. The spread of plasticity across grain boundaries during fatigue should be similar to that which occurs during unidirectional straining. Therefore, the Hall-

Petch theory of yielding relating the lower yield stress to the grain size should also apply here. However, as shown by experiments[8], there is virtually no correlation between the yield stress and fatigue limit for a range of grain sizes. The suggestions of Oates and Wilson of two different mechanisms for fine and coarse grained steels, cannot explain why the fatigue limit has a linear relationship with $d^{-\frac{1}{2}}$ (d is the grain diameter). Moreover, there is not a dividing line to separate the 'fine' grains from the 'coarse' grains.

Kettunen's[100] suggestion followed much the same line as the proposal of Oates and Wilson for fine grained steels. However, his work contained some inconsistencies. While he supported strain ageing before fatigue as the fatigue limit mechanism, he also reported that Armco iron heat-treated to have carbon in solution (thus with a propensity for strain ageing) had a knee position at a shorter life than specimens heat treated to have low amounts of carbon in solution. Also, his suggesttion of pre-strain ageing is ambiguous since fatigue limits of steels are usually obtained in the as-treated condition with no pre-strain ageing.

Ferro and Montalenti[4], Bishop *et al*[106], and Bergström *et al*[5], provided some good evidence that strain ageing was not solely responsible for the existence of fatigue limits. Ferro and Montalenti purified their steel by removing carbon and nitrogen, Bishop *et al* performed experiments at very low temperatures where ageing was not possible, and Bergström *et al* tied down the active interstitials by adding a strong carbo-nitride former, titanium, and in all cases, definite fatigue limits were still present.

As mentioned earlier, in order to produce suitable materials to study the effects of strain ageing, often other side effects are introduced during specimen preparation. This, together with the vast statistic scatter inherent in fatigue failures, makes the end results even more scattered so that the many experiments performed could not yield a single accurate

account of the fatigue process. The best conclusion that can be drawn from previous work is that there is no one mechanism responsible for the entire fatigue behaviour of ferritic materials. Two important factors however, emerged from the work so far, viz., dynamic strain ageing and grain size effects. Individually, these two factors have been shown to have significant influence on the fatigue behaviour of steel. It is the object of this project to study their combined effects on the fatigue of low carbon steel so that a better understanding of the fatigue limit mechanism can be achieved.

The proposition[103] that the fatigue limit is a consequence of the competitive process between strengthening and damage provides the basis for this research. However, the author does not agree with Levy[103] that the strengthening mechanism during fatigue is solely strain age hardening. It is felt that the strengthening is a combined effect of strain age hardening and cyclic strain hardening.

Published results[6,7] have shown that there appears to be some differences between the fatigue process in fine and coarse grained steels. This may be explained if it can be shown that the individual contribution of the two forms of hardening are functions of grain size. As mentioned in Section 3.1, it is difficult to isolate these two forms of hardening. However, the contribution of strain age hardening can be indirectly assessed by comparing the fatigue performances of two steels of identical chemical composition and grain size, but of different ageing propensities. Furthermore, if one of the two steels is a non-ageing steel, then by using its fatigue performance as a reference, it may be able to deduce the strain hardening effect by measuring some property changes associated with fatigue.

Properties which are known to change during fatigue include damping, temperature, microstructure and dislocation structure. It should be noted that these property changes all basically emanate from one single effect, the

behaviour of dislocations during fatigue. Thus, studying these properties and the resultant dislocation structure associated with their changes may provide an explanation to the fatigue process.

CHAPTER FIVE

DYNAMIC YIELDING

5.1 INTRODUCTION

Under the application of a sufficiently high stress, some dislocations in a material will move. The effects of such dislocation movements include dislocation generation, annihilation, pile-up against obstacles, cross-slip, etc., and the extent to which each of these occurs is dependent on factors such as the stress level, the mode of stress, temperature, grain size, and others.

Again, because of the mode of stressing, it is easier to study the dislocation behaviour in a static test than in a fatigue test. The first major effect of static loading is to cause yielding. Yielding is usually defined as the beginning of macro-plastic deformation, but it is more exact to define yielding as the instant dislocation movement starts. (This latter case is usually termed micro-yielding.) Therefore, for any strain to be imparted, it is first necessary to have mobile dislocations in the matrix. The creation of mobile dislocations by the unlocking process has been discussed in Chapter Two. Another model[54] of yielding, a dynamical model which considers dislocations being heterogeneously nucleated, will be discussed in the following section. This model, together with observations on micro-yielding[107], provide an explanation for the dependence of yielding and hardening on grain size in static tests. Even though the actual hardening mechanisms may be different between tensile and fatigue testing, the similarity between the dislocation structures produced[42] suggests that some sort of parallel exists. Hence, the dependence on grain size of yielding and hardening in tension may also apply in the case of fatigue.

5.2 YIELDING UNDER STATIC LOADING - A DYNAMIC MODEL

The concept of dislocation locking by interstitial impurities and

precipitates developed by Cottrell is well established[48]. For the case of iron and related b.c.c. metals, the dependence of the yield drop and discontinuous yielding on interstitial impurities[108], the kinetics of strain ageing[49], and direct observation by transmission electron microscopy of particles formed on dislocations[109] provide a consistent body of evidence supporting this concept.

The explanation of the abrupt yield drop[48], the Luders strain, the Luders Band velocity[110] and the delay time phenomenon[111] in terms of unlocking of dislocations are, however, not satisfactory. For example, the temperature[112], strain rate[113,114] and grain size[115] dependence of the upper and lower yield stress and of subsequent flow stress values are very similar. Yet the flow stress cannot be governed by the unlocking mechanism at ambient and low temperatures where the pinning points are essentially stationary. The grain size dependence of unlocking presents other difficulties. While the observed $d^{-\frac{1}{2}}$ dependence of the lower yield stress (2d is the grain diameter) is in accord with the unlocking theory[55,116], it frequently is not influenced by the test temperature in the manner expected[112,117]. Moreover, f.c.c.metals which do not show discontinuous yielding also display this dependence of flow stress in grain size[118]. Finally, the Hall-Petch equation relating the yield stress and $d^{-\frac{1}{2}}$ requires dislocation pile-ups at grain boundaries and so cannot account for the presence of yield points in single crystals[119].

For the above reasons, a different approach to yielding was developed by Johnston and Gilman[120]. They studied the effects of stress, temperature, radiation damage, impurities and crystal strength on the dislocation velocities in LiF single crystals, and found that a minimum stress, lower than the lower yield stress of LiF, was required to cause dislocation movements in these crystals. The dislocation velocity was found to be extremely sensitive to the applied stress, but the flow stress

was relatively insensitive to any dislocation velocity changes. The strain rate sensitivity of the flow stress was also very slight. This means that if the strain rate was increased tenfold, the dislocations would move ten times as fast but this could be accomplished by only a few per cent increase in the flow stress.

Gilman[121] found that mobile dislocations in LiF were heterogeneously nucleated and were not created by unlocking. He also observed that to produce large macroscopic strains, large numbers of dislocations had to be in motion. The rate of dislocation multiplication was found to be sensitive to the applied stress, and the dislocation density was shown to vary linearly with plastic strain.

Using this experimental information on dislocation velocity and density, Johnston and Gilman[120] produced a mathematical model to describe the deformation curve. The model appeared to be well founded, particularly in the region just prior to and just after yielding. At small strains the linear relationship between strain and dislocation density did not hold, hence the model did not match the experimental curve exactly. Also, the model did not consider strain hardening so that a departure from the actual curve at large strains was observed.

Following Johnston and Gilman's model closely, Hahn[54] developed a similar model to account for the yield characteristics of iron and other b.c.c. metals.

5.2.1 Hahn's Model

It was noted that the strain rate imposed by the machine during tensile or compressive test $\dot{\varepsilon}_M$ had to be matched by the total strain rate of the specimen, $\dot{\varepsilon}_S$.

$$\dot{\varepsilon}_M = \dot{\varepsilon}_S = \dot{\varepsilon}_e + \dot{\varepsilon}_p \qquad \text{Equation (5.1)}$$

where $\dot{\varepsilon}_e$ = elastic strain rate

$\dot{\varepsilon}_p$ = plastic strain rate.

From the definition of Young's modulus, E,

$$E = \frac{\sigma}{\varepsilon_e}$$

$$\therefore \quad \dot{\varepsilon}_e = \frac{1}{E} \cdot \frac{d\sigma}{dt} \qquad \text{Equation (5.2)}$$

(This is assuming total rigidity.)

For single isotropic crystals,

$$\dot{\varepsilon}_p = \phi b L v \qquad \text{Equation (5.3)}$$

where ϕ is the orientation factor, b the Burger's vector, v is the dislocation velocity, and L the total length of dislocation line in motion per unit volume.

0.5 is the value assigned to ϕ and 0.5ϕ represents the contribution of a single dislocation of unit length and unit velocity moving in a direction close the the maximum resolved shear stress.

Combining Equations (5.1), (5.2), and (5.3),

$$\dot{\varepsilon}_M = \frac{1}{E} \cdot \frac{d\sigma}{dt} + \phi b L v \qquad \text{Equation (5.4)}$$

Dislocation Multiplication

As a first approximation, the quantity L is assumed to be a fixed fraction f, of the dislocation density ρ[120].

$$L = f\rho \qquad \text{Equation (5.5)}$$

where $f \approx 0.1$. Etching pitting[120] and studies involving transmission electron microscopy[122] show that dislocation multiplication on straining in the range $10^{-3} < \varepsilon_p < 10^{-1}$ can be described by a parabolic equation of the form

$$\rho = C\, \varepsilon_p^{F} \qquad \text{Equation (5.6)}$$

where C and F are parameters obtained by direct measurements of densities.

Generally, F lies between 0.7 and 1.5 while C varies between 10^9 to 2000 x 10^9 cm/cm^2 per unit strain for steel.

In order to extend the description to the small strains, the extrapolation

$$\rho = \rho_o + C \varepsilon_p^F \qquad \text{Equation (5.7)}$$

is assumed valid to a first approximation. In the absence of dislocation locking $\rho = \rho_o$ ($\varepsilon_p = 0$) represents the grown-in dislocation density, normally about 10^6 - 10^8 lines/cm^2 in annealed f.c.c. metals. When dislocations are locked, ρ_o is regarded as an average density of unlocked dislocations - those dislocations nucleated heterogeneously at inclusions or other discontinuities below the nominal stress level associated with significant dislocation mobility. Above this stress level the multiplication process, presumably, governs the increase in density.

Dislocation Velocity

Stein and Low[123] found a relationship between the stress and dislocation velocity of the form

$$v = \left(\frac{\tau}{\tau_o}\right)^n \qquad \text{Equation (5.8)}$$

where τ = resolved shear stress = $\frac{\sigma}{2}$

τ_o = resolved shear stress corresponding to unit velocity

n = dislocation mobility factor, temperature dependent

and $n \alpha \frac{1}{T}$

Gilman and Johnston[124] found that $\Delta\sigma$, the change in flow stress accompanying work hardening in LiF, closely approximates the stress increment needed to maintain a given velocity. The result, accepted conditionally as valid for metals, provides a means of introducing the effect of strain hardening, such as a simple linear hardening law:

$$\Delta\sigma = q\varepsilon_p \qquad \text{Equation (5.9)}$$

as follows:

$$v = (2\tau_o)^{-n} (\sigma - \Delta\sigma)^n$$

$$= (2\tau_o)^{-n} (\sigma - q\varepsilon_p)^n \qquad \text{Equation (5.10)}$$

where q, about 30-40 x 10^8 N/m^2 for mild steel, is the macroscopic work hardening coefficient and σ the tensile stress corresponding to τ.

Equation (5.10) is regarded as a general functional relationship and together with appropriate values of τ_o, n and q, is used to describe dislocation velocity in b.c.c. metals.

Combining Equations (5.4), (5.5), (5.7), (5.9) and (5.10),

$$\dot{\varepsilon}_M = \frac{1}{E} \cdot \frac{d\sigma}{dt} + \phi bf \left(\frac{\sigma - q\varepsilon_p}{2\tau_o}\right)^n (\rho_o + C\,\varepsilon_p^F) \qquad \text{Equation (5.11)}$$

When deformation proceeds at constant stress, the elastic contribution is approximately zero.

$$\therefore \quad \dot{\varepsilon}_M = \dot{\varepsilon}_p = \phi bf \left(\frac{\sigma - q\varepsilon_p}{2\tau_o}\right)^n (\rho_o + C\,\varepsilon_p^F) \qquad \text{Equation (5.12)}$$

Rearranging gives

$$\sigma = q\,\varepsilon_p + 2\tau_o \left[\frac{\dot{\varepsilon}_M}{\phi bf(\rho_o + C\varepsilon_p^F)}\right]^{\frac{1}{n}} \qquad \text{Equation (5.13)}$$

This model flow curve gives an abrupt yield drop, the upper yield point being given by Equation (5.13) for $\varepsilon_p = 0$. The dependence of the yield drop on the dislocation density is well described by the model, increasing the initial dislocation density reduces the yield drop. The yield drop had always been explained in terms of unlocking - the sudden release of stationary locked dislocations at a critical stress. Hahn's model shows that a sizable yield drop could be accounted for without recourse to unlocking, the abrupt yield drop displayed by the model is a consequence of rapid multiplication and the stress dependence of dislocation velocity.

Hahn's model assumes total rigidity and does not take into consideration elastic yielding. Consequently, the model does not provide for pre-yield

micro-strain[125], and dislocation movements concurrent with loading in the elastic range and pre-yield dislocation multiplication (pre-yield means before macro-yielding).

Hahn's model may be modified in various ways by using different velocity-stress relationships and using different approximations to strain hardening.

An important omission from the model is the effect of grain size. Hutchison[126] measured the upper and lower yield stresses for steels of different grain sizes and found that the yield drop increases with decreasing grain size. According to his test results at room temperature, there would be no yield drop for coarse grained steels if $d^{-\frac{1}{2}} < \sim 3.0$ (d is the grain diameter in mm). For 3¼% Silicon-iron Suits and Chalmers[107] observed no yield drop for $d^{-\frac{1}{2}} = 2.43\ mm^{-\frac{1}{2}}$.

5.3 MICRO-YIELDING IN STATIC TESTS

In deriving the final relationship described in Equation (5.13), Hahn considered two important factors for his model: (1) at the upper yield point, rapid multiplication of dislocation occurs, and (2), the dislocation velocity is extremely sensitive to the applied stress. As mentioned earlier, Hahn assumed total rigidity so that no dislocation movement or multiplication was possible before the macroscopic yield point.

(In considering micro-plasticity, the terminology of Brown *et al*[127] is commonly used, see Figure 5.1. The elastic limit, σ_E, is the lowest stress determined by a load-unload method in tension or compression from which the stress-strain curve on unloading is not linear, but the hysteresis loop is closed, see Figure 5.1. σ_E therefore represents the lowest stress at which dislocation movement can be detected directly and it was suggested[127] that σ_E truly represents the friction stress of the material, since it is the stress level which must be exceeded before appreciable dislocation movement is possible. It was also suggested[127] that at σ_E only the most mobile part of the dislocation array is moved and most probably only the mobile edge

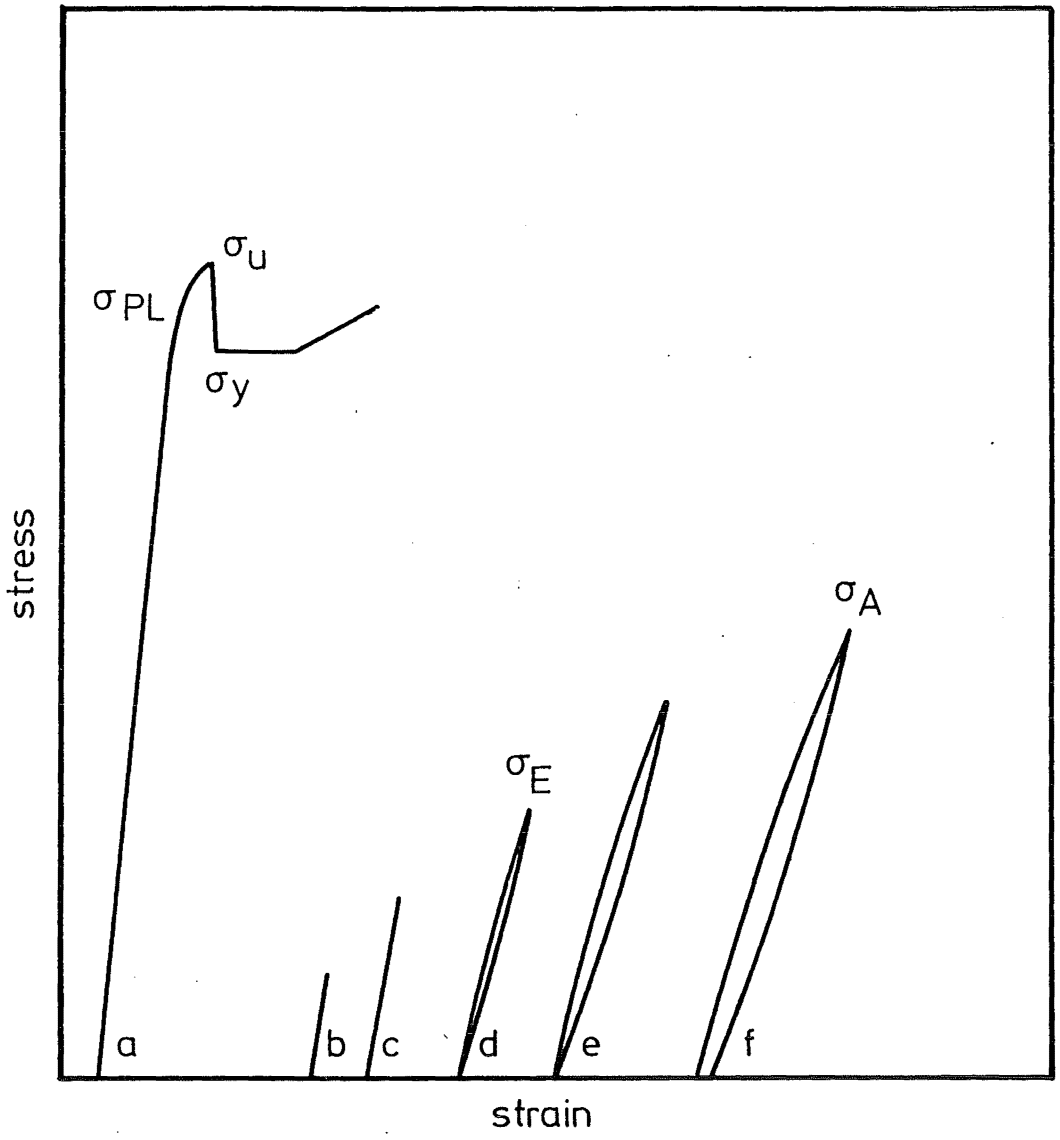

FIG 5·1 TYPE OF YIELD POINTS IN IRON
(Ref. 127)

dislocations are involved. The value of σ_E is, however, very much dependent on the sensitivity of the measuring instrument. In a series of loading and unloading tests with increasing stress amplitude, it is possible to determine a minimum stress for which loading and unloading results in an open hysteresis loop. This stress is called the anelastic limit, σ_A. Above σ_A, dislocations move irreversibly and the movement of screw components is believed to cause the observed permanent strain[129].

It has been proved experimentally that dislocations do move at stresses well below the macroscopic yield stress, i.e., micro-yielding occurs first. Brentnall and Rostoker[130] showed that for iron, slip activity was possible before the upper yield point was reached. By using etch pitting techniques and micro-yielding measurements, they found that yielding was a progressive process starting at stresses anywhere from 25 - 75% of the macroscopic yield stress. For nickel and Fe - 3% Si, the micro-yield stress was found to vary linearly with $d^{-\frac{1}{2}}$ (d is the grain size) while for pure iron, this stress was unaffected by the grain size. Similar observations were made by Suits and Chalmers[107]. The found that slip activity of 3¼% Silicon iron occurred at a stress below the yield point and the micro-yield stress was independent of grain size. Slip activity after initial micro-yielding was, however, very much a function of grain size. Suits and Chalmers[107] explained these observations for fine grained steel by suggesting that yielding starts in individual grains at a stress considerably below the macroscopic yield stress. As the stress is increased, more and more grains yield and this is followed by clusters of grains yielding at the fillet region of the specimen, indicating yield propagation. These clusters grow in size with increasing stress until the upper yield point is reached, at which stage a cluster has grown large enough to cover the entire specimen cross-section at the fillet. This forms the first Luders band front and the Luders band now propagates at the macroscopic lower yield stress of the material. The situation is slightly different for coarse grained material

where more than one cluster tend to grow in both the fillet region and in the bulk of the gauge length. Many of these clusters can grow quite large and the stress at which they coalesce and cover the entire specimen gauge length is the macroscopic yield stress of the material.

The results of Brentnall and Rostoker[130] and Suits and Chalmers[107] indicate that the micro-yielding which occurs initially (i.e., before the upper yield point is reached) is dependent on the grain size. Therefore, two specimens with the same initial mobile dislocation density but with different grain sizes, will have different dislocation densities after they have been loaded to a stress below the upper yield point. In other words, at their respective upper yield points, their dislocation densities would be quite different. Hahn's model only describes the flow stress starting from the upper yield point and he assumed a fixed dislocation density, ρ_o, without considering the grain size, hence his model is not affected by grain size. The process of micro-yielding therefore, has a significant influence on the upper and lower yield points and the subsequent flow curve. According to Suits and Chalmers[107] results, micro-yielding appears to be easier in coarse grained materials.

5.4 DYNAMIC YIELDING IN FATIGUE

In a similar manner to the micro-yielding observed in tensile loading, "dynamic yielding" of specimens has been observed in fatigue tests at stress amplitudes below the fatigue limit of the material. To distinguish from micro-yielding which occurs during unidirectional tensile loading, the term "dynamic yielding" is used here to mean pre-yielding at a stress below the fatigue limit under dynamic loading conditions.

There are various ways in which dynamic yielding may be detected during fatigue loading; for example, by strain amplitude monitoring[8], temperature measurement[6], damping measurement[131] or strain amplitude measurement under constant stress amplitude fatigue[132].

Eshelby[133] showed by a mathematical model that dislocation movement can cause mechanical damping in metals. Consider an edge dislocation in an otherwise perfect lattice structure. Surrounding the edge dislocation is a strain field. Suppose a dislocation at point A now moves to a new position, B. The strain at A decreases while the strain at B increases. Associated with these changes in stress and strain is a change in local temperature at points A and B. A thermal gradient is thus set up and heat flow is accompanied by the dissipation of mechanical energy. This is known as Zener's theory of thermoelastic damping[133].

A significant change in damping can therefore be produced when the effects of all the moving dislocations are summed. Thus, by measuring the damping changes of a material under fatigue loading, it is possible to detect large scale dislocation movements.

Lazan and Wu[131,134] studied the effects of fatigue stress on the damping capacity of mild steel. They measured the damping capacity indirectly using a rotating cantilever beam machine. The machine was designed on the principle that a rotating beam of symmetrical cross-section would not deflect exactly in the direction of the applied load, but would also have a lateral deflection. The amount of lateral deflection depends on the damping capacity of the beam.

Using SAE 1020 steel, Lazan and Wu measured the damping capacity of specimens subject to different fatigue stress amplitudes, see Figure 5.2(a). At stresses well below the fatigue limit, no change in damping was observed up to 10^7 cycles. For stresses just below the fatigue limit, a gradual increase in damping was observed with increasing number of cycles until a stabilised level was attained. At stresses above the fatigue limit, damping increased rapidly initially, but the increase became more gradual later until failure occurred. Replotting these results in a different way, Lazan and Wu obtained a diagram which was very similar to a S-N diagram, Figure 5.2(b).

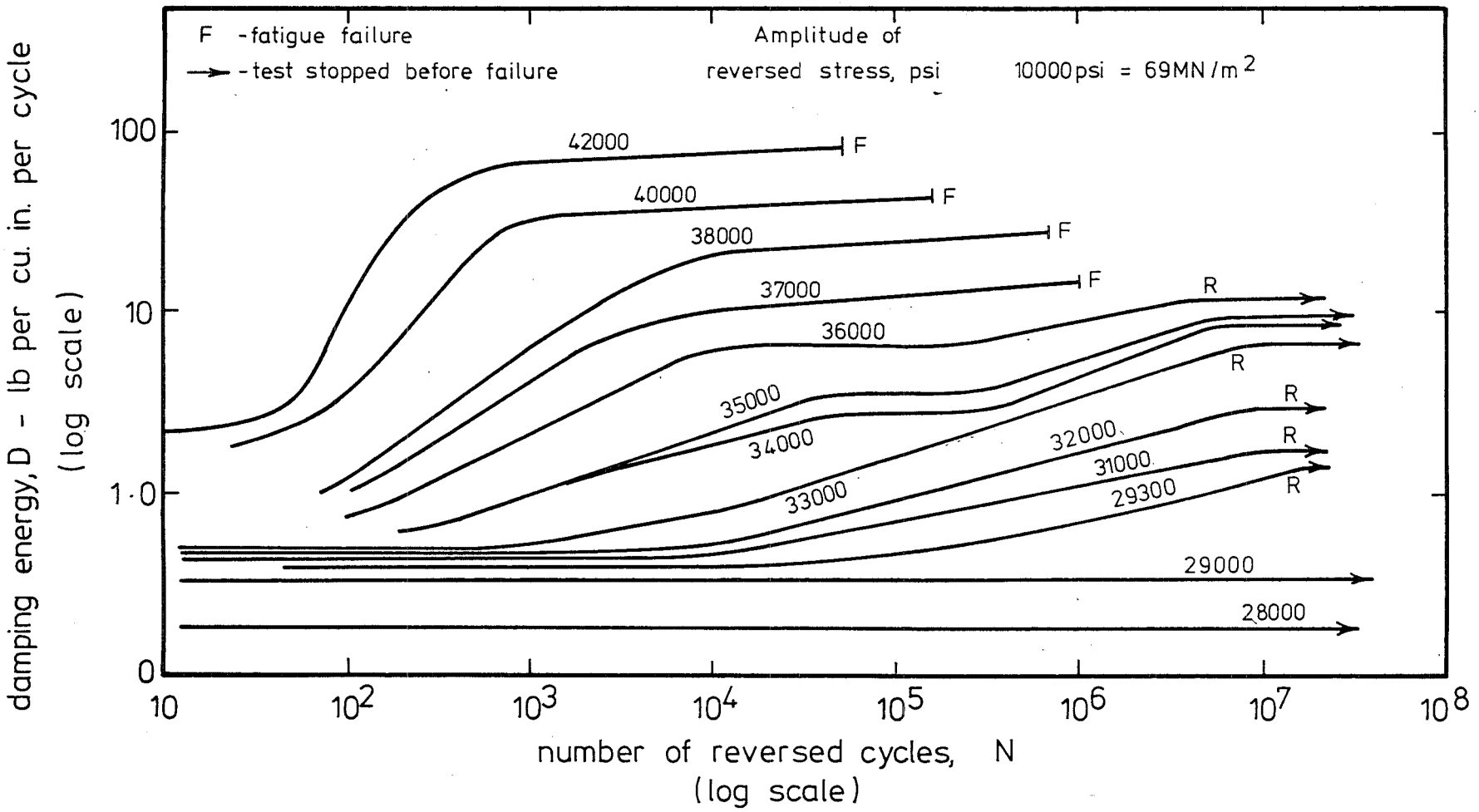

FIG 5·2 (a) VARIATION OF DAMPING ENERGY WITH STRESS AMPLITUDE (Ref. 134)

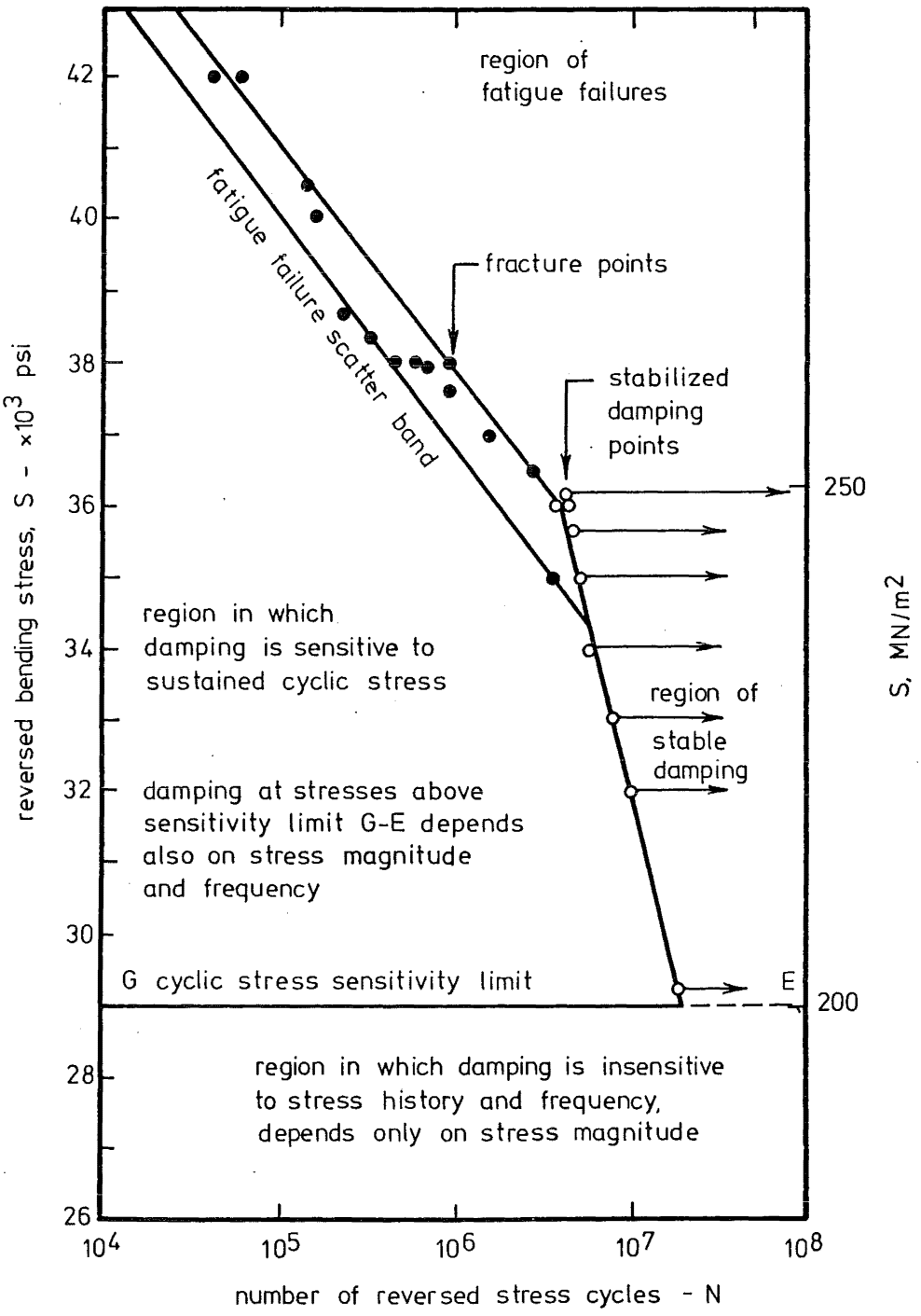

FIG. 5·2(b) S-N-N FATIGUE DIAGRAM EXTENDED TO INCLUDE STABILIZED DAMPING LINE FOR STRESS RELIEVED MILD STEEL. (Ref 134)

The diagram showed that the maximum stress amplitude for stabilised damping was very close to the fatigue stress-limit of the steel. Lazan and Wu[134] claimed that since the damping data had a smaller statistical scatter, the fatigue limit could be obtained this way with fewer specimens. However, the chemical composition of the steel, and more important, the amount of nitrogen in the steel was not given. Since ageing is known to affect the fatigue behaviour of steels, this is an important omission. According to their results from tests where specimens were rested, it would appear that the steel contained a considerable quantity of nitrogen, since resting the steel for 10^4 minutes caused a substantial drop in damping capacity. This drop in damping capacity could be attributed to strain age hardening.

A noteworthy result of Lazan and Wu's[134] experiment is that failures of specimens occurred at the peak of damping capacity. In other words, all their specimens either showed continuous softening (dislocation multiplication) until failure (at high stress) or softening until a stable state was attained without failure (at moderately high stress below the fatigue limit) or no softening at all (at low stress levels). It seems more logical that specimens would strain harden at some stage of cyclic loading and reduce damping capacity particularly when there was active nitrogen in the steel making strain ageing possible.

Other methods of monitoring micro-yielding in fatigue tests and results are summarised in a paper by Morrow[135]. These include measuring the cyclic stress amplitude[136] (or strain amplitude), internal friction[137], plastic strain energy and energy per cycle[132] under constant strain (or stress) cycling. It was noted that different transient behaviours exist under cyclic loading conditions and they are dependent on the material, its initial state, the magnitude and history of previous cyclic strain, and the test temperature. In the fully annealed state, polycrystalline copper hardens initially when fatigue cycled; if previously cold-worked, it softens, and if partially annealed, it shows an intermediate behaviour. Single crystals of copper

respond to cycling in a manner similar to that of fully annealed polycrystalline copper. However, the amount of transient hardening achieved can be increased by orientating the crystal to have more than one slip system under maximum stress. Snowden[138] reports that aluminium crystals hardened by previous cycling at a higher strain amplitude, cyclically soften at a low strain amplitude. This behaviour is similar to that demonstrated by cold-worked polycrystalline copper. It thus appears that for f.c.c. materials, the type of transient behaviour is not affected by the strain (or stress) amplitude or the method used to harden the material before cycling.

For mild steel, the dependence of transient behaviour on the stress amplitude is demonstrated by the results of Benham and Ford[132]. It was observed that mild steel cyclically hardens at high amplitude and softens at low amplitude. This is characteristic of a material with an initial yield point which disappears with cycling[132]. Benham and Ford also found that regardless of the control conditions, most of the fatigue life of steel is spent at essentially a constant stress, strain and plastic energy per cycle, i.e., the transient stage (softening or hardening or both) only occupies a small part of the total life; most of the cycling time is occupied by the saturation strain stage with zero hardening.

Klesnil *et al*[8] showed that the transient behaviour depends on the grain size. For fine-grained specimens, the fatigue limit was below the static yield stress and cyclic loading of a specimen at a stress between them caused initial softening followed by hardening. But if the stress was below or just above the fatigue limit, only slight softening occurred. Thus, there appeared to be some limiting value of stress amplitude above which the initial softening was followed by hardening. Below this limiting value, no hardening took place. This limiting value lay between the fatigue limit and static yield stress and decreased with increasing grain size. For the coarse grained specimens ($d^{-\frac{1}{2}} < 3.8\ mm^{-\frac{1}{2}}$), the fatigue limit was above the lower yield stress and Klesnil *et al*[8] found that when the specimen was fatigue cycled, only

hardening occurred. This is hardly surprising since the cyclic amplitude used was above the fatigue limit (and well above the lower yield stress); consequently, the first quarter cycle would produce plastic strain of 1 - 3% and plastic softening could not possibly occur in this instance. The distinction of Klesnil *et al*[8] between fine and coarse grained materials behaviour under cyclic loading is thus not exactly correct, since the test conditions were varied. In one instance the stress was below the static yield stress, and in the other, it was above the yield stress. Nevertheless, their results showed that grain size does have some influence over the type of initial transient behaviour.

5.5 CYCLIC STRAIN HARDENING

Most materials in the annealed state cyclically harden initially before attaining a saturation strain. Direct observation of dislocation structures produced by fatigue[139] indicate that the initial rapid hardening process is caused predominantly by the accumulation of dislocation debris in the form of complex braids of dipoles and monopoles. These debris, produced by cross-slip of screw dislocations act as effective obstacles to dislocation movements. Hardening is achieved when large numbers of dislocations are rendered immobile by being entangled.

Unlike the rapid hardening explanation[139] which is popularly accepted, various different theories have been proposed to account for the zero hardening plastic flow in saturation. These theories have all been based on the type of dislocation structures observed. Thus, for high amplitude cycling which produces a cell structure, the mechanism proposed is different from that suggested for low amplitude cycling, which produces a dislocation-forest structure. For a mechanism that can accommodate non-hardening plastic flow, it must either be one of dynamic balance between competing processes or a reversible, or at least regenerative, process.

Models of the first type were proposed by Alden[140] and Alden and

Backofen[141]. Basically the argument put forward to explain the absence of cyclic strain hardening during saturation is that cross-slipping of screw dislocations of opposite signs may be able to annihilate each other and thus set up a dynamic recovery process similar to the Stage III hardening in tensile deformation. Avery and Backofen[42] also suggested the possibility that saturation was due to the reversible bowing of free dislocation lengths back and forth under cyclic stress.

Most researchers favour a mechanism of the second type, and models have been put forward to describe the hardening mechanism in both high and low amplitude fatigue. For high amplitude fatigue, where three- dimensional cells are the predominant dislocation structure, Feltner and Laird[142] proposed the cell shuttling model. It employs Kuhlmann-Wilsdorf's concept[66] of Stage II unidirectional strain hardening where the saturation flow stress is controlled by the reactions of free meshlengths of dislocations $\bar{\ell}$, against bowing out. When stress is applied, the free meshlength at the cell wall bows out and the link increases in size until certain "critical" length is reached when it is free to move through the clear volume between cell walls. A loop emitted from a link continues to grow in size until it comes into contact with a cell wall in the vicinity. Segments of the loop will experience both attractive and repulsive interactions as they enter the stress field of the cell walls and destruction by annihilation. Upon entering the cell walls, the attractive interaction entangles the loop in the walls and its free meshlength is reduced to $\bar{\ell}$. The process repeats itself when the stress is reversed.

Transmission electron microscopy studies have shown that the characteristic feature of low amplitude fatigue is the production of large quantities of dislocation loops[143,144], the densities ranging as high as 10^{15} - 10^{16} loops per cm^3. The loops produced are prismatic loops and they generally account for 80 - 90% of the total dislocation density[145]. These observat-

ions led Feltner[145] to propose a Dipole Flip-Flop mechanism. It was suggested that the initial stage of hardening is caused by entanglement of mobile dislocations by debris loops. Thus in the early stage of hardening, the rate of hardening is determined by the formation of debris obstacles. As the material fills up with debris, the motion of screw dislocations diminishes and the enforced strain is accommodated by the motions of prismatic loops. The basic motion of the prismatic loop is a flip-flop motion from one stable equilibrium position to another. Because this process is reversible, the net hardening rate is nearly zero and the saturation stage is attained.

Several objections to the model have been raised, notably by Grosskreutz[146] and Finney and Laird[147]. The question arises as to whether loop-flipping makes sufficient contribution to the total strain to sustain the stress in the saturation state, since the observed loop density is much lower than that required theoretically[146]. It is established that loops do exist within the matrix structure, both within patches and 'clear' areas. Dipoles are also plentiful within the walls comprising the persistent slip bands (PSB's) near the surface. The loop density in the 'clear' area between PSB's is very low (10^9 per cm^2)[147] and Piqueras *et al*[148] have examined and rejected the possibility that part of the strain is taken up by motions of dislocations tangled in walls. Thus the majority of the dipoles are in such a configuration (walls and patches) that they would find it difficult to move, whereas those in the "easy flip" location ('clear' areas) are insignificant in number It appears that loop-flipping, if it occurs, contributes little to the saturation strain. A further criticism of the flip-flop mechanism is that, because the process is completely reversible, it cannot cope with structure changes which occur in saturation, and makes no allowance for crack formation.

The formation of PSB's on surfaces and the development of cracks from

these, coupled with evidence that PSB's are soft relatively to the matrix[149,150], suggest that there is a heavy concentration of strain within PSB's. Finney and Laird[147] observed that there was a considerable difference in the dislocation structures at the surface and at the interior of the material. In saturation, PSB's were observed to traverse the whole section of their copper crystal and that all the imposed plastic strain was manifested as slip steps on the surface as traces of the PSB's. Their PSB results demonstrated that not only the crystal surface was not uniformly hardened, but the internal matrix also hardened to such a degree that it could support the saturation stress elastically.

The similarity between the dislocation structure at the surface in low amplitude fatigue, observed by Lukas *et al*[151] as cylinder structure and by Woods[152] as wall structure, and the cell structure at the interior in high amplitude fatigue led Finney and Laird[147] to propose a model for saturation hardening based on the cell shuttling model of Feltner and Laird[142]. It was suggested in low amplitude fatigue, edge links at the surface of the specimen bow out from the walls comprising the PSB structure until they become incorporated in the opposite wall. As this is taking place, the stress imbalance will cause a link in the opposite wall to become active, producing a snowballing effect. On reverse loading, the same or a similar link travels in the opposite direction and reversibility is thus accomplished. Further strain can come from the traversing of screw dislocations formed from the bowing process between the walls, but annihilation of these screw dislocations can readily occur. The links which emerge at the free surface are not completely reversible and crack formation is simply a geometrical consequence of the irreversibility of this dislocation emergence in the PSB traces.

It should be noted that all the models on saturation hardening were derived from experimental observations of copper crystal. However, there is

ample evidence to show that the dislocation structures of fatigued iron and low carbon steel are similar, i.e., cell wall formation at high amplitude cycling[8], elongated tangles of helical dislocations and loops[5,31,153] in specimen interior at low amplitude cycling, with the surface showing PSB structures of loops, entangled dislocations and bow outs from PSB walls[154]. Therefore, it is likely that the same saturation hardening mechanism proposed for f.c.c. metal also applies for b.c.c. metals.

5.6 THE EFFECT OF CYCLIC PRESTRESS ON SUBSEQUENT STATIC YIELDING

Klesnil *et al*[8] showed that cyclic prestressing mild steel can lead to changes in the tensile flow curve characteristics during a subsequent tensile test. Unfortunately, they did not specify the grain size of the specimens and the amplitude of cyclic prestress used. It seems reasonable to assume that a fine grained specimen was used and that the stress amplitude used was above the fatigue limit but below the yield stress. This would cause softening and then hardening of the material. Nevertheless, their results showed that increasing the number of prestress cycles (using the same stress amplitude) had four major effects on the subsequent tensile curve:

1) the yield drop could be suppressed or eliminated;
2) the Luders strain could be reduced or eliminated;
3) the plastic deformation below the yield point could be increased, i.e., the initial stress-strain curve departs from linearity at an earlier point;
4) the strain hardening rate could be increased.

A combination of these four effects is that with a sufficient number of prestressing cycles, a completely smooth stress-strain curve could be obtained from subsequent tensile tests of fatigued specimens. This effect was attribued to the generation of free dislocations and the expansion of the plastically deformed volumes formed during cyclic stressing[8].

Luther and Williams[128] found that for complete reversed loading, cycling at 50 Hz at a stress below the fatigue limit ($< \sigma_y$) had no effect on the subsequent tensile flow curve. However, when the cyclic stress was raised above the fatigue limit (below σ_y), the yield drop was suppressed after 7×10^4 cycles and a smooth tensile curve obtained after 1.2×10^5 cycles of pre-stress. Raising the test frequency to 100 Hz did not introduce other effects and similar results were obtained.

Luther and Williams[155] found that strain hardening occurs preferentially on the surface layer of a steel cyclically loaded to $0.7\ \sigma_y$, and since the elastic limit of low carbon steel was estimated at $0.5 - 0.6\ \sigma_y$, they suggested that the effect of cyclic stress is to generate mobile dislocations in the surface to cause hardening and suppress the yield drop and Luders strain in a subsequent tensile test.

While Klesnil *et al*[8] and Luther and Williams[128] found that the yield drop could be gradually suppressed by increasing the number of cyclic prestressing cycles, Abel and Muir[156] found that similar effects could be achieved by increasing the cyclic prestress amplitude. They also found that if the cyclic prestress was unidirectional, the stress ampltidue required for the removal of the yield point had to be greater than σ_A, ($< \sigma_y$) whereas if the cyclic prestress was complete reversed (i.e. zero mean stress), the stress amplitude required to produce the same effect was lower than σ_E. In other words, complete reversed cyclic prestressing was more effective in suppressing the yield point of a subsequent tensile flow curve than unidirectional cyclic prestressing. Abel and Muir[156] suggested that different mechanisms were operative with the different forms of loading. For unidirectional cyclic loading, an exhaustion hardening mechanism was proposed whereby the supply of the mobile edge dislocations is exhausted and at cyclic stress below the static lower yield stress, the number of new mobile dislocations generated is very small and is insufficient to satisfy

the strain rate imposed by the tensile machine during subsequent tensile tests. At stresses above the static lower yield stress, the normal mechanisms of plastic deformation take over to produce sufficient number of mobile dislocations and result in the suppression of the yield point phenomenon. For complete reversed cyclic stressing, it was suggested that a micro-Bauschinger effect is operating, and when an edge segment of a dislocation is forced against a barrier on loading in one direction, its potential to move with the reversed load is increased. Consequently, plastic flow can occur in the compression half-cycle immediately following a tension half-cycle at a much lower stress than that attained in the preceding half-cycle. It was also suggested that the reverse strain will be larger than the forward strain so that the mobile dislocations can consequently be generated to satisfy the strain rate imposed by the tensile machine during a subsequent tensile test at cyclic prestresses below the static yield stress.

Abel and Muir[156] suggested that since the hysteresis loop was closed between σ_E and σ_A and that unidirectional cyclic prestressing at amplitudes below σ_A could not remove the yield point of a subsequent tensile test flow curve, no new mobile dislocations were generated. However, the fact that loading to a stress between σ_E and σ_A and unloading creates a loop (a closed loop) means that there is dislocation movement, and with dislocation movement new dislocations must be created.[121]. Because the stress amplitude is low compared to the static yield stress, dislocations will only move over very short distances. Therefore, they are unlikely to be blocked and can return to the original positions upon unloading. No net strain is thus imparted and the hysteresis loop remains closed.

For the case of complete reversed cyclic prestress, the values of σ_E and σ_A could not be appropriately used for comparison, the reason being that these values were determined from load-unload (or unidirectional cyclic

loading) method as described previously.

The results and explanations of Abel and Muir[156] and the results of Klesnil *et al*[8] appear complementary to the dynamic yield theories and model of Gilman and Johnston[53] and Hahn[54]. According to Hahn's model for yielding in iron, one of the three main criteria for a sharp yield drop is a low initial mobile dislocation, the higher the initial dislocation density the smaller the yield drop. Since prolonged cyclic prestressing at a sufficiently high amplitude can eliminate the yield point and yield drop during a subsequent tensile test, it may be concluded that the effect of cyclic prestressing is to increase the mobile dislocation density. Moreover, the mobile dislocation density attained is both a function of the cyclic prestress amplitude and the number of prestress cycles.

If the above conclusion is correct, then fatigue cycling of a steel specimen can eliminate its yield point in a subsequent tensile test if the fatigue stress is sufficiently high to generate mobile dislocations, even if the fatigue stress is below the fatigue limit of the steel. Since an increase in damping is an indication of dislocation movement and hence dislocation generation[121], it follows that when the fatigue stress is high enough to cause an increase in damping, it must also be high enough to eliminate the yield point in a subsequent tensile test.

CHAPTER SIX

THE REDUCTION OF ACTIVE NITROGEN IN STEELS BY THE PRECIPITATION OF ALUMINIUM NITRIDE AND THE CONTROL OF GRAIN SIZE

6.1 KINETICS OF ALUMINIUM NITRIDE PRECIPITATION

Aluminium is often added to steels to render them non-strain ageing. This process involves the combination of nitrogen in the steel with the aluminium to form aluminium nitride. The fact that the reaction $Al + N \longrightarrow AlN$ is reversible is, however, not always fully appreciated, the assumption often being made that all the nitrogen in steels containing aluminium is combined as AlN, regardless of the preceding thermal history.

Since it is known that the fatigue limit in steels is dependent on strain ageing, it is necessary to know the "active" nitrogen content before attempting to assess variations in fatigue limit brought about by strain ageing.

Reversible reactions such as this can be described by the Law of Mass Action, which states that the velocity of a reaction at a given temperature is proportional to the product of the active masses of the reacting substance[157].

Consider the reaction

$$AlN \rightleftharpoons Al + N \qquad \text{Equation (6.1)}$$

The forward rate of this reaction is given by

$$v_f = k_f [AlN] \qquad \text{Equation (6.2(a))}$$

and the rate of the reverse action is

$$v_r = k_r [Al] [N] \qquad \text{Equation (6.2(b))}$$

where v_f = rate of forward reaction

v_r = rate of reverse reaction

k_f and k_r are proportionality constants

Since equilibrium is a dynamic one and is achieved when the rates of forward and reverse reactions are equal, we have $v_f = v_r$

i.e. $$k_f [AlN] = k_r [Al] [N]$$

or $$\frac{k_f}{k_r} = \frac{[Al] [N]}{[AlN]} = k_c \qquad \text{Equation (6.3)}$$

where k_c is the concentration equilibrium constant and is temperature dependent.

Now since the concentration term for the compound aluminium nitride is constant at constant temperature, Equation (6.3) can be written as

$$[Al] [N] = k_c [AlN] = k_s \qquad \text{Equation (6.4)}$$

where k_s is a new constant called the solubility product.

According to the Arrhenuis Equation, which can be deduced from the Vant Hoff isochore equation and the Law of Mass Action, the effect of temperature on the rate of a reaction is given by

$$v = \theta e^{-\frac{Q}{RT}} \qquad \text{Equation (6.5(a))}$$

or $$\ln v = \ln \theta - \frac{Q}{RT} \qquad \text{Equation (6.5(b))}$$

or $$\log v = \log \theta - \frac{Q}{2.303\ RT} \qquad \text{Equation (6.5(c))}$$

where v = specific reaction rate

θ = integration constant

Q = activation energy

R = gas constant

T = absolute temperature

Now from Equations (6.2(b)) and (6.4), it can be established that

$$v \propto k_s$$

and since from Equation (6.5(c)) that

$$\log v \propto \frac{1}{T}$$

it follows that

$$\log k_s \propto \frac{1}{T} \qquad \text{Equation (6.6)}$$

The relationship was first proved by Darken[158] for aluminium nitride dissolving in austenite to form a solid solution of aluminium and nitrogen. The solubility product was taken as the product of the weight-percentages of aluminium and nitrogen in solution in austenite in equilibrium with aluminium nitride, these being considered equivalent to the activities, i.e.

$$k_s = [\%\ N]\ [\%\ Al] \qquad \text{Equation (6.7)}$$

$$\therefore \quad k_s = [C_N - C_C]\ [C_{Al} - \frac{27}{14} C_C] \qquad \text{Equation (6.8)}$$

where C_N = wt % acid soluble nitrogen

C_{Al} = wt % acid soluble aluminium

C_C = wt % N combined as aluminium nitride

$(\frac{27}{14} C_C)$ = wt % aluminium combined as acuminium nitride

The values of C_N and C_{Al} can be determined by chemical analysis[159], as can the nitrogen combined as aluminium nitride[160].

For low carbon steels, the relationship between $\log k_s$ and temperature

in the form of Equation (6.5(b)) is given by[161]

$$\log k_s = -\frac{6180}{T} + 0.725 \qquad \text{Equation (6.9)}$$

where k_s is given by Equation (6.7) and T = absolute temperature in Kelvin.

Equation (6.9) refers to low carbon steels in the austenite condition, i.e., at temperatures in excess of 900°C and can be considered to be a reasonable approach to equlibrium conditions. The precipitation of aluminium nitride has been investigated in some detail[161,162,163,164]. Erasmus[161,162,163] studied the effects of both isothermal "down-quenching" (i.e., quenching to some intermediate temperature from a higher temperature and holding at this temperature to allow for isothermal precipitation) and isothermal "up-quenching" (i.e., rapid heating from room temprature to some isothermal precipitation temperature, having previously quenched the specimen to room temperature from temperatures above the aluminium nitride solution temperature). All the above studies have shown that the precipitation of aluminium nitride during "down-quenching" and continuous slow cooling conditions to be extremely sluggish - see Figures 6.1(a) & 6.1(b). i.e. Aluminium nitride will not necessarily be formed in steels containing aluminium and that its formation is largely dependent on the solubility product k_s, the heat treatment temperature, the time at temperature and the final cooling rate. Consequently, steels containing aluminium may still be susceptible to strain ageing, and susceptible to any effect of strain ageing on the fatigue properties. A graph of % N_{AlN} vs T(°C) is plotted for a steel with 0.006% N_{sol} and 0.027% Al, i.e., typical of experimental steel - see Figure (6.2).

6.2 THE EFFECT OF ALUMINIUM ADDITION ON THE GRAIN SIZE OF STEELS

Grain growth of steels is a thermally activated process and the grain size which is developed depends mainly on both the austenising temperature

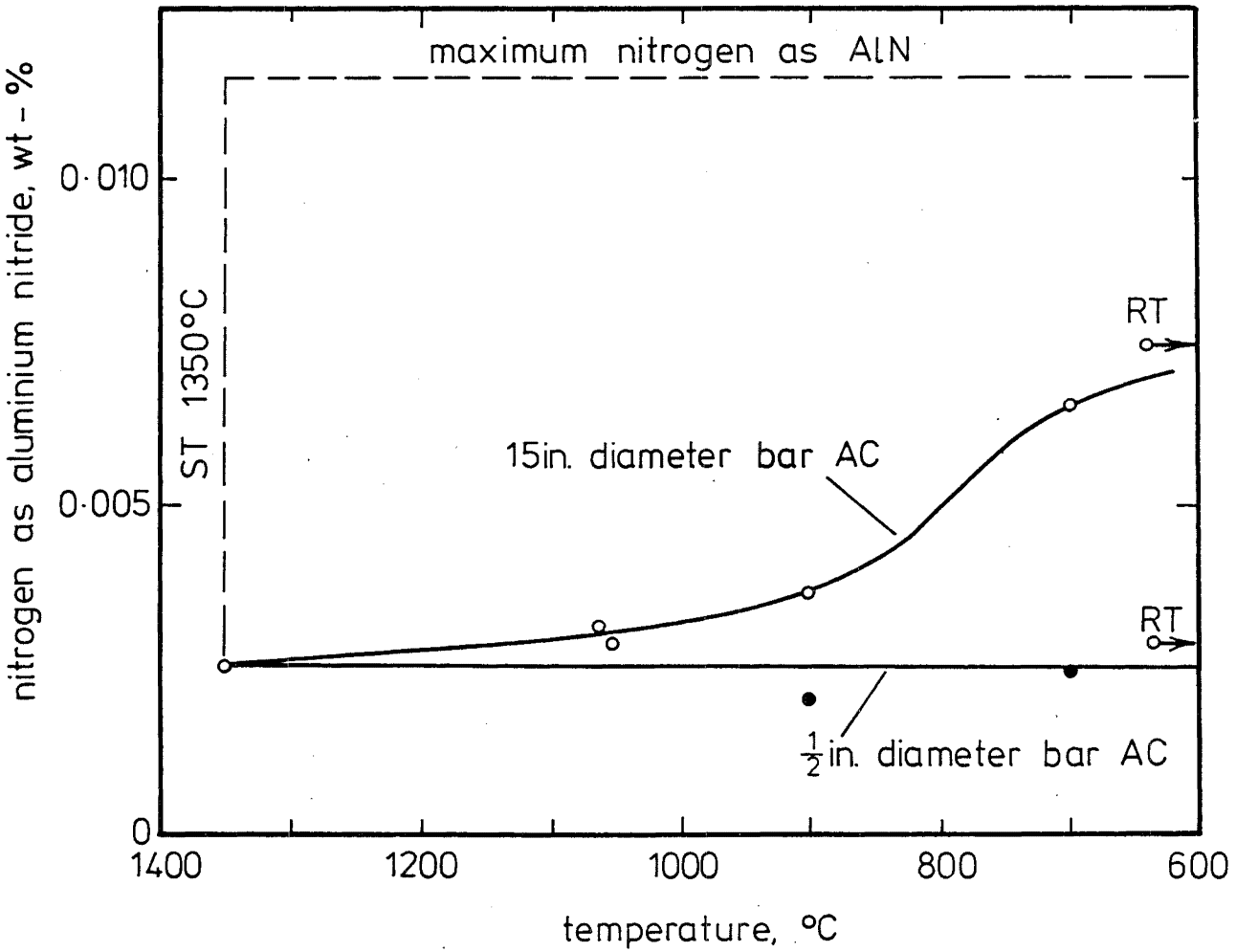

FIG 6·1 (a) PRECIPITATION OF ALUMINIUM NITRIDE IN A 0·08% Al STEEL DURING CONTINUOUS COOLING (Ref. 166)

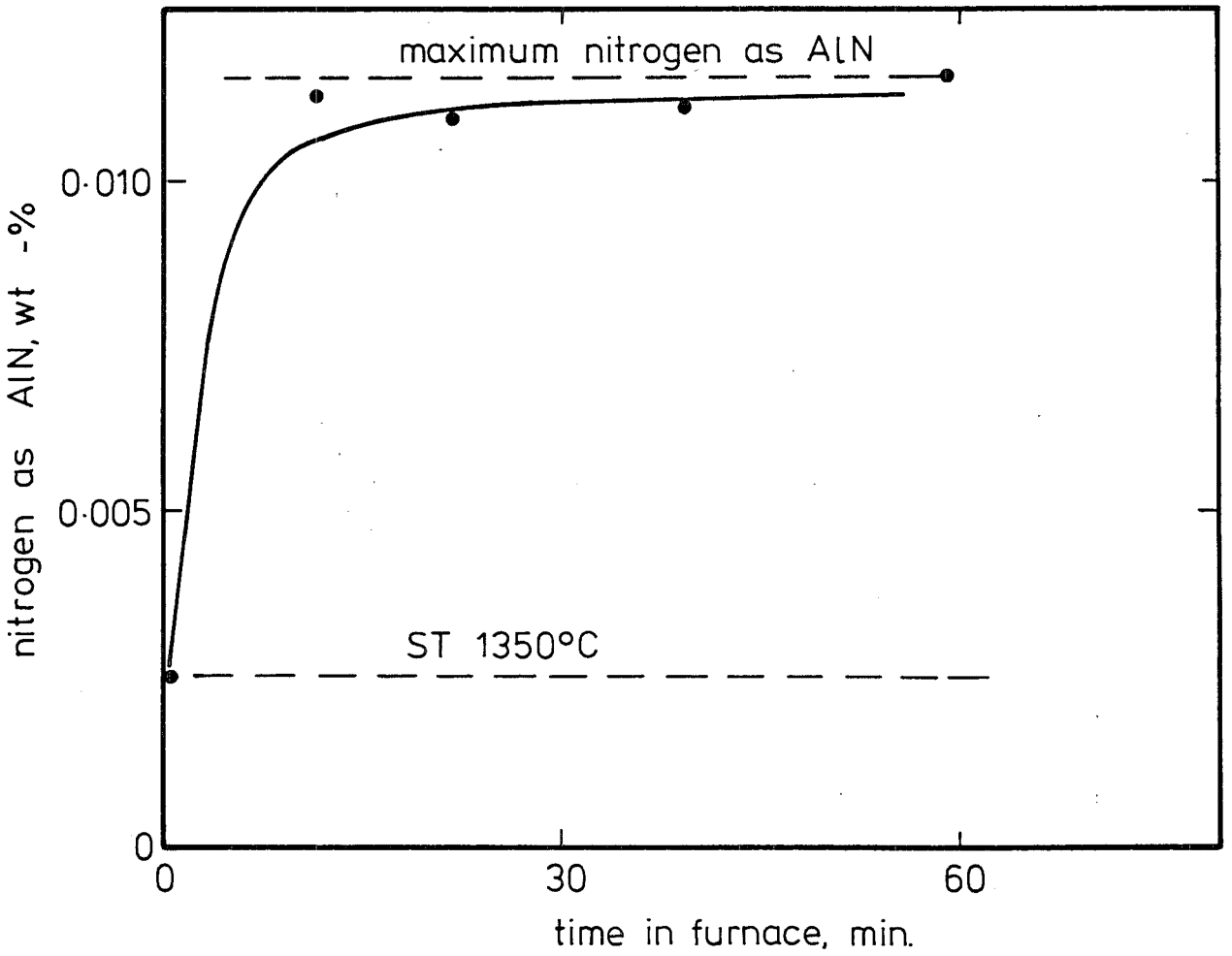

FIG. 6·1 (b) PRECIPITATION OF ALUMINIUM NITRIDE IN A 0·08% Al STEEL DURING UP-QUENCHING TO 950°C (Ref 166)

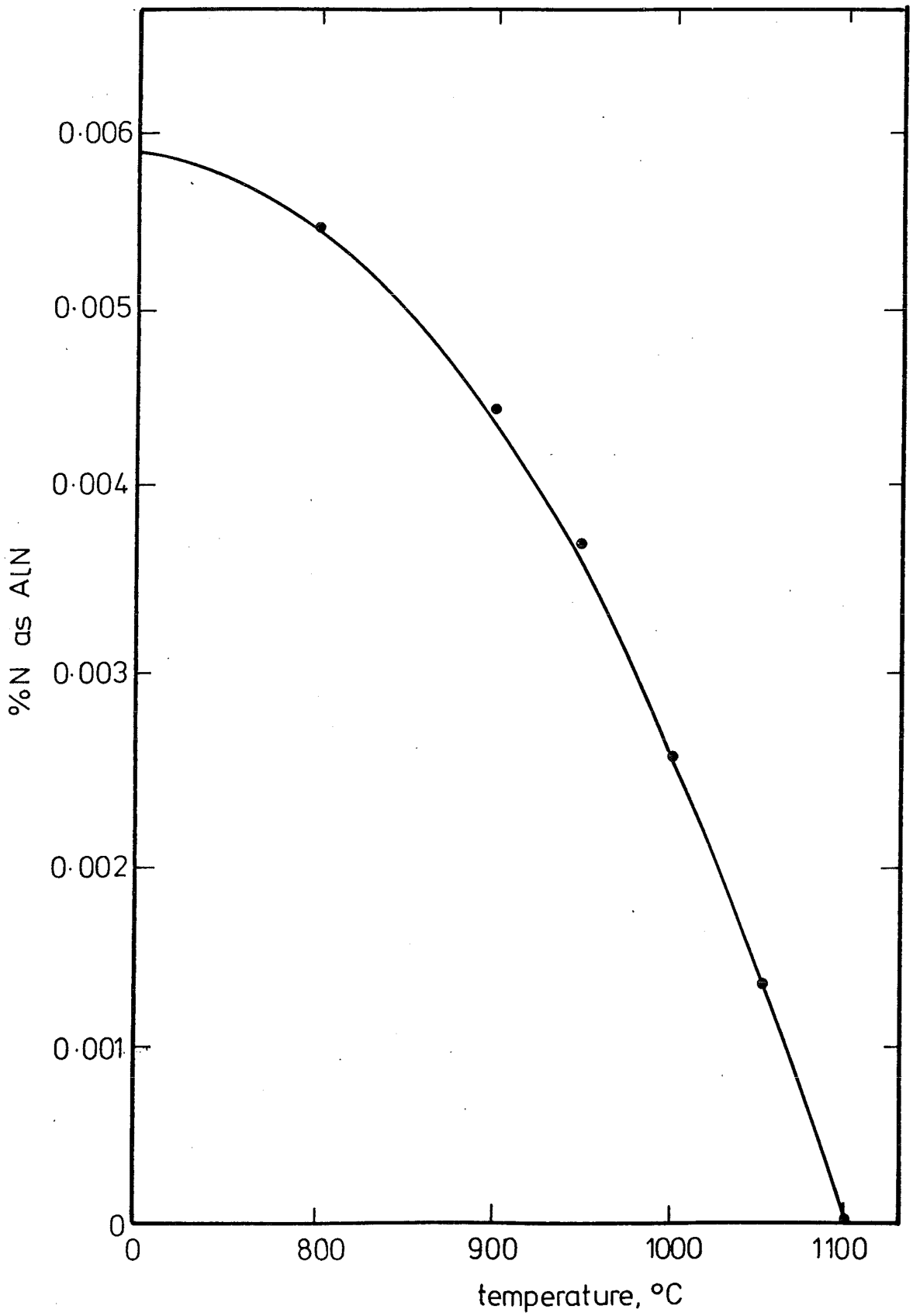

FIG 6·2 EQUILIBRIUM N_{AlN} CONTENT IN AUSTENITE OF A LOW CARBON STEEL WITH N_{sol} = 0·006%, Al_{sol} = 0·027%

and the soaking time.

Other factors, however, are known to influence the migration of grain boundaries, and these include the concentration of solute elements at grain boundaries which can introduce a frictional drag on the moving boundary, and second phase particles, which decrease the grain boundary area, and hence the overall grain boundary energy[165]. Thus the grain growth of austenite can be modified by the additions of elements such as aluminium, niobium, vanadium, titanium, etc., all of which produce small, sparingly soluble precipitates[166].

Bain and Paxton[167] found two principal types of grain coarsening curves. Plain carbon steels without, for example, aluminium additions, show gradual growth of all grains as the austenising temperature is increased. The second type of grain growth is observed in steels containing additions of grain refining elements. In this case, the grain size remains small (ASTM 6-8) at temperatures up to the grain coarsening temperature, and then on heating above this temperature, only a few of the grains grow, resulting in a mixture of coarse and fine grains. When the temperature is raised sufficiently, all the grains become coarse (ASTM 0-2).

Different solute elements have different effects on the grain coarsening temperature. For aluminium, Halley[168] found that increasing the aluminium content to 0.04% increased the grain coarsening temperature. Increasing the aluminium content above about 0.04% then caused a lowering of the grain coarsening temperature. Chatterjea and Nijhawan[169] found a similar effect and Rickett and Leslie[170] in discussing the results of Chatterjea and Nijhawan, expressed the opinion that fine dispersions of aluminium nitride inhibited grain growth. They further suggested that at high aluminium contents, the precipitation occurred at extremely high temperatures, due to the limited solubility. This resulted

in the agglomeration of particles giving rise to a few large particles which were ineffective in inhibiting grain growth[169,170]. Studies of the effects of niobium and titanium on the grain coarsening characteristics of austenite[168,171] have shown that the grain coarsening temperature increased progressively with increasing alloy addition and that there was apparently no optimum alloy content. Erasmus[91] studied the effect of vanadium on the grain coarsening characteristics of austenite and found a progressive increase in grain coarsening temperature with increasing vanadium content. Small additions of vanadium were relatively more effective than large additions, and the behaviour of vanadium might well be analogous to that of aluminium. Also, grain coarsening always started at temperatures well below the solubility limit of vanadium nitride.

The original microstructure of the steel and the heating rate have also been found to have some influence on the eventual grain size. However, their effects are usually small. The variation in grain size produced by using a wide range of heating rates or prior microstructure is usually of the order of one ASTM number[172].

The effects of temperature and aluminium content on the grain coarsening characteristics of low carbon steels have been studied by Gladman and Pickering[166]. Figures (6.3(a)) and (6.3(b)) are reproductions of their results.

6.3 THE CONTROL OF "ACTIVE" NITROGEN AND GRAIN SIZE IN THE EXPERIMENTAL STEELS

In order to fully investigate the effects of strain ageing and microstructures on the fatigue limit of steels, specimens of different grain sizes at two levels of "active" nitrogen were prepared. The heat treatments used to achieve these conditions are shown in Table 6.1 and are briefly summarised as follows:

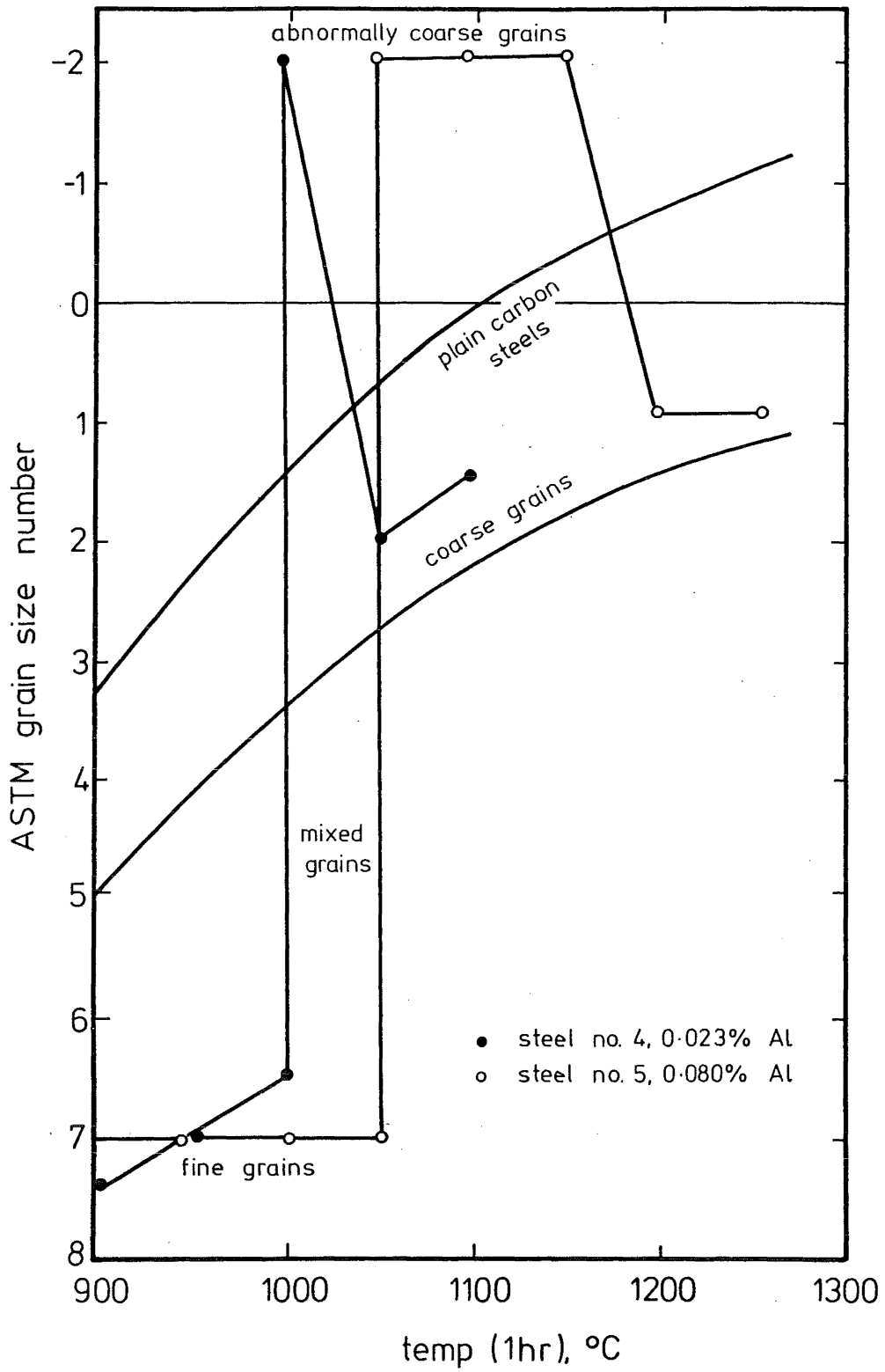

FIG. 6·3 (a) GRAIN-COARSENING CHARACTERISTICS OF GRAIN-REFINED STEELS. (Ref. **166**)

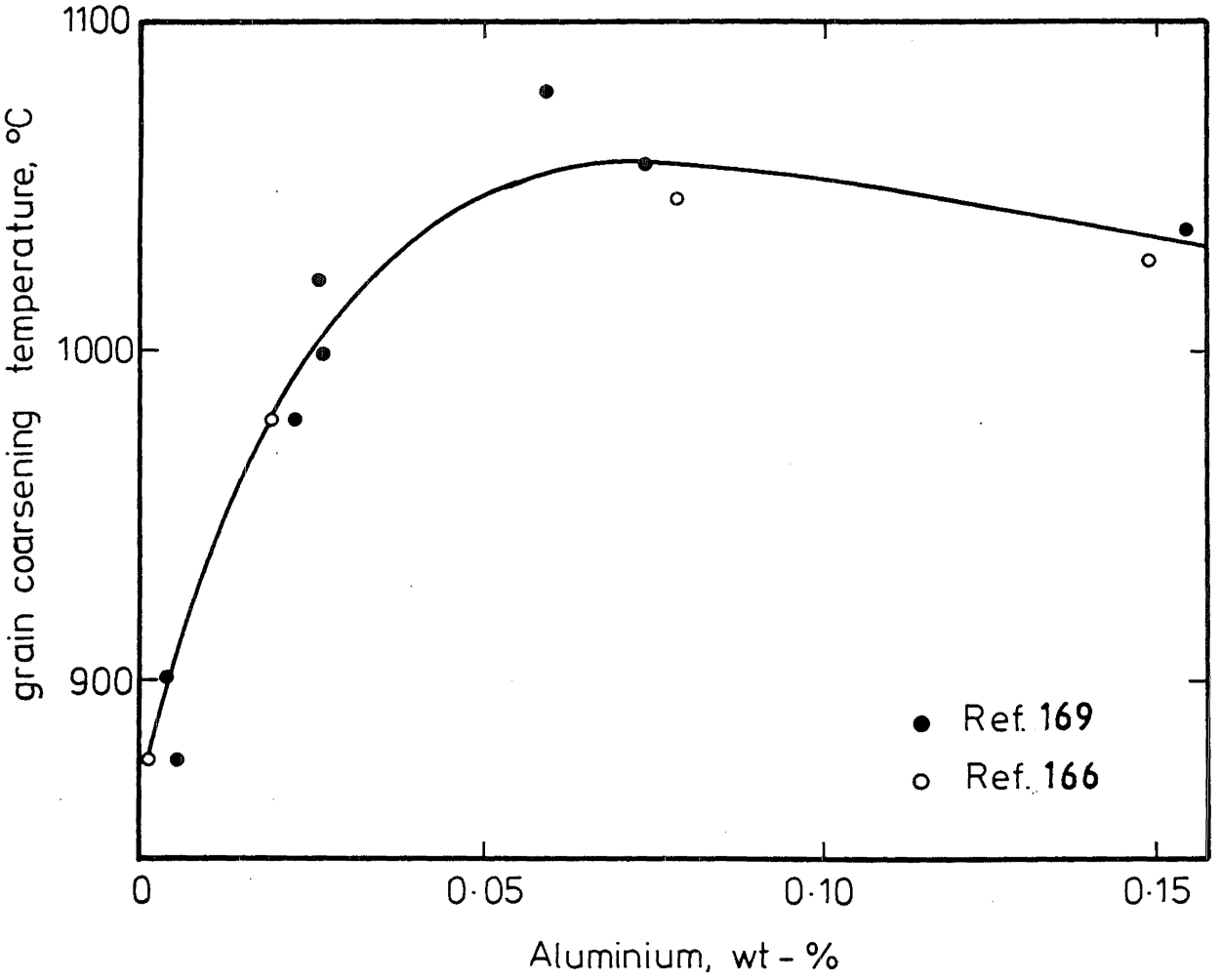

FIG. 6·3 (b) THE EFFECT OF ALUMINIUM ON GRAIN-COARSENING TEMPERATURE IN 'AS ROLLED' STEEL (Ref 166)

(a) Coarse grained - low "active" nitrogen specimens (A):

High temperatures (> 1100°C) were used to introduce large austenite grain sizes followed by very slow cooling (controlled cooling from 950°C to 650°C over 49 hours). This ensured extensive precipitation of aluminium nitride. The slow cooling rate also encouraged the precipitates to grow in size and larger aluminium nitride precipitates are less effective in restricting grain growth compared to fine precipitates.

(b) Fine grained - low "active" nitrogen specimens (A):

A low austenising temperature (900°C) was used to obtain the fine grained structure. As shown in Figure 6.2, for equilibrium conditions, heat treatments at about 900°C should result in the combination of most of the nitrogen as aluminium nitride. To ensure a closer approach to the equilibrium condition, a multiple (repeated) heat treatment was used for these specimens.

(c) Coarse grained - high "active" nitrogen specimens (B):

High austenising temperatures (> 1100°C) were again used to obtain the coarse structures. Faster cooling rate was used to reduce the precipitation of aluminium nitride.

(d) Fine grained - high "active" nitrogen specimens (B)

The fine grained structure required low austenising temperatures. However, the low temperature under equilibrium conditions would result in extensive precipitation of aluminium nitride. It was found, however, that when the soaking time was short and the cooling rate reasonably rapid, the precipitation of aluminium nitride was slow. The specimens were thus normalised at 900°C for one hour and air-cooled.

TABLE 6.1

METHODS OF HEAT TREATMENT FOR EXPERIMENTAL STEEL

Specimen Identification	Soaking Temperature °C	Soaking Time (Hrs)	Method of Cooling
A(1)	900 and 880	2 + 1 + 1	Normalised at 900°C for 2 hours. Air-cooled to < 650°C. Normalised at 900°C for 1 hour. Air-cooled to < 650°C. Normalised at 880°C for 1 hour. Air-cooled.
A(2)	1100	2	Control cooled from 950°C - 650°C over 49 hours; then furnace cooled.
A(3)	1350	3	Control cooled from 950°C - 650°C over 49 hours; then furnace cooled.
B(1)	900	1	Air cooled.
B(2)	1100	2	Air cooled.
B(3)	1100	2	Furnace cooled from 1100°C.
B(4)	1200	2½	Furnace cooled from 1200°C.
B(5)	1350	3	Furnace cooled from 1350°C.

By variations of the aforementioned heat treatment procedures, intermediate grain sizes were produced for specimens with the two levels of "active" nitrogen. Altogether, eight groups of specimens were prepared, five with high "active" nitrogen content, designated B(1), B(2), B(3), B(4) and B(5), and three groups with low "active" nitrogen content, A(1), A(2), and A(3). The heat treatment methods are summarised in Table 6.1.

The experimental steel for all the specimens came from a common bar stock of 32 mm diameter. Heat treatments were carried out before specimens were machined to shape. In order to reduce decarburisation, non-oxidising atmospheres were used during soaking and cooling when the temperature was above 800°C. For steels A(1) and B(1), this was done by burning the gas curtain in the furnace. For the other six steels, argon was fed into the furnace.

The following example using the most extreme case shows that the specimens were not significantly affected by decarburisation during the heat treatments. Steel B(5) was soaked at 1350°C for three hours.

The diffusion rate of carbon in γ iron is given by[173]

$$D_\gamma(T) = 0.21 \frac{cm^2}{S} \cdot e^{(-\frac{1}{RT})} \quad (33800 \text{ mole/cal.})$$

$$R = 1.98 \text{ cal/mole . K}$$

$$T = 1623 \text{ K}$$

$$\therefore \quad D_\gamma(1623) = 0.21 \frac{cm^2}{S} \; e^{-\frac{33800}{1.98 \times 1623}}$$

$$= 5.68 \times 10^{-4} \frac{mm^2}{S}$$

Using Fick's Second Law of Diffusion

$$\frac{C_x - C_s}{C_o - C_s} = \text{erf} \left(\frac{x}{2\sqrt{Dt}} \right) \qquad \text{Equation (6.10)}$$

where C_x = carbon concentration at distance x from bar surface

x = 0 at surface

C_o = carbon content of "as-received" steel, 0.16%

C_s = carbon content at steel/atmosphere interface, assumed zero

t = time in seconds, 3 x 3600s

By putting in the appropriate values, Equation 6.10 becomes

$$\frac{C_x - 0}{0.16 - 0} = \text{erf.} \left(\frac{x}{2\sqrt{5.68 \times 10^{-4} \times 3 \times 3600}} \right)$$

$$\Rightarrow \quad C_x = 0.16 \text{ erf.} \left(\frac{x}{4.95}\right) \% \qquad \text{Equation (6.11)}$$

The profile of carbon concentration across the section of the bar may now be obtained by plotting C_x against x for $0 < x < 16$mm and using symmetry to obtain the profile for $16 < x < 32$mm. This is shown in Fig. 6.4.

Since the largest specimen size machined from the bar was 15mm diameter, it may be seen that the specimen gauge length was not significantly affected by decarburisation.

Some decarburisation would, of course, continue to occur during the cooling stage. However, the cooling rate (of furnace atmosphere) was fast and diffusion rate drops rapidly with temperature, e.g. D_γ (1200°C) = $\frac{1}{3}$ D_γ (1350°C).

Thus, with the provision of non-oxidising atmospheres during heat treatment, it can be said decarburisation at the core of the bar was insignificant and that all the specimens still contained the same amount of carbon.

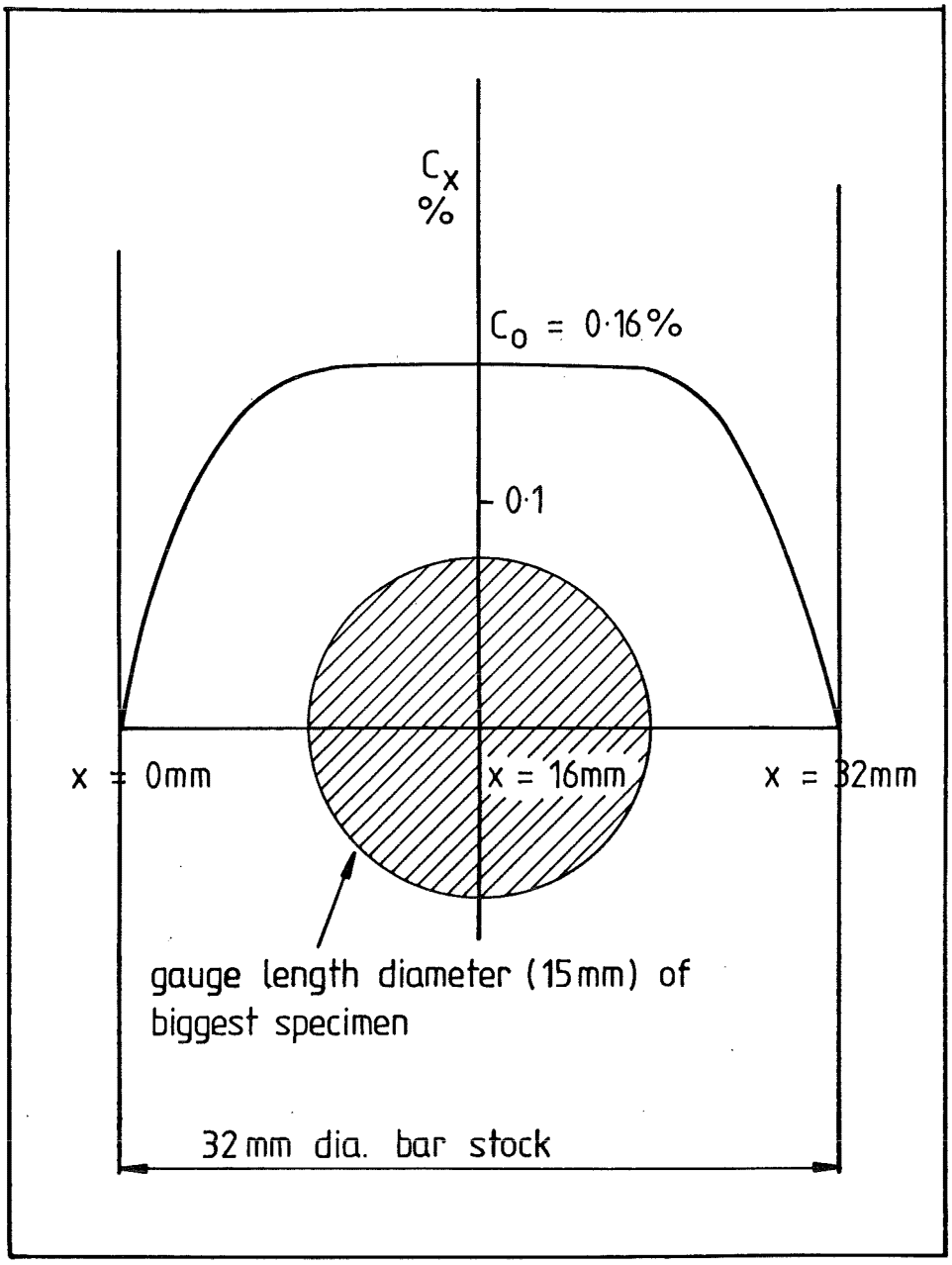

FIG. 6·4 CARBON CONCENTRATION PROFILE OF A 32 mm DIA. LOW CARBON STEEL BAR (C = 0·16%) AFTER HEATING AT 1350°C FOR 3 HOURS

CHAPTER SEVEN

EXPERIMENTAL PROCEDURES AND RESULTS

7.1 CHEMICAL ANALYSIS

The chemical composition of the steel supplied by the manufacturer is given in Table 7.1. In addition, nitrogen analysis was carried out to determine the "free" nitrogen in each of the eight experimental steels.

The method used was that of the United Steel Companies Ltd[159]. It included separate determinations of nitrogen as acid soluble and acid insoluble nitrides. Since the soluble part consists mainly of aluminium nitride and "free" nitrogen, it may therefore be assumed that

$$\%\ N_{\text{as free interstitials}} = \%\ N_{\text{as soluble nitrides}} - \%\ N_{\text{as AlN}}$$

The full detail of this analysis method is given in Appendix A.

These results, see Table 7.1, show that there was a considerable difference in the "free" nitrogen contents of the Steels 'A' (low "free" nitrogen) and the Steels 'B' (high "free" nitrogen).
(Note: The low "free" nitrogen steels, Steels 'A', were steels with low contents of nitrogen as interstitials and hence were steels with little ageing propensity. For simplicity, Steels 'A' will be referred to as the low nitrogen steels. Similarly, the high nitrogen steels were Steels 'B' which contained high levels of nitrogen as interstitials and were capable of severe ageing.) However, the amount of "free" nitrogen present in Steels 'A' was still enough to cause some strain ageing. It must therefore be noted that the three low nitrogen steels (Steels 'A') were not non-ageing steels but represented steels with a lower propensity for strain ageing than the five high nitrogen steels (Steels 'B').

TABLE 7.1

CHEMICAL COMPOSITION AND NITROGEN ANALYSIS

OF EXPERIMENTAL STEELS (wt %)

C = 0.16%
Mn = 0.54%
Si = 0.12%
S = 0.037%
P = 0.015%

Experimental Steel	Al_{SOL}	N_{SOL}	N_{INSOL}	N_{AlN}	N_{ACTIVE}	
A(1)	0.027	.0055	.0008	.0042	.0013	Low nitrogen steels. LoN
A(2)	0.027	.0062	.0009	.0045	.0017	
A(3)	0.027	.0044	.0018	.0043	.0001	
B(1)	0.027	.0065	.0009	.0009	.0056	High nitrogen steels, HiN.
B(2)	0.027	.0062	.0013	.0003	.0059	
B(3)	0.027	.0057	.0013	.0002	.0055	
B(4)	0.027	.0058	.0008	.0009	.0049	
B)5)	0.027	.0047	.0014	.0012	.0035	

7.2 GRAIN SIZE MEASUREMENT

Micro specimens were prepared from the eight sets of steel to determine the grain sizes. Specimens were obtained from used fatigue and tensile specimens at a region away from the gauge length. The average grain size of the two specimens was taken as the grain size of that particular specimen batch.

The linear intercept method[174] was used for grain measurement on the photomicrograph of the specimens. In this method, parallel straight lines of total length L were drawn on the micrographs. The total number of intercepts, N_i, made by these lines with the grain boundaries, were counted and the average grain diameter was calculated as follows:

$$d = \frac{L}{N_i \times M}$$

M = photomicrograph magnification.

At least 300 intercepts were obtained in each case for an accurate assessment of the grain size. The grain sizes, as determined by the above method, are given in Table 7.2.

7.3 TENSILE TESTS

Standard 15 mm diameter tensile specimens with 90 mm gauge lengths as specified in BS 18 (see Figure 7.1) were prepared from the eight sets of steel. Testing was carried out on a 250 kN Instron Universal Testing Machine at a strain rate of about 2×10^{-4}/sec. The lower yield stresses and tensile stresses for these steels are tabulated in Table 7.2.

Prior to testing, all the specimens were given a 3-hour treatment at 100°C to ensure as many dislocations as possible were pinned by precipitates. Erasmus[175] had shown that the mobile dislocation density could vary from specimen to specimen due to the different heat treatments, and since yielding is dependent on the initial mobile dislocation density[54], it was

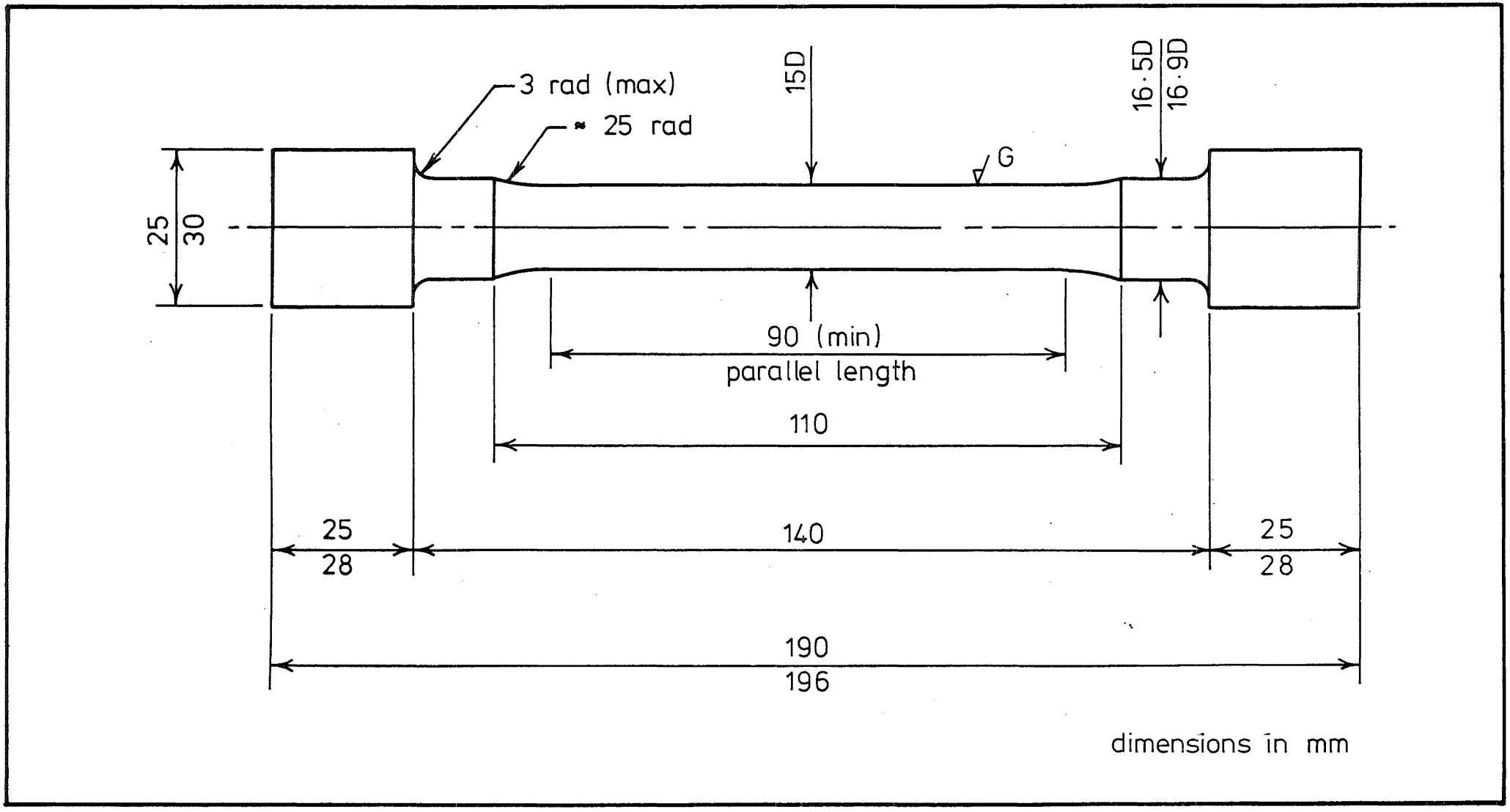

FIG. 7·1 TENSILE SPECIMEN

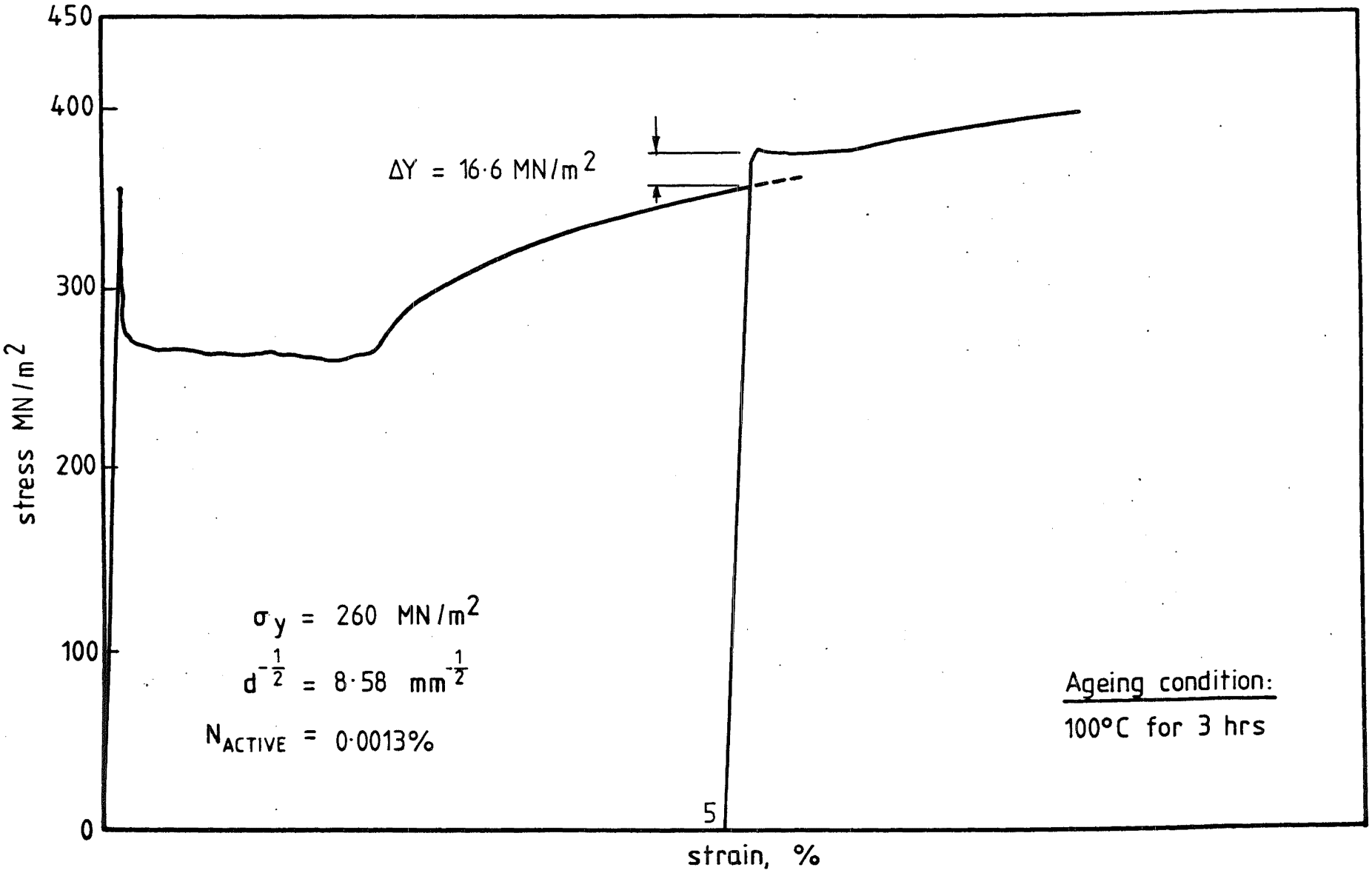

FIG. 7·2 STRESS-STRAIN OF STEEL A(1) BEFORE AND AFTER STRAIN-AGEING

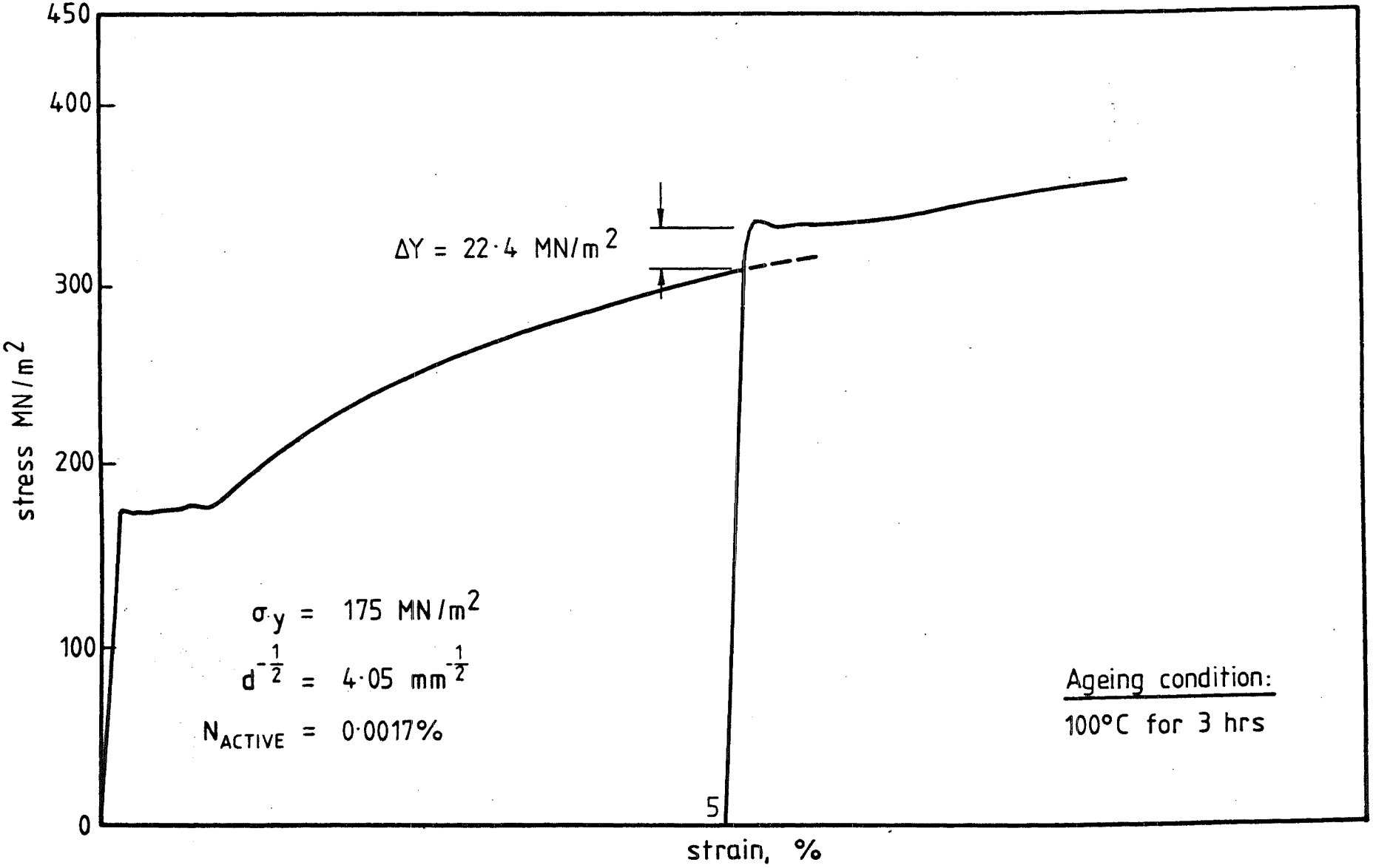

FIG. 7·3 STRESS-STRAIN OF STEEL A(2) BEFORE AND AFTER STRAIN-AGEING

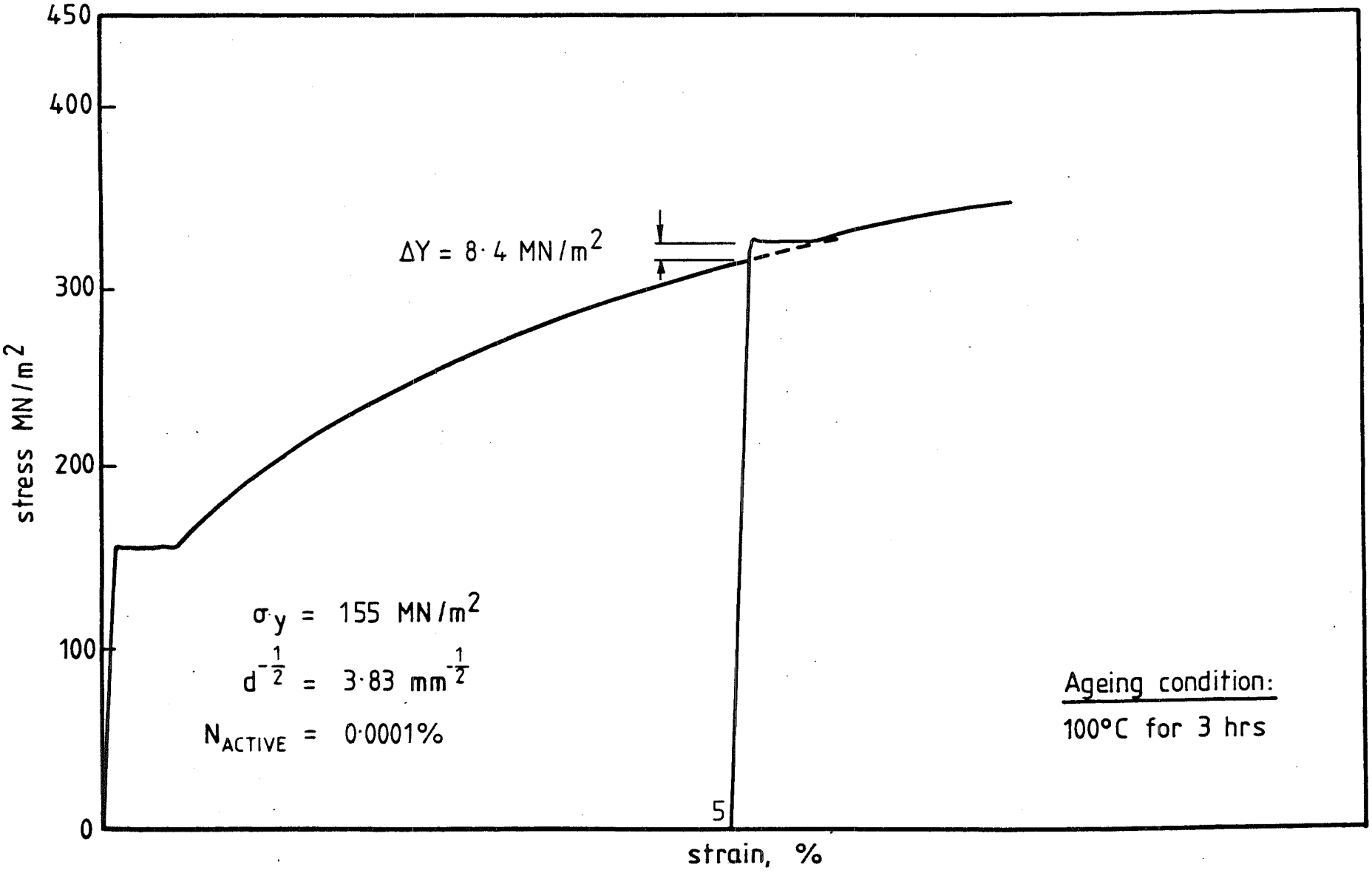

FIG. 7·4 STRESS-STRAIN OF STEEL A(3) BEFORE AND AFTER STRAIN-AGEING

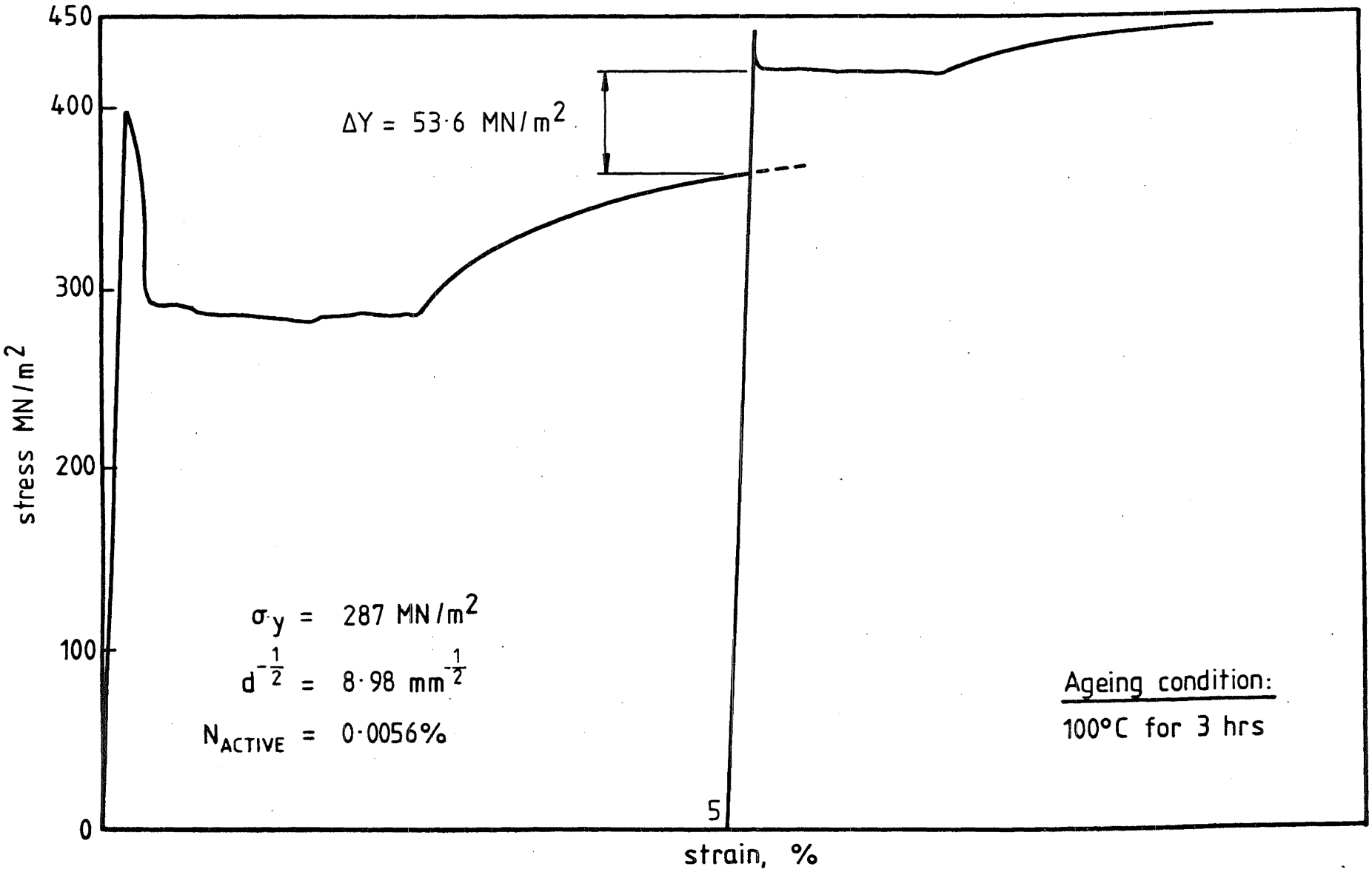

FIG. 7·5 STRESS-STRAIN OF STEEL B(1) BEFORE AND AFTER STRAIN-AGEING

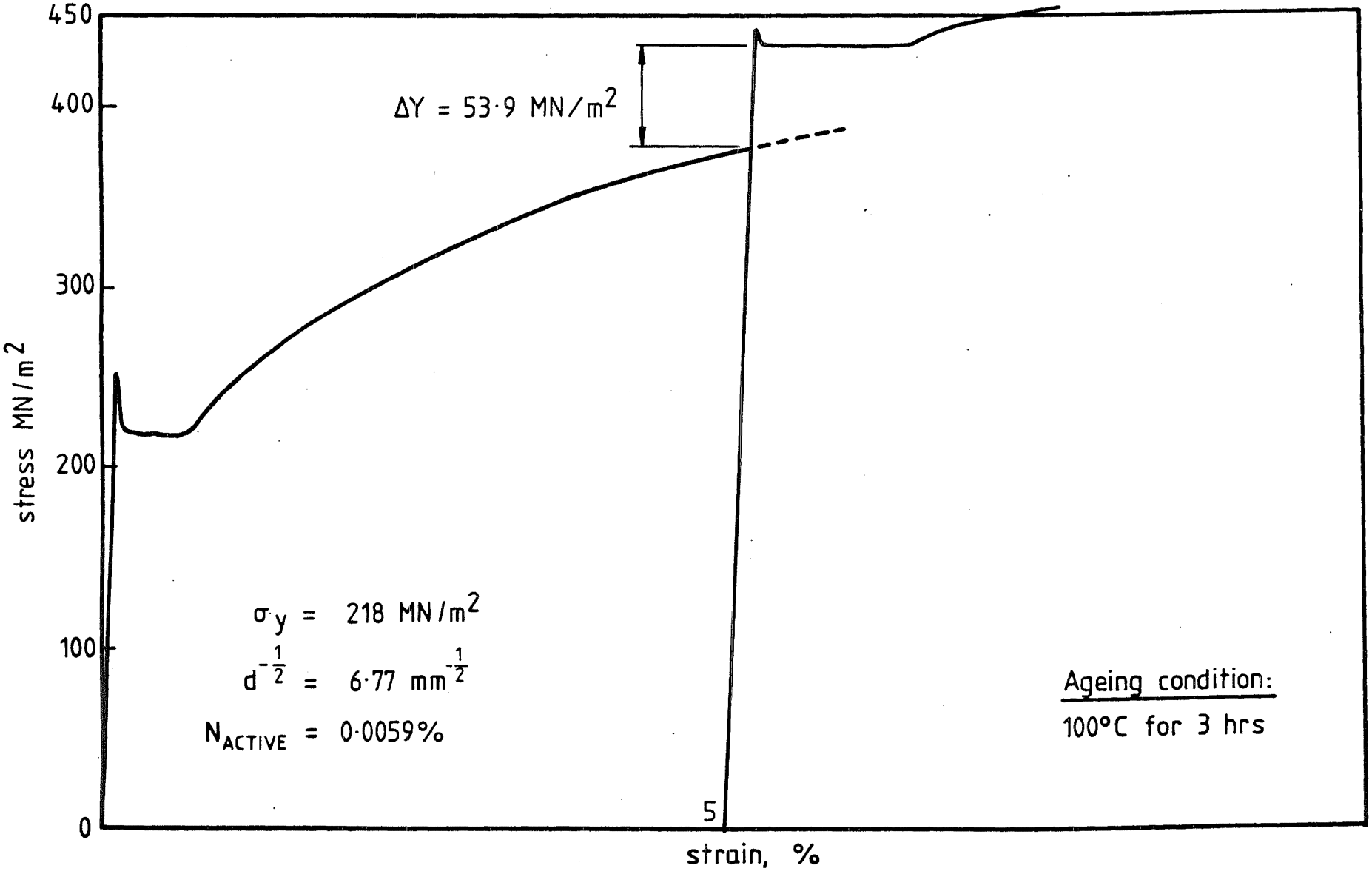

FIG. 7·6 STRESS-STRAIN OF STEEL B(2) BEFORE AND AFTER STRAIN-AGEING

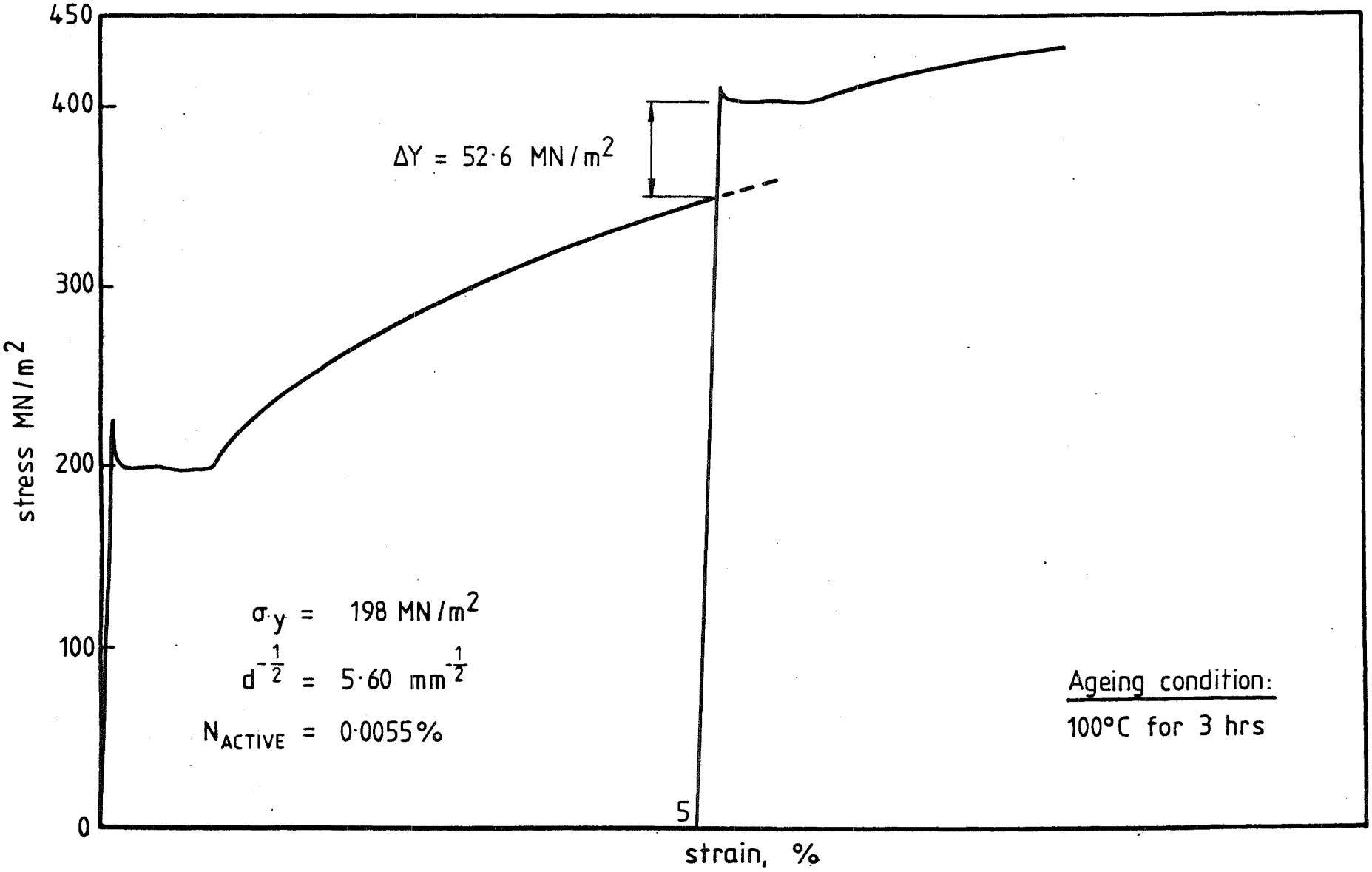

FIG. 7·7 STRESS-STRAIN OF STEEL B(3) BEFORE AND AFTER STRAIN-AGEING

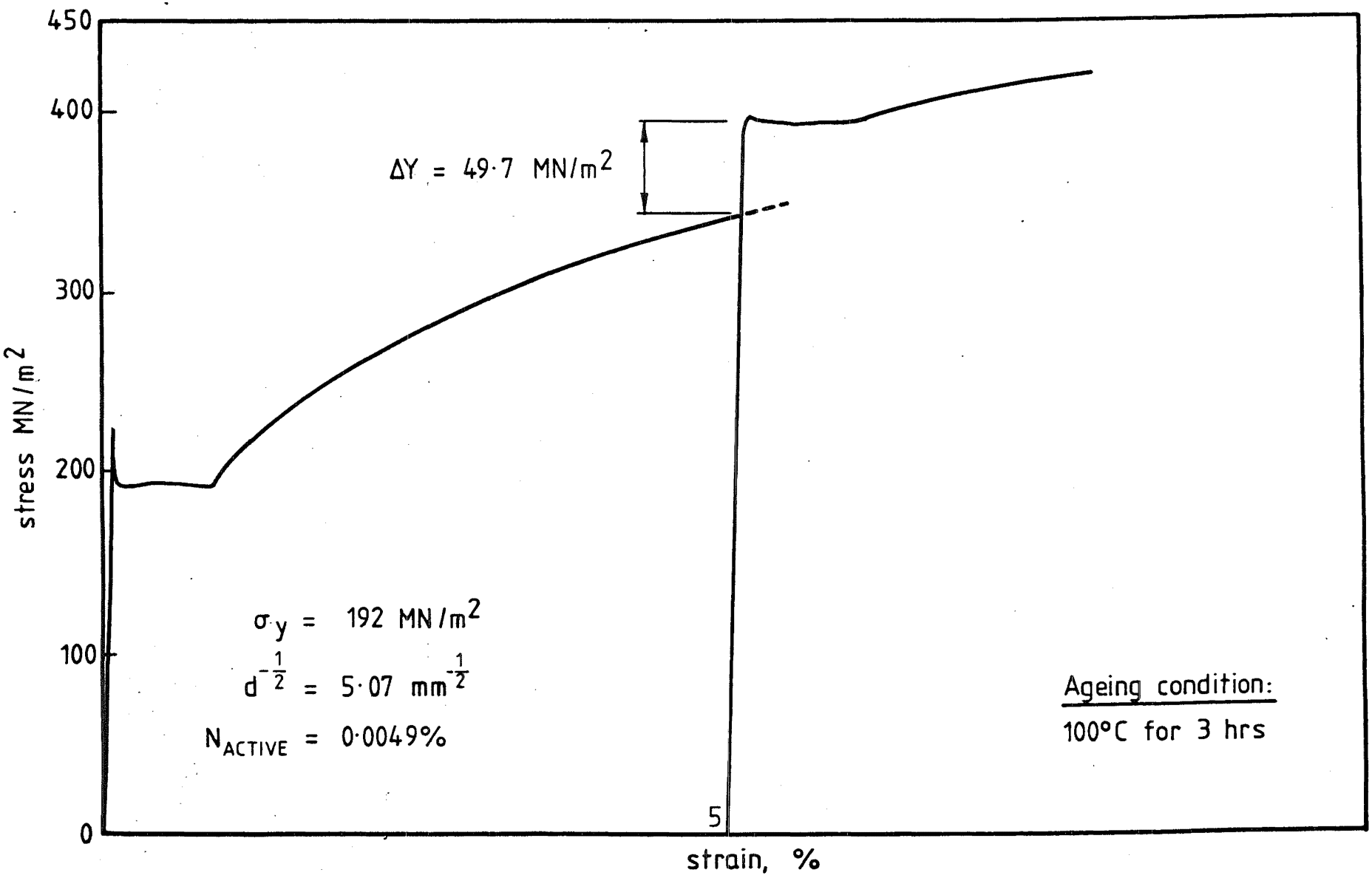

FIG. 7·8 STRESS-STRAIN OF STEEL B(4) BEFORE AND AFTER STRAIN-AGEING

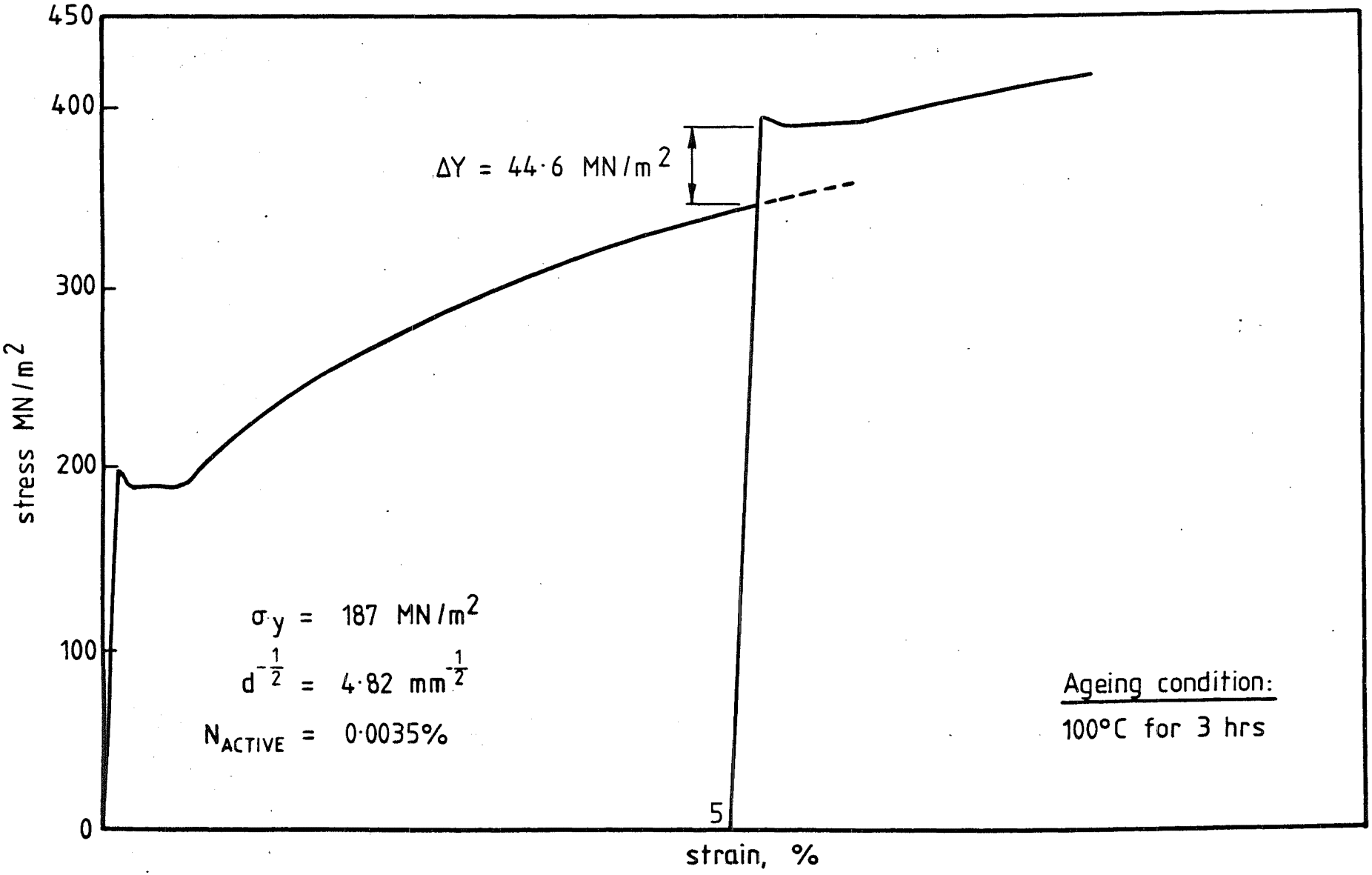

FIG. 7·9 STRESS-STRAIN OF STEEL B(5) BEFORE AND AFTER STRAIN-AGEING

hoped that this prior treatment would standardize conditions, making comparison of all the high (or low) nitrogen steels possible. It was, however, realised that complete locking of dislocations, as a result of this heat treatment, in the low nitrogen steels would be difficult.

Tensile tests were also done to ascertain the ageing propensities of the steels. After the initial treatment of 3 hours at 100°C, tensile specimens were strained 5% and then artificially aged at 100°C for 3 hours. A second test was then carried out to obtain the aged tensile curves and these are shown in Figs. 7.2 to 7.9.

It may be seen that all the eight steels showed a return of yield point after ageing. However, the ageing indices, ΔY, for the low nitrogen A steels were considerably smaller than those for the high nitrogen B steels. These results were correctly predicted by the nitrogen analysis in Section 7.1.

7.4 FATIGUE TESTS

Direct stress fatigue testing was carried out in an Amsler Vibrophore at a frequency of about 170 Hz. Sixteen specimens were prepared from each of the eight sets of steels for the determination of fatigue limits. Special specimens were prepared as shown in Fig. 7.10. This specimen shape gives a relatively low volume of highly stressed material and with the long shoulders, the elasticity of the specimen is increased. A high elasticity is necessary because the specimen forms part of the vibrating system and low carbon steel specimens have a very high damping capacity. This specimen shape was found to be satisfactory.

The screw heads of the specimen were turned in a lathe. These threads have been shown by the manufacturer of the machine to have excellent fatigue strength so that the ratio between the smallest diameter part of the test piece and the threaded core could be kept relatively low with central

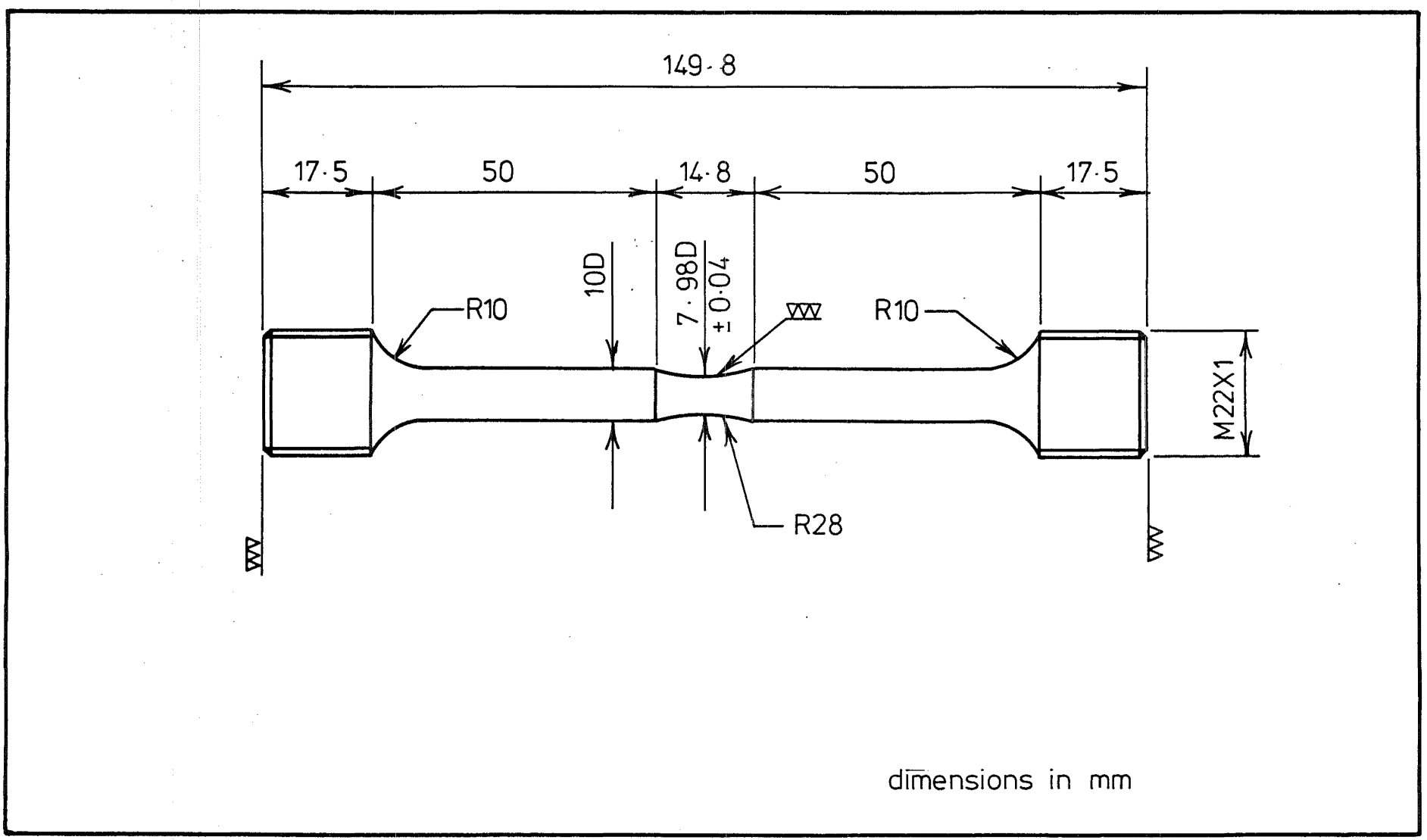

FIG 7·10 DIRECT STRESS SPECIMEN FOR AMSLER VIBROPHORE

fractures still being obtained in all tests. The screw heads of the specimens used were actually larger than that specified by Amsler in order to obtain better alignment. The ends of the specimens, which are the contact surfaces during the compression half cycles, were ground to ensure that they were perfectly flat and smooth and perpendicular to the specimen axis. The gauge length of the specimen was ground to shape before polishing. Polishing was first done longitudinally using Grade I emery paper, followed by 1/0 paper. 2/0 paper was then used to polish the specimen circumferentially and polishing was completed longitudinally using 3/0 emery paper.

Again, all fatigue specimens were aged at 100°C for three hours to achieve similar starting conditions as far as possible.

The machine was checked for its alignment before any tests were carried out. This was done by using a specimen with four strain gauges attached at 90°C to each other around the gauge length. The alignment of the machine was found to be better than 35 micro strain, which corresponded to a bending stress caused by this misalignment of less than 5% of the maximum stress used.

The positions of the crack initiation on all specimen surfaces relative to the machine were recorded and they indicated that there was no preferred position for a crack initiation. This further confirmed the good alignment of the direct stress machine.

All fatigue testings were carried out with zero mean stress and the fatigue limit of each set of steel determined using the staircase method as outlined in BS 3518. A description of the method, and the results, are given in Appendix B. The fatigue limits of these steels obtained by this method are tabulated in Table 7.2.

TABLE 7.2

TENSILE AND FATIGUE PROPERTIES AND GRAIN SIZE OF EXPERIMENTAL STEELS

Steel	Grain Size $d^{-\frac{1}{2}}$	Lower Yield Stress σ_y	Maximum Tensile Stress σ_{UTS}	Fatigue Limit σ_ℓ	$\frac{\sigma_y}{\sigma_\ell}$	$\frac{\sigma_{UTS}}{\sigma_\ell}$
	$mm^{-\frac{1}{2}}$	MN/m^2	MN/m^2	MN/m^2		
A(1)	8.58	260	420	183	1.42	2.30
A(2)	4.05	175	389	165	1.06	2.37
A(3)	3.83	155	371	164	0.95	2.26
B(1)	8.98	287	427	184	1.56	2.32
B(2)	6.77	218	410	179	1.22	2.29
B(3)	5.60	198	405	177	1.12	2.29
B(4)	5.07	192	403	178	1.08	2.26
B(5)	4.82	187	396	176	1.06	2.25

The relative values of the upper yield point, lower yield point and fatigue limit are shown in Figure 7.11 as a function of $d^{-\frac{1}{2}}$, where d is the grain diameter of the steel. The lower yield stress and the fatigue limit both obeyed the Hall-Petch type relationship and the A (low nitrogen) and B (high nitrogen) steels showed the dependence of fatigue limit (stress) on the active nitrogen content.

It is interesting to note that, although there is no apparent correlation between the lower yield stress and the fatigue limit of low carbon steels, a plot of $\frac{\sigma_y}{\sigma_\ell}$ against $d^{-\frac{1}{2}}$, where d is the grain size, yielded some form of relationship. This is shown in Figure 7.12. Published results are also shown in the figure and it may be seen that all the data appear to follow a similar trend. Assuming the simple linear relationship, a line of best fit was obtained using linear regression. This gave a correlation coefficient r of 0.95.

The good correlation between all the results is remarkable considering the fact that the results were obtained from steels of varying carbon content (0.08% - 0.16%), nitrogen content (0.0001% - 0.006%) and that the direct stress fatigue limits were determined using different test frequencies (30 Hz - 200 Hz). By extrapolating the line to intercept $d^{-\frac{1}{2}} = 0$, the $\frac{\sigma_y}{\sigma_\ell}$ ratio may be expressed in terms of $d^{-\frac{1}{2}}$ as

$$\frac{\sigma_y}{\sigma_\ell} = 0.65 + 0.09\, d^{-\frac{1}{2}}$$

The relationship between $\frac{\sigma_{UTS}}{\sigma_\ell}$ and grain size is shown in Figure 7.13. The results obtained from the experimental steels showed that $\sigma_{UTS} \approx 2.3\ \sigma_\ell$ irrespective of the free nitrogen content and grain size of the steel. However, not sufficient published data could be found to make such a generalisation for low carbon steel valid. The few results of other works quoted (Fig. 7.13) suggest that there might not be a general relationship.

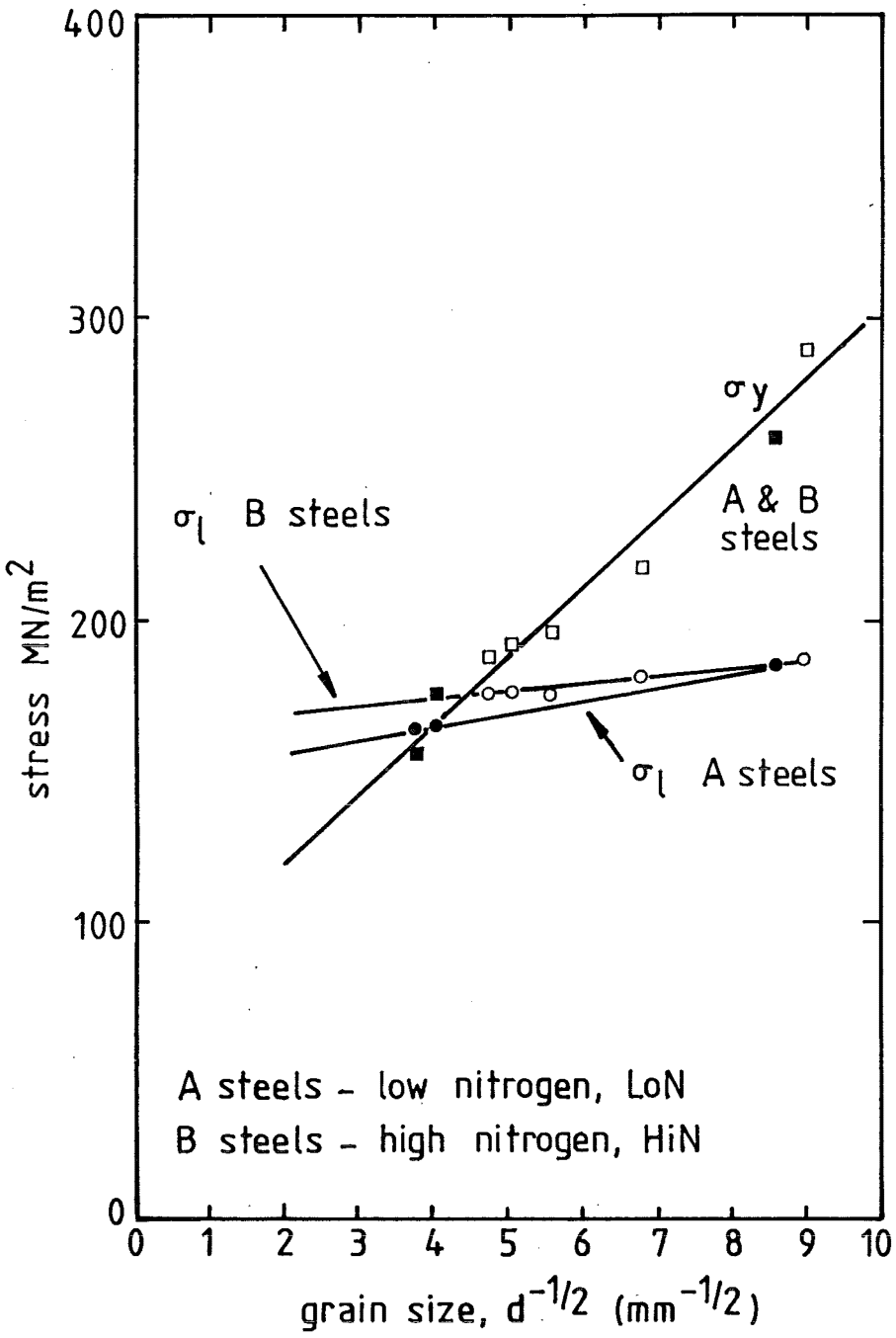

FIG. 7·11 EFFECTS OF FREE NITROGEN CONTENT AND GRAIN SIZE ON THE YIELD STRESS AND FATIGUE LIMIT OF LOW CARBON STEEL

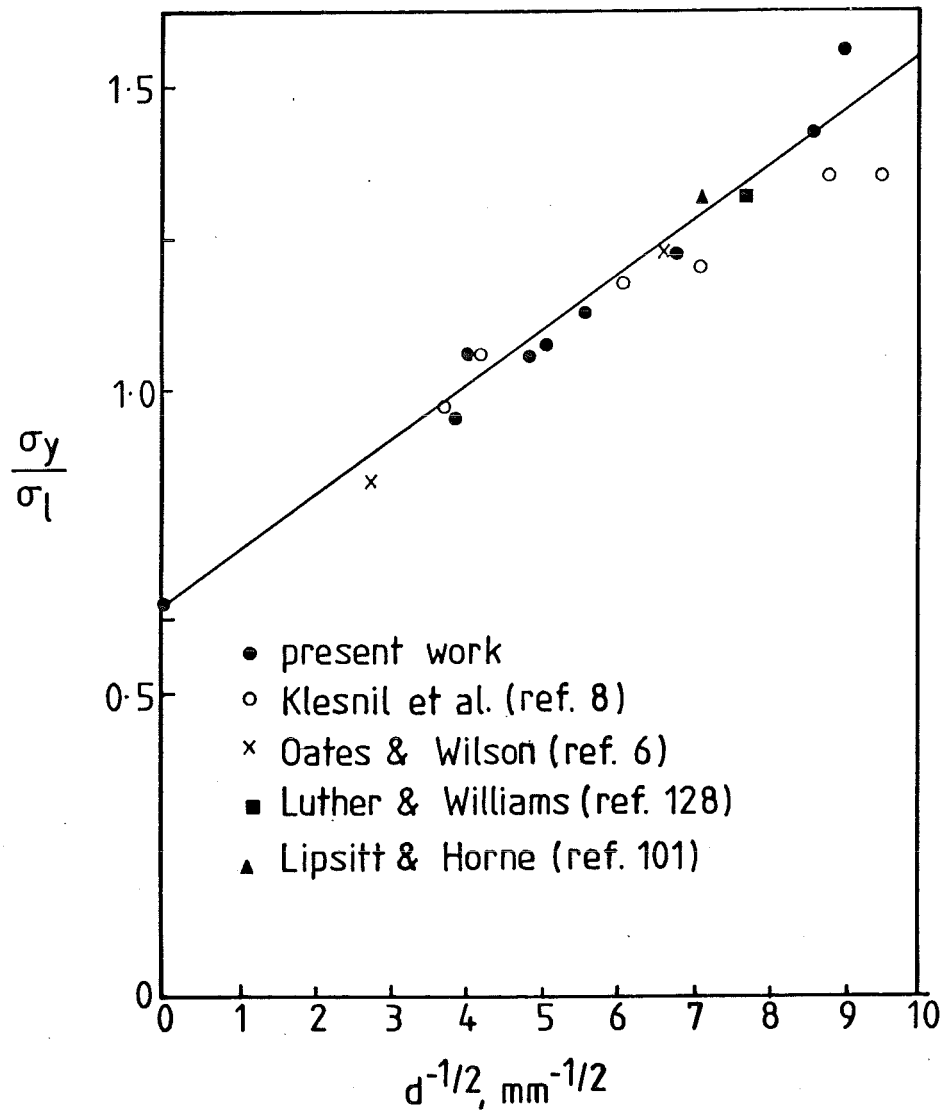

FIG. 7·12 INFLUENCE OF GRAIN SIZE ON THE YIELD STRESS/FATIGUE LIMIT RATIO OF LOW CARBON STEEL

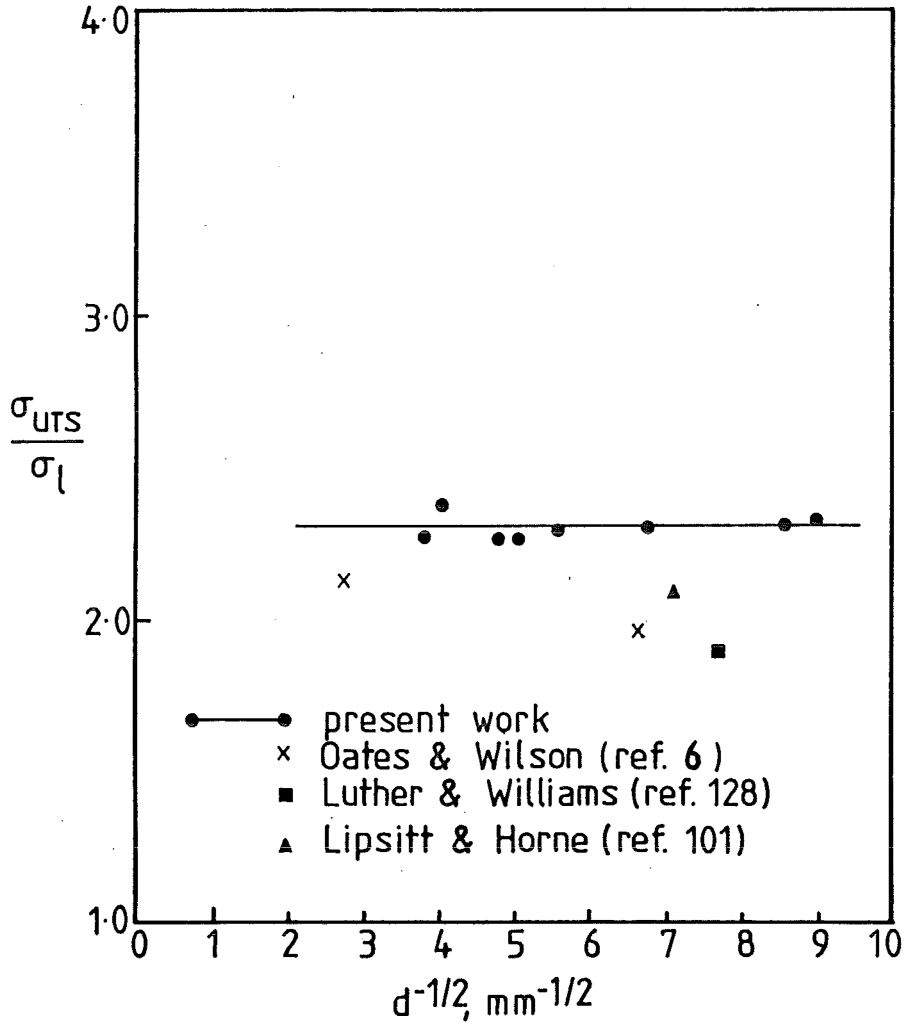

FIG. 7·13 INFLUENCE OF GRAIN SIZE ON MAX. TENSILE STRESS/FATIGUE LIMIT RATIO OF LOW CARBON STEEL

CHAPTER EIGHT

MONITORING FATIGUE DAMAGE, PROCEDURES AND RESULTS

8.1 DAMPING TESTS

8.1.1 Measurement of Specimen Damping

The operational principle of the Amsler High Frequency Vibrophore provides an ideal basis for damping measurement in that it involves vibration at the resonant frequency of the specimen/machine system.

The high frequency vibrophore operates as a 2-mass system linked together by the specimen, see Figure 8.1. The active masses are the main mass m_1, and opposing mass, m_2. The latter is the machine base and is supported flexibly on springs. The elastic element of the vibrating system is made up of the specimen and the load cell. The natural frequency of the system is established by the magnitudes of the masses m_1 and m_2, and the spring constants of the specimen and load cell. An electromagnetic actuator ensures that the machine will always be excited at this frequency and the damping losses are replaced to maintain a constant load amplitude. The electronic load cell measures the amplitude of the dynamic load and a feedback system controls the actuator, thus completing a closed loop control system.

The system may be represented by a diagram as shown in Figure 8.2. When the machine is switched off, the vibration of the system will die down, the decay being described by a negative exponential curve of the form (this is assuming a single degree of freedom system since $m_2 \gg m_1$, and the vibration of m_2 is small), [176],

$$\sigma(t) = \sigma_{max}\, e^{-\delta t} \sin(\omega_d t + \phi) \qquad \text{Equation (8.1)}$$

where $\sigma(t)$ = instantaneous stress amplitude, time dependent

σ_{max} = maximum stress amplitude

δ = logarithmic decrement

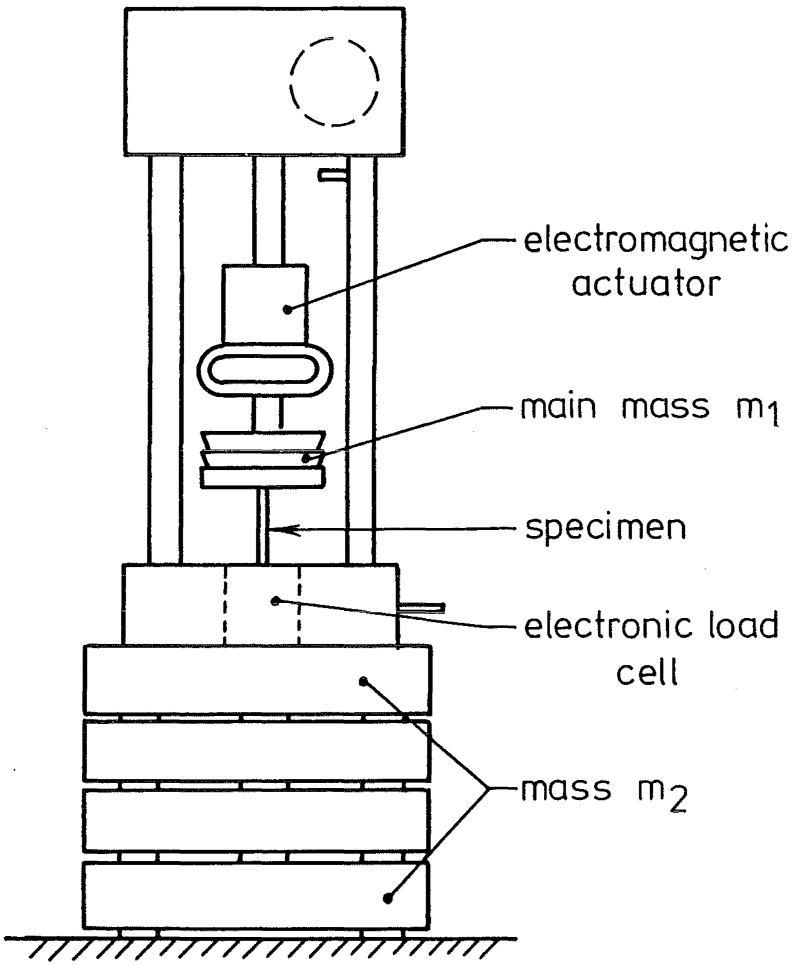

FIG. 8·1 SCHEMATIC DIAGRAM OF AMSLER HIGH FREQUENCY VIBROPHORE

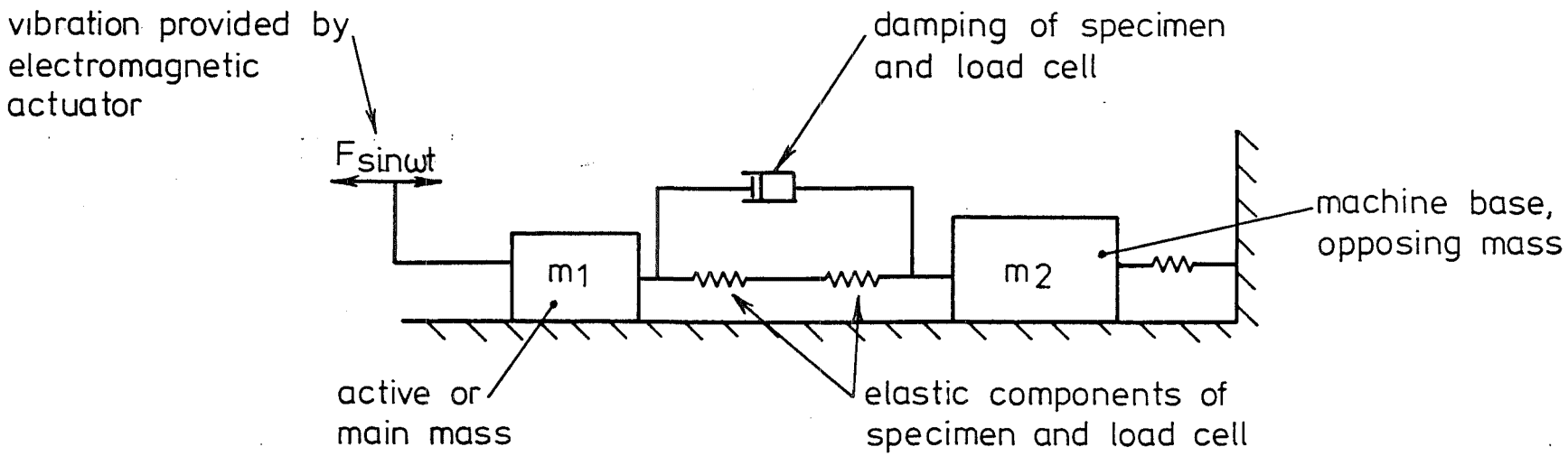

FIG 8·2 SCHEMATIC REPRESENTATION OF THE AMSLER VIBRATING SYSTEM

ω_d = damped natural frequency

t = time

ϕ = phase angle

Figure 8.3 shows the waveform of the stress as the vibration gradually reduces to zero.

Consider the maximum stress amplitude of two successive cycles, at times t_1 and t_2

$$\sigma_1(t_1) = \sigma_{max}\, e^{-\delta t_1} \sin(\omega_d t_1 + \phi) \qquad \text{Equation (8.2)}$$

$$\sigma_2(t_2) = \sigma_{max}\, e^{-\delta t_2} \sin(\omega_d t_2 + \phi) \qquad \text{Equation (8.3)}$$

$$\therefore \quad \frac{\sigma_1(t_1)}{\sigma_2(t_2)} = \frac{\sigma_{max}\, e^{-\delta t_1} \sin(\omega_d t_1 + \phi)}{\sigma_{max}\, e^{-\delta t_2} \sin(\omega_d t_2 + \phi)}$$

$$= \frac{e^{-\delta t_1}}{e^{-\delta t_2}}$$

$$= e^{-\delta(t_1 - t_2)} \qquad \text{Equation (8.4)}$$

But $t_2 = t_1 + T$ where T, a constant, is the period of the vibration

$$\therefore \quad \delta = \frac{1}{T} \ln\left(\frac{\sigma_1}{\sigma_2}\right) \qquad \text{Equation (8.5)}$$

δ, the logarithmic decrement, is a measure of the damping capacity of the material. If δ is small, Equation (8.5) indicates that the ratio $\frac{\sigma_1}{\sigma_2}$ is small, thus the damping is low. Conversely, a large value of δ indicates a case of high damping.

Since the damping of a system represented by Equation (8.1) is provided

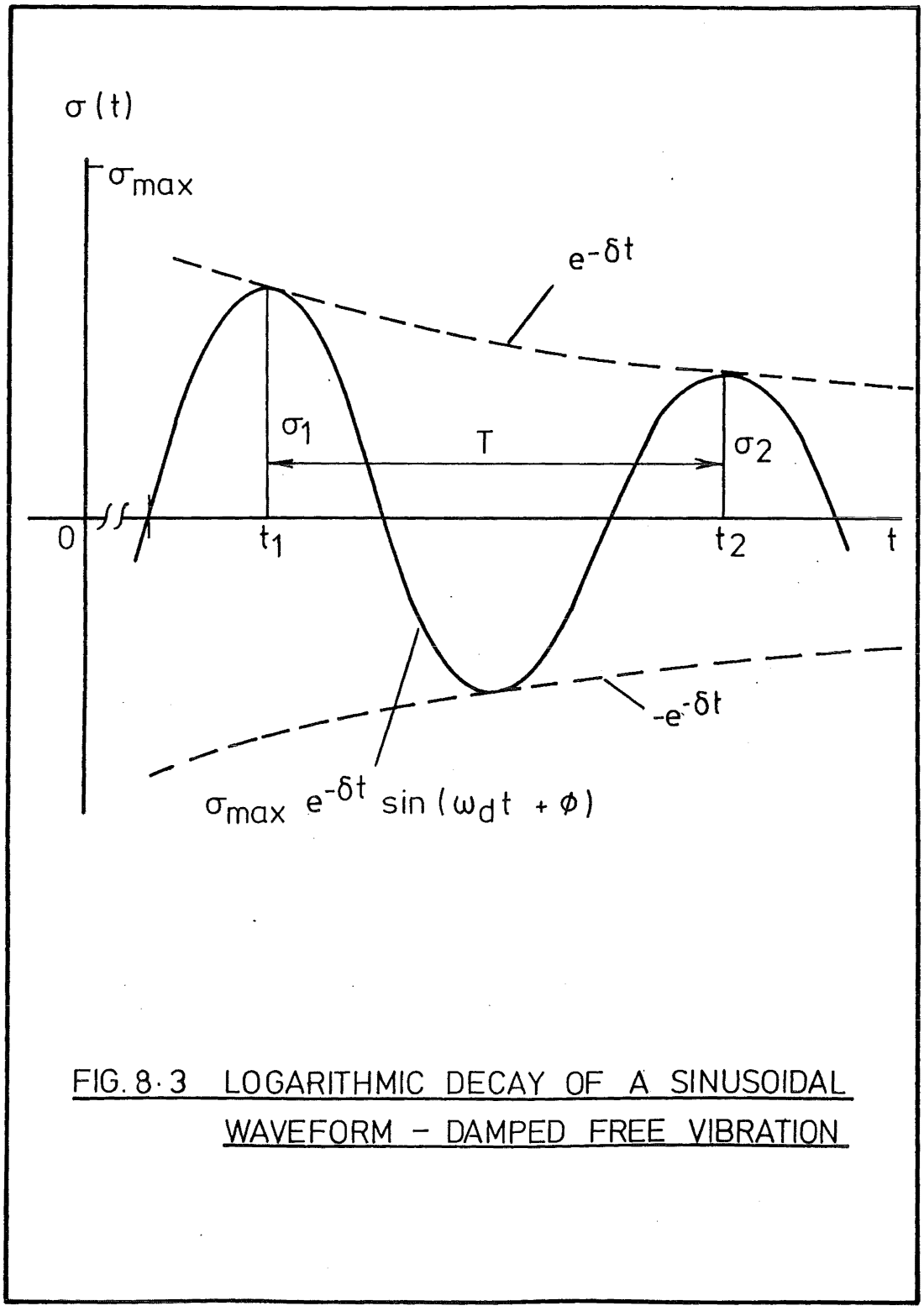

FIG. 8·3 LOGARITHMIC DECAY OF A SINUSOIDAL WAVEFORM – DAMPED FREE VIBRATION

by the specimen and the load cell, and that the damping of the load cell is constant, any change in damping can be attributed to the damping changes of the specimen alone.

The method of recording the decaying waveform employed to obtain values of δ of the specimen used the output signal from the alternating load unit of the Amsler Control console. When the machine was switched off, a signal was triggered off in the oscilloscope and the decaying waveform was recorded on the storage oscilloscope screen. A photograph was immediately taken of the waveform and from it, the δ value of the waveform was easily calculated.

8.1.2 Damping Measurement Specimens

The specimens used were slightly different from those used for the determination of fatigue limits. Instead of a continuous curve gauge length, these specimens had a parallel section gauge length, see Figure 8.4. The reason for introducing a longer gauge length was to increase the bar volume under maximum stress and so achieve higher damping. Higher damping values were required in this case to make measurement easier and more accurate.

All specimens were aged at 100°C for three hours in order to achieve similar initial conditions as far as possible (see Section 7.3). The specimens were then polished with emery paper and the polishing was finished with 3/0 emery paper, longitudinally.

8.1.3 Testing Procedures

Four groups of steels were tested for their damping behaviour during fatigue. These were steels A(1) and A(3) [low free nitrogen, fine and coarse grained steels] and steels B(1) and B(5) [high free nitrogen, fine and coarse grained steels - refer to Tables 7.1 and 7.2]. For each group, damping changes of specimens tested at different stress levels were recorded. For each specimen, the damping behaviour was studied by obtaining its logarithmic decrement values at various stages of a test. Thus, if the

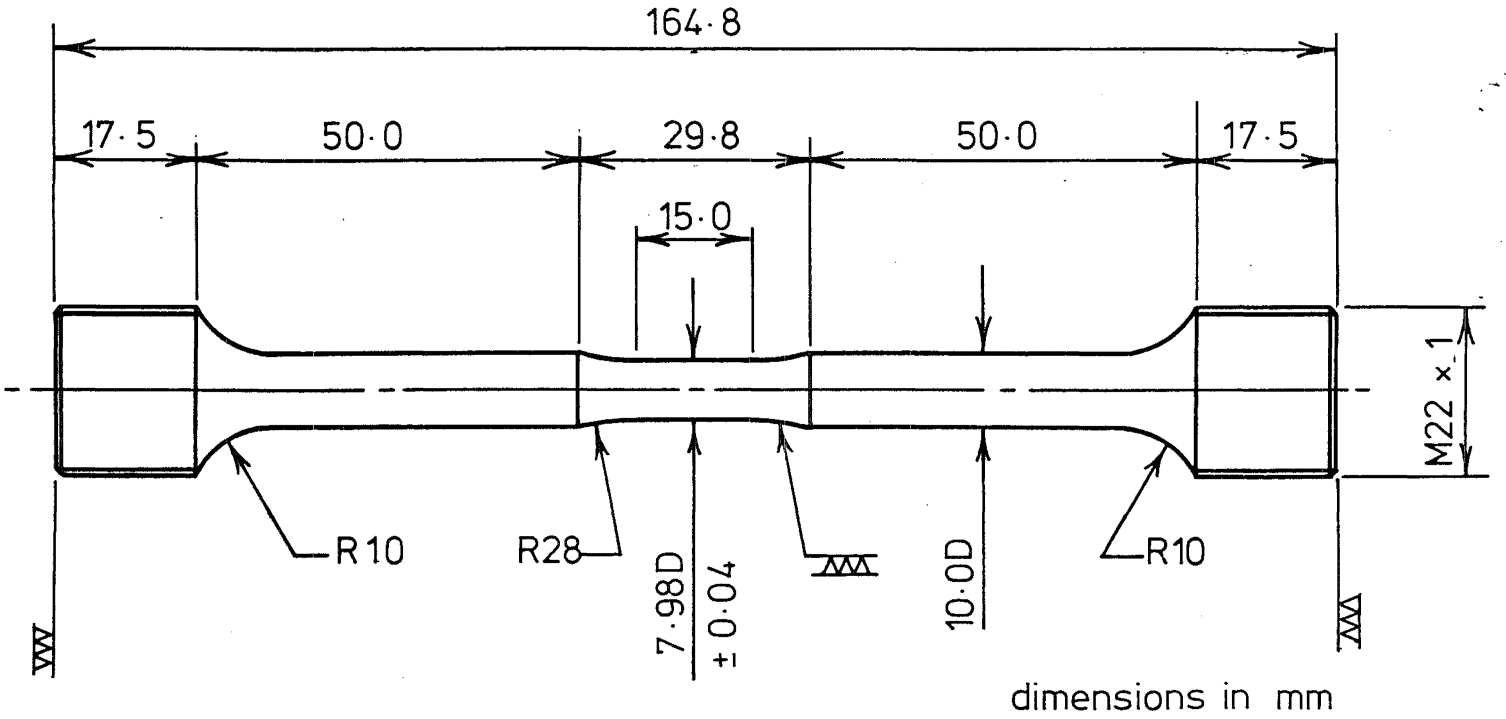

FIG. 8·4 DIRECT STRESS FATIGUE SPECIMEN FOR THE AMSLER AND INSTRON MACHINES.

specimen had undergone some changes, for example, plastic deformation, the change would be indicated by a change in the logarithmic decrement. A measurement was taken as soon as the machine had been started and the load stabilised. Thereafter, readings were taken at intervals until the specimen ran out at 5×10^7 cycles. For comparison purposes, all values of δ were divided by the first value obtained, δ_o. The reason for this normalisation of values is because it was realised that the steels were not in similar initial condition prior to testing, i.e., because of the different heat treatments and free nitrogen contents, the steels would still have different initial dislocation densities despite a three-hour ageing treatment at 100°C prior to testing. The absolute values were not important in this case, only the relative values, hence all δ values were divided by δ_o.

8.1.4 Damping Test Results

The damping test results are presented in Figures 8.5 - 8.8 as graphs of $(\frac{\delta}{\delta_o})$ versus log (number of cycles). δ_o, the first value recorded was taken at $N = 10^4$ and hence all the graphs started from $N = 10^4$. This was necessary since the vibrophore operates at high frequency and 10^4 cycles was reached in less than one minute after the machine was switched on. Because some time was required for load to stabilise, it was decided that readings taken too soon would not be accurate. $N = 10^4$ was thus chosen to represent the starting value. All the damping tests were conducted at stress levels below the direct stress fatigue limit.

Steel A(1) - Low Nitrogen Fine Grained, Figure 8.5.

At a stress amplitude of 145 MN/m^2, no significant change in the specimen damping was recorded throughout the entire test run of 5×10^7 cycles. Similarly, at 150 MN/m^2, the specimen damping remained unaltered.

At 155 MN/m^2, a slight decrease in damping was noted early on but this was followed at $N \approx 6 \times 10^5$ by a large increase. The onset of this increase

was rapid and a steady damping value was reached after the rapid increase. The damping value remained high until the test was stopped at 5×10^7 cycles with no failure.

Thus, for this steel 155 MN/m^2 appears to be the limiting stress, below which the damping of the specimen remained virtually constant even with prolonged cycling. We shall refer to this as the "critical damping stress", σ_{CD}, and cycling at σ_{CD} caused a large and sudden increase in the specimen damping capacity. Since damping increase implies softening and hence a larger strain amplitude, it is related to dislocation movement and σ_{CD} can be regarded as the minimum stress amplitude required to cause dislocation movement on a large scale. Because mobile dislocations are required for dislocation motion, it may be assumed that cycling at σ_{CD} causes significant dislocation generations.

Steel A(3) - Low Nitrogen Coarse Grained - Figure 8.6.

At 145 MN/m^2, no increase in damping was recorded although there appeared to be a slight decrease towards the end of the test.

At 150 MN/m^2, the steel showed a slight decrease in damping in the early part of the test. A rise was recorded from about $N = 10^6$ cycles and the rise was steady and relatively slow compared to that for steel A(1). After reaching the maximum value at $N = 10^7$ the damping remained constant for the last 80% of the test run.

σ_{CD} for this steel was thus established at 150 MN/m^2.

Steel B(1) - High Nitrogen Fine Grained - Figure 8.7.

A feature of the results of this group of steel is that at all the stress levels used, the steel showed an initial hardening stage. The decrease in damping was recorded before 5×10^5 cycles in all cases. At 155 MN/m^2, the steel, after showing the initial hardening, returned to its original state and at the end of the test, no apparent change was noticeable.

However, at 160 MN/m^2, after the initial drop in damping, a rapid increase was recorded after about 3×10^6 cycles of loading. The maximum was reached in a very short period of time and thereafter the damping remained constant until run out.

Cycling at 165 MN/m^2 produced a similar effect, but the damping rise was recorded earlier on in the test, after about 7×10^5 cycles. The maximum damping reached was virtually the same as in the previous case.

σ_{CD} for this steel was consequently taken as 160 MN/m^2.

Steel B(5) - High Nitrogen Coarse Grained - Fig. 8.8

As for the case of Steel B(1), this steel showed initial hardening (indicated by a decrease in damping) during the test, but this occurred at a later stage than that of Steel B(1).

Fatigue cycling at 145 MN/m^2 caused a slight drop in damping which was insignificant. At higher stresses, however, damping increases were recorded after the initial drop, with the maximum damping attained being higher with increasing stress amplitude. It is surprising that the rise at 155 MN/m^2 occurred earlier than that at 160 MN/m^2.

σ_{CD} for steel B(5) was 150 MN/m^2.

Comparing the results, it may be seen that σ_{CD} was better defined for fine grained steels than for coarse grained steels. The damping increase was much larger in magnitude for the fine grained steels, indicating that dislocation generation was on a larger scale in the fine grained steels.

It may be seen from the damping measurements (Figures 8.5 - 8.8) that in all cases where a rise in damping was recorded, the steels' damping capacity remained high throughout the tests. In other words, these measurements indicated only softening during fatigue. Since low carbon steels are known to be capable of hardening after initial softening[8,136],

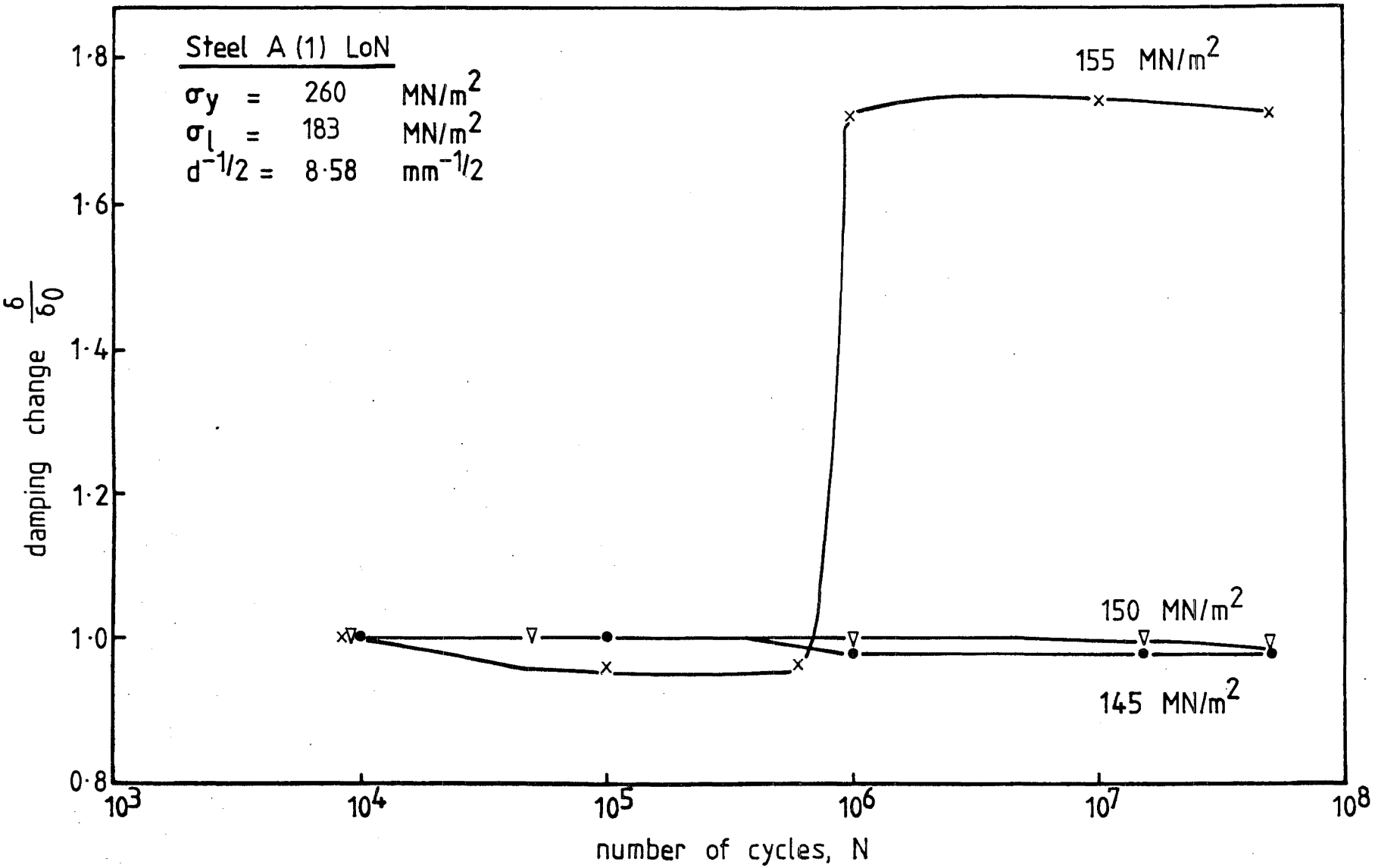

FIG 8·5 EFFECT OF CYCLIC STRESS ON DAMPING OF STEEL A (1)

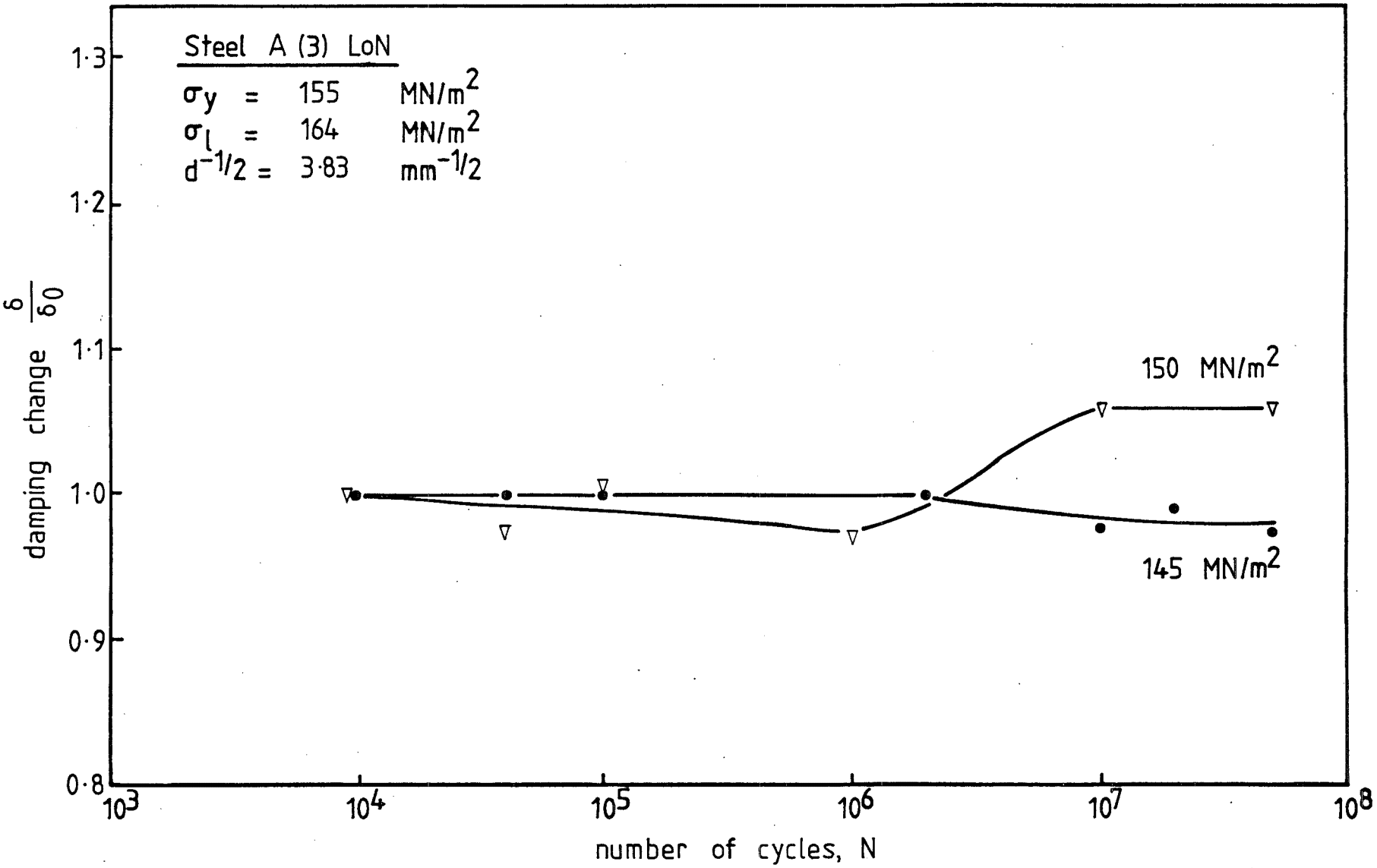

FIG 8·6 EFFECT OF CYCLIC STRESS ON DAMPING OF STEEL A (3)

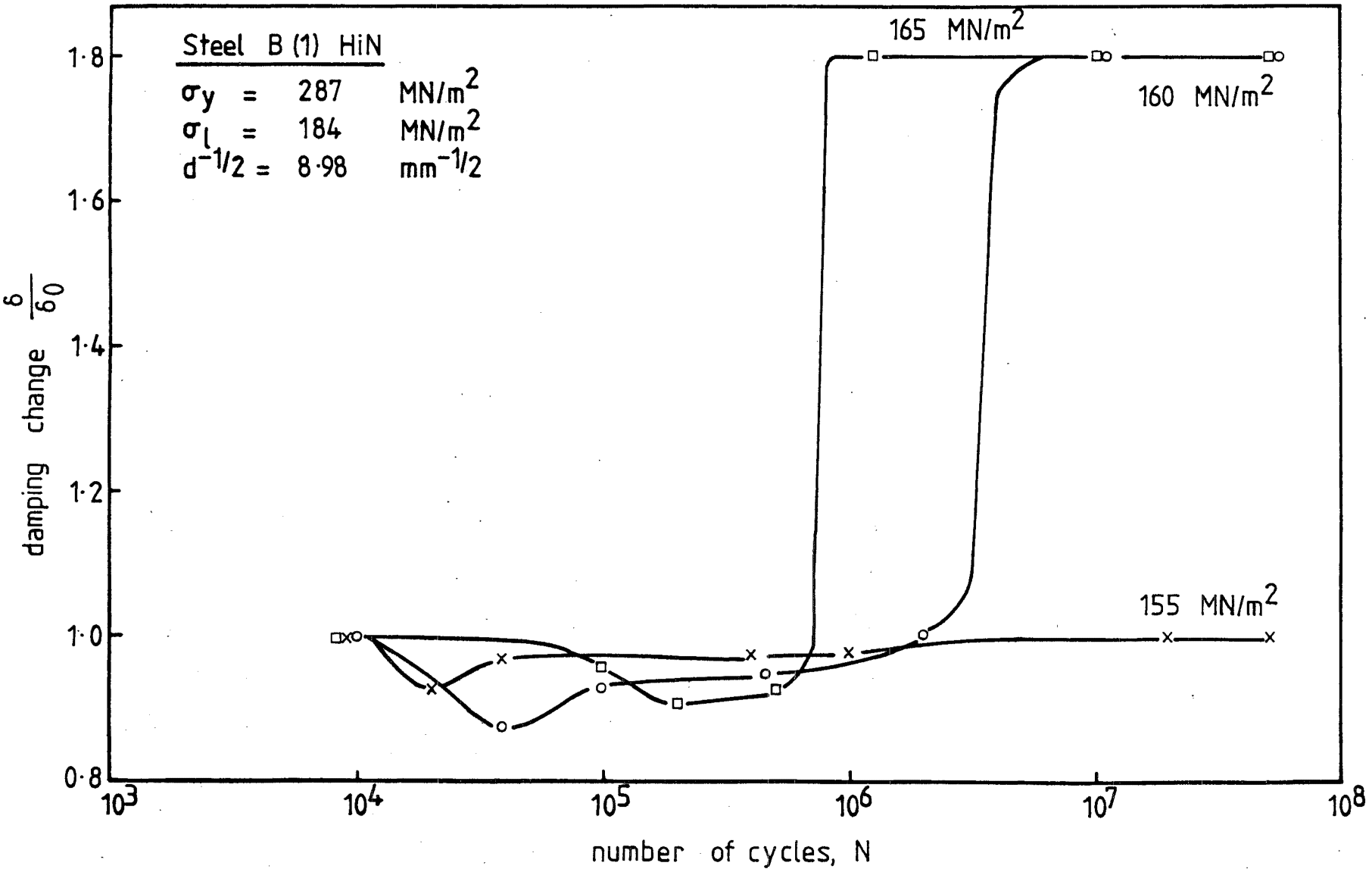

FIG. 8·7 EFFECT OF CYCLIC STRESS ON DAMPING OF STEEL B (1)

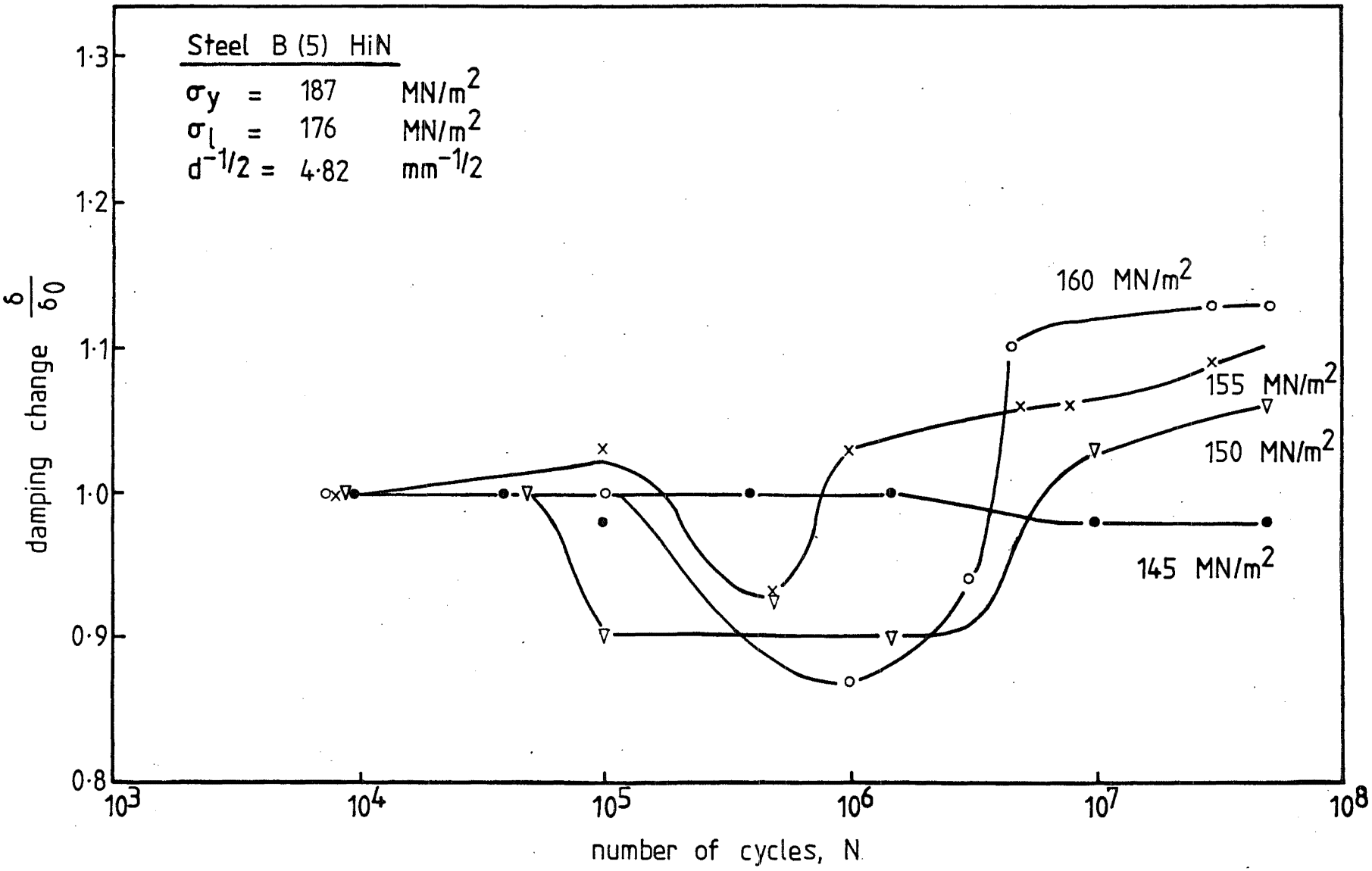

FIG. 8·8 EFFECT OF CYCLIC STRESS ON DAMPING OF STEEL B (5)

it is possible that hardening was not indicated by the damping measurements. This may be due to the high operating frequency used which caused rapid damping energy generation. If the energy dissipation was slower than its generation, then hardening, indicated by a drop in damping energy, would not be indicated.

The initial decrease in damping for the high nitrogen steels B(1) and B(5) may be due to a gradual relocking of dislocations by nitrogen, since this ageing was not observed in the A steels with lower active nitrogen content. It would suggest that the pre-ageing treatment (at 100°C for 3 hours) did not cause complete locking of all the mobile dislocations in the B steels. This is surprising since the B steels contained high levels of active nitrogen.

These damping results agree in some respects with the work of Klesnil *et al*[8] on their fine grained steel where they measured the strain amplitude of a specimen under constant stress amplitude fatigue. In each case, a limiting stress which was necessary for softening to occur, was established. However, while Klesnil *et al*[8] found that such a limiting stress existed only for fine grained steel and that it was above the direct stress fatigue limit, the results here show that limiting stresses existed for both fine and coarse grained steels, and that they were about 10-15% below the fatigue limit.

8.2 TEMPERATURE MONITORING

Temperature rises of fatigue specimens were also recorded for the four steels fatigued at different stress levels. The temperature change was measured by a differential thermocouple comprising two Philips PR 6462B/60 thermocouples with Ni-NiCr elements. One thermocouple was attached to the specimen gauge length with PVC tape and the reference thermocouple, connected in series to the main thermocouple to compensate for room temperature

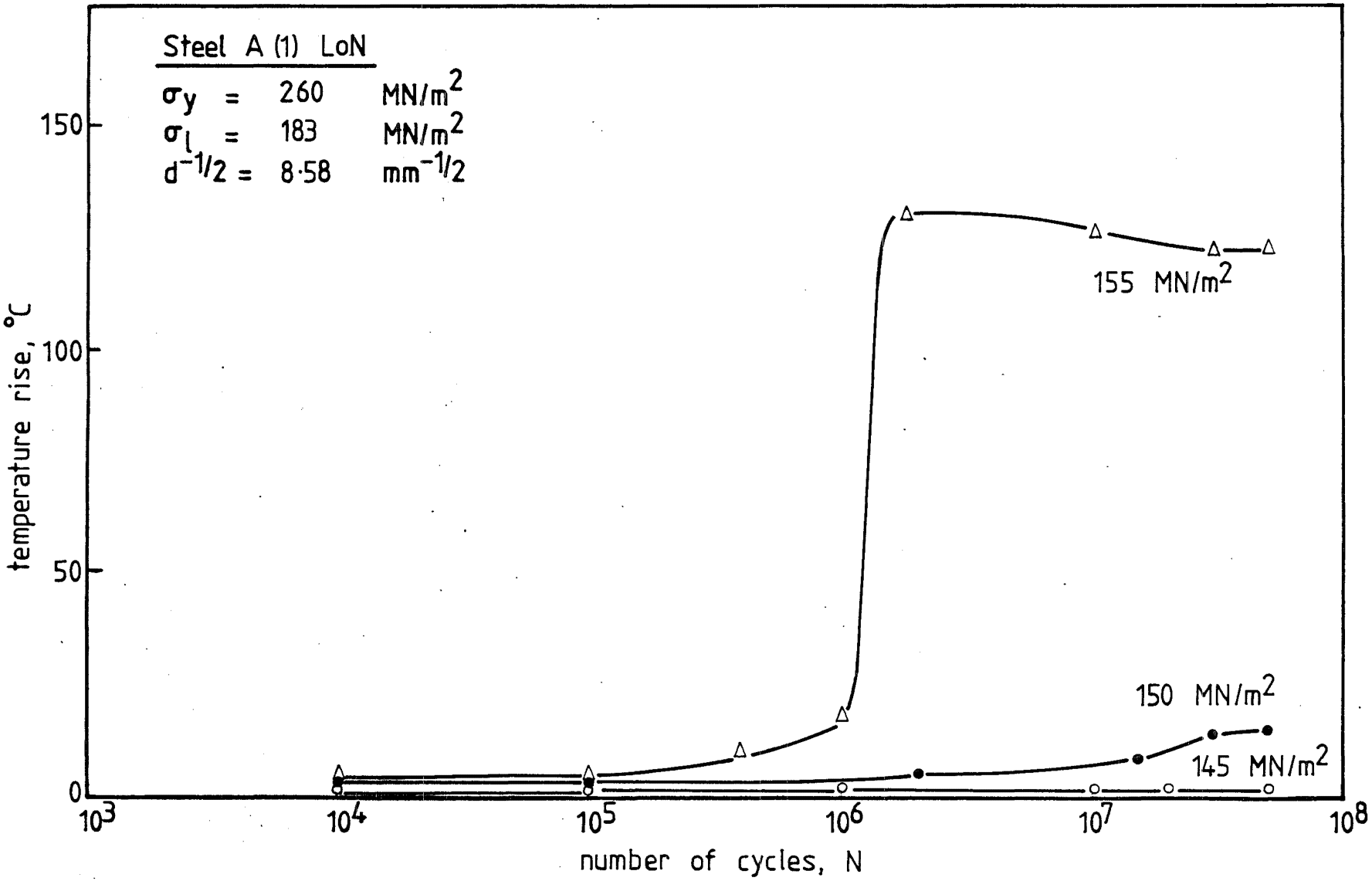

FIG. 8·9 EFFECT OF CYCLIC STRESS ON TEMPERATURE RISE OF STEEL A (1)

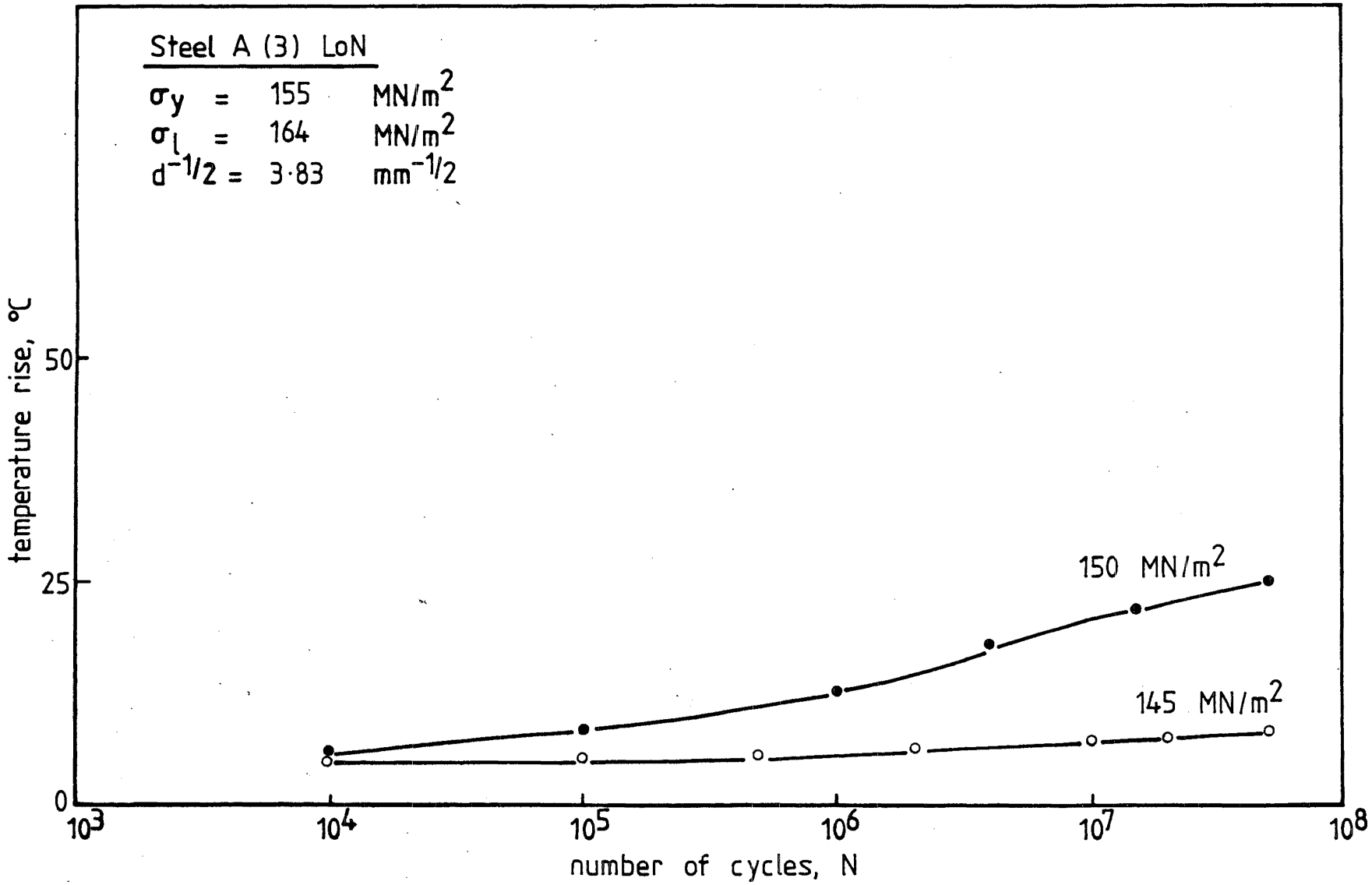

FIG. 8·10 EFFECT OF CYCLIC STRESS ON TEMPERATURE RISE OF STEEL A (3)

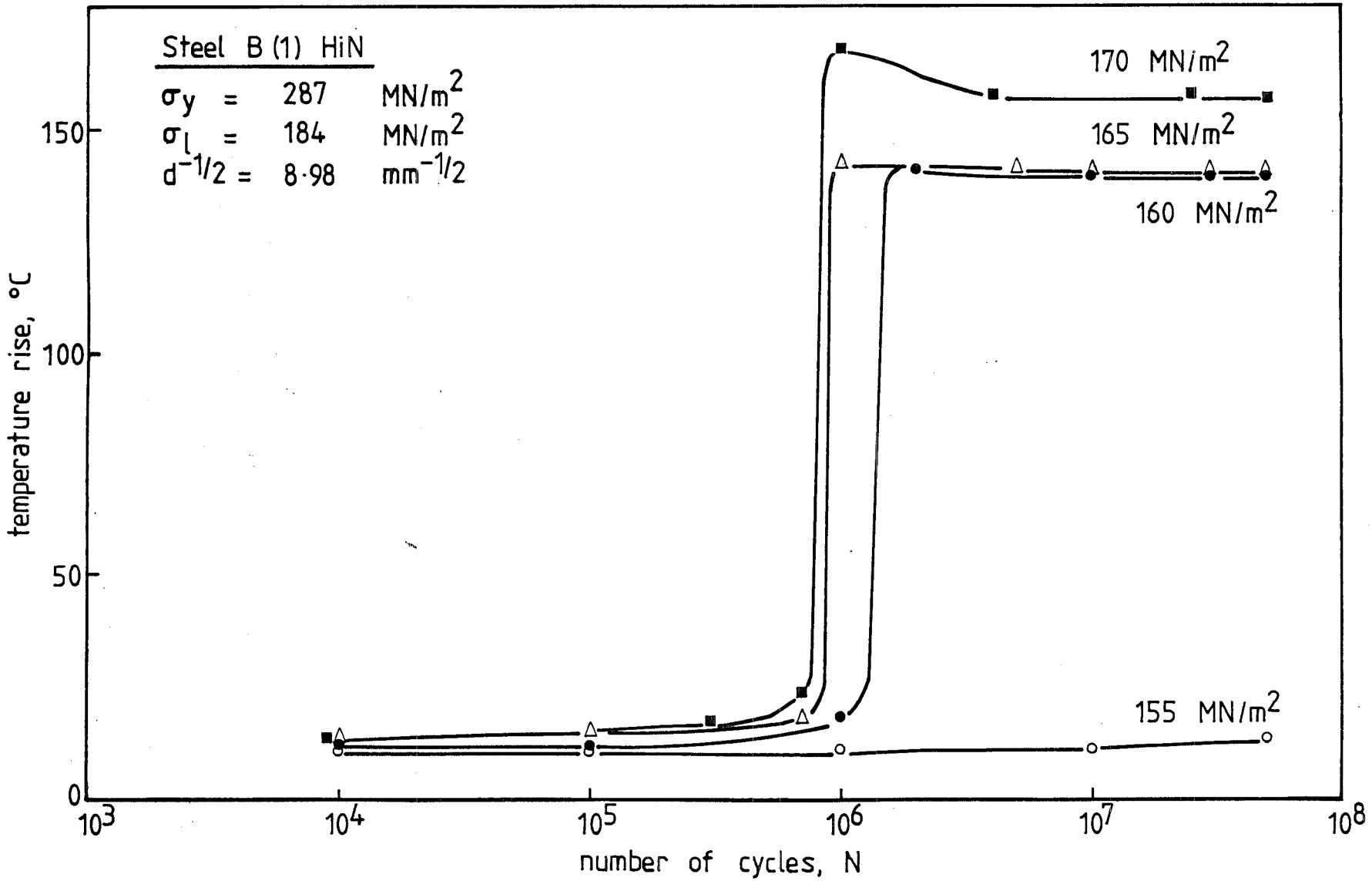

FIG. 8·11 EFFECT OF CYCLIC STRESS ON TEMPERATURE RISE OF STEEL B (1)

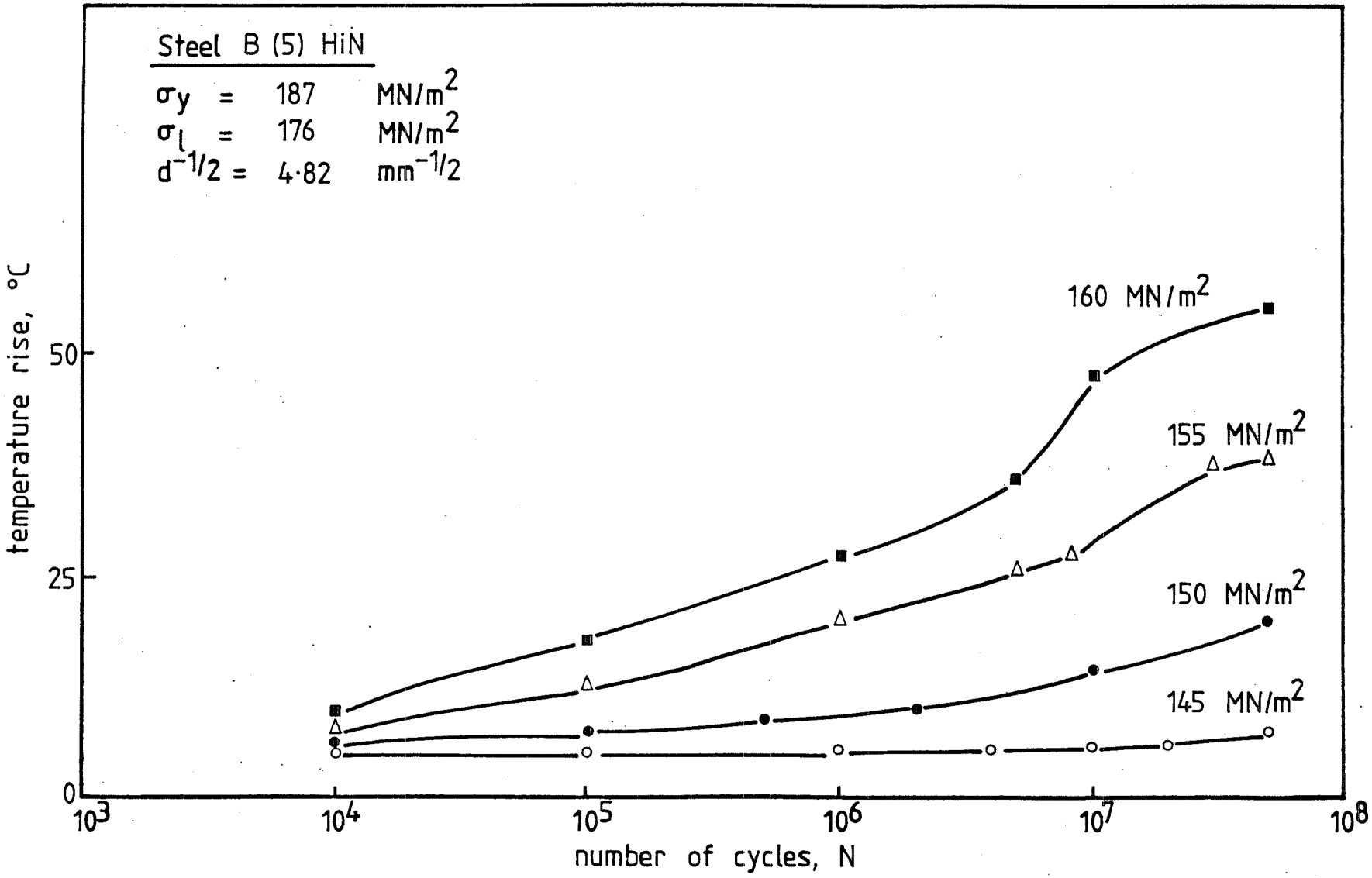

FIG. 8·12 EFFECT OF CYCLIC STRESS ON TEMPERATURE RISE OF STEEL B (5)

fluctuation, was attached to the fatigue machine.

The temperature curves for the four steels are shown in Figures 8.9 - 8.12. As expected, the results indicated by these measurements agree well with those obtained using damping capacity. In all cases, cycling at stresses below σ_{CD} produced a temperature rise of less than 4°C. For the coarse grained steels A(3) and B(5), cyclic stressing at σ_{CD} produced a temperature rise of about 20°C at the end of the test and in all cases where the stress was at or above σ_{CD}, the temperature did not reach a constant value, i.e., it was still increasing at the end of the test.

The fine grained steels, however, produced large temperature increments (~150°C) when cycled at σ_{CD} or above. The temperature rise was rapid and was completed within a few thousand cycles (i.e., less than a minute of testing time). As in the case for damping, hardening was not depicted by the temperature curves.

The damping and temperature curves were obtained from different specimens; this explains why the temperature and damping rise occurred, in some cases, at a different number of cycles for the same steel fatigued at the same stress amplitude, e.g., Steel A(1) at 155 MN/m^2; B(1) at 160 MN/m^2.

8.3 THE EFFECT OF DIRECT STRESS FATIGUE ON TENSILE PROPERTIES

To investigate the significance of the critical damping stress further, specimens of the type shown in Figure 8.4 were fatigued at various stress levels near σ_{CD} and then tested in tension. All specimens were run to 5×10^7 cycles at ~170 Hz.

Tensile testing was carried out using the 250 kN Instron Universal Testing machine at a strain rate of about 2×10^{-4}/sec. Special adaptors were made for specimen gripping so that the self-aligning hemispherical head attachment of the Instron could be used. To check the specimen

alignment, three strain gauges were attached to a specimen at 120° apart around the gauge length circumference. The maximum error due to misalignment was found to be not more than 3% and the specimen gripping method was considered satisfactory.

8.3.1 The Effect of Cyclic Pre-Stress Amplitude

The results of these tests are shown in Figures 8.13 - 8.16.

Steel A(1) - LoN - Figure 8.13

For steel A(1), cyclic pre-stressing at 145 MN/m^2, i.e. below σ_{CD}, did not have any significant effect on the tensile properties of the steel. Both the yield drop and Luders strain remained and there was no hardening. At 150 MN/m^2, the Luders strain was not distinct, and there was still some indication of a drop; some strain hardening was noticed. At 155 MN/m^2, the stress-strain curve was completely smooth and substantial hardening was produced by the cyclic pre-stress.

The partial removal of the discontinuous yield point suggests that mobile dislocations were generated by fatigue cycling and that little hardening was achieved implied minimal dynamic ageing or cyclic strain hardening. Comparing the curves for stresses at 150 MN/m^2 and 155 MN/m^2, it appears that the true value of σ_{CD} was probably slightly below 155 MN/m^2.

Steel A(3) - LoN - Figure 8.14

The yield drop was removed when steel A(3) was cyclic pre-stressed at 145 MN/m^2, but part of the Luders strain was still retained and insignificant hardening resulted. When fatigue at 150 MN/m^2, i.e. σ_{CD}, a smooth tensile curve was obtained and some hardening was clearly noticeable. However, the amount of hardening gained was less than that for steel A(1). Raising the stress to 160 MN/m^2 produced a similar result, but the gain in hardening was small.

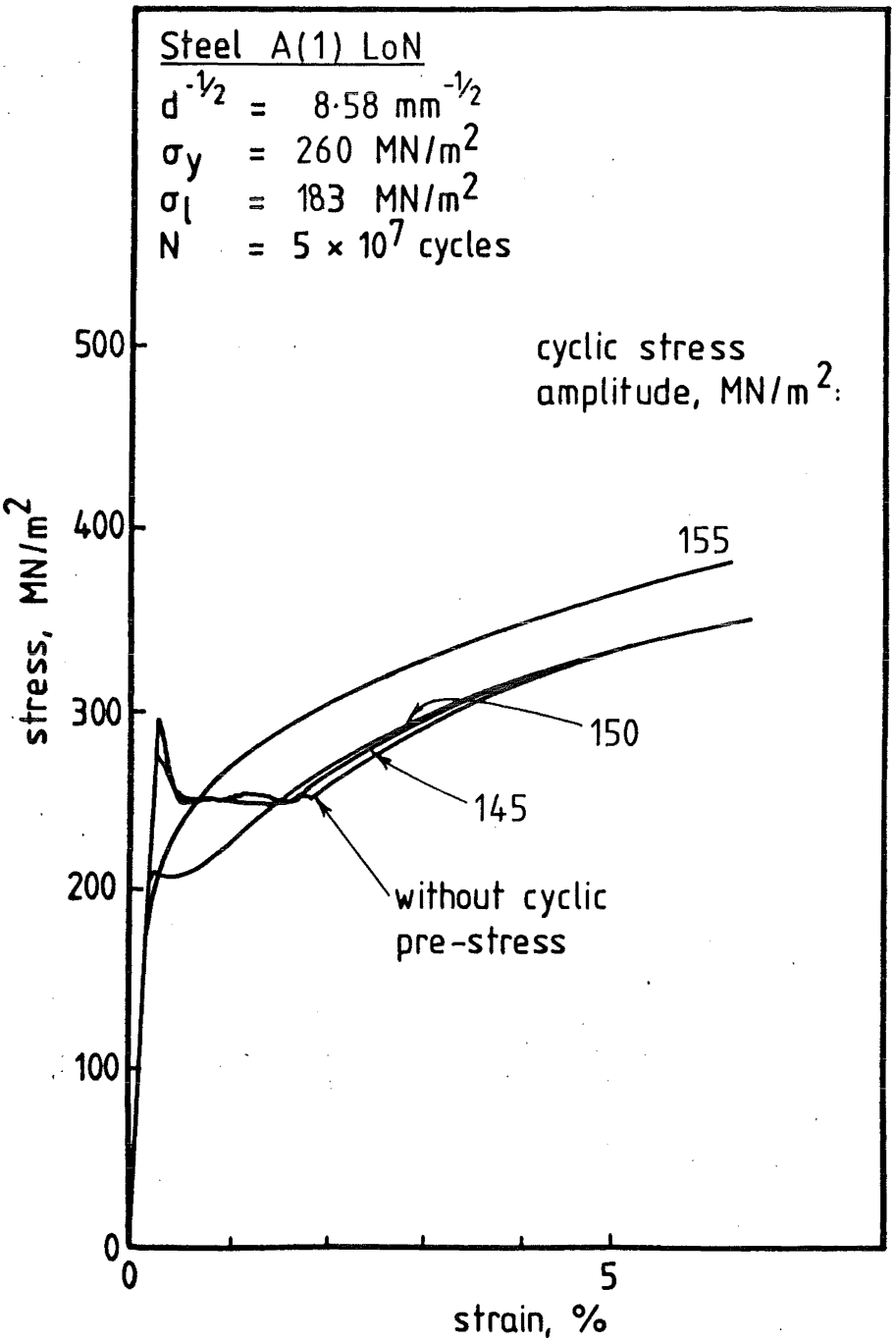

FIG. 8·13 EFFECTS OF CYCLIC PRE-STRESS ON THE TENSILE CURVES OF STEEL A(1)

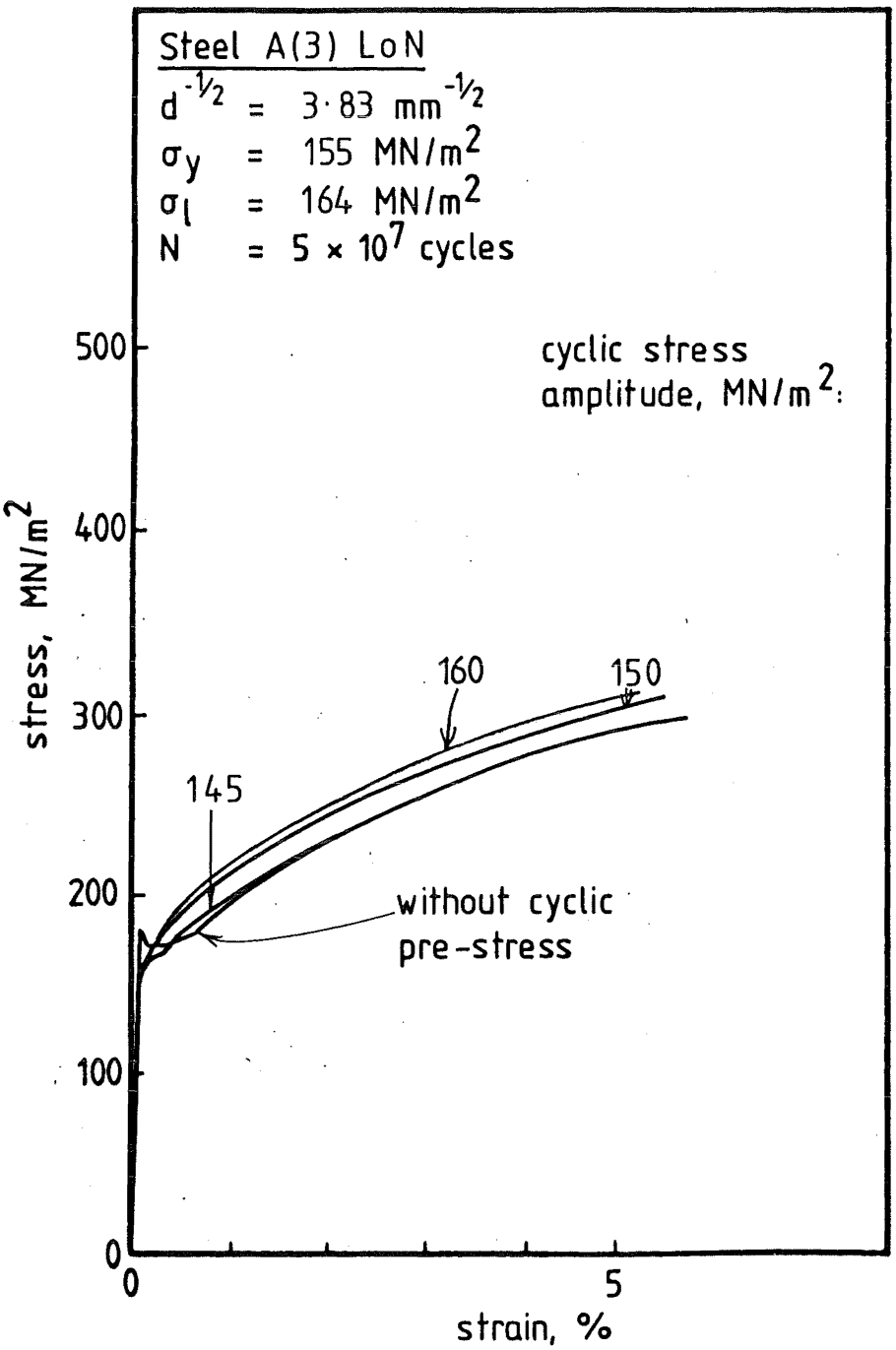

FIG. 8·14 EFFECTS OF CYCLIC PRE-STRESS ON THE TENSILE CURVES OF STEEL A(3)

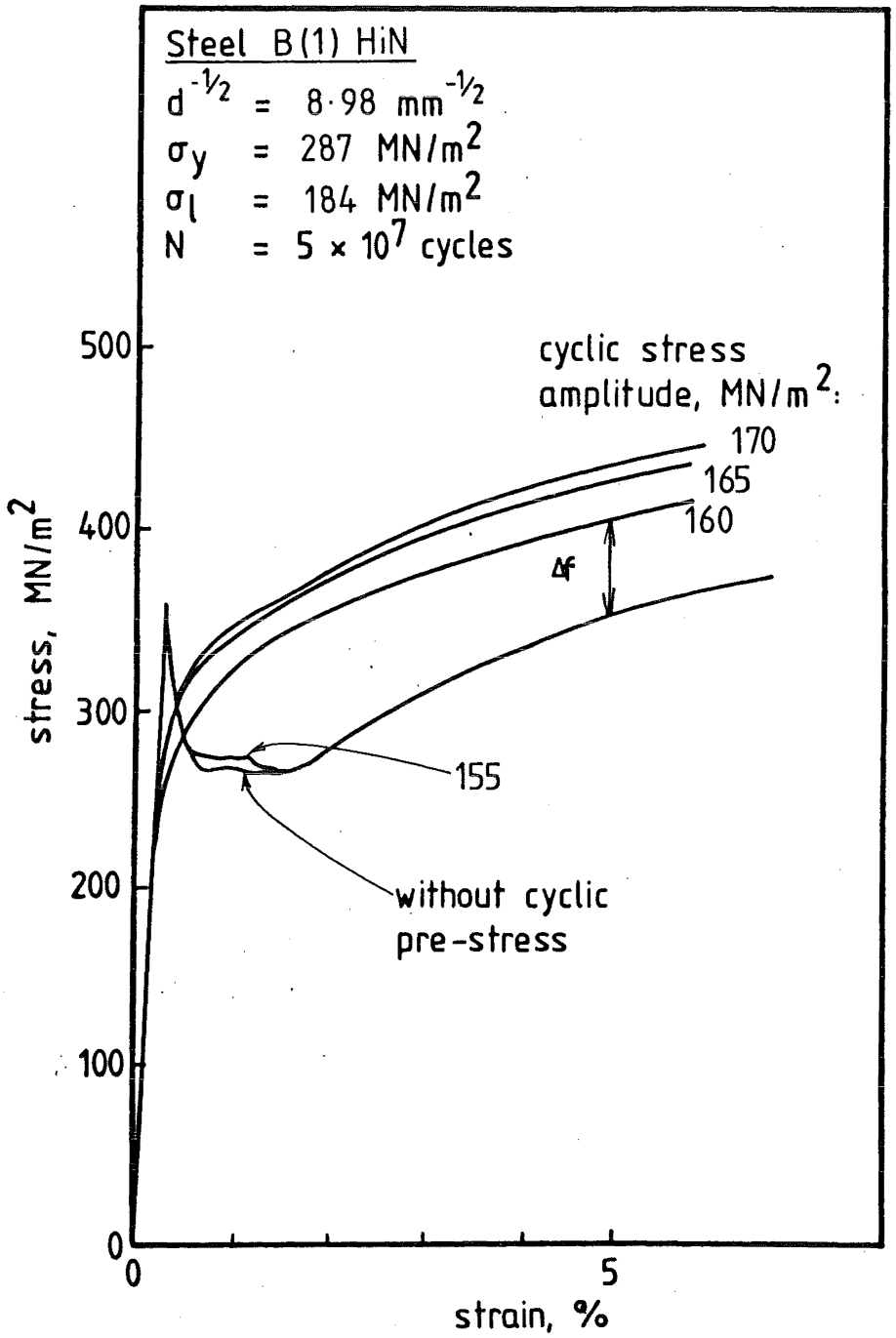

FIG. 8·15 EFFECTS OF CYCLIC PRE-STRESS ON THE TENSILE CURVES OF STEEL B(1)

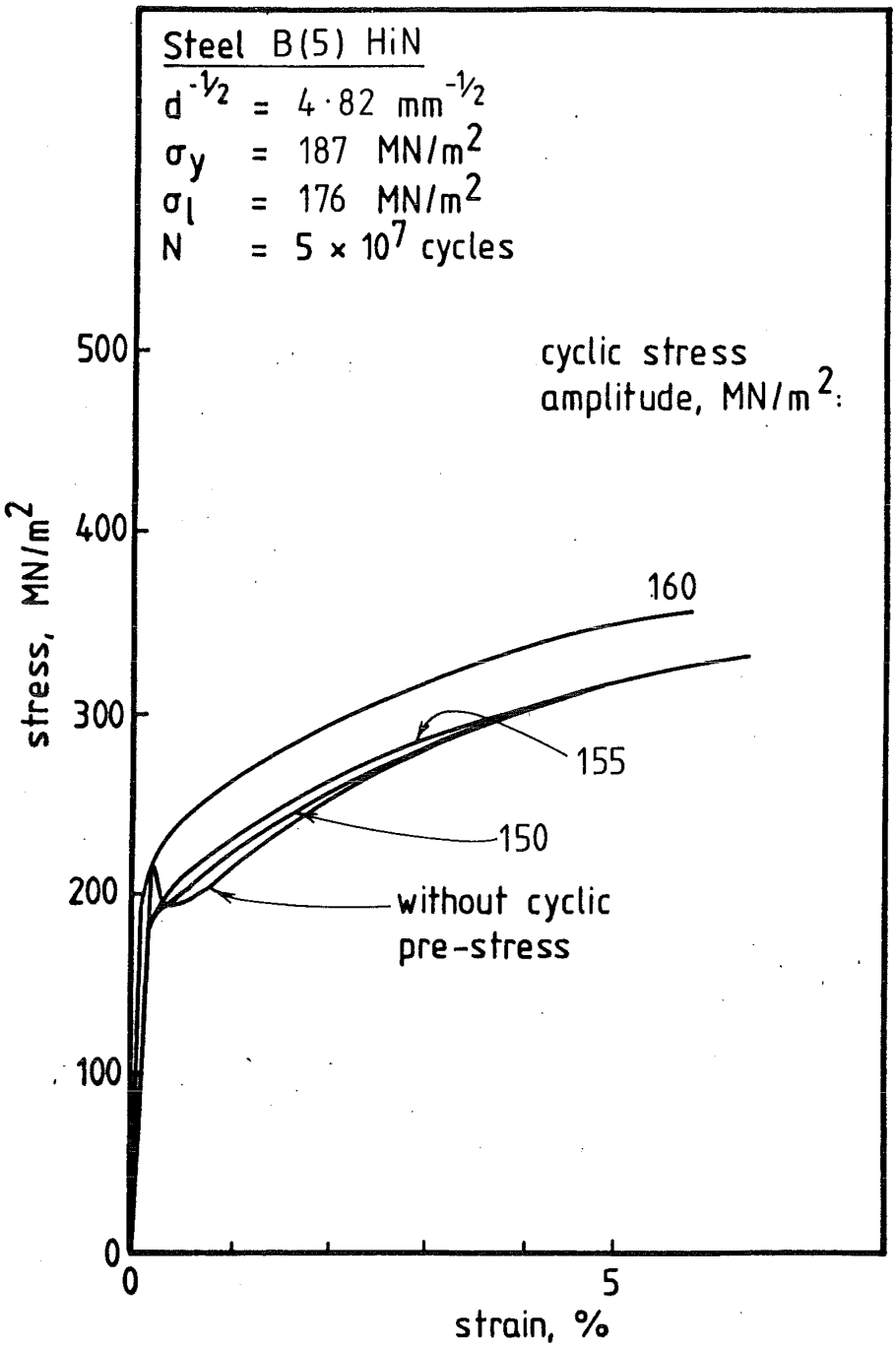

FIG. 8·16 EFFECTS OF CYCLIC PRE-STRESS ON THE TENSILE CURVES OF STEEL B(5)

Steel B(1) - HiN - Figure 8.15

The results of this group of steel were very similar to those for Steel A(1). Cycling at a stress below σ_{CD} (160 MN/m^2) produced no effect on the subsequent tensile curve, but when the stress was at σ_{CD} or above, smooth tensile curves were obtained. The amount of hardening, indicated by Δf (see Figure 8.15 for definition of Δf), increased with the cyclic pre-stress amplitude.

Steel B(5) - HiN - Figure 8.16

Cyclic pre-stressing this steel at σ_{CD} (150 MN/m^2) caused the removal of the yield drop and Luders strain, and a little hardening was observed. Fatigued at 155 MN/m^2, the tensile curve was smooth with a little more hardening recorded. At 160 MN/m^2, the hardening was substantial.

These tensile curves of cyclic pre-stressed specimens agree well with the damping and temperature recordings. At cyclic stresses below σ_{CD}, no significant change in material properties was effected. At σ_{CD}, fatigue cycling caused an increase in damping capacity and temperature rise for the steel, and removed the yield drop and Luders strain, resulting in a smooth tensile curve. Cycling at stresses above σ_{CD} caused hardening and the amount of hardening was dependent on the cyclic pre-stress amplitude.

The important point revealed is that σ_{CD} is below σ_ℓ. Most researchers e.g., Luther & Williams[128], Stephens[177], suggested that for the yield drop and Luders strain to be eliminated, the cyclic stress had to be above σ_ℓ. The above results clearly indicate that this can be achieved even if the stress is below σ_ℓ, provided it is at or above σ_{CD}, with $\sigma_{CD} < \sigma_\ell$.

8.3.2 The Effect of Number of Pre-Stress Cycles

Specimens of steel B(1) were fatigued at σ_{CD}, 160 MN/m^2, for different lengths of time and then tested in tension. Figure 8.17 shows that during fatigue cycling, the yield point was gradually removed, due to dislocation generation. The specimen fatigued to 1.1×10^6 cycles was tested after its temperature had started to rise during fatigue cycling, see Fig.8.11. This confirms

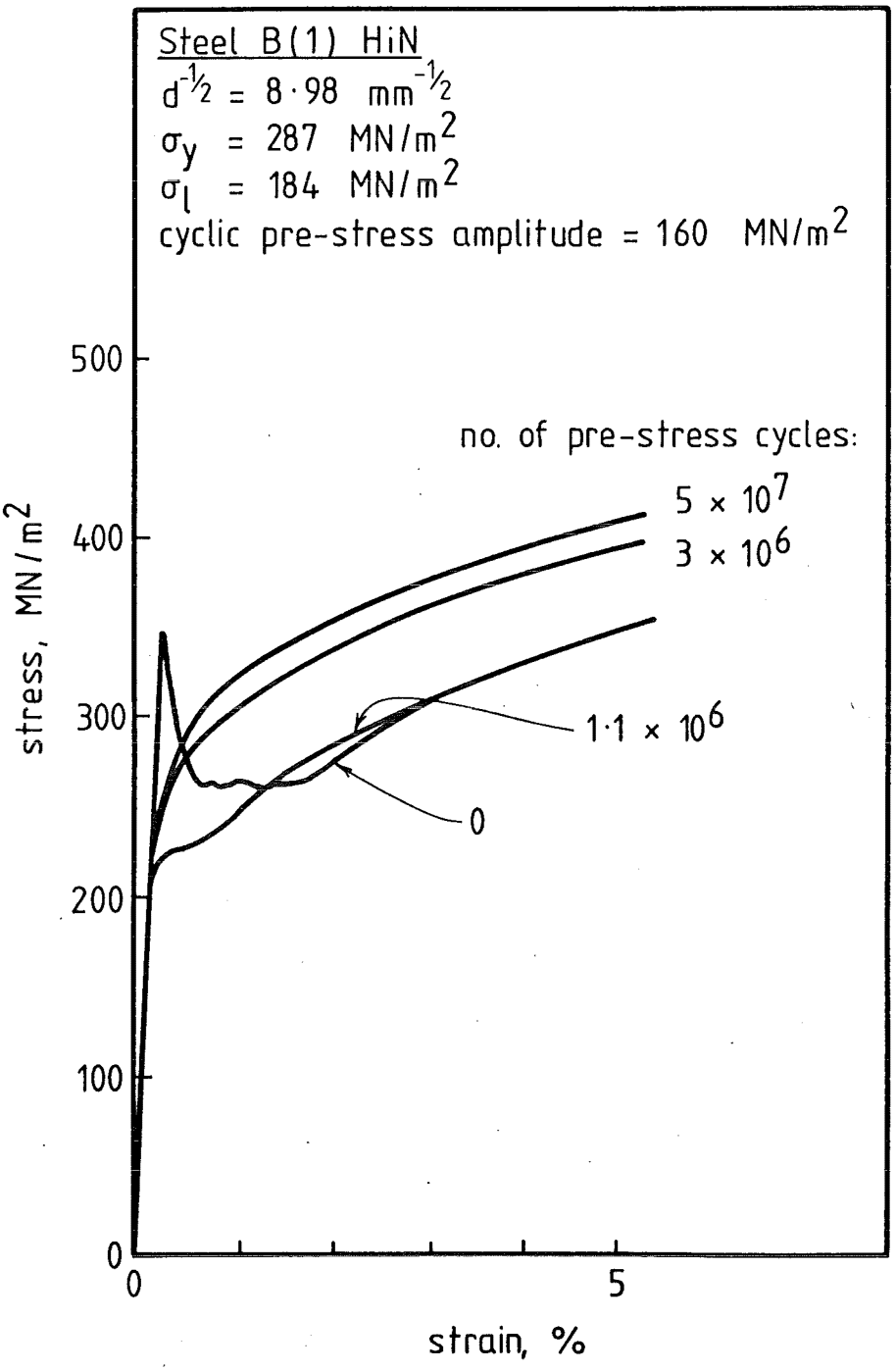

FIG. 8·17 EFFECTS OF NUMBER OF PRE-STRESS CYCLES ON THE TENSILE CURVE OF STEEL B(1).

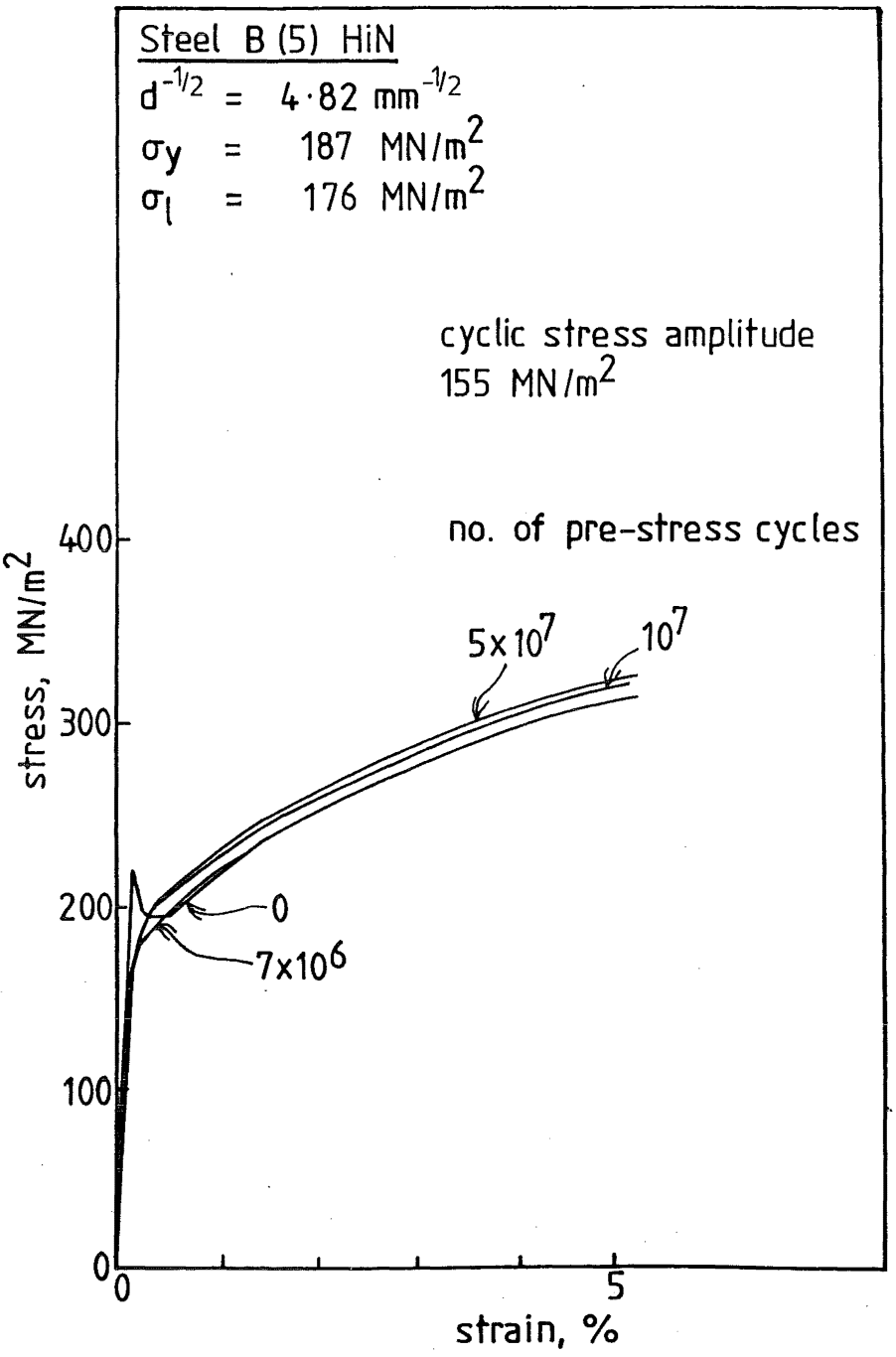

FIG. 8·18 EFFECTS OF NUMBER OF PRE-STRESS CYCLES ON THE TENSILE CURVE OF STEEL B(5)

the prediction that damping and temperature rise are due to dislocation generation and motion. After 3×10^6 cycles, corresponding to the maximum temperature value, the removal of yield point was complete and significant hardening was observed. Cycling for another 4.7×10^7 cycles only increased the hardening by a small margin. Thus, most of the hardening was achieved during and immediately after the damping and temperature rise.

Specimens of steel B(5) were also subjected to different number of pre-stress cycles at 155 MN/m^2 before tensile testing. Figure 8.18 shows that the original yield point was removed after 7×10^6 cycles of pre stress but no hardening was recorded, refer to Fig. 8.12. After 10^7 cycles hardening was clearly evident and further cycling to run-out at 5×10^7 cycles produced increased hardening although the gain was slight.

In all cases of cyclic pre-stressing, the tensile curve of both the fine and coarse grained steels did not display a returned yield point to suggest that dynamic strain ageing was present. The degree of hardening gained by cyclic stressing appeared to be lower in the coarse grained steel than in the fine grained steel. This is in accord with the observed temperature measurements.

8.3.3 The Effect of Static Ageing after Cyclic Pre-Stressing

Specimens of steels B(1) and B(5) after cyclic stressing at their respective σ_{CD} for 5×10^7 cycles were aged at 100°C before being tested in tension.

Figure 8.19 shows the results for steel B(1). It was found that ageing at 100°C for 3 hours did not bring about the return of a sharp discontinuous yield point and well-defined Luders strain. No further hardening was gained by static ageing. This ill-defined yield point was surprising in view of the fact that mobile dislocations were generated during fatigue and that the steel contained a high level of active nitrogen

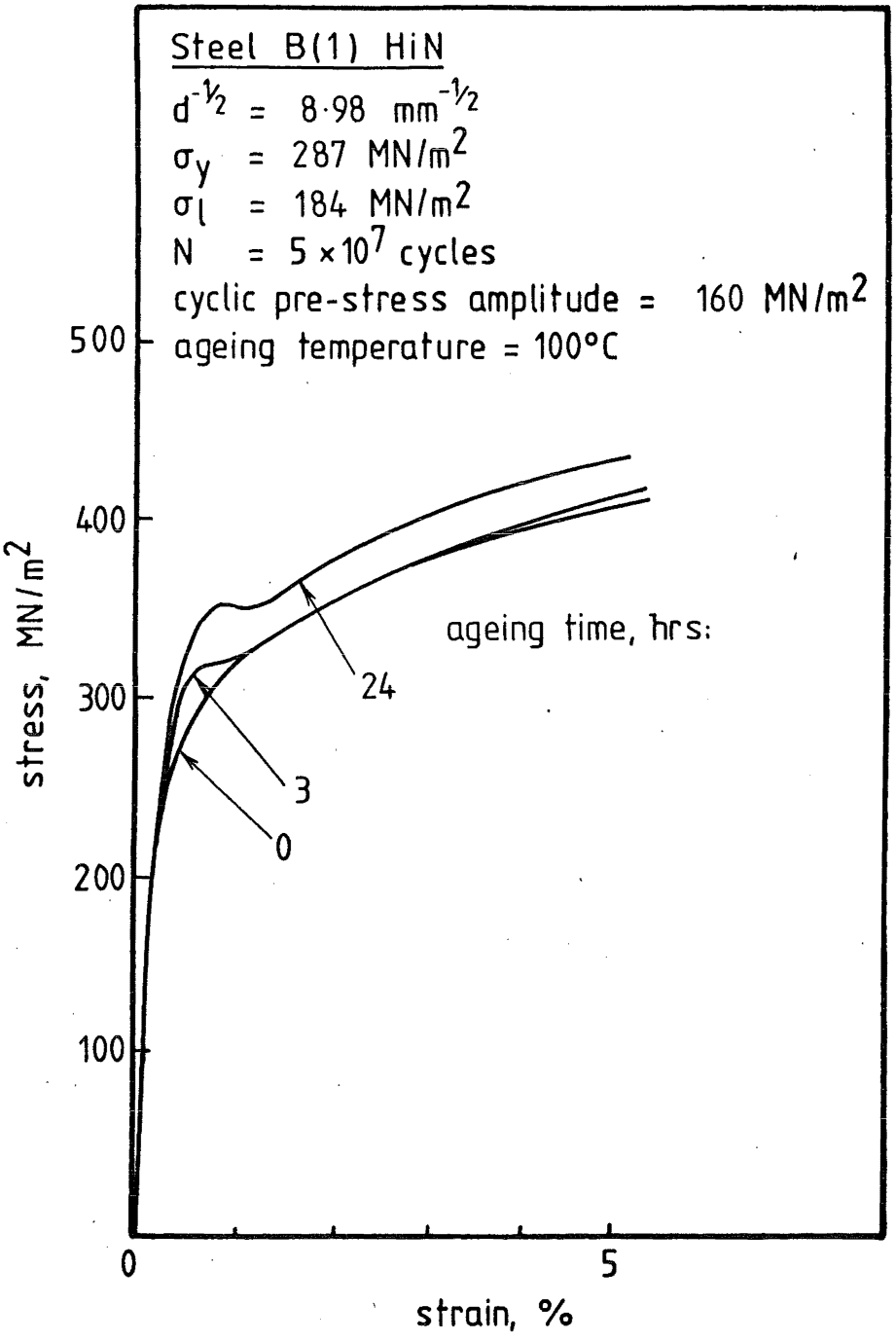

FIG. 8·19 EFFECTS OF AGEING AT 100°C AFTER CYCLIC PRE-STRESSING ON THE TENSILE CURVE OF STEEL B(1).

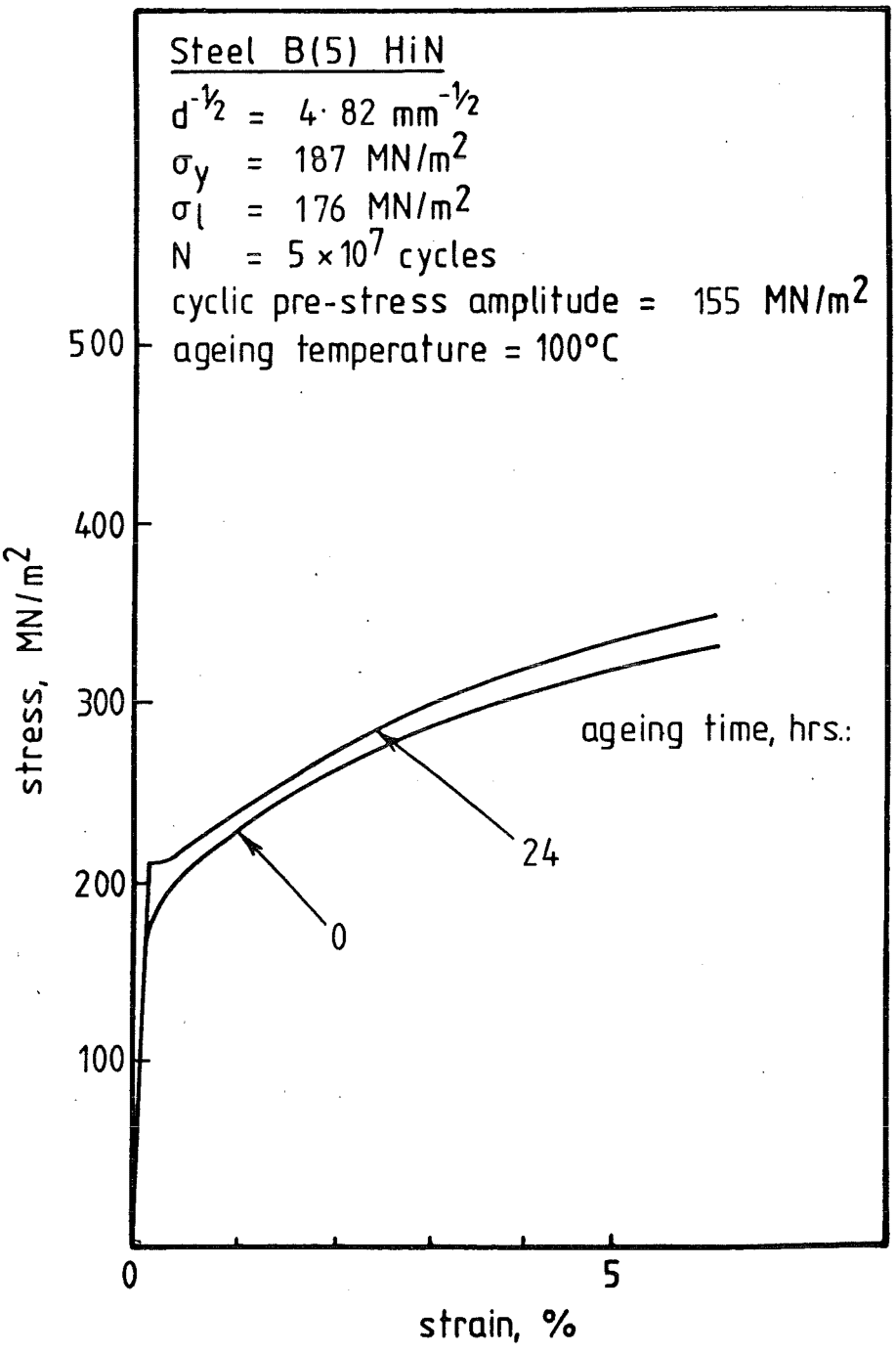

FIG. 8·20 EFFECTS OF AGEING AT 100°C AFTER CYCLIC PRE-STRESSING ON THE TENSILE CURVE OF STEEL B(5).

Ageing for 24 hours at the same temperature produced a more distinct yield point and some hardening. This specimen was fatigued at a stress slightly above σ_{CD} (~162 MN/m^2) so that the increased hardening may be partially due to the increased cyclic pre-stress.

For the coarse grained steel, ageing for 24 hours after cycling produced a definite Luders strain, but a true yield drop was still absent, (see Figure 8.20). Some strain age hardening was observed.

8.3.4 The Effect of Surface Damage caused by Fatigue

The results so far on the effect of cyclic pre-stress on tensile properties appear inconsistent. Figure 8.17 clearly shows that mobile dislocations were generated during fatigue and the smooth tensile curve obtained after 5×10^7 cycles of stressing suggests a high mobile dislocation density after fatigue. However, despite an abundance of mobile dislocations and the high active nitrogen content of the steel, prolonged artificial ageing after fatigue could not introduce a well-defined yield point in a subsequent tensile test, Figure 8.19. The ineffectiveness of artificial ageing would be expected if the active nitrogen content was low, but as yet there is no evidence to suggest that dynamic strain ageing occurred during fatigue to cause a depletion in the active nitrogen available for locking.

Persistent slip bands are known to form on polished specimen surfaces during fatigue, and Finney and Laird[147] observed differences in dislocation structures at the surface region and in the bulk of the specimen after fatigue. Therefore, it may be that dynamic ageing did take place during fatigue, but the returned yield point (due to dynamic strain ageing) was masked out by the effects of surface irregularities after fatigue.

Lloyd and Greenough[178] found that austenising followed by the removal of a surface layer from the specimen produced a yield point. They

concluded that surface roughness developed by fatigue stressing provided many regions of effective stress concentrations at the surface of the specimen, so suppressing the yield drop. In other words, they considered the disappearance of the original yield point was due to surface stress concentration and not dislocation generation. This conclusion is unacceptable because firstly, while surface roughness might obliterate the yield drop, it would not cause the disappearance of the Luders strain. Secondly, the yield point they observed in their polished specimen was almost certainly due to the effect of austenising and not due to the removal of a surface layer. Thirdly, the experimental results here have shown that dislocations were generated during fatigue to eliminate the original yield point, Figures 8.17 and 8.18.

To investigate the effect of surface damage, a B(1) specimen was fatigued at σ_{CD} (160 MN/m^2) for 5 x 10^7 cycles. After fatigue, the specimen was transferred to the Instron tensile machine and a hysteresis loop was obtained. A layer of 100 μm was then polished away from the specimen and its hysteresis loop again recorded. Tensile testing was then carried out and the stress strain curve recorded.

Figure 8.21 shows that polishing away a surface layer did not have any effect on the stress strain curve. Thus the specimen surface irregularities did not play any part in shaping the tensile curve of a fatigued specimen.

Figure 8.22 compares the hysteresis loops of the specimen before and after polishing away a surface layer. If the suggestion of Finney and Laird[147] that all the plastic strain after transient changes were taken up by surface PSB's was correct, and that the specimen core hardened sufficiently to sustain the applied stress elastically, then the polished specimen should give a different shaped hysteresis loop with perhaps a harrower width. This was shown not to be the case since the loops were almost identical, Figure 8.22. This implies that either dislocation

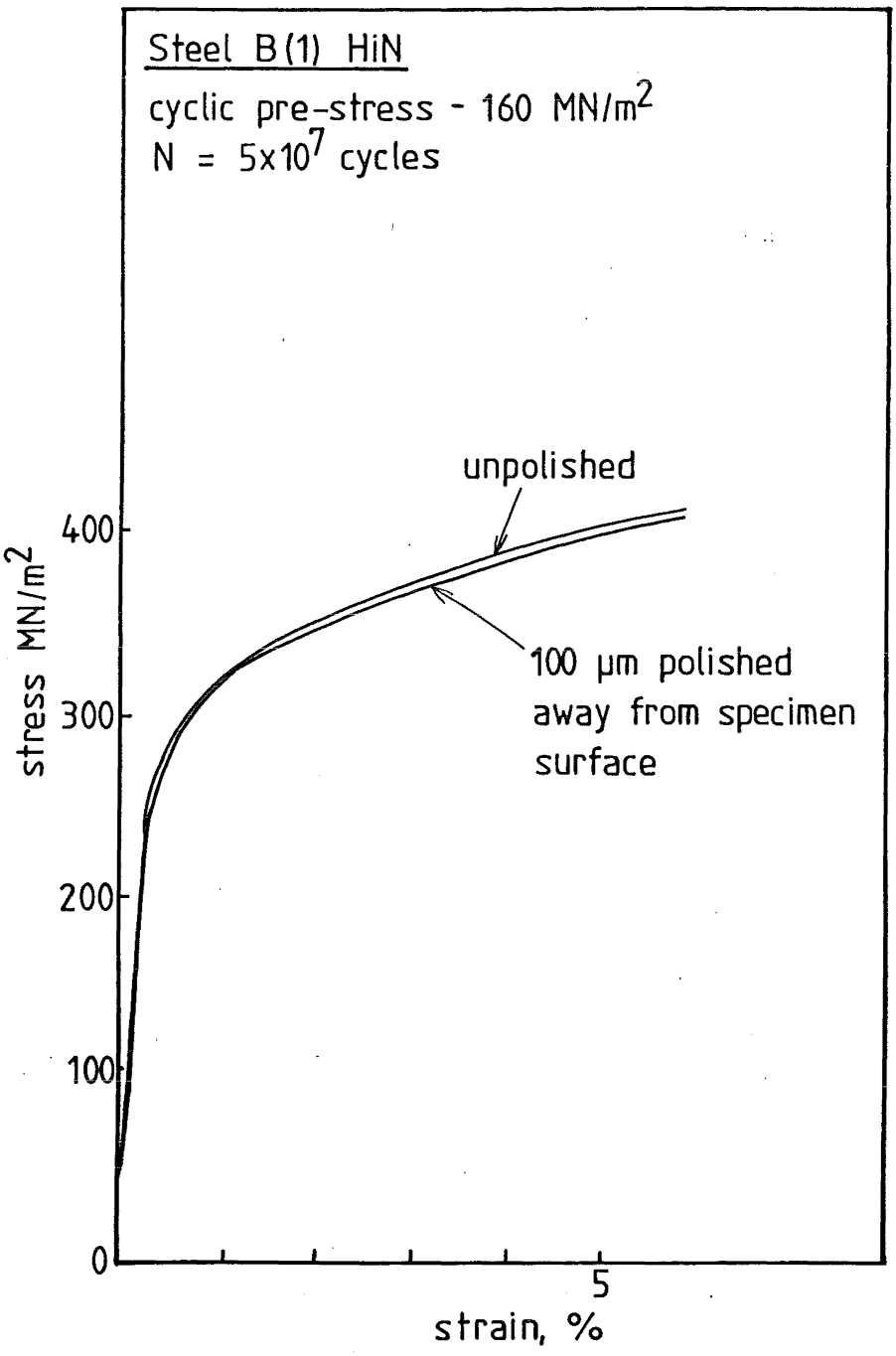

FIG. 8·21 EFFECT OF SURFACE LAYER ON THE STRESS-STRAIN CURVE OF FATIGUED SPECIMENS STEEL B(1)

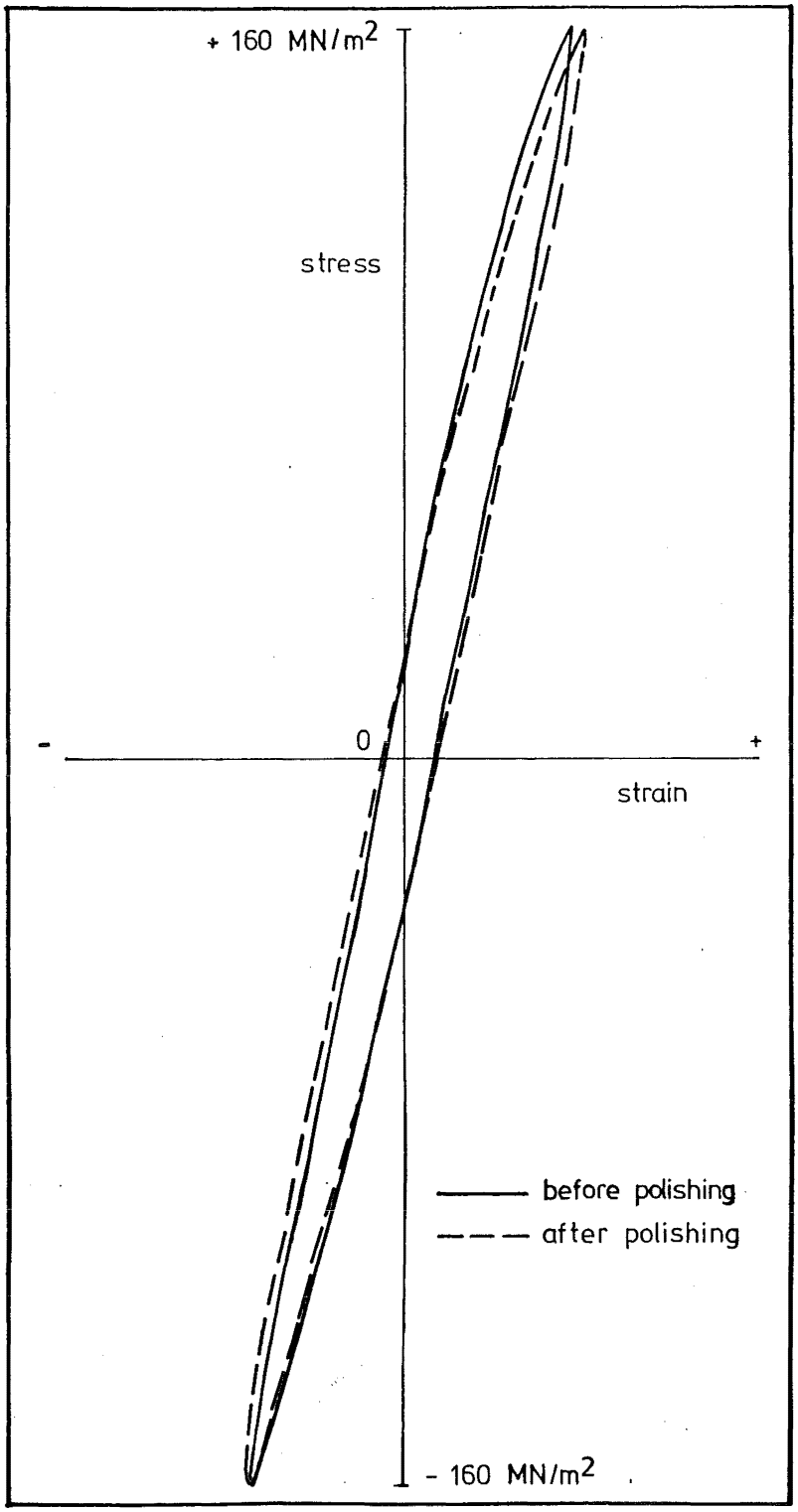

FIG. 8·22 HYSTERESIS LOOPS OF FATIGUED STEEL B(1) BEFORE AND AFTER REMOVAL OF SURFACE LAYER (100 μm) FATIGUED AT 160 MN/m^2 FOR 5×10^7 CYCLES

behaviour in the core of the material was no different from that at the surface region of the specimen or that surface behaviour was not dominant.

8.3.5 Further Investigation on the Effect of Number of Pre-Stress Cycles

Results obtained so far indicate that when the temperature and damping of a specimen fatigued at σ_{CD} started to rise, mobile dislocations were being created. For the case of steel B(1), the specimen temperature rose to about 170°C and this temperature coupled with an abundance of mobile dislocations, must result in some dynamic strain ageing. However, dynamic strain ageing has not been shown by a return of a yield point in a subsequent tensile test.

It appears that most of the micro-structural and property changes occurred during the period when the specimen temperature increased rapidly. To show this, specimens of B(1) were fatigue cycled at σ_{CD}, 160 MN/m^2, to different lives and the results shown in Figure 8.23. The insert indicates the approximate points relative to the temperature curve at which fatigue cycling was stopped. The results clearly show that dynamic strain ageing occurred during the cyclic pre-stressing stage, i.e. dynamic strain ageing occurred during fatigue in this steel - see curves 2 and 3. However curve 4 shows that the returned yield point (shown in curve 3) was rapidly being eliminated so that at run-out (5×10^7 cycles), a completely smooth tensile curve was obtained, curve 5.

Because the coarse grained steels, when fatigued at their σ_{CD}, did not show a sudden and large temperature rise, changes in the steel properti apparently occurred at a slow rate. It was therefore difficult to detect whether strain ageing was occurring or not. Figure 8.18 shows that cycling the high nitrogen coarse grained steel B(5) at 155 MN/m^2 (σ_{CD} = 150 MN/m^2) to various stages did not indicate any sign of dynamic strain ageing, but some hardening was observed.

To obtain evidence of dynamic strain ageing in the coarse grained B steels, B(5) specimens were fatigued at 165 MN/m^2, i.e. below σ_ℓ (176 MN/m^2) and above σ_{CD} (150 MN/m^2). It was found that fatigue cycling at this stress amplitude caused a rapid temperature rise similar to that observed for the fine grained steels. The maximum temperature of about 120°C was reached after about 2.5×10^4 cycles of stressing. Figure 8.24 shows the tensile curves of B(5) specimens fatigued to various stages at this stress amplitude. After 5×10^4 cycles, a distinct returned yield point was obtained (curve 2), and a substantial gain in hardening was observed. After 2×10^6 cycles, the yield point, although diminished, was still evident (curve 3) and there was further hardening. After 5×10^7 cycles, a smooth tensile curve was recorded (curve 4) and very little additional hardening was achieved. Dynamic strain ageing was thus proved to be part of the fatigue process in a coarse grained low carbon steel.

By comparison, dynamic strain ageing was shown to be absent in the A (low N) steels. Steel A(1) was fatigued at its σ_{CD} (155 MN/m^2) and although there was a large temperature rise (~150°C), Figure 8.25 shows tha there was no trace of a return of yield point to indicate dynamic strain ageing. This was due to the low active nitrogen content of the steel. Similarly, steel A(3) when fatigued at 160 MN/m^2 (σ_ℓ = 164 MN/m^2) showed a rapid and large temperature rise (~100°C) but did not exhibit a returned yield point in the tensile curves, Figure 8.26. However, both Figures show strain hardening.

The identical results shown by B(1) and B(5) and by A(1) and A(3) suggest that there is no difference in the fatigue mechanism of fine and coarse grained steel. This is at least true for stress amplitudes above and just below σ_ℓ. Fatigue cycling in this region caused rapid temperatu rise in steels of all grain sizes, and if the steel contained sufficient free nitrogen, dynamic strain ageing occurred. The only difference was

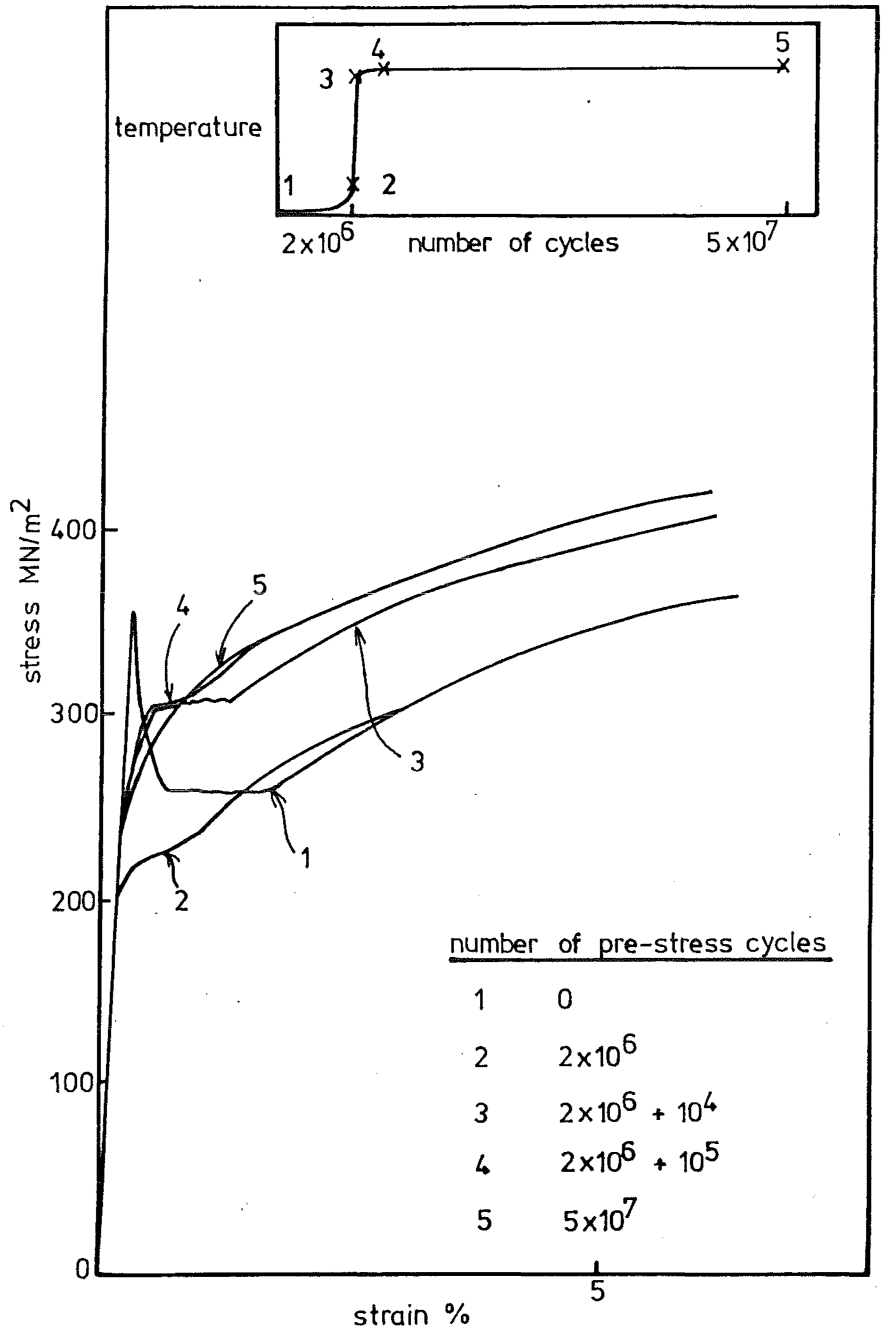

FIG. 8·23 EFFECTS OF NUMBER OF PRE-STRESS CYCLES ON THE TENSILE CURVE OF STEEL B(1). CYCLIC STRESS AMPLITUDE 160 MN/m^2 (σ_{c_D})

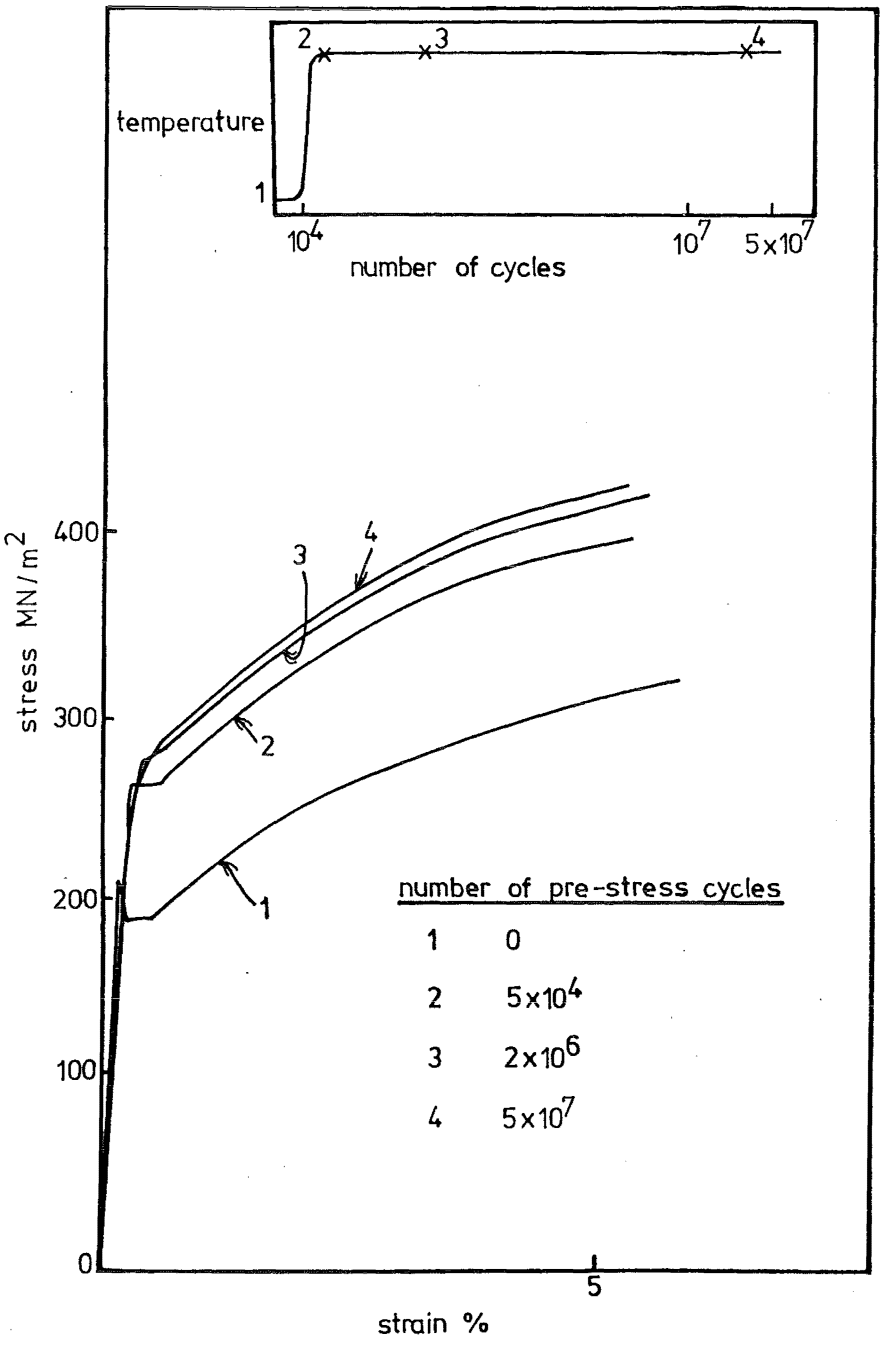

FIG. 8·24 EFFECTS OF NUMBER OF PRE-STRESS CYCLES ON THE TENSILE CURVE OF STEEL B(5). CYCLIC STRESS AMPLITUDE 165 MN/m^2 (σ_{CD} = 150MN/m^2)

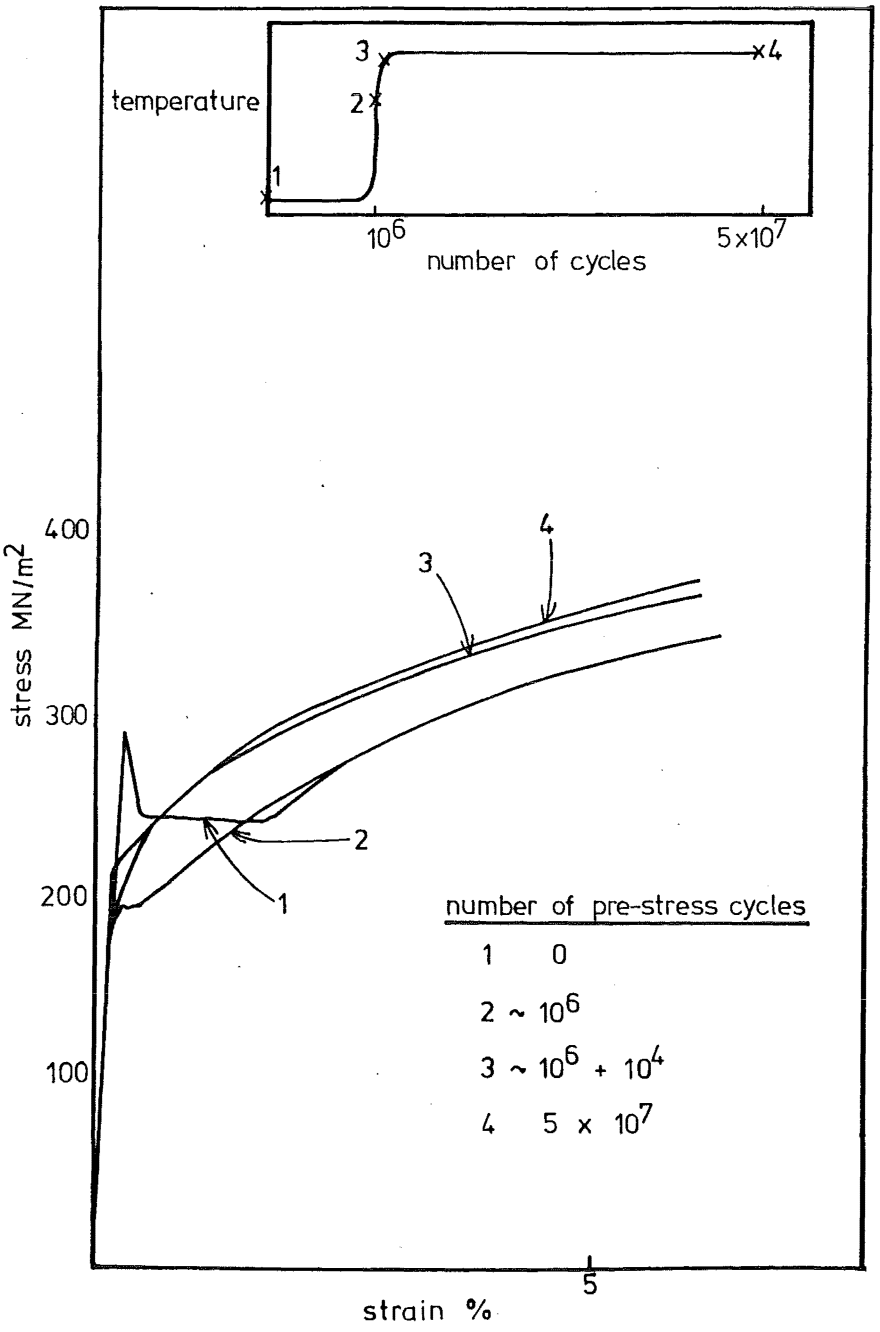

FIG. 8·25 EFFECTS OF NUMBER OF PRE-STRESS CYCLES ON THE TENSILE CURVE OF STEEL A (1). CYCLIC STRESS AMPLITUDE = 155 MN/m² (σ_{CD})

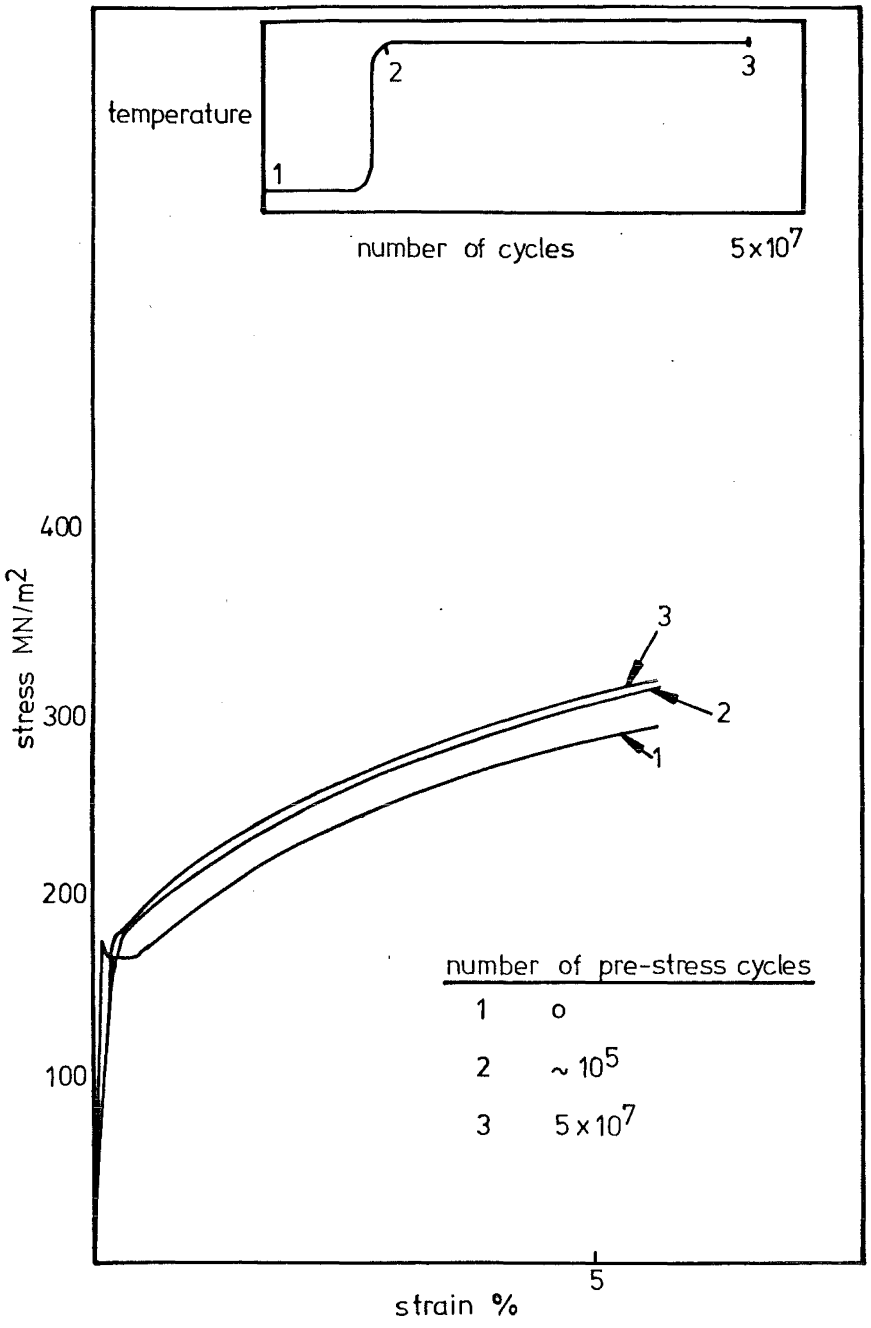

FIG. 8·26 EFFECTS OF NUMBER OF PRE-STRESS CYCLES ON THE TENSILE CURVE OF STEEL A (3). CYCLIC STRESS AMPLITUDE: 160 MN/m^2 (σ_{CD} = 150 MN/m^2)

at the lower stress amplitudes close to σ_{CD} where cyclic stressing of the coarse grained steels did not give a large temperature rise and dynamic strain ageing was not observed. This may be attributed to a slower dislocation generation rate which could not induce large temperature increases to facilitate ageing dynamically.

8.4 THE EFFECT OF DIRECT STRESS FATIGUE ON THE MICROSTRUCTURE AND DISLOCATION STRUCTURE

The effects of fatigue on structural changes of steel were studied by comparing surface behaviour, internal microstructure and dislocation structures of specimens fatigued for 5×10^7 cycles at σ_{CD} and at stresses below σ_{CD}.

8.4.1 Optical Microscopy - Surface Behaviour

Two specimens from each of the four groups A(1), A(3), B(1) and B(5) were mechanically polished to produce a fine finish over the specimen gauge length. Polishing was finished with ¼ micron diamond paste. However, it was difficult to get a good finish because non-metallic inclusions tended to become detached and cause scratching of the surface. These scratch marks were clearly seen on the surface, but they did not affect the results.

For each steel, one specimen was fatigued at σ_{CD} and one at a stress below σ_{CD}, e.g. steel A(1) at 155 MN/m^2 and 150 MN/m^2; B(1) at 160 MN/m^2 and 155 MN/m^2.

All four steels showed similar results; when fatigued at their respective σ_{CD} for 5×10^7 cycles, persistent slip bands were formed on the specimen surface, Figures 8.27 - 8.30. It may be seen that the PSB formation was more widespread in the fine grained steels, A(1) and B(1), than in the coarse grainedsteels A(3) and B(5). Thus, while most of the surface grains of steel A(1) and B(1) appeared to be covered by PSB's, only isolated grains showed such striations in the coarse grained steels. Also,

groups of neighbouring grains showing PSB's were more common in the fine grained steel.

When fatigued at stresses below their respective σ_{CD}, PSB's were not observed on any of the four steels.

A B(1) specimen was polished and then fatigued at σ_{CD} (160 MN/m^2). Cyclic stressing was stopped at various stages and the specimen taken out for surface observation. The following points were noted:

1) After 10^6 cycles (i.e. before the temperature rise), no striations were observed on the specimen surface, Figure 8.31(a).

2) After 2.1×10^6 cycles (just after the temperature started to rise), not fully developed PSB's were observed in isolated grains, Figure 8.31(b); the density of PSB's was estimated at <10% of that observed on a run-out specimen fatigued at the same stress, Figure 8.29.

3) After 2.105×10^6 cycles (when the maximum temperature was attained) the specimen surface was densely covered with PSB's, Figure 8.31(c).

4) After 3×10^6 cycles, very little change was observed although some striations became better developed.

5) At 5×10^7 cycles, no further changes were observed. The PSB density was not increased by the additional 4.7×10^7 cycles of fatigue.

These observations are in accord with those results presented earlier, that there appears to be major changes at the surface and in the bulk of the material associated with a rise in damping capacity and temperature. Whatever these changes might be, it is obvious that they did not start until a rise in temperature (or damping) was recorded. In the fine grained steels, because the temperature rise was sudden and steep, the changes were completed in a very short period of time (compared to the length of the test)

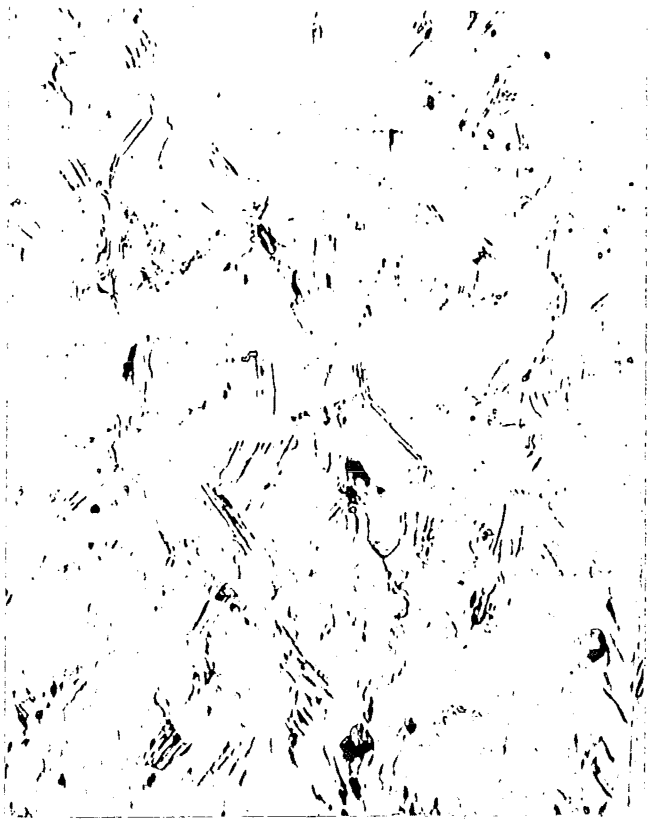

FIG 8·27 Persistent slip bands on surface of specimen A(1) fatigued at σ_{CD} (155MN/m^2) for 5×10^7 cycles.
Specimen surface shows wide-spread PSB formation.

0·1mm

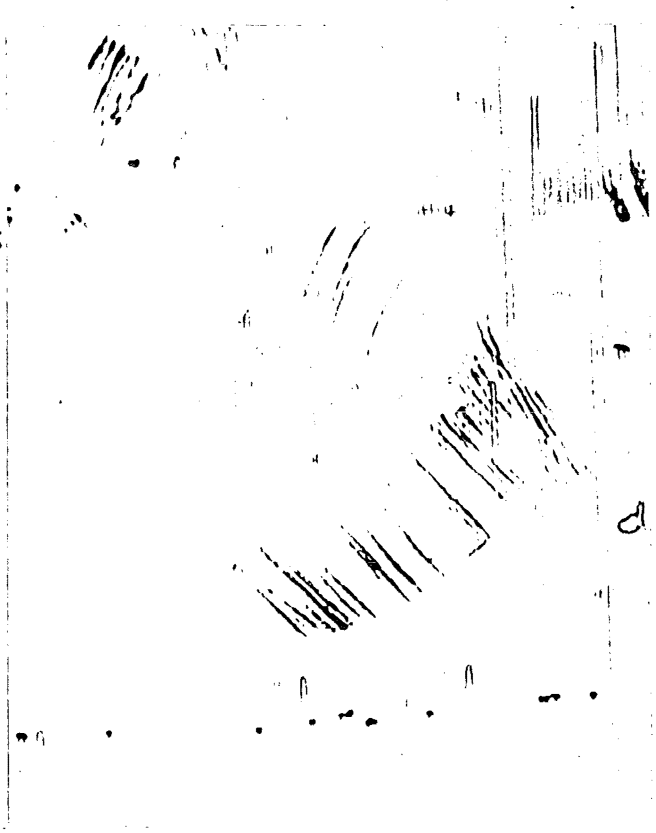

FIG 8·28 Persistent slip bands on surface of specimen A(3) fatigued at σ_{CD} (150MN/m^2) for 5×10^7 cycles.
PSB's formed on specimen surface.

0·1mm

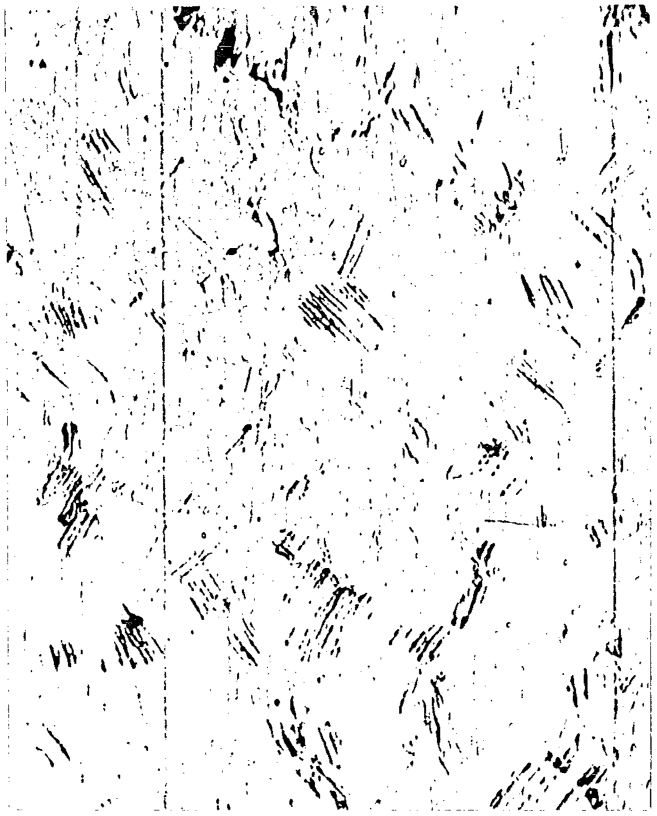

FIG 8·29 Persistent slip bands on surface of specimen B(1) fatigued at σ_{CD} (160MN/m^2) for 5×10^7 cycles.
Specimen surface shows wide-spread PSB formation.

0·1mm

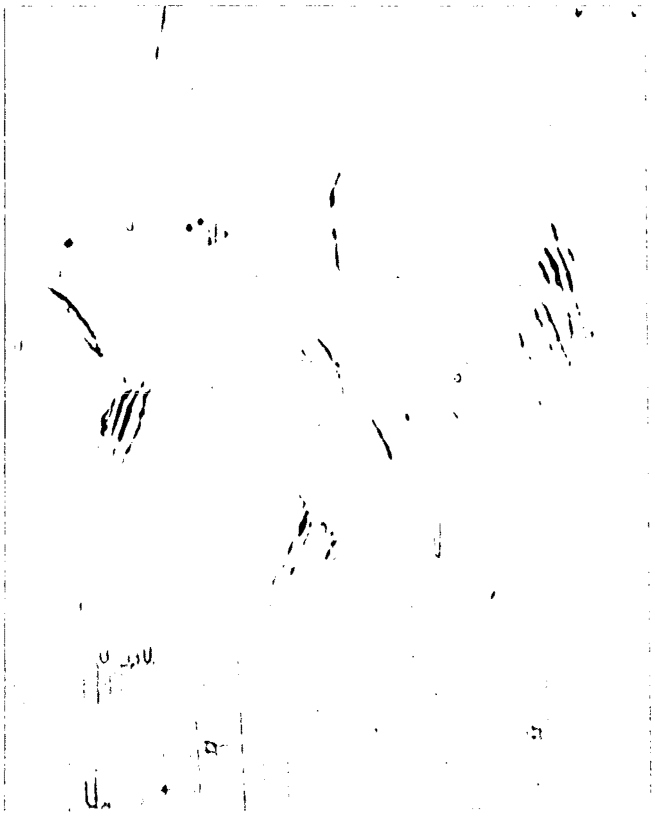

FIG 8·30 Persistent slip bands on surface of specimen B(5) fatigued at σ_{CD} (150MN/m^2) for 5×10^7 cycles.
PSB's formed on specimen surface.

0·1mm

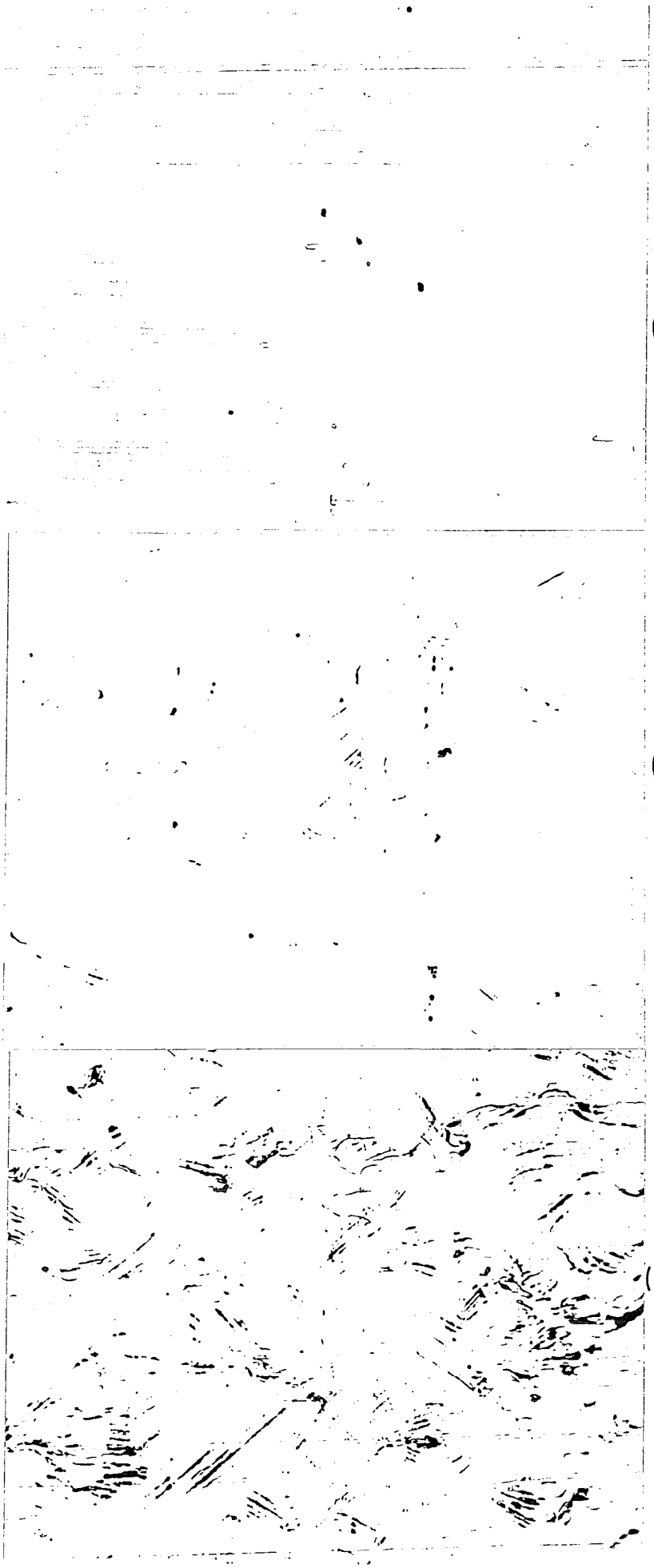

FIG 8·31 Persistent slip band formation on specimen surface of steel B(1) fatigued at σ_{CD} to various stages.

and that no further changes were apparent for the rest of the test (up to 90% of the total time). For the coarse grained steel, where the temperature rise was not so dramatic, it appears that these changes took place more slowly and were less easily detected.

8.4.2 Optical Microscopy - Internal Microstructure

Steels A(1), A(3), B(1) and B(5) were fatigued at their respective σ_{CD} for 5 x 10^7 cycles. After fatigue, micro-specimens were taken from each specimen for observation, the area examined being perpendicular to the stress axis in each case. For comparison, the effect of cycling at a stress below σ_{CD} was also studied.

The micro-specimens were first hand polished with emery paper and diamond paste and then electropolished with a Buehler Electro-Polishing Cell. The electrolyte used was of the following composition:

50 ml of Perchloric Acid, 70%, S.G. 1.67

750 ml of ethanol

140 ml of distilled water.

After electropolishing, the micro-specimens were etched in 2% nital.

Typical examples of the etched structure are shown in Figures 8.32 - 8.35. It may be seen from the micrographs that preferential etching of some ferrite grains occurred. To ascertain that this was not an effect of polishing, an annealed specimen was polished and etched in a similar manner. Figures 8.36 and 8.37 show that the grains were free from such roughening effect.

The roughening appearance of ferrite grains was due to dislocation etch pits. These were similar to those observed by Wilson[80] in yielded grains at the Luders band front of a tensile specimen. Thus the grains that showed etch pits could be considered to have yielded plastically

FIG 8·32 Yielding in steel A(1) shown by etch-pitting. Fatigued for 5×10^7 cycles at σ_{CD} (155MN/m^2)

×1000

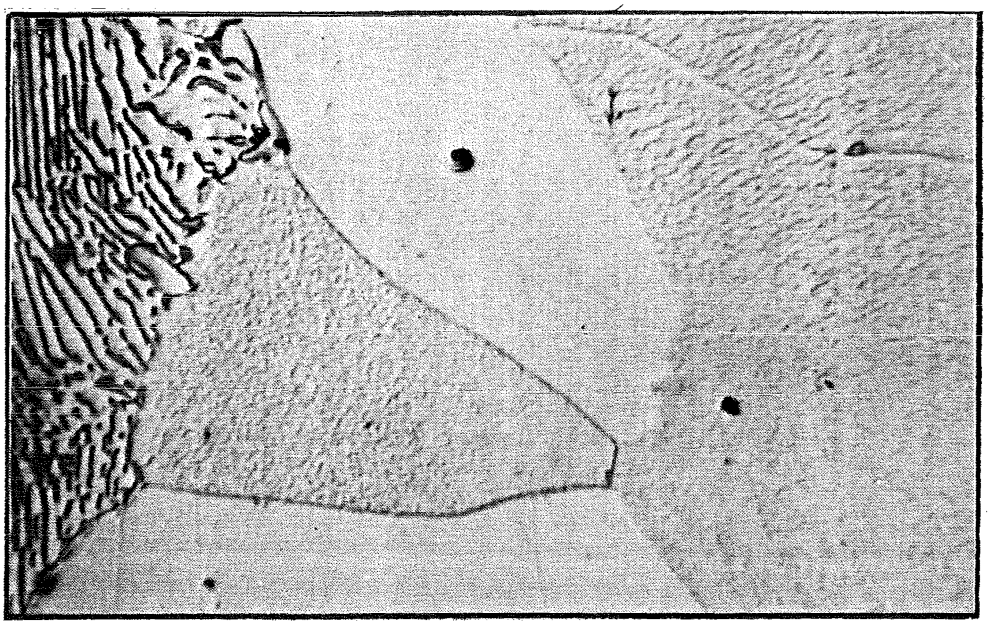

FIG 8·33 Yielding in steel A(3) shown by etch-pitting. Fatigued for 5×10^7 cycles at σ_{CD} (150MN/m^2)

×1500

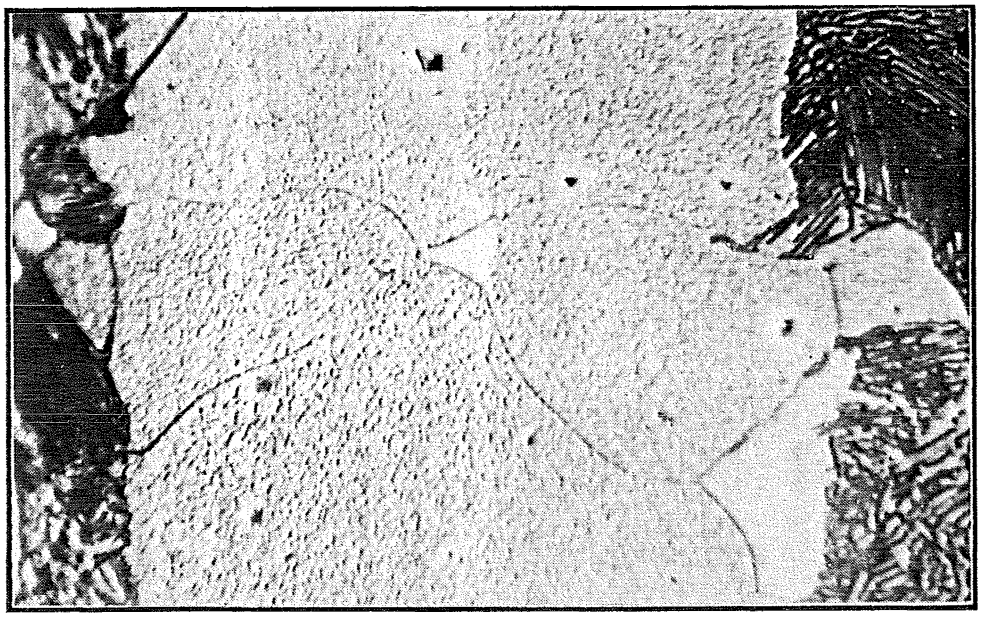

FIG 8·34 Yielding in steel B(1) shown by etch-pitting. Fatigued for 5×10^7 cycles at σ_{CD} ($160 MN/m^2$)
×1500

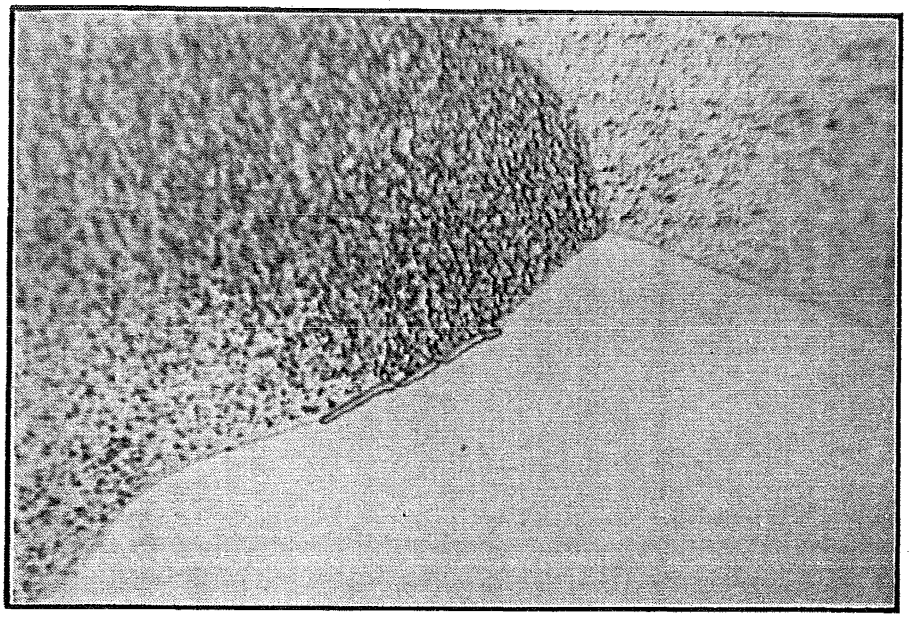

FIG 8·35 Yielding in steel B(5) shown by etch-pitting. Fatigued for 5×10^7 cycles at σ_{CD} ($150 MN/m^2$)
×1500

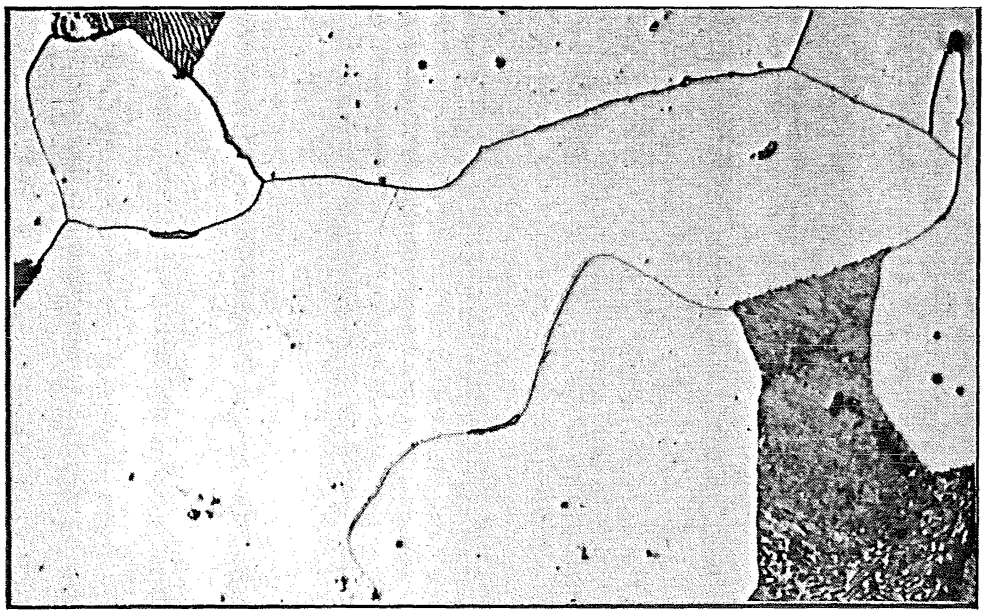

FIG 8·36 Annealed steel A(3) - no etch-pitting.
×1000

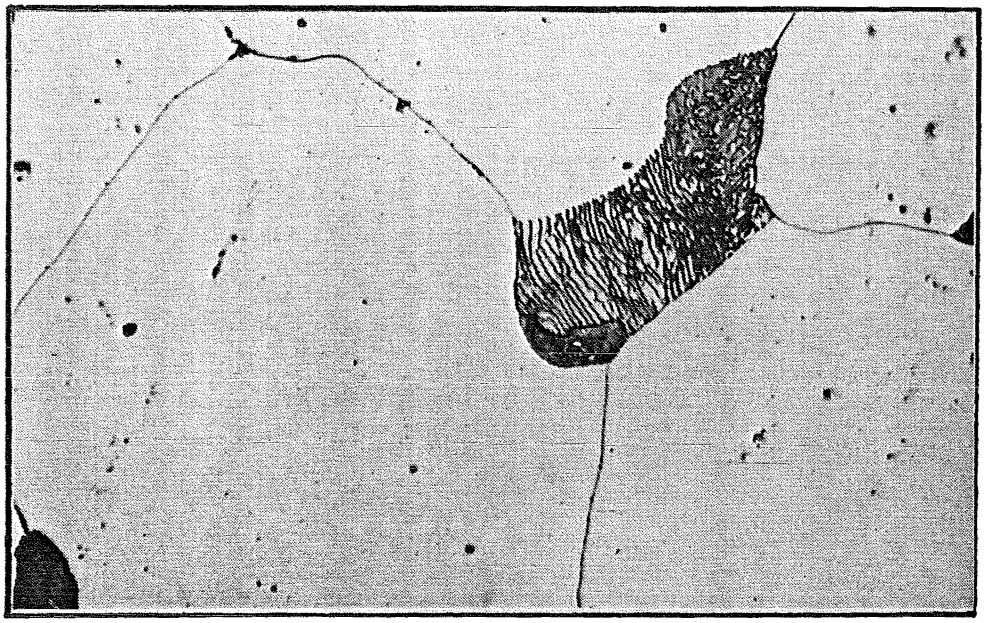

FIG 8·37 Annealed steel B(5) - no etch-pitting.
×1000

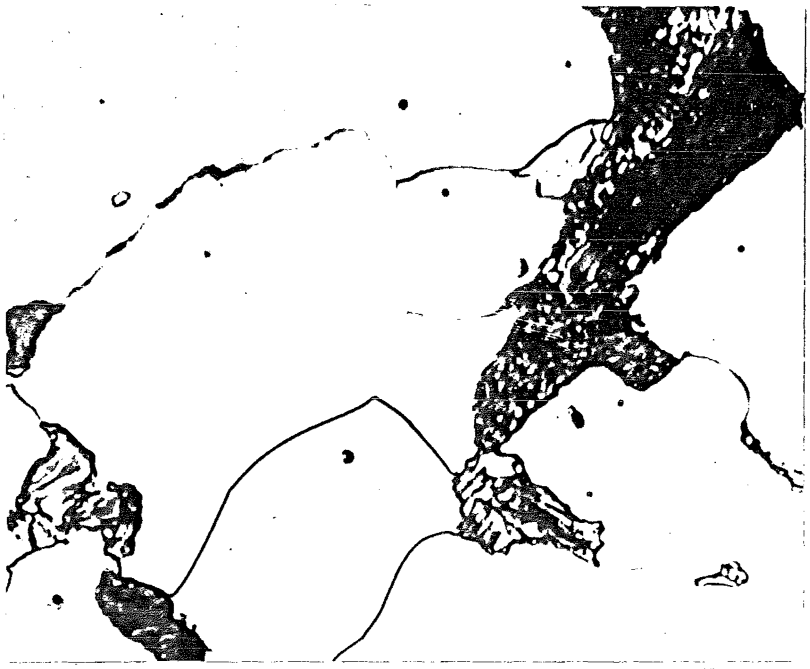

FIG 8·38 Steel B(1) fatigued for 5×10^7 cycles at $155 MN/m^2$ (below σ_{CD}) yielding in isolated grains only.

×1500

FIG 8·39 Steel A(1) fatigued for 5×10^7 cycles at $150 MN/m^2$ (below σ_{CD}) very low etch pitch density.

×1500

during fatigue.

Since the grains either showed uniform roughening or no roughening at all, it appears that yielding of grains occurred individually. It was also observed that fine grained steels showed a higher proportion of yielded grains than coarse grained steels. This is consistent with the observation on PSB formation on the specimen surface.

Specimens fatigued at stresses below σ_{CD} did not show such extensive yielding. Etch pits were observed only in isolated grains and the density of pits was lower, Figures 8.38 and 8.39.

NOTE: To obtain magnifications of 1000 and 1500 times, an oil immersion lens was used. This resulted in some distortion of the picture at the edges. Also, in order to accentuate the appearance of etch pits, it was necessary to alter the focus at the expense of sharp grain boundary and pearlite images.

8.4.3 Transmission Electron Microscopy (T.E.M.)

Fine grained steel B(1) and coarse grained steel B(5) were fatigued at their respective σ_{CD} for 5×10^7 cycles. After fatigue, thin foil specimens for T.E.M. observations were taken from the core of gauge lengths of fatigued specimens, the discs taken being perpendicular to the axis of loading. For comparison a B(1) steel was fatigued at 155 MN/m^2 (i.e. below σ_{CD}) for 5×10^7 cycles and similar foils made for study.

Discs 3mm diameter and 0.75mm thick were cut with a Buehler Wafer Disc before polishing with emery down to a thickness of 0.25mm. This was followed by electro-polishing using a Polaron M401 Electropolishing unit which employs the jetting technique.

Electropolishing was done in two stages. The first or profiling stage, was done using 20% Perchloric Acid (70%) in ethanol at 30 volts.

15 seconds of polishing time was allowed for each side. The second, or perforating stage, used 10% Perchloric Acid in ethanol at 10-12 volts. After perforating, the foil was washed in dilute acetic acid and then in ethanol.

Observations were carried out using a 100 kV JEM-7A electron microscope and Figures 8.40 - 8.43 show the dislocation structures resulting from fatigue. The dislocation structures of fine grained and coarse grained steels appeared different.

The fine grained steel revealed an unexpected dislocation cell structure, Figures 8.40 and 8.41.

The formation of a cell structure was surprising since this type of structure had always been associated with high amplitude fatigue and the stress used in this case was below σ_{ℓ}. The cell walls were well defined and in some cases, it was possible to resolve the cell wall to show dislocations. The cell interiors were not entirely free of dislocations.

The coarse grained steel showed some well-defined sub-grain boundaries, Figure 8.42. It is apparent that the sub-grain boundaries (or bands) were formed by interactions of long screw dislocations, Figure 8.43.

Steel B(1) fatigued at 155 MN/m^2 (below σ_{CD}) did not show cell structures or heavy dislocation tangles. Some dislocations appeared unaffected by the cyclic stress, Figure 8.44 and others revealed some interactions. Dipole loops were also observed in this specimen, Figure 8.45. Although no actual dislocation count was done, it was quite clear that the dislocation density in this specimen was much lower than for the specimens tested at above σ_{CD} (160 MN/m^2).

FIG 8·40 Formation of dislocation cell structure in steel B(1) fatigued for 5×10^7 cycles at σ_{CD}, 160MN/m^2. $d^{-1/2} = 8 \cdot 98 mm^{-1/2}$

1μ

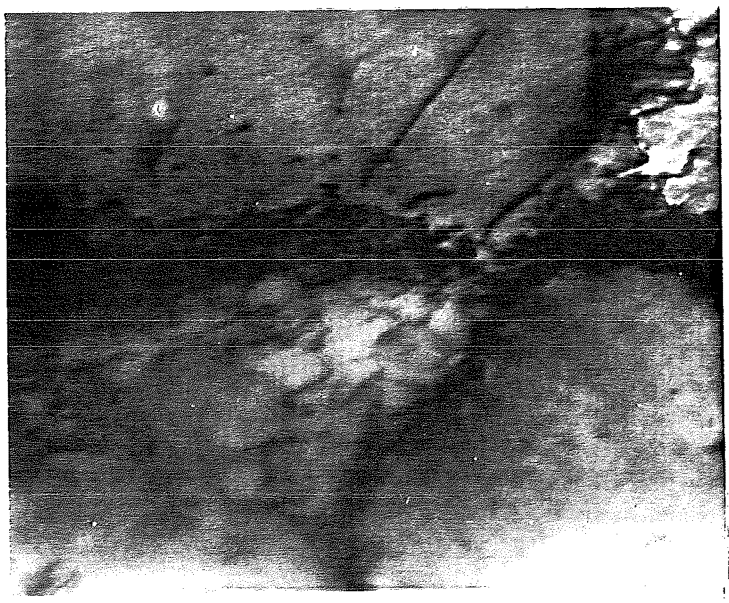

FIG 8·41 Formation of dislocation cell structure in steel B(1) fatigued for 5×10^7 cycles at σ_{CD}, 160MN/m^2. $d^{-1/2} = 8 \cdot 98 mm^{-1/2}$

0·5μ

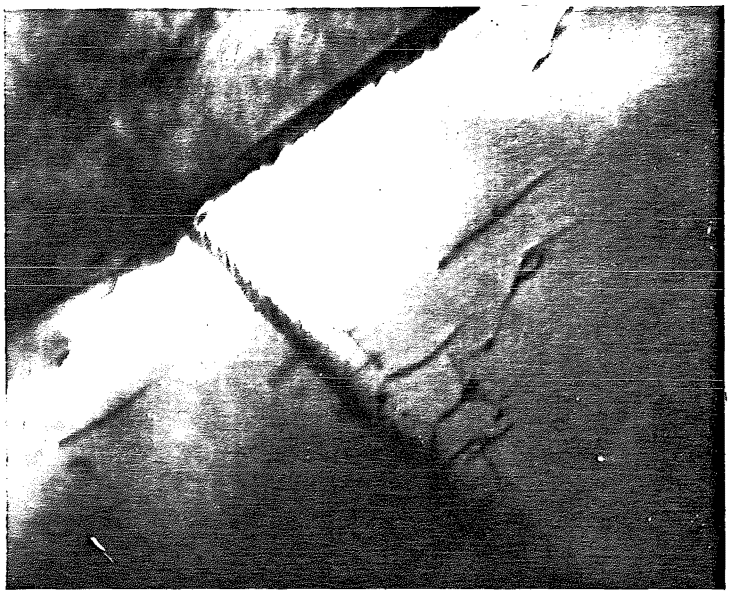

FIG 8·42 Formation of subgrain boundaries in steel B(5) fatigued for 5×10^7 cycles at σ_{CD}, 150MN/m^2. $d^{-1/2} = 4{\cdot}82 mm^{-1/2}$

0·5 μ

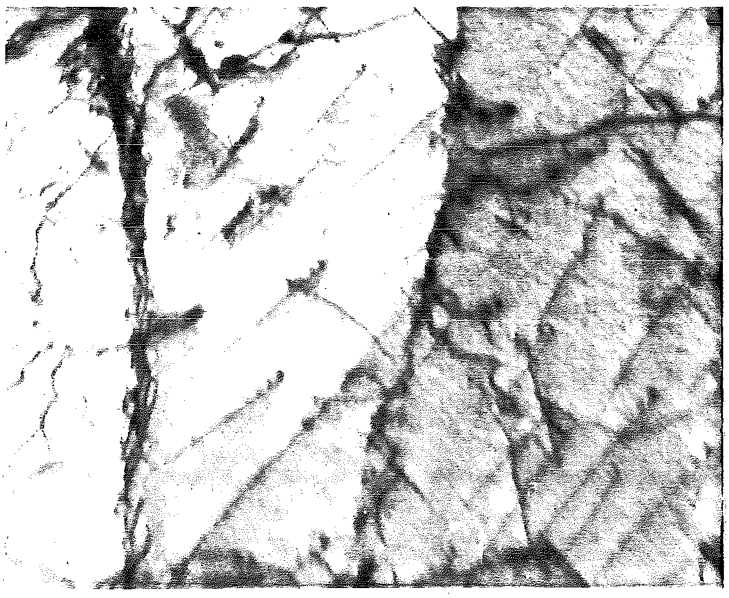

FIG 8·43 Dislocations forming band structures in steel B(5) fatigued for 5×10^7 cycles at σ_{CD} 150MN/m^2. $d^{-1/2} = 4{\cdot}82 mm^{-1/2}$

0·5 μ

FIG 8·44 Undisturbed dislocations in steel B(1) fatigued for 5×10^7 cycles at $155 MN/m^2$ (below σ_{CD}). $d^{-1/2} = 8 \cdot 98 mm^{-1/2}$

0·5μ

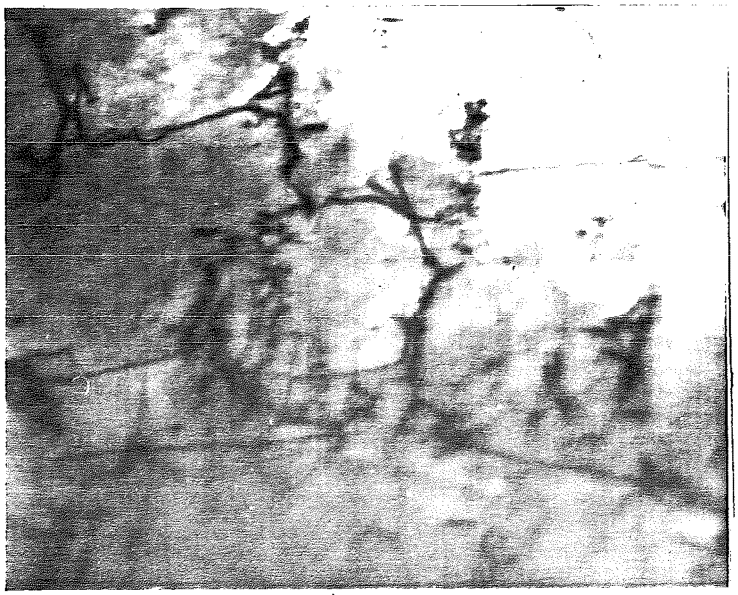

FIG 8·45 Dislocation dipole loops in steel B(1) fatigued for 5×10^7 cycles at $155 MN/m^2$ (below σ_{CD}). $d^{-1/2} = 8 \cdot 98 mm^{-1/2}$

0·5μ

CHAPTER NINE

DISCUSSION

9.1 THE EFFECTS OF GRAIN SIZE AND ACTIVE NITROGEN CONTENT ON THE FATIGUE LIMITS

It may be seen from Fig. 7.11 that the fatigue limit of low carbon steel varies linearly with $d^{-\frac{1}{2}}$ in the range of grain sizes considered (d is the grain diameter). This Hall-Petch type relationship has previously been verified by Klesnil *et al*[8]. The σ_ℓ vs $d^{-\frac{1}{2}}$ plot was different for the two steel groups and since the A and B steel groups contained different amounts of active nitrogen, this difference in fatigue limit for the same grain size may be attributed to the effect of active or free nitrogen, i.e. free nitrogen causes hardening so that the fatigue limit of the steel is raised to a higher level.

Nitrogen in a steel can cause two forms of hardening, viz., strain hardening and strain age hardening. In fatigue it is difficult to differentiate between the two forms of hardening. However, the contribution of nitrogen strain hardening may be indicated by studying the effects of active nitrogen on the flow stress of the two steels in tensile tests. Fig. 9.1 shows the flow stress of the eight experimental steels. These values were taken at 5% plastic strain from the tensile curves (see Figs 7.2 - 7.9). The low flow stress value of steel B(1) was due to the larger Luders strain of this steel, i.e., the flow curve was pushed to the right on the stress-strain curve. Fig. 9.1 shows that there is a distinct difference between the flow stress of the high and low nitrogen steels. Since these values were obtained prior to any ageing, the difference may be considered to be the effect of active nitrogen on strain hardening. This strain hardening by nitrogen was more predominant in a steel with a finer grain size.

Assuming that cyclic strain hardening is analogous to tensile strain hardening, (this will be qualified in a later Section, 9.5), then the

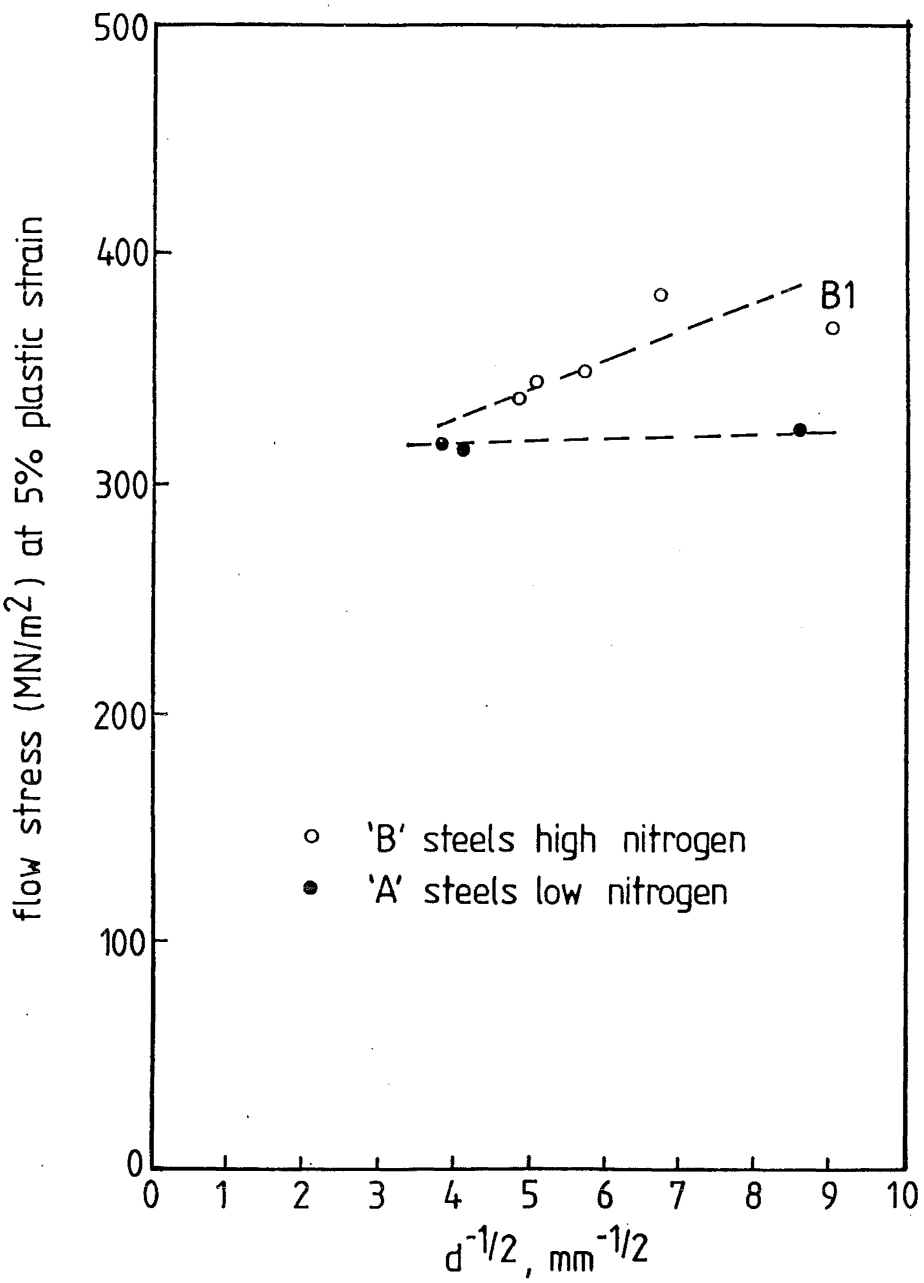

FIG. 9·1 EFFECTS OF FREE NITROGEN CONTENT AND GRAIN SIZE ON THE FLOW STRESS (AT 5% PLASTIC STRAIN) OF LOW CARBON STEEL

contribution of nitrogen strain hardening to improving the fatigue performance of low carbon steel may be assessed. Fig. 9.2 illustrates this diagrammatically. Lines 1 and 2 represent the fatigue limits (stress) of the low and high nitrogen steels respectively. The difference between the two lines is the result of total nitrogen hardening, i.e., nitrogen strain hardening plus strain age hardening. The total nitrogen hardening increases with increasing grain size. From the assumed analogy, nitrogen strain hardening is more effective as the grain size is reduced, hence a line (the dotted line in Fig. 9.2) can be drawn relative to line 1 to show this effect. It is now obvious from the diagram that the contribution from nitrogen strain hardening is only minimal (in the absolute sense). Hence, if any hardening was achieved by the high nitrogen steels during fatigue, it was gained mainly by way of strain age hardening. Because the magnitude of nitrogen strain hardening is small, it shall be assumed that its contribution approximates to zero, i.e., the difference between the fatigue limits of the high nitrogen and low nitrogen steels will be assumed to be due entirely to strain age hardening. It should also be noted that the low nitrogen A steels were not entirely free of active nitrogen and that their fatigue limits might have been slightly raised due to nitrogen strain hardening. Again, because of the small magnitude, nitrogen strain hardening will be ignored from here on.

Strain age hardening appeared to be more effective in improving the fatigue limit stress of coarse grained steels, whereas its effect on fine grained steels, say $d^{-\frac{1}{2}} \sim 9.0mm^{-\frac{1}{2}}$, was minimal. Oates and Wilson[6] using a different method of study, found that strain ageing had little effect on the fatigue performance of fine grained steels and at the same time, concluded that the fatigue limit of coarse grained steel was most probably controlled by its strain ageing propensity.

Although strain age hardening was not effective in fine grained steel B(1), that strain ageing still took place in the course of fatigue was established

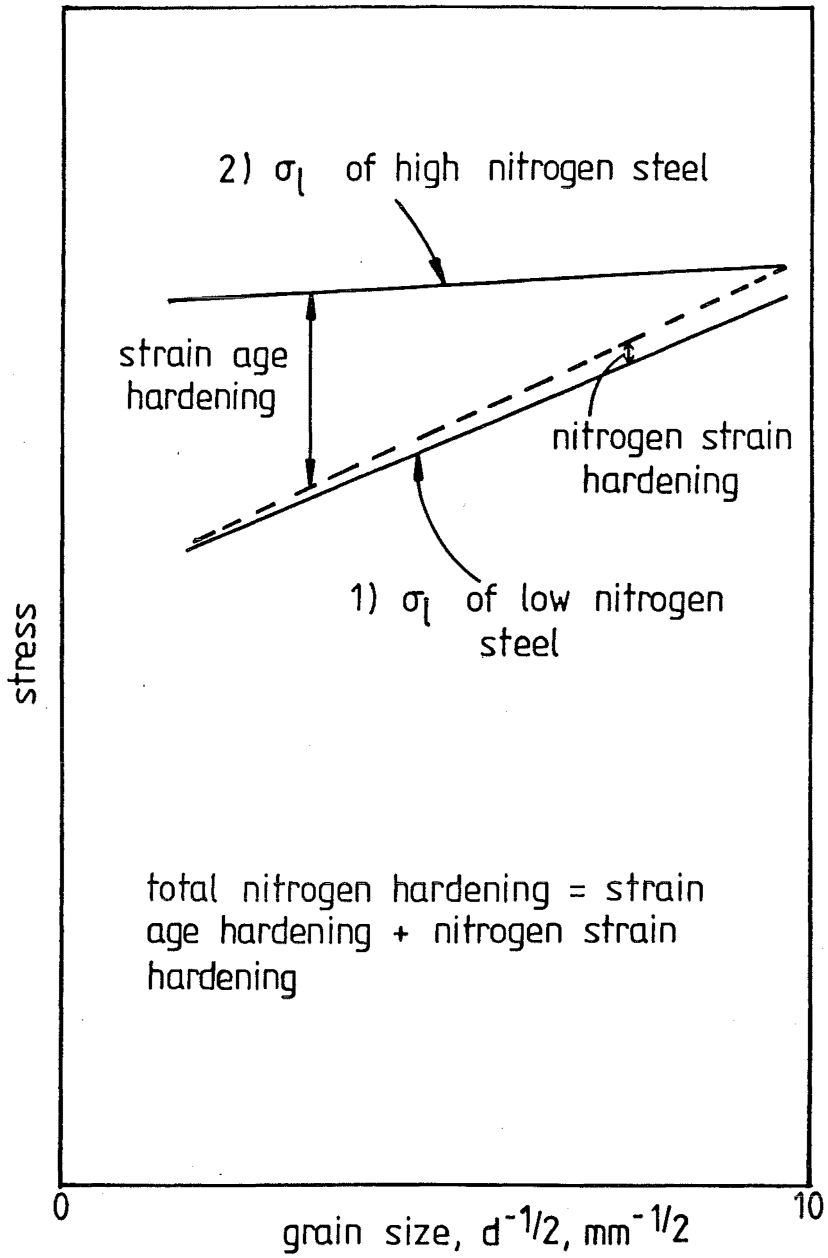

FIG. 9·2 DIAGRAMMATIC REPRESENTATION OF HARDENING DUE TO ACTIVE NITROGEN

beyond any doubt. Fig. 8.23 clearly shows a return of yield point in a tensile test after fatigue. It is difficult to assess how complete the ageing process was, since it was dynamic ageing. If it is assumed that strain ageing here was similar to the case of static ageing (i.e., where dislocations are stationary and solute atoms can diffuse to and segregate at dislocation sites) and if it is further assumed that complete static ageing would need a year at room temperature, then dynamic strain ageing would have been completed within a few hours considering the very high temperature reached during fatigue (over 100°C). However, the rapid removal of the returned yield point and the appearance of a smooth tensile curve after extended cycling time suggest that the strain ageing effect was overshadowed by some other factor after its completion, Fig. 8.23.

For the coarse grained steel B(5), proof of dynamic ageing (by the display of a returned yield point) during fatigue at σ_{CD} could not be obtained. The damping and temperature measurements taken during fatigue at σ_{CD} or just above, indicated a very slow change in the material properties, Figs 8.8 and 8.12. Since the specimen temperature remained low (below 40°C), ageing, if it did occur, would have been very gradual. The absence of a returned yield point in tensile curves of specimens fatigued to different lives (Fig. 8.18) suggest that ageing was absent and that hardening was purely due to cyclic strain hardening.

However, when the stress amplitude was raised to 165 MN/m^2, steel B(5) behaved in a similar manner to steel B(1) fatigued at σ_{CD}. A rapid damping and temperature rise was recorded and dynamic ageing was found to occur, Fig. 8.24. Considerable hardening was obtained during fatigue at this stress. Dynamic strain ageing was thus proved to be present in steels of all grain sizes provided there was sufficient active nitrogen.

By comparison to the yield stress, the fatigue limit of low carbon steel was relatively insensitive to changes in grain size. This is not

surprising when the type of dislocation motions is considered under these two forms of stressing. In uniaxial tension, dislocations are forced to move in one direction only. Because grain boundaries are effective barriers to mobile dislocations, more dislocation pile-ups would occur in a fine grained structure and hence raise the yield stress. The yield stress is therefore sensitive to grain size changes. In fatigue, dislocations move along slip planes back and forth with the alternating stress; pile-ups against grain boundaries are therefore less severe and the spread of yielding becomes less dependent on grain size.

9.2 THE EFFECT OF GRAIN SIZE AND ACTIVE NITROGEN CONTENT ON THE CRITICAL DAMPING STRESS, σ_{CD}

σ_{CD}, as defined in Section 8.1.4, is the minimum stress amplitude required to cause dislocation generation during fatigue cycling of low carbon steel. Associated with this increase in dislocation density is an increase in specimen damping and temperature and the removal of the original discontinuous yield point of the steel.

Although only two steels from each of the two nitrogen groups were tested, the results show that σ_{CD} was not influenced by the amount of active nitrogen in the steel. The graduation on the load scale of the Amsler Vibrophore control unit was such that loading could only be recorded with an accuracy of ± 2.5 MN/m^2. Since the maximum difference in σ_{CD} displayed by the high and low nitrogen steels was 5 MN/m^2 in the range of grain sizes considered, it may be said that within the experimental accuracy there was no difference in the critical damping stresses between the high and low nitrogen steels, i.e., it was possible to draw a straight line through the four points on a plot of σ_{CD} against $d^{-\frac{1}{2}}$, where d is the grain diameter, Figure 9.3.

That σ_{CD} is independent of the amount of active nitrogen in the steel is not unexpected if the definition of σ_{CD} is considered. σ_{CD} is the minimum

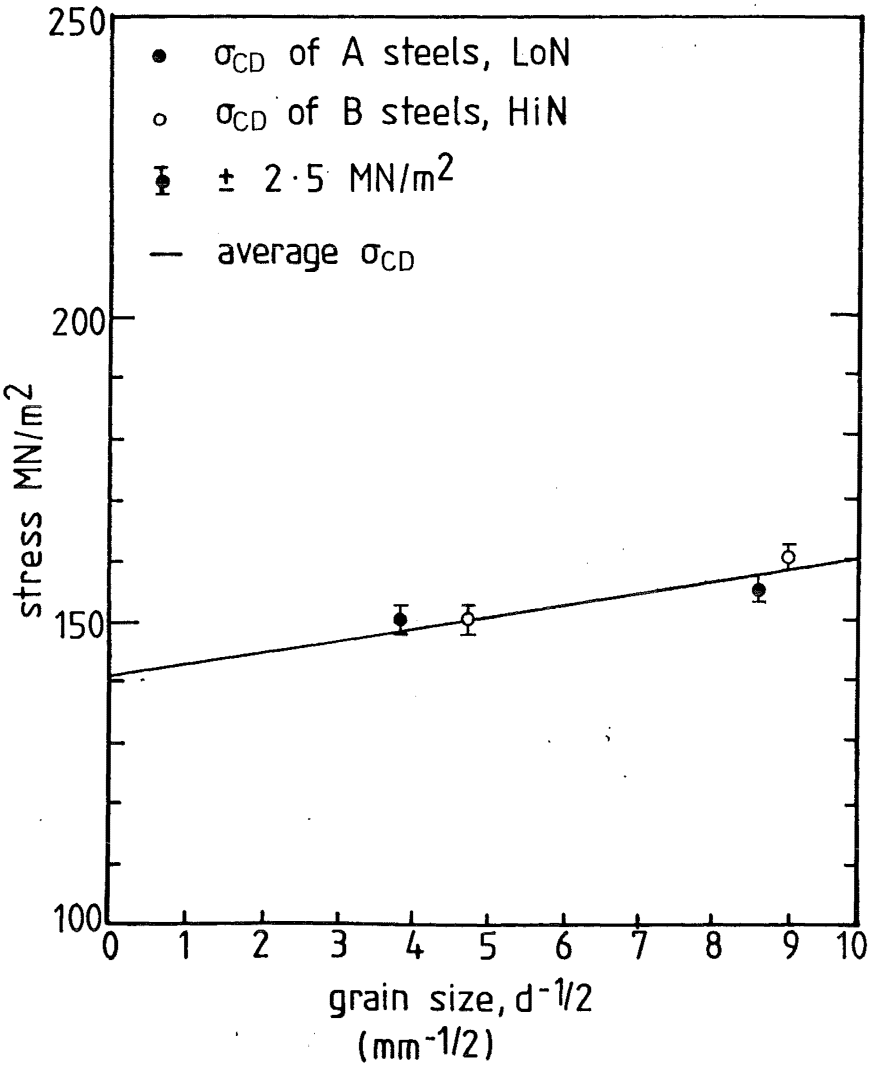

FIG. 9·3 EFFECT OF FREE NITROGEN CONTENT AND GRAIN SIZE ON THE CRITICAL DAMPING STRESS (σ_{CD}) OF LOW CARBON STEEL

stress required for a significant number of mobile dislocations to be generated. In uniaxial tension, mobile dislocations may be created by two different proposed mechanisms; by unlocking according to Cottrell's model, or by heterogeneous nucleation according to Hahn's model. Since σ_{CD} is below σ_y, unlocking in the Cottrell sense is unlikely to occur here and dislocations are most likely created by heterogeneous nucleation. Consequently σ_{CD} is not greatly affected by the locking effects of solute nitrogen atoms. (Note from Fig. 7.11 that the lower yield stress was also unaffected by the active nitrogen contents.)

The slope of σ_{CD} vs $d^{-\frac{1}{2}}$ line is small, (Fig. 9.3) and this suggests that σ_{CD} is not greatly affected by the grain size of the steel. This is analogous to microyielding of pure iron in uniaxial tension where initial slip occurs at a stress below the lower yield stress, σ_y. The microyielding stress is not affected by grain size[107] but subsequent yielding behaviour after initiation is very much dependent on d. In fatigue, σ_{CD} is only mildly dependent on the grain size, but the type of yielding behaviour produced by fatigue cycling at σ_{CD} varies with the grain size, e.g., compare Fig. 8.5 and Fig. 8.6.

9.3 THE EFFECTS OF FATIGUE CYCLING AT THE CRITICAL DAMPING STRESS, σ_{CD}

Fatigue cycling of low carbon steel specimens at its σ_{CD} produced considerable changes in the properties of the steel. At first sight, there appeared to be some differences in the effects of fatigue on coarse and fine grained steels; however, closer examination indicated that similarities could be found.

Cyclic stressing of the fine grained steels A(1) and B(1) at σ_{CD} revealed that there were three distinct stages characterised by different damping behaviour, Fig. 8.5 and 8.7. The first stage of cycling produced no apparent changes in the material. If there were any changes, these were not detected by damping and temperature measurements and observations for surface damage.

This stage usually lasted for about 10^6 to 3 x 10^6 cycles.

The transition from the first to second stage occurred very abruptly and this second stage, the transient stage, occupied a very short period of the total cycling time and was completed in less than 10^5 cycles (~ 10 minutes of running time). Even though this was the shortest stage by far, most of the changes associated with fatigue appeared to occur during this time. The characteristic of this period was the steep and large rise in the specimen damping capacity and temperature, Figures 8.5, 8.7, 8.9 and 8.11. The first noticeable property change accompanying this damping/temperature rise was provided by a specimen fatigued to the beginning of this stage. Curve 2 in Fig. 8.23 shows that the tensile curve of such a fatigued specimen had a suppressed original yield drop and Luders strain. This could be attributed to the generation of mobile dislocations during fatigue so that with an increased mobile dislocation density, the original yield point was being eliminated. For the high nitrogen steel B(1), cyclic stressing to the end of the second stage (i.e. until the specimen temperature had reached the maximum) caused dynamic strain ageing to take place. This is proved by curve 3 in Fig. 8.23, which shows the tensile curve of a specimen fatigued to this stage. A return of the yield point at a higher stress was recorded. Dynamic strain ageing at this stage was not unexpected considering the increased mobile dislocation density and the high temperature of the specimen (~170°C). A considerable amount of hardening was achieved up to this stage of cycling. For the low nitrogen steel A(1), dynamic strain ageing did not take place since the tensile curve of a specimen fatigued to this stage did not exhibit a returned yield point, curve 3 in Fig. 8.25. However, there was still a substantial gain in hardening.

For both steels A(1) and B(1), occurring almost simultaneously with these property changes was the widespread formation of persistent slip bands on the surfaces of the specimens. At the end of this second stage, the

formation of PSB's was almost complete, Fig. 8.31.

The final stage of fatigue cycling at σ_{CD} was the saturation strain stage where equilibrium was established and prolonged cycling produced no further changes. At the transition from the second to third stage, the returned yield point in steel B(1) was suppressed so that by the end of the test at 5×10^7 cycles, a smooth stress-strain curve was recorded for the specimen, curve 5 in Fig. 8.23. Persistent slip bands formation remained visibly unchanged and further hardening was negligible. The saturation stage occupied up to 90% of the total cycling time. At the end of the test, observations of microstructure revealed widespread yielding in the steels, Fig 8.32 and 8.34, and steel B(1) also exhibited cellular dislocation structure, Fig. 8.40.

Fatigue cycling of the fine grained steels at stress amplitudes above σ_{CD} produced similar effects, viz., rapid damping/temperature rise at some stage after cycling had commenced, removal of the original yield point, hardening, etc. The only difference was that, as the stress amplitude was increased, the damping/temperature rise occurred at an earlier stage, e.g. Fig. 8.7.

Fatigue cycling of fine grained steels at stress amplitudes below σ_{CD} did not effect any change. No damping/temperature rise was recorded and the steel tensile properties remained unaltered. No PSB's were observed on the specimen surface and micro-examination revealed no widespread plastic yielding, Figs 8.38 and 8.39. The dislocation structure consisted of both undisturbed dislocations and some dipole loops. No heavy clusters or cells were formed, Figs 8.44 and 8.45.

The clearcut difference between fatigue cycling at σ_{CD} and below σ_{CD} observed for fine grained steels was not so obvious for the coarse grained steels A(3) and B(5), e.g., see Figs 8.6, 8.8, 8.10 and 8.12. Instead of

the sudden and spectacular rise in specimen damping and temperature, the increases were gradual and the maximum temperature attained was only 25°C (compared to over 100°C for steels A(1) and B(1)). However, the effects of cycling at σ_{CD} on the tensile properties were similar. The original yield points of the steels were eliminated and a smooth tensile curve resulted after 5 x 10^7 cycles of loading, Figs 8.14 and 8.16. Some hardening was achieved but this was small compared to that in a fine grained steel. A major difference from the fine grained steel B(1) was that dynamic strain ageing could not be detected during fatigue of steel B(5), even when the stress was 155 MN/m^2 (above σ_{CD}), Fig. 8.18. PSB's were formed on the surface of specimens during fatigue, but these were fewer in numbers compared to the fine grained steels, Figs 8.28 and 8.30. Considering the gradual temperature rise and the slower hardening rate, Fig. 8.18, the formation of PSB's appeared to take place over a longer cycling period, compared to the sudden burst seen in fine grained steels. Transmission electron microscopy studies showed that sharp sub-grain boundaries were formed by dislocations after 5 x 10^7 cycles of fatigue, Fig. 8.42, and cellular structure was absent. Etch-pitting studies indicated that yielding occurred in some grains but was not generally as widespread as in the fine grained steels, Figs 8.33 to 8.35.

Fatigue cycling of the coarse grained steels A(3) and B(5) at stress amplitudes below their respective σ_{CD} produced no changes in the steel properties. The damping and temperature of the specimens remained low, Figs 8.6, 8.8, 8.10 and 8.12, and the steel tensile curves were unaltered after fatigue, Figs 8.14 and 8.16. However, at some stress amplitude above σ_{CD} but below σ_{ℓ}, rapid temperature/damping rise was recorded during fatigue of these two steels, Figs 8.24 and 8.26. In the case of steel B(5), dynamic strain ageing was detected (curves 2 and 3 in Fig. 8.24) and a big increase in hardening was recorded. Although this transient stage was also detected for steel A(3), the hardening achieved was small, probably due to a lack of strain age hardening, Fig. 8.26.

Since rapid temperature/damping rise and dynamic ageing were observed in both fine and coarse grained high nitrogen steels, it may be said that there is essentially no difference in their fatigue processes. The apparent difference observed at lower stresses, i.e., at their respective σ_{CD}, may be attributed to the difference in dislocation generation rates in the two steels. It is well established that in uniaxial tension, a fine grained steel, when plastically strained, shows a higher dislocation density than a coarse grained steel strained to the same degree[43,44], hence a fine grained steel has a higher rate of dislocation generation. If this also holds in the case of fatigue, then fatigue cycling at σ_{CD} (which is the minimum stress required for dislocation generation) would cause more dislocations to be generated in the fine grained steel. This, in turn, increases the damping energy released so that the specimen temperature is raised to accelerate ageing. For the coarse grained steel, cycling at σ_{CD} produces sufficient mobile dislocations to eliminate the original yield point, but the temperature is not raised significantly to induce accelerated ageing due to a smaller number of dislocations generated. To obtain accelerated ageing, the specimen temperature has to be raised and this may be achieved by using a higher fatigue stress amplitude to increase the dislocation generation rate. For the experimental steel B(5), a stress of 160 - 165 MN/m^2, i.e. above σ_{CD} but below σ_{ℓ} was sufficient to cause dynamic ageing.

Thus, at stresses just below σ_{ℓ} and above σ_{ℓ}, i.e. in the S-N curve region of the steel, it may be said that fine and coarse grained steels respond in a similar manner to fatigue stressing. Fatigue cycling at these stress amplitudes would cause hardening and dynamic ageing to occur regardless of the grain size of the steel provided the steel contains a sufficient level of active nitrogen.

9.4 THE RELATIONSHIP BETWEEN THE YIELD STRESS, FATIGUE LIMIT AND CRITICAL DAMPING STRESS

The fact that the lower yield stress line (σ_y) and the fatigue limit

line (σ_ℓ) cross on a plot of stress versus $d^{-\frac{1}{2}}$ (d is the grain diameter), Fig. 7.11, gives an impression that two different mechanisms are operative in fatigue of low carbon steels; one for fine grained steels where $\sigma_y \geq \sigma_\ell$ and the second for coarse grained steels, $\sigma_y < \sigma_\ell$. Oates and Wilson[6] proposed such a theory. They suggested that the fatigue limit of a coarse grained steel was a direct result of strain ageing while that of a fine grained steel was due to the effect of initial dislocation locking. If their suggestion for the fine grained steel is correct, then the fatigue limit line (for the fine grained steels) should be approximately parallel to the yield stress line, since the yield stress is a consequence of initial dislocation locking. Therefore, a plot of σ_ℓ vs $d^{-\frac{1}{2}}$ would not yield a straight line but a line with two different slopes. The straight line relationship between σ_ℓ and $d^{-\frac{1}{2}}$ has been proved by Klesnil *et al*[8] and confirmed in Figure 7.11. It has also been shown that the fatigue mechanism is the same for steels of all grain sizes. Thus the differentiation by Oates and Wilson[6] of the two mechanisms appears doubtful.

It must be noted that σ_y is the stress at the beginning of macro plastic yielding while σ_ℓ represents the stress amplitude required to cause failure after a considerable amount of plastic deformation. σ_y and σ_ℓ are therefore not exactly comparable and the significance of the relationship shown on Fig. 7.12 is not clear. It is perhaps more appropriate to compare σ_ℓ with the tensile stress, σ_{UTS}.

Although the physical meaning of σ_y/σ_ℓ is not obvious, the good correlation shown by these two important properties may be useful information. This relationship may also be obtained by assuming a Hall-Petch type relationship for both σ_y and σ_ℓ and expanding their ratio as a series.

Thus if $\sigma_y = \sigma_i + k_y d^{-\frac{1}{2}}$

$\sigma_\ell = \sigma_{i\ell} + k_{y\ell} d^{-\frac{1}{2}}$, σ_i, $\sigma_{i\ell}$, k_y, $k_{y\ell}$ are constants,

then $$\frac{\sigma_y}{\sigma_\ell} = \frac{\sigma_i + k_y\, d^{-\frac{1}{2}}}{\sigma_{i\ell} + k_{y\ell}\, d^{-\frac{1}{2}}}$$

$$= \left(\frac{\sigma_i}{\sigma_{i\ell}}\right) + \left(\frac{k_y}{k_{y\ell}} - \frac{\sigma_i}{\sigma_{i\ell}}\right)\left[\left(\frac{k_{y\ell}}{\sigma_{i\ell}}\, d^{-\frac{1}{2}}\right) - \left(\frac{k_{y\ell}}{\sigma_{i\ell}}\, d^{-\frac{1}{2}}\right)^2 + \left(\frac{k_{y\ell}}{\sigma_{i\ell}}\, d^{-\frac{1}{2}}\right)^3 \ldots\right]$$

$$= \frac{\sigma_i}{\sigma_{i\ell}} + \left(\frac{k_y}{k_{y\ell}} - \frac{\sigma_i}{\sigma_{i\ell}}\right) \sum_{n=1}^{\infty} (-1)^{n+1} \left(\frac{k_{y\ell}}{\sigma_{i\ell}}\, d^{-\frac{1}{2}}\right)^n \qquad \text{Equation (9.1)}$$

Now, the series is convergent if $\left| \frac{k_{y\ell}}{\sigma_{i\ell}}\, d^{-\frac{1}{2}} \right| < 1$

This requires $\left| d^{-\frac{1}{2}} \right| < \frac{\sigma_{i\ell}}{k_{y\ell}}$

The values of $\sigma_{i\ell}$ and $k_{y\ell}$ may be obtained from Fig. 7.11, e.g., for the A steels,

$$\sigma_{i\ell} = 147 \text{ MN/m}^2$$

$$k_{y\ell} = 4.3 \text{ MN/m}^2/\text{mm}^{-\frac{1}{2}}$$

$$\therefore \quad \left| d^{-\frac{1}{2}} \right| < \frac{147}{4.3} \text{ mm}^{-\frac{1}{2}}$$

$$= 34.19 \text{ mm}^{-\frac{1}{2}}.$$

Hence, in the range $0 < d^{-\frac{1}{2}} < 10$, convergence is satisfied. Similarly, it can be shown that the expansion is convergent using $\sigma_{i\ell}$ and $k_{y\ell}$ values of the B steels.

For $0 < d^{-\frac{1}{2}} < 10$, terms higher than the second order are small and may be neglected. Equation 9.1 is reduced to

$$\frac{\sigma_y}{\sigma_\ell} = \frac{\sigma_i}{\sigma_{i\ell}} + \left(\frac{k_y}{k_{y\ell}} - \frac{\sigma_i}{\sigma_{i\ell}}\right) x \left(\frac{k_{y\ell}}{\sigma_{i\ell}}\, d^{-\frac{1}{2}}\right) x \left[1 - \left(\frac{k_{y\ell}}{\sigma_{i\ell}}\, d^{-\frac{1}{2}}\right)\right] \qquad \text{Equation (9.2)}$$

This is an equation of a parabola.

From Fig. 7.11,

	$\sigma_i = 70 \text{ MN/m}^2$	$k_y = 23 \text{ MN/m}^2/\text{mm}^{-\frac{1}{2}}$
A Steels	$\sigma_{i\ell} = 147 \text{ MN/m}^2$	$k_{y\ell} = 4.3 \text{ MN/m}^2/\text{mm}^{-\frac{1}{2}}$
B Steels	$\sigma_{i\ell} = 163 \text{ MN/m}^2$	$k_{y\ell} = 2.6 \text{ MN/m}^2/\text{mm}^{-\frac{1}{2}}$

Substituting into Equation 9.2,

A Steels, $$\left(\frac{\sigma_y}{\sigma_\ell}\right)_A = 0.48 + 0.14 \left[d^{-\frac{1}{2}} - 0.027 \left(d^{-\frac{1}{2}}\right)^2\right] \quad \text{Equation (9.3)}$$

B Steels, $$\left(\frac{\sigma_y}{\sigma_\ell}\right)_B = 0.43 + 0.13 \left[d^{-\frac{1}{2}} - 0.016 \left(d^{-\frac{1}{2}}\right)^2\right] \quad \text{Equation (9.4)}$$

Equations 9.3 and 9.4 are plotted on Fig. 9.4. Also shown is the parabola fit to the experimental data given in Fig. 7.12. The curvilinear regression gave the expression

$$\frac{\sigma_y}{\sigma_\ell} = 0.56 + 0.12 \left[d^{-\frac{1}{2}} - 0.023 \left(d^{-\frac{1}{2}}\right)^2\right] \quad \text{Equation (9.5)}$$

Correlation factor R = 0.96.

The curves were almost identical and this gave further indication that σ_ℓ and $d^{-\frac{1}{2}}$ followed a Hall-Petch type relationship for $0 < d^{-\frac{1}{2}} < 10$ mm$^{-\frac{1}{2}}$. Consequently, there can only be a single mechanism of fatigue for steels of all grain sizes in this range.

It is interesting to note that Shih *et al*[179] found some correlation between the anelastic limit and endurance limit of 0.4%C steel. Although their endurance limit was obtained by rotating bending fatigue and the anelastic limit by loading-unloading in tension, they nevertheless, showed that the two properties were similar functions of the tempering temperature and hardness of the steel.

A plot of the fatigue limits and critical damping stress, σ_ℓ and σ_{CD} against $d^{-\frac{1}{2}}$ is shown in Fig. 9.5. σ_{CD} as defined in Section 8.1.4 and verified experimentally was the minimum stress in fatigue required to create mobile dislocations, eliminate the discontinuous yield point in a tensile curve and cause PSB formation on the specimen surface. For the fine grained steel B(1), it was also the minimum stress required for dynamic ageing to occur.

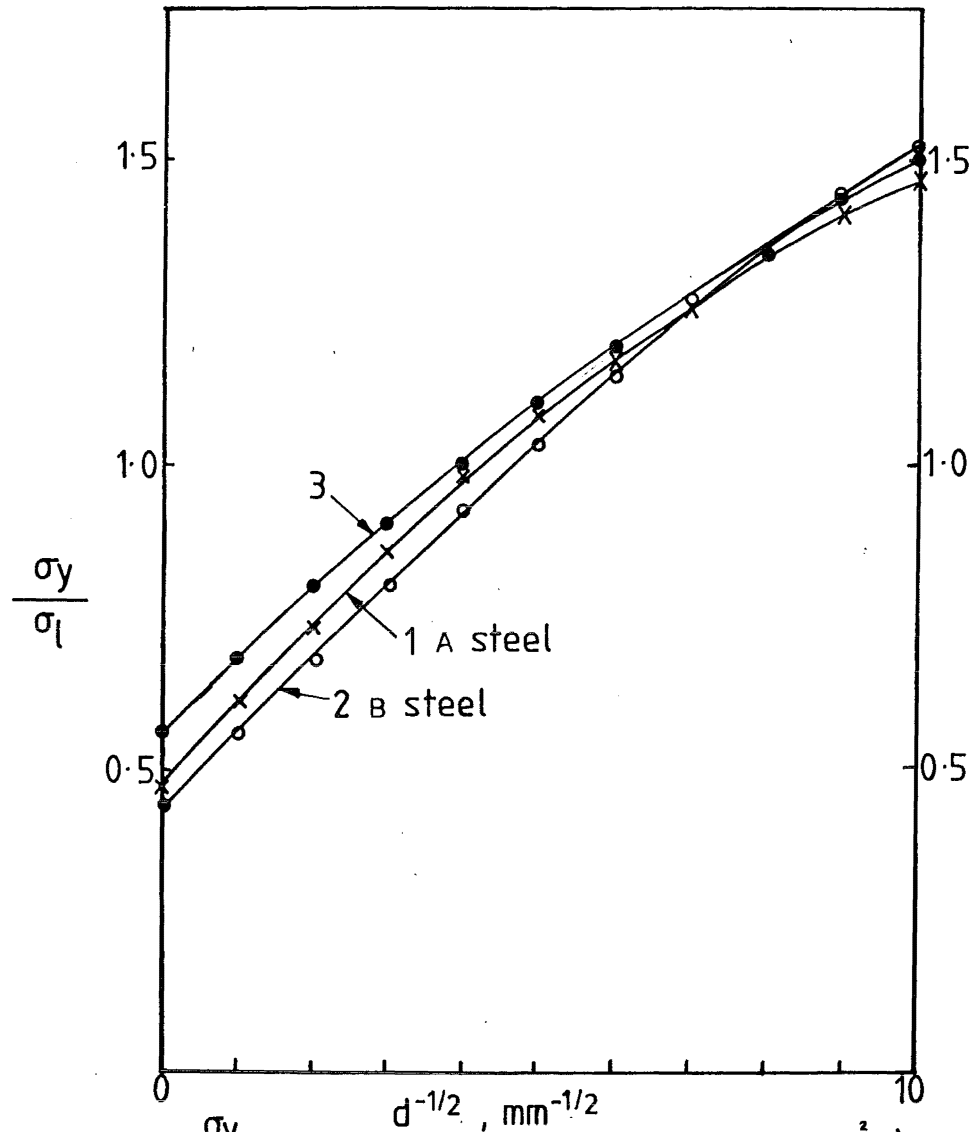

1. equation (9·3). $(\frac{\sigma y}{\sigma_l})_A = 0{\cdot}48 + 0{\cdot}14\,[\,d^{-1/2} - 0{\cdot}027\,(d^{-1/2})^2\,]$
2. equation (9·4). $(\frac{\sigma y}{\sigma_l})_B = 0{\cdot}43 + 0{\cdot}13\,[\,d^{-1/2} - 0{\cdot}016\,(d^{-1/2})^2\,]$ } by expansion
3. equation (9·5). $(\frac{\sigma y}{\sigma_l}) = 0{\cdot}56 + 0{\cdot}12\,[\,d^{-1/2} - 0{\cdot}023\,(d^{-1/2})^2\,]$ - from experimental data

FIG. 9·4 INFLUENCE OF GRAIN SIZE ON THE YIELD STRESS/ FATIGUE LIMIT RATIO OF LOW CARBON STEEL

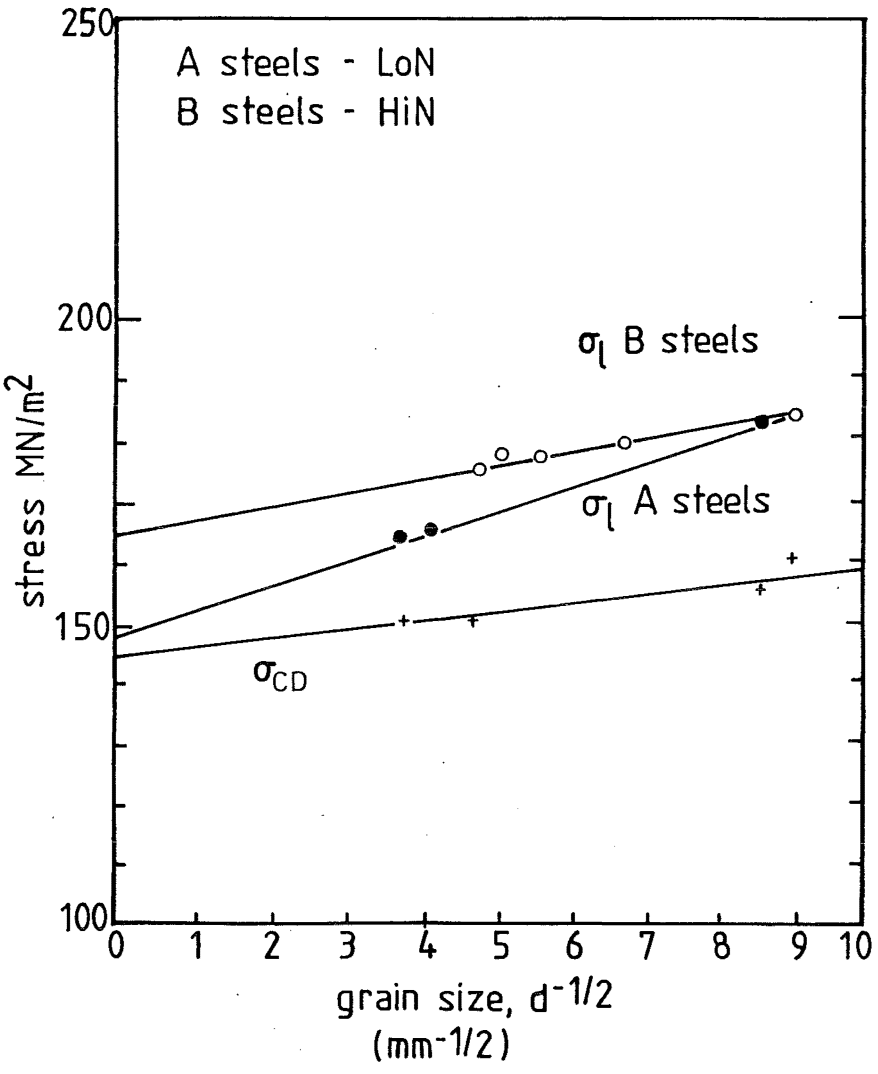

FIG. 9·5 EFFECTS OF FREE NITROGEN CONTENT AND GRAIN SIZE ON THE FATIGUE LIMITS AND CRITICAL DAMPING STRESS OF LOW CARBON STEEL

The experimental results showed that fatigue cycling at stresses below σ_{CD} could not cause cyclic strain hardening or strain ageing, Figs 8.13 to 8.16. Thus, σ_{CD} could be considered as the fatigue limit of a "perfect" steel which would not cyclically strain harden and dynamically strain age harden.

The A steels contained low levels of active nitrogen, A(1) with 0.0013%N and A(3) with 0.0001%N did not show dynamic strain ageing during fatigue, Figs 8.25 and 8.26. Since the fatigue limit of an A steel (non-ageing steels) was above its σ_{CD} the difference could be attributed to cyclic strain hardening, i.e., because all steels are capable of strain hardening, the fatigue limits are raised. (The contribution of interstitial nitrogen to strain hardening is assumed zero, see 9.1). Likewise, since the fatigue limit of a B steel (ageing steel) was above that of an A steel, the difference could be due to strain age hardening. Thus, in general, the total hardening achieved in a low carbon steel is a sum of cyclic strain hardening and strain age hardening, provided there is sufficient active nitrogen in the steel to allow for ageing.

It was mentioned earlier in Section 9.1 that strain age hardening was more extensive in a coarse grained steel than a fine grained steel. Fig. 9.5 shows that an opposite trend was observed for cyclic strain hardening. The different contributions of the two forms of hardening for steels of different grain sizes may be shown by comparing tensile curves of cyclically pre-stressed steels.

Figs 8.23 and 8.25 show the tensile curves of steels B(1) and A(1) fatigued at their respective σ_{CD} to different stages. Consider only the tensile curve of a run-out specimen in each case (curve 5 in Fig. 8.23, curve 4 in Fig. 8.25). For steel A(1), the hardening achieved by fatigue was due to cyclic strain hardening only (ignoring again the effect of nitrogen), and for steel B(1), it was a combination of cyclic strain hardening and strain age hardening. For steel B(1), the contribution of cyclic strain

hardening may be estimated by comparing it with that of steel A(1). If these two steels were of the same grain size and fatigued at the same stress, then they would achieve the same amount of cyclic strain hardening. However, B(1) steel had a finer grain structure and it was also fatigued at a higher stress amplitude; therefore, the amount of cyclic strain hardening must be higher than that achieved by steel A(1). Thus, by comparing the magnitudes of hardening from Figs 8.23 and 8.25, and taking into account the different grain sizes and cyclic stress amplitudes, it appears that cyclic strain hardening was the chief contributor to the total strengthening of fine grained steel B(1).

Steel B(5), coarse grained, when fatigued at its σ_{CD} (150 MN/m^2) and 155 MN/m^2 did not show dynamic strain ageing, Fig. 8.18, and the hardening, purely cyclic strain hardening, was small compared to that achieved by the fine grained steels. However, when the stress amplitude was raised to 165 MN/m^2 dynamic ageing was observed and the hardening was vastly improved, Fig. 8.24. This demonstrates that strain age hardening was the major strengthening mechanism for the coarse grained steel B(5). Referring to Fig. 8.16, the large improvement gained by cycling at 160 MN/m^2 indicated that ageing was probably occurring at that stress amplitude. From the temperature reading, Fig. 8.12 and using Hundy's Equation (Equation 3.1), calculations showed that ageing was almost half completed in this case. This explains the large increase in hardening. It is interesting to note that from Fig. 9.5, a non-ageing steel of the same grain size as B(5), $d^{-\frac{1}{2}} = 4.82$ mm$^{-\frac{1}{2}}$ has a fatigue limit of about 165 MN/m^2.

Further proof of the importance of strain age hardening in coarse grained steels may be obtained by comparing steels A(3) and B(5). Steel A(3) did not exhibit any dynamic ageing when fatigued at 160 MN/m^2, Fig. 8.26, and the amount of cyclic strain hardening was small. Steel B(5), which showed dynamic ageing when fatigued at the same stress, hardened more significantly due to the contribution of strain age hardening, Fig. 8.16.

9.5 MECHANISM OF FATIGUE - SUGGESTED THEORY

Before the grain size dependence of strain age hardening and cyclic strain hardening can be explained, it is necessary to understand the dislocation mechanics during fatigue. Hence, at this point of the discussion, an attempt will be made to describe the mechanism of fatigue in terms of dislocation behaviour under cyclic stress conditions.

It has been shown by the experimental results that fatigue cycling of the fine grained steels A(1) and B(1) at their σ_{CD} produced a 3-stage behaviour, Section 9.3. This was also observed in the coarse grained steels B(5) and A(3) when the stress amplitude was raised above their σ_{CD} but below σ_{ℓ}. Thus, in the area of main interest, i.e., at stresses just below or above σ_{ℓ}, the S-N curve region, it may be said the fatigue cycling of a low carbon steel of any grain size may be divided into three stages. These three stages, as mentioned in Section 9.3, are:

1) An initial stage where no damping/temperature changes are noticeable, no persistent slip bands are formed and the original discontinuous yield point of the steel is not eliminated.

2) Transient stage, which occupies a very small proportion of the total cycling time. During this stage, rapid damping and temperature rises are recorded, the original yield point of the steel is eliminated, dynamic strain ageing may occur depending on the amount of free nitrogen in the steel, and widespread formation of PSB's occur on the specimen surface. Initial softening (removal of yield point) is followed by rapid strain hardening, and in steels with active nitrogen, also by strain age hardening.

3) The saturation strain stage. Prolonged fatigue cycling causes little or no further strain hardening. Persistent slip band formation is completed in the early part of this stage and the returned yield point, if there was dynamic strain ageing, is rapidly suppressed. No further changes

are noticeable until run-out if the cyclic stress is below σ_ℓ. Fig. 9.6 shows diagrammatically this 3-stage behaviour of a steel fatigued at a stress (below σ_ℓ) sufficiently high to cause rapid temperature or damping rise.

(Note: As the cyclic stress amplitude is increased, the initial stage is shortened. When the stress is at or above fatigue limit stress, the initial stage may be completely absent, i.e., temperature rise starts immediately).

Opinions are varied among workers as to whether cyclic stressing is analogous to uniaxial tension. Certainly some aspects of fatigue are unique to cycling, the most notable being the saturation strain. However, the overall effects of cyclic stressing are similar to those produced by uniaxial tension. This may be seen by comparing the tensile curves of steels pre-strained to different degrees (assuming no ageing has occurred in between tests) with those of steels fatigued at different stress amplitudes, see Fig. 9.7. (Note: Strictly speaking, the effects of cyclic pre-stress should be compared to the effects of tensile pre-stress and not tensile pre-strain. Tensile pre-strain was chosen here so as to make the comparison more easily understood.) The amount of hardening increases with the pre-strain in tension, and with the cyclic stress amplitude in fatigue. Small pre-strains and lower cyclic stress amplitudes ($\sim\sigma_\ell$) tend to produce dipole loops and dislocation clusters. As the pre-strain and cyclic stress amplitude are increased, there is a tendency for cell dislocation structures to form[5,32,43]. Therefore, it may be said that cyclic stressing is analogous to uniaxial tensile straining. In other words, the effect of cyclic stressing at a stress above σ_{CD} is equivalent to straining a steel past its Luders strain extension in tension, except that there is no visible physical changes, i.e., no elongation and that the strain hardening rate is lower. Since all the major changes in fatigue occur during the transient stage, the analogy can be more specifically drawn between tensile strain

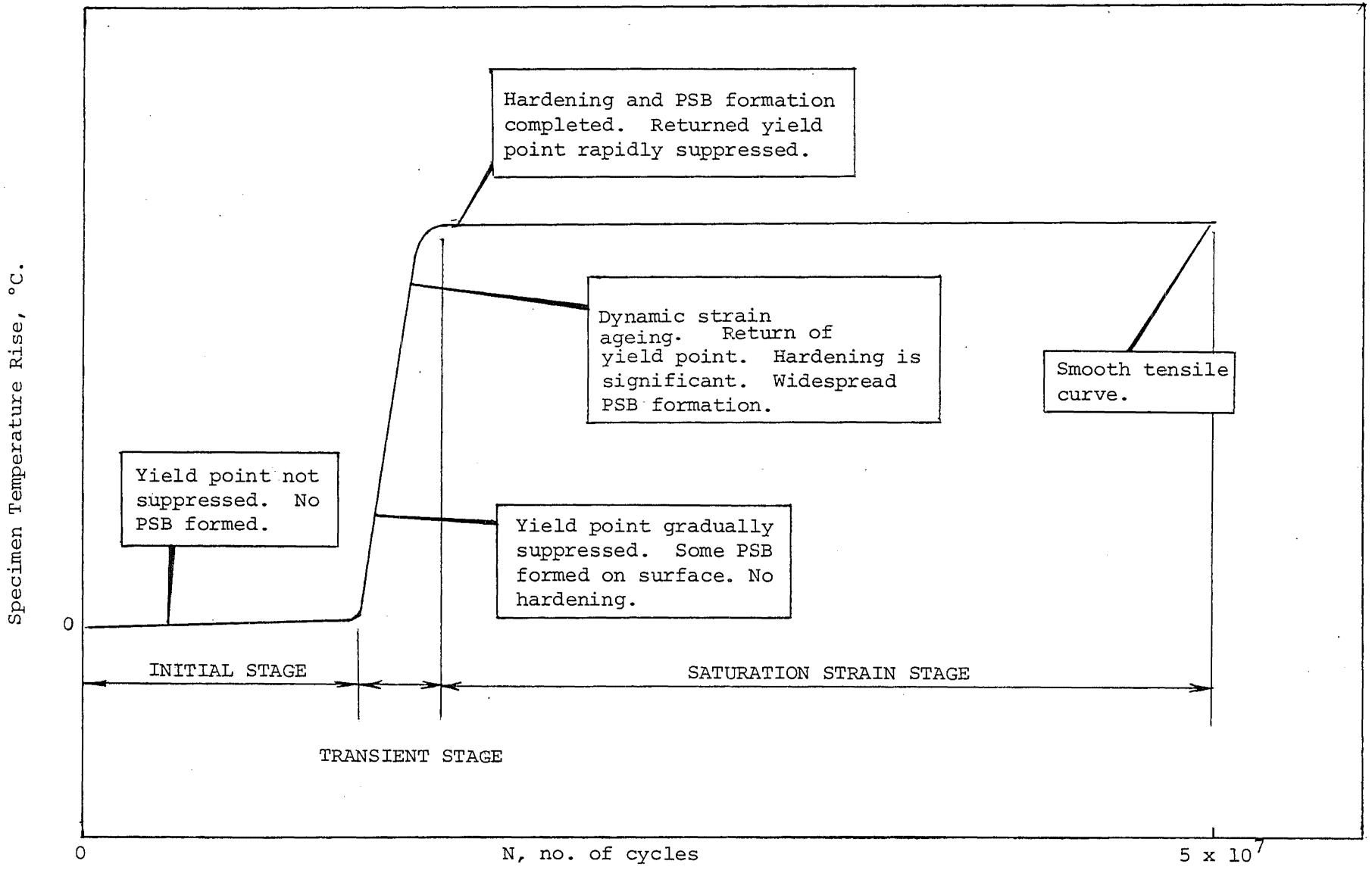

FIG. 9.6: Schematic Representation of the 3-Stage Fatigue Cycling Process

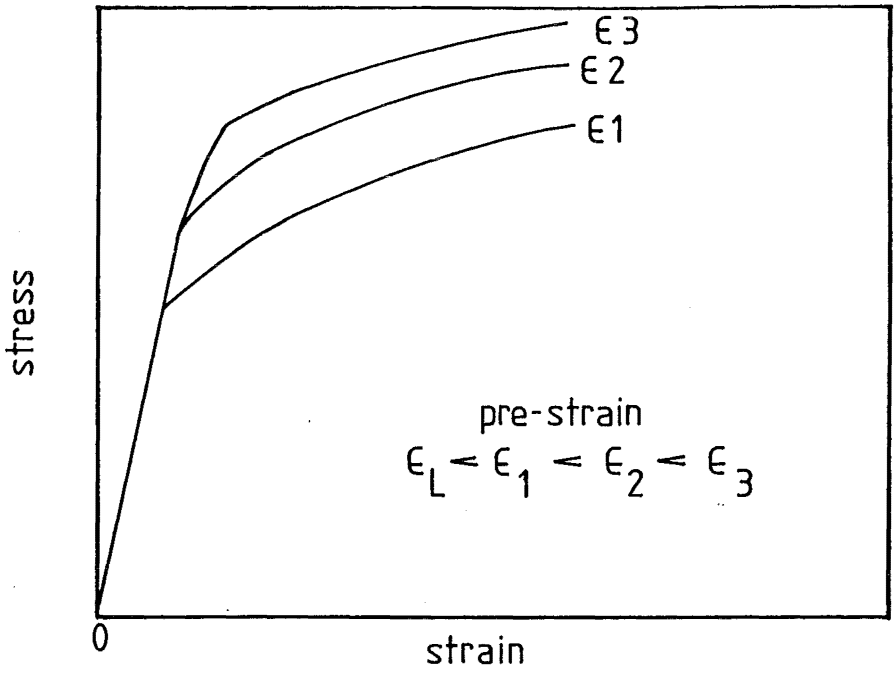

FIG. 9·7 (a) EFFECT OF TENSILE PRE-STRAINING ON STRESS-STRAIN CURVE OF LOW CARBON STEEL

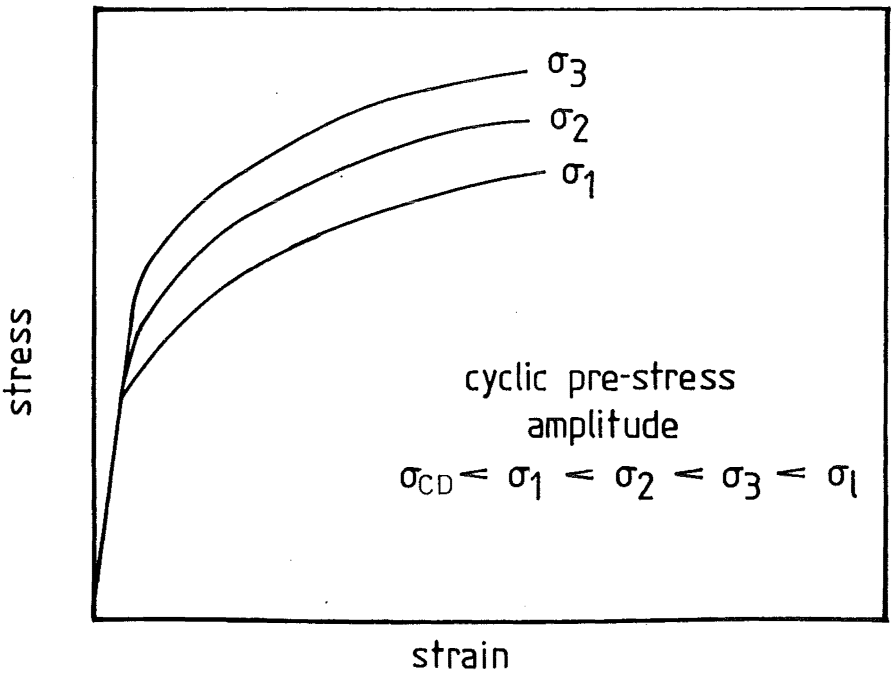

FIG. 9·7 (b) EFFECT OF CYCLIC PRE-STRESSING ON STRESS-STRAIN CURVE OF LOW CARBON STEEL

hardening and softening/rapid strain hardening in fatigue[42]. This assumption seems valid since it has been shown in both uniaxial tension[180] and fatigue[139] that hardening is due to and dependent on the increase in dipole loop density.

For simplicity, various terms which will be used in the following discussion are represented by symbols; these are:

ρ = total dislocation density

ρ_i = immobile dislocation density

ρ_m = mobile dislocation density, $\rho = \rho_m + \rho_i$

n = dislocation velocity exponent from Equation 5.8 or dislocation mobility factor

s = mean-free-path or mobile dislocations.

In the first stage of cycling, all the strain is taken up by existing mobile dislocations which can move relatively freely due to a low ρ. The initial s is a function of ρ at this stage[181], and it is also a function of the grain size[182].

When damping starts to increase, i.e., the beginning of stage two, mobile dislocations are being created and ρ_m increases. This causes a suppression of the original discontinuous yield point, see Fig. 8.23, curve 2. Little hardening is achieved at this point, an indication that ρ_i has not increased. The generation of large numbers of mobile dislocations and their simultaneous motions cause the release of damping energy in the form of heat, and the ensuing temperature rise (100°C - 150°C at a test frequency of 170 Hz) accelerates the ageing process if the steel contains sufficient solute atoms. This is indicated by a return of the yield point at a higher stress, curve 3 in Fig. 8.23. In the case of a steel with a low level of solute nitrogen atoms, ageing does not take place, curve 3,in Fig. 8.25. When dynamic strain ageing commences, some dislocations become immobilised. These pinned dislocations act as effective obstacles to other mobile

dislocations so that further immobilisation takes place by entanglement. Also, mobile dislocations interacting with each other cause the creation and accumulation of large numbers of primary and coplanar dipoles[139] and these dipole loops act as further obstacles for moving dislocations. It has been shown in cases where ageing is absent, hardening in fatigue is determined by the extent of cross-slip and the increase in dipole density[145,183,184]. Therefore, ρ_i is increased by both dislocation locking and dislocation interaction and hardening is a combination of strain age hardening and cyclic strain hardening. Since ρ_i continuously increased at the expense of ρ_m, and s is decreased and since a certain ρ_m must be maintained to cope with the applied strain, dislocation generation must be a continuous process during the entire transient stage. The regions of high dislocation density, i.e., tangles or clusters, provide ideal sites for nitrogen atoms to diffuse to and consequently the interstitial nitrogen content is rapidly depleted.

Further cycling causes a rearrangement of the dislocations into cells or bands (i.e. subgrain boundaries) and the regions between cell walls or bands are relatively free of dislocations. s now becomes constant and since mobile dislocations can move freely within the 'clear' area, hardening virtually ceases at this stage. Thus, at the end of the softening/rapid hardening stage (transient stage), ρ_i has been greatly increased, dislocations immobilised by locking or entanglement are arranged in some structures (cells or bands) and almost all the nitrogen is segregated to these regions of high dislocation density, i.e. cell walls and bands. (For complete segregation of all nitrogen atoms to these areas in a steel with 0.006%N, ρ_i has to be about 3×10^{10} lines/cm^2, see Appendix C.)

Stage 3 of fatigue cycling (saturation strain stage) is characterised by almost zero hardening. ρ_m may increase initially until a constant value is reached when the number of mobile dislocations with a constant s can sustain the applied strain. The final value of ρ_m is not known, but

judging by the rapid suppression of the returned yield point, Fig. 8.23, it may be quite high. In tensile straining, it has been shown that past the Luders strain extension, ρ_m remains constant at ~10^8 lines/cm^2 (185). ρ_i is the component that increases with strain and is responsible for the increase in flow stress. Thus if analogy is assumed between cyclic and tensile straining, then the effect of cyclic stressing a low carbon steel to its saturation strain stage is to introduce a ρ_m of the order of 10^8 lines/cm^2.

In a tensile test, whether a yield drop is exhibited depends on two factors, ρ_m and n. Increasing the value of either or both tends to suppress the yield drop and Luders strain(54). Now, if ρ_m after fatigue cycling is about 10^8 lines/cm^2, then according to Hahn's model there would be no yield drop. Furthermore, n is increased by both plastic straining(186) and dynamic ageing(187,188,189) so that its value after fatigue is higher than its initial value (prior to fatigue). This further ensures that a smooth tensile curve is obtained after cyclic pre-stress.

The dependence of cyclic strain hardening and strain age hardening on grain size may now be explained using the suggested mechanism. In a fine grained steel, the dislocation generation rate is high. The high value of ρ_m, coupled with a small s (s is a function of initial dislocation density and grain size) means that cross-slip can take place readily so that the dipole 'debris' density is rapidly built up. Thus, while locking by nitrogen may provide some immobilisation, the increase in ρ_i is probably due mainly to the trapping of mobile dislocations by these 'debris' obstacles. Hence, most of the hardening in a fine grained steel is due to cyclic strain hardening. In a coarse grained steel, dislocations are generated at a slower rate and since the mean free path of dislocations is proportional to the grain size initially(182), cross-slipping and interactions become less frequent and hardening is slower and lesser. However, if nitrogen is present, locking of mobile dislocations can contribute significantly to ρ_i. Hence

dynamic strain age hardening is more important in a coarse grained steel than in a fine grained steel.

9.6 INTERPRETATION OF PUBLISHED WORK IN TERMS OF THIS SUGGESTED THEORY

The basic area of dispute on the subject of fatigue in low carbon steels is whether the fatigue limit mechanism is affected by dynamic strain ageing. The experimental results of this work showed that the fatigue limit of the steel was dependent on its grain size as well as its free nitrogen content, i.e., its ability to strain harden and strain age harden under cyclic loading. It was found that fatigue limit was determined by the combined effect of these two factors. For example, the steel with a fine grained structure and a high free nitrogen level exhibited only slight strain age hardening during fatigue.

Published results[6,7,100] indicated that the fatigue limit of a steel was related to its tensile strength. In other words, if the tensile strength of a steel could be improved, its fatigue limit would also increase so that the Tensile Strength/Fatigue Limit ratio was approximately preserved at all times.

It appears that the confusion over the role of strain ageing during fatigue was due to the fact that conclusions were drawn from experiments which did not consider the three aforementioned factors together, viz., the grain size of the steel, its free nitrogen level or strain ageing propensity, and its strength.

For example, Lipsitt and Horne[101] found that by decarburising their steel (reducing its carbon content from 0.09% to 0.003%C), a 36% reduction in fatigue limit stress was obtained. However, they failed to consider the effect of grain size which increased from ASTM No.7-9 to ASTM No.3-5. The coarsening of the grain size caused a reduction in tensile strength and furthermore, decarburisation caused a loss of precipitation hardening. Therefore the drop in fatigue limit stress could not be attributed to the lack of strain ageing in the decarburised steel.

The effects of strain ageing during fatigue had always been studied by comparing the fatigue performance of steels that would age and those that would

not age. Different methods had been used to render the steel non-ageing, and in most cases these methods introduced side-effects which were not considered. For example, decarburising and denitriding caused a loss in precipitation hardening and this in turn, reduced the strength and fatigue limit of the steel[2,101], and coaxing of specimens caused strain hardening[102].

Pre-straining and ageing a specimen did nothing more than improve its tensile strength since in both cases, the dislocations remained locked and there was essentially no difference in the grain size. The annealed steel and strain aged steel could therefore be considered as two similar steels with different tensile strengths and hence different fatigue strengths. Kettunen's[100] results may be interpreted this way.

The suggestion of Oates and Wilson[6] that two different fatigue mechanisms for fine and coarse grained steels was not satisfactory. Their conclusion on the strain ageing effect on coarse grained steel was confirmed by the work. However, their suggestion that strain ageing was the cause of the presence of a fatigue limit seemed unlikely. This work and others[4,5,7] clearly showed that fatigue limits were still present even if the steel had little or no ageing propensity. Oates and Wilson[6] observed that there was extensive plastic deformation associated with failure in coarse grained steels with fatigue striations spreading across grain boundaries on the specimen surface. Since no such spread of plasticity was observed in fine grained steel specimens that failed at stresses near to the fatigue limit, and that ageing had no effect on the steel's fatigue limit, they concluded that the fatigue limit for a fine grained steel was not due to strain ageing but initial dislocation locking. It was suggested that strong dislocation lockings inhibited the spread of plasticity across grain boundaries in essentially the same manner as in static yielding.

However, yielding in the sense described by the Hall-Petch model cannot be expected to spread across grain boundaries during fatigue of a fine grained steel because, for this to occur, the stress has to be equal to the static yield stress of the steel. For a fine grained steel of say, $d^{-\frac{1}{2}} = 9.0\ mm^{-\frac{1}{2}}$, the fatigue limit is typically about 40% below the static yield stress.

Therefore, failure occurring at or near the fatigue limit stress (well below the static yield stress) is unlikely to be due to a spread of plasticity. It is suggested here and confirmed by Figures 8.32 - 8.35 that plastic deformation in fatigue is basically confined to the region within the grain boundary of the individual grains. However, for a coarse grained steel, say $d^{-\frac{1}{2}} < 4\ mm^{-\frac{1}{2}}$, because the fatigue limit stress and the static yield stress are about the same in magnitude, this spread of plasticity is possible and this was observed by Oates and Wilson[6].

The results of Oates and Wilson[6] on pre-strained fine grained steel showed that the fatigue limit was not eliminated at room temperature. Since pre-straining should remove the principal effect of dislocation locking, their proposed mechanism of initial dislocation locking for a fine grained steel seems unlikely. This current work suggests that the fatigue limit of a fine grained steel is the direct result of the strain hardening ability of the steel under cyclic loading conditions. Both fatigue damage and cyclic strain hardening are functions of stress and at some value of stress, viz., the fatigue limit, fatigue damage outpaces hardening to cause failure. For a coarse grained steel, the same mechanism applies but with strain age hardening also contributing to the strengthening process. Thus the fatigue limit of a coarse grained steel is also affected by its ageing propensity.

The results of Ferro and Montalenti[4] can also be explained this way. Even though their steels contained insufficient carbon and nitrogen as interstitials for ageing to occur, fatigue limits were still recorded due to the competitive process between cyclic strain hardening and damage.

Although this work agrees with that of Oates and Wilson[6], that the influencing factors on fatigue limit are different for fine and coarse grained steels, this suggestion does not point to two different mechanisms. The

same mechanisms hold for steels of all grain sizes, but the dominant strengthening mechanism is dependent on the grain size. For a fine grained steel, cyclic strain hardening predominates the strengthening process. As the grain size is increased, its effect gradually diminishes while strain age hardening begins to take over. For a coarse grained steel, say $d^{-\frac{1}{2}} \simeq 3.5\ mm^{-\frac{1}{2}}$, strengthening by strain age hardening becomes very significant.

The suggested theory implies that all materials which are capable of cyclic strain hardening should possess fatigue limits, e.g., copper, aluminium and their alloys. Indeed, Erasmus[175] found that commercially pure aluminium EIC possessed a definite fatigue limit, and work by Helgeland[149] on single crystal copper, and more recently by Lukas and Klesnil[191] on polycrystalline pure copper and Copper - 31% Zinc, showed that a fatigue limit existed in each case. Helgeland[149] used constant stress amplitude cycling to get a fatigue limit at 28.4 MN/m^2, but Kettunen[190] in repeating the experiment could not establish such a limit and he obtained a smooth S-N curve. This discrepancy was rectified by Lukas and Klesnil[191], who found that the fatigue limit could be easily identified by using constant strain amplitude cycling. The fatigue strain limit was found to be 8×10^{-5}. Thus it appears that the strain amplitude may be the more appropriate parameter to use than the stress amplitude for materials that do not show a definite fatigue stress limit. The situation is slightly different for steels (see Section 1.4). Lukas *et. al.*[192] found that for a typical medium carbon steel, there was no difference in the Coffin-Manson plots obtained from strain cycling and from stress cycling. Hence the same fatigue limit could be obtained from either constant strain amplitude cycling or constant stress amplitude cycling.

It was later found[193] that in the fatigue of copper single crystals, a threshold strain was required to form the first single persistent slip band

and with continued cycling, the number of persistent slip bands would increase[147]. Since fatigue cracks have been shown to form in persistent slip bands[195,196], this threshold strain should be the fatigue strain limit of a copper single crystal. This was confirmed by Mughrabi[193] who obtained a threshold strain of 8×10^{-5} and the same threshold in terms of stress was established at 28.4 MN/m^2 [194,197], the value of 28.4 MN/m^2 being the fatigue limit of single crystal copper[149].

There appears to be no experimental value of the threshold strain for the first persistent slip band to form in polycrystalline copper. However, the results of Lukas and Klesnil[191] showed that the fatigue strain limits of polycrystalline copper and single crystal copper were the same. Therefore the fatigue limit and threshold strain for persistent slip band formation are unaffected by the grain size. This provides further evidence to the argument that in fatigue, deformation is basically confined to the region within the grain boundary of individual grains. Hence the threshold stress (or strain) is determined by the slip system of the material and not by the grain size, and if the stress is sufficient to cause persistent slip band to form in a single crystal, it is also high enough to cause the same effect in a polycrystalline specimen.

The work and results of Mughrabi[193] and Lukas and Klesnil[191] provide an interesting comparison with the current work. In this work, a threshold stress, the critical damping stress, σ_{CD}, was found to be necessary for softening/hardening to occur and for PSB to form. This threshold stress was only slightly affected by the grain size of the steel, and it was about 11% below the fatigue limit of a fine grained steel ($d^{-\frac{1}{2}} \simeq 9\ mm^{-\frac{1}{2}}$) and 9% below that of a coarse grained steel ($d^{-\frac{1}{2}} \simeq 4\ mm^{-\frac{1}{2}}$). Since persistent slip bands have been observed at stresses below the fatigue limit in carbon steels[198], and that σ_{CD} was the threshold stress for plastic deformation to occur and for PSB to form, σ_{CD} can be considered to be analogous to the threshold strain

found by Mughrabi[193] required to form the first persistent slip band.

Laird[194] in his paper concluded that a true fatigue stress limit and fatigue strain limit (connected directly through the cyclic stress-strain curve) existed for most crystalline materials. These limits were based on the stress-strain requirements to form persistent slip bands, and since the formation of persistent slip bands is a general phenomenon in metals and all kinds of alloys[194], it is reasonable to assume that most metals and alloys possess some sort of fatigue limit. Laird[194] also pointed out that the fatigue stress limit (based on persistent slip band formation) for a given material could be increased by dislocation locking and precipitation hardening. This is consistent with the finding of this work.

CHAPTER TEN

CONCLUSION

Damping and temperature measurements of fatigue specimens cyclically stressed at different stress amplitudes, showed that a threshold limit, called the Critical Damping Stress, σ_{CD}, existed for low carbon steels of various grain sizes and different free nitrogen contents. σ_{CD} was defined as the minimum cyclic stress amplitude required to cause a change in the damping of a fatigue specimen within 5×10^7 cycles of loading. In the experimental steels, σ_{CD} was found to be about 11% below the fatigue limit of a fine grained ($d^{-\frac{1}{2}} = 9.0\ mm^{-\frac{1}{2}}$) steel, and 9% below that of a coarse grained steel ($d^{-\frac{1}{2}} = 4.0\ mm^{-\frac{1}{2}}$); the reference fatigue limits used were those of steels with little ageing propensities, the A steels. The value of σ_{CD} was not affected by the amount of free nitrogen in the steel and it was only slightly dependent on the grain size, increasing with decreasing grain size.

Under constant stress amplitude cycling conditions, the damping capacity and temperature rise of a specimen are directly related to the strain amplitude. Since the strain amplitude is proportional to the mobile dislocation density[185], an increase in specimen damping also means an increase in the mobile dislocation density. Thus the initial effect of cyclically stressing a specimen at its σ_{CD} is to produce mobile dislocations. This was shown by tensile tests of specimens cyclically pre-stressed at σ_{CD}. The tensile curves showed that the original yield point of the steels were eliminated, this being a consequence of a high initial dislocation density ("initial" here means before the tensile test).

The electron micrographs showed that fatigue stressing of a specimen at its σ_{CD} caused a rearrangement of dislocations into some structures. A significant finding is that a cell structure was observed for a fine grained

steel [B(1)] even though the cyclic stress amplitude was below the fatigue limit. For the coarse grained steel [B(5)], subgrain boundaries and bands were formed.

In uniaxial tensile loading, when a steel is plastically strained, strain hardening occurs. If the steel contains sufficient nitrogen as free interstitials and that sufficient time is allowed for ageing to occur, strain age hardening will also take place. The same phenomena were observed during fatigue of low carbon steels. For the two low nitrogen steels A(1) and A(3), cyclic strain hardening resulted from fatigue. In the case of the high nitrogen steels B(1) and B(5), dynamic strain ageing was detected during the course of fatigue so that strain age hardening and cyclic strain hardening contributed to the total strengthening.

From the experimental results, it was observed that the fatigue limit of an ageing steel was higher than that of an equivalent steel of similar grain size but with little ageing propensity. This difference was attributed to strain age hardening. Furthermore, the fatigue limit of a non-ageing steel was higher than its σ_{CD}. This was considered to be due to the effect of cyclic strain hardening. A schematic representation of the effects of these two strengthening mechanisms on the fatigue limit of low carbon steel is given in Figure 10.1.

Line 1 is the Critical Damping Stress line and represents the fatigue limit of a perfect plastic steel that neither strain hardens nor strain age hardens. Fatigue cycling at stresses below this line does not cause any damping or temperature rise and no strain hardening or strain ageing results. The original discontinuous yield property of the steel is not eliminated and persistent slip bands are not formed on the surface. Hence no failure can occur.

Cyclic stressing at σ_{CD} causes dislocation generation in the steel.

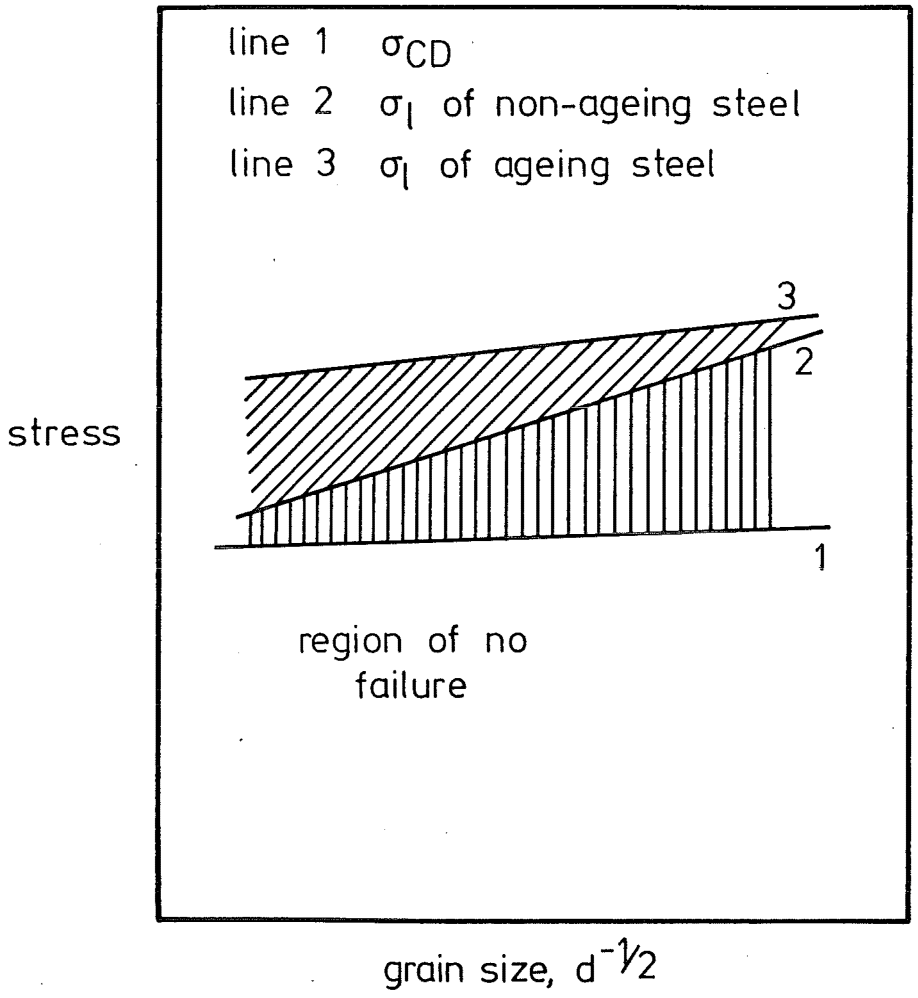

FIG. 10·1. SCHEMATIC REPRESENTATION OF STRENGTHENING BY STRAIN AGE HARDENING AND CYCLIC STRAIN HARDENING DURING FATIGUE.

Because of the increased mobile dislocation density, the total dislocation motions are also increased and this causes energy to be released in the form of heat. The increased mobile dislocation density results in widespread dislocation interactions which produce large quantities of dipole 'debris'. Cyclic strain hardening is achieved when dislocations are trapped by these 'debris' obstacles and the immobile dislocation density increased. Thus, although persistent slip bands are formed on the specimen surface, the strain hardened structure ensures that the persistent slip bands do not develop into propagating cracks. For failure to occur, the stress amplitude must be raised to line 2 for sufficient damage to overcome the hardened structure. The fatigue limit of a non-ageing steel is hence defined by line 2. Between lines 1 and 2, no failure will occur. Because dislocation densities in fine grained steels are higher than those in coarse grained steels, and because the dislocation means free path is proportional to the grain size, dislocation interactions become more widespread as the grains get smaller, so that cyclic strain hardening is more significant in fine strained steels than in coarse grained steels.

If the steel contains active nitrogen and if the temperature of the specimen is raised sufficiently during fatigue (~100°C for example), then the increased mobile dislocation density due to cyclic stressing means that dynamic strain ageing will readily take place. Immobilisation of dislocations by solute locking contributes to the total immobilised dislocation density and further hardening is gained by way of dynamic strain age hardening. Because the total hardening is improved, cyclic stressing at line 2 will not cause failure. For failure to occur, the cyclic stress must be raised to line 3, which now defines the fatigue limit of an ageing steel. In a coarse grained steel, because of the lower dislocation density and larger mean free path (compared to that of a fine grained steel), dislocation interactions occur to a lesser degree so that cyclic hardening is small. In this case, immobilisation by solute atoms locking will contribute significantly to the

total hardening. This means strain age hardening is more significant as the grain size gets larger.

On account of this, fatigue of low carbon steels is a combination of three simultaneous processes (viz., damage, strain hardening and strain age hardening), or two if the steel is a non-ageing steel. The experimental results on damping and tensile tests of fatigued specimens show that during fatigue at a stress amplitude above σ_{CD}, cyclic strain hardening and strain age hardening were completed very quickly, i.e.,during the transient stage. This implies that after the completion of the transient stage, hardening is no longer a function of time, whereas damage may be time dependent. Thus, whether prolonged cycling can cause failure or not depends simply upon the degree of hardening gained. Although the total hardening increases with cyclic stress amplitude, it appears to tend to a limit with increasing stress amplitude. This may be seen by plotting Δf (see Figure 8.15 for definition of Δf) against the stress amplitude. Figure 10.2 shows that for both the fine and coarse grained steels, Δf tends to a limit. (These values of Δf were obtained from Figures 8.14 and 8.15). Consequently, beyond a certain point, Δf is not a function of the stress amplitude. Since damage is likely to be a function of stress amplitude, then at some limit, damage will outpace the hardening. This is the fatigue limit.

These results,which show opposite grain size dependence of cyclic strain hardening and strain age hardening, explain the apparent difference in fatigue behaviour of fine and coarse grained steels when these two forms of hardening are not considered together. This work has clearly established that a single fatigue mechanism is operative for low carbon steel of all grain sizes.

In this work, σ_{CD} was found to be the minimum stress amplitude required for persistent slip band formation in a low carbon steel. This is analogous to Mughrabi's[193] definition of threshold limit for persistent slip bands to

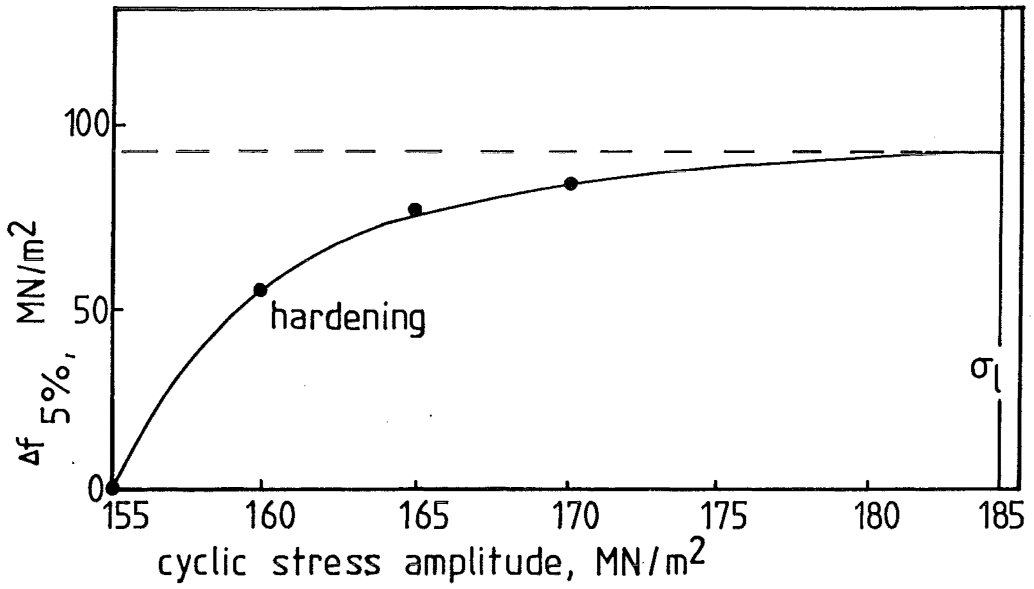

FIG. 10·2 (a) TOTAL HARDENING GAINED BY FATIGUE STRESSING AT DIFFERENT AMPLITUDES, STEEL B (1)

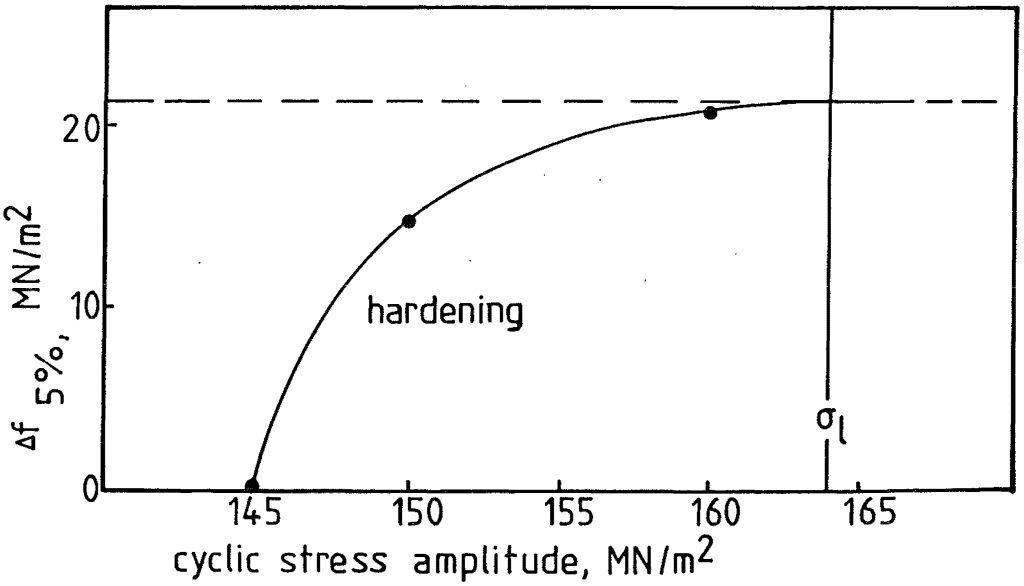

FIG. 10·2 (b) TOTAL HARDENING GAINED BY FATIGUE STRESSING AT DIFFERENT AMPLITUDES, STEEL A (3)

form in copper crystals. This implies that the fatigue mechanism of b.c.c. and f.c.c. structures are similar. This seems a likely possibility after recent discoveries of fatigue limits in aluminium[175], copper[193] and Cu-30% Zn alloy[191].

REFERENCES

1. RANKINE, W.J.M., 1843, Proc. Instn Civ. Engrs, vol.2, p. 105.

2. RALLY, F.C. & SINCLAIR, G.M., 1955, Report No. 87, University of Illinois, Dept of Theoretical and Applied Mechanics.

3. LEVY, J.C. & SINCLAIR, G.M., 1955, Proc. Amer. Soc. Test. Mater., 55, p. 866.

4. FERRO, A. & MONTALENTI, G., 1963, Phil. Mag., vol.8, p. 105.

5. BERGSTROM, Y., VINGSBO, O. & LAGERBERG, G., Mater. Sci. Eng, 1969/70, vol.5, p. 153.

6. OATES, G. & WILSON, D.V., 1964, Acta. Met., vol.12, p.21.

7. YOSHIKAWA, A. & SUGENO, T., 1965, Trans. Met. Soc. AIME, vol.233, p.1314.

8. KLESNIL, M., HOLZMANN, M., LUKAS, P., RYS, P., 1965, J.I.S.I., vol.203, p.47.

9. THOMPSON, N., WADSWORTH, N. & LOUAT, N., 1956, Phil.Mag., vol.1 p.113.

10. FUJITA, F.E., 1963, "Fracture of Solids", Ed. Drucker, D.C.and Gilman, J.J., Interscience, London, p.657.

11. GATES, R.G. & WOOD, W.A., 1968, J.I.M., vol.96, p.242.

12. McMILLAN, J.C. & HERTZBERG, R.W., 1968, "Electron Fractography" A.S.T.M. Spec. Tech.Publ. No.436, Philadelphia, Pa., p.89.

13. PLUMBRIDGE, W.J. & RYDER, D.A., 1969, Metallurgical Reviews No. 136, vol.14, p.119.

14. FORSYTH, P.J.E., 1961, "A Two Stage Process of Fatigue Crack Growth", Proceedings, Crack Propagation Symposium, Cranfield.

15. LAIRD, C., 1967, "Fatigue Crack Propagation, A.S.T.M., STP.No.415, Philadelphia, Pa., p.131.

16. FORSYTH, P.J.E., 1963, Acta. Met., vol.11, p.703.

17. FORSYTH, P.J.E., STUBBINGTON, C.A. & CLARK, D., 1961, J.I.M., vol.90, p.238.

18. HERTZBERG, R.W., 1967, "Fatigue Crack Propagation", A.S.T.M. STP. 415, Philadelphia, Pa., p.205.

19. FORSYTH, P.J.E. & RYDER D.A., 1961, Metallurgia, vol.63, p.117.

20. MEYN, D.A. , 1968, Trans. Am. Soc. Metals, vol.61, No.1, p.42.

21. PELLOUX, R.M.N., 1969, Trans. Am. Soc. Metals, vol.62, p.281.

22. KOTERAZAWA, R., MORI, M., MATSUI, T. & SHIMO, D., 1973, Trans. A.S.M.E., vol.95, p.202.

23. ERASMUS, L.A., 1970, "The Failure of Metals in Service", D.S.I.R., Auckland University Symposium, p.57.

24. ERASMUS, L.A., 1971, Tech. Report E.1148, Dept of Mech. Engineering, University of Canterbury, Christchurch, N.Z.

25. YEN, C.S., 1969, "Metal Fatigue", Ed. Madoyag, A.F., Wiley, N.Y., p.107.

26. ---------- 1964, Annual Report for 1963, National Engineering Laboratory, Reviewed in Metal Industry, vol.104, p.731.

27. WOOD, W.A., COUSLAND, S.M. & SARGANT, K.R., 1963, Acta. Met., vol.11, p.643.

28. MANSON, S.S., 1966, "Thermal Stress and Low Cycle Fatigue", McGraw-Hill, N.Y.

29. HIRSCH, P.B., PARTRIDGE, P.G. & SEGALL, R.L., 1959, Phil. Mag., vol.4, p.721.

30. GROSSKREUTZ, J.C., 1964, "Fatigue - an Interdisciplinary Approach", Syracuse University Press, N.Y., p.27.

31. McGRATH, J.T. & BRATINA, W.J., 1965, Phil. Mag., vol.12, p.1293.

32. GROSSKREUTZ., J.C., 1963, J. Appl. Physics, vol.34, p.372.

33. GROSSKREUTZ., J.C. & WALDOW, P., 1963, Acta. Met., vol.11, p.717.

34. LUKAS, P., KLESNIL, M., KREJCI, J., & RYS, P., 1966, Physica Status Solidi, vol.15, p.71.

35. WILSON, D.V. & TROMANS, J.K., 1970, Acta. Met., vol.18, p.1197.

36. KLESNIL, M. & LUKAS, P., 1965, J.I.S.I., vol.203, p.1043.

37. HEMPEL, M., 1956, Proc. International Conf. Fatigue of Metals, Inst. Mech. Eng, London, p.543.

38. WOOD, W.A., REIMANN, W.H. & SARGANT, K.R., 1964, Trans. Met. Soc. A.I.M.E., vol.230, p.511.

39. ADAIR, A.M. & LIPSITT, H.A., 1966, Trans. A.S.M.E. vol.236, p.1235.

40. MANN, J.Y., 1967, "Fatigue of Materials", Melbourne University Press, Victoria, Australia.

41. HAYDEN, H.W., MOFFAT, W.G. & WULFF, J., "The Structure and Properties of Materials", vol.3, Wiley, p.104-111.

42. AVERY, D.H. & BACKOFEN, W.A., 1963, Acta. Met., vol.11, p.653.

43. CONRAD, H., FEUERSTEIN, S., & RICE, L., 1967, J. Mat. Soc. Eng, vol.2, p.157.

44. SOH , K.S., 1970, M.E. Thesis, Mechanical Eng Dept, University of Canterbury, N.Z.

45. HALL, E.O., 1970, "Yield Point Phenomena in Metals and Alloys", MacMillan, p.2.

46. DALBY, W.E., 1913, Proc. Roy. Soc., vol.A88, p.281.

47. KURODA, M., 1938, Sci. Pap. Inst. Phys.Chem. Research, vol.34, p.1528.

48. COTTRELL, A.H., 1948, Report of Conference on Strength of Solids, Phys. Soc. p.30.

49. COTTRELL, A.H. & BILBY, B.A., 1949, Proc. Phys. Soc., vol.A.62, p.49.

50. ---------- 1961, Metal Treatment and Drop Forging, vol.28, p.279.

51. KENT, K.G. & KELLY, A., 1965, J.I.M., vol.93, p.536.

52. HALL, E.O., 1968, J.I.M., vol.96, p.21.

53. GILMAN, J.J. & JOHNSTON, W.G., 1957, "Dislocations and Mechanical Properties of Crystals", John Wiley, N.Y., p.116.

54. HAHN, G.T., 1962, Acta. Met., vol.10, p.727.

55. HALL, E.O., 1951, Proc. Phys. Soc., vol.B.64, p. 747.

56. CRACKNELL, A. & PETCH, N.J., 1955, Acta. Met. vol.3, p.186, p.200.

57. HESLOP, J. & PETCH, N.J., 1956, Phil. Mag., vol.1, p.866
Phil. Mag., vol.2, p.649.

58. FISHER, R.M., 1961, Ph.D. Thesis, University of Canterbury.

59. ARMSTRONG, R., CODD, I., DOUTHWAITE, R.M. & PETCH N.J., 1962, Phil. Mag. vol.7, p.45.

60. EVAN, J.T. & RAWLINGS, R., 1968, Metal. Sci. Journal, vol.2, p.221.

61. MORRISON, W.B., 1966, Trans. Am. Soc. Metals, vol.59, p.824.

62. TEGART, W.J.M., "Elements of Mechanical Metallurgy", MacMillan, p. 13-19.

63. KOVÁCS, I., 1967, Acta Met., vol.15, p.1731.

64. HIRSCH, P.B., 1960, Acta. Cryst., vol.13, p.1114.

65. MOTT, N .F, 1960, Trans. AIME, vol.218, p.962.

66. KUHLMANN-WILSDORF, D., 1962, Trans. AIME, vol.224, p.1047.

67. SEEGER, A., KRONMÜLLER, H., MADER, S., & TRÄUBLE, H., 1961, Phil.Mag., vol.6, p. 639.

68. SEEGER, A., DIEHL, J., MADER, S. & REBSTOCKS, H., 1957, Phil. Mag, vol.2, p.1.

69. SESTÁK, B. & SEEGER, A., 1971, Phys. Stat. Sol., vol.43, p.433.

70. KEH, A.S. & NAKADA, Y., 1967, Canadian J. Phys. vol.45, p.1101.

71. KOVÁCS, I. & ZSOLDOS, L., "Dislocations and Plastic Deformation", Pergamon, p.258.

72. ESSMANN, U., 1963, Phys. Stat. Sol., vol.3, p.932.

73. BAIRD, J.D. 1963, Iron & Steel, vol.36,pp.186, 400 and 450.

74. BAIRD, J.D. 1971, Metallurgical Review, vol.16, p.1.

75. WILSON, D.V. & RUSSELL, B., 1960, Acta. Met., vol.8, p.468.

76. HUNDY, B.B., 1954, J.I.S.I., vol.178, p.34.

77. BUTLER, J.F., 1962, Trans. Met. Soc. AIME, vol.224, p.89.

78. WILSON, D.V. & RUSSELL, B., 1960, Acta. Met.,vol.8, p.36.

79. COTTRELL, A.H., 1963, "The Relation betweeh Structure and Mechanical Properties of Metals", N.P.L. Symp. No.15. H.M.S.O., p.456.

80. WILSON, D.V., 1968, Acta. Met., vol.16, p.743.

81. RITCHIE, I.G. & RAWLINGS, R., 1967, Acta. Met., vol.15, p.491.

82. LEAK, D.A., THOMAS, W.R. & LEAK G.M., 1955, Acta. Met., vol.3, p.501.

83. DE KAZINCZY, F. & AXNAS, A., 1963, Jernkont Ann., vol.147, p.931.

84. MORGAN, E.R. & SHYNE, J.C., 1957, J.I.S.I., vol.185, p.156.

85. FOUNTAIN, R.W. & CHIPMAN, J., 1962, Trans. AIME, vol.224, p.599.

86. SHOENBERGER, L.R., 1958, Trans. Met. Soc. AIME, vol.212, p.402.

87. CHAN, B.K., 1976, Proj.Rep. MM/69/76, Mech. Eng Dept, University of Canterbury, N.Z.

88. IRVINE, K.J., PICKERING F.B. & GLADMAN, T., J.I.S.I., vol.205, p.161.

89. GEORGE, T.J. & IRANI, J.J., 1968, J. Australian Inst. Metals, vol.13, p.94.

90. SMAILL, J.S., KEOWN, S.R., & ERASMUS L.A., 1976, Metals Technolgy, vol.3, p.194.

91. ERASMUS, L.A., 1964, J.I.S.I., vol.202, p.128.

92. EPSTEIN, S., CUTLER, H.J. & FRAME, J.W., 1950, Journal of Metals, vol.188, p.830.

93. FRAME, J.W. & SCHUNK F.B., 1958, "Deep Drawing Steels", IMD. Spec. Rep., Series No.6, AIME, p. 57.

94. JONES, W. & COOMBS, G., 1953, J.I.S.I., vol.174, p.9.

95. RASHID, M.S., 1975, Metallurgical Trans., vol.6A, p.1265.

96. MORRISON, W.B., 1963, J.I.S.I., vol.201, p.317.

97. SAGE, A.M. & COPLEY, F.E., 1960, J.I.S.I., vol.195, p.422.

98. STUART, H., BURTON, D., & ROTHWELL, A.B., BISRA REPORTS MG/C/54/69, MG/C/55/59.

99. PUSSEGODA, L.N., 1978, Ph.D. Thesis, University of Canterbury, N.Z.

100. KETTUNEN, P.O., 1964, J.I.S.I, vol.202, p.209.

101. LIPSITT, H .A, & HORNE, G.T., 1957, Proc.Am. Soc. Test. Matls, vol.57, p.587.

102. LEVY, J.C. & KANITKAR, S.L., 1961, J.I.S.I., vol.197, p.296.

103. LEVY, J.C., 1957, Metallurgia, vol.56, p.71.

104. KNOTT, J.F., 1971, Mat. Sci. Eng, vol.7, p.1.

105. DE FOUQUET, J., 1961, Mem. Sci. Rev. Met., vol.58, p.129.

106. BISHOP, S.M., SPRETNAK, J.W. & FONTANA, M.G., 1952, Trans. Amer. Soc. Met., vol.45, p.993.

107. SUITS, J.C. & CHALMERS, B., 1961, Acta Met. vol.9, p.854.

108. LOW, J.R. & GENSAMER, M., 1944, Trans. AIMME, vol. 158, p.207.

109. --------- 1961, Report by Metallurgy Divison, N.P.L. Metal Treatment and Drop Forging, vol.28, p.279.

110. FISHER, J.C. & ROGERS, H.C., 1956, Acta. Met., vol.4, p.180.

111. FISHER, J.C., 1955, Trans. Amer. Soc.(Metals), vol.47, p.451.

112. CONRAD, H. & SCHOEK, G., 1960, Acta. Met., vol.8, p. 791.

113. MANJOINE, M.J., 1944, Trans. Am. Soc. Mech. Engrs, vol.66, p.A.244.

114. CARREKER, R.P. & GUARD, R.W., 1956, Trans. Amer. Inst. of Min. (Metall) Engrs., vol.206, p.178.

115. TJERKSTRA, H.H., 1964, Acta Met., vol.9, p.259.

116. PETCH, N.J., 1953, J.I.S.I., vol. 174, p.25.

117. DE KAZINCZY, F., BACKOFEN, W.A. & KAPADIA, B., 1959, "Fracture", John Wiley, N.Y., p.65.

118. BALDWIN Jr, W.M., 1958, Acta. Met., vol.6, p.139.

119. SCHWARTZBART, H. & LOW Jr, J.R., 1949, Trans. Amer. Inst. of Min. (Metall) Engrs, vol.195, p.637.

120. JOHNSTON, W.G. & GILMAN, J.J., 1956, J. Appl. Physics, vol.30, p.129.

121. GILMAN, J.J., 1959, J. Appl. Physics, vol.30, p.1584.

122. KEH, A.S. & WRIEDT, H.A., 1962, Trans. Amer. Inst. of Min.(Metall) Engrs, vol.224, No.3, p.560.

123. STEIN, D.F. & LOW Jr J.R., 1960, J. Appl. Physics, vol.31, p.362.

124. GILMAN, J.J. & JOHNSTON, W.G., 1960, J. Appl.Physics, vol.31, p.687.

125. OWEN, W.S., COHEN, M. & AVERBACH, B.L., 1958, Trans. Amer. Soc. Metals, vol.50, p.517.

126. HUTCHISON, M.M. 1962, Phil. Mag., vol.8, p.121.

127. BROWN, N. & EKVALL, R.A., 1962, Acta. Met., vol.10, p.1101.

128. LUTHER, R.G. & WILLIAMS, T.R.G., 1977, Metal Science, vol.5, p.164.

129. BROWN, N. & KOSSOWSKY, R., 1966, Acta. Met., vol.14, p.131.

130. BRENTNALL, W.D. & ROSTOKER, W., 1965, Acta. Met., vol.13, p.187.

131. LAZAN, B.J., 1950, Trans. Amer. Soc. Metals, vol.12, p.499.

132. BENHAM, P.P. & FORD, H., 1961, J. Mechanical Engineering Sc., vol.3, No.2, p.119.

133. ESHELBY, J.D., 1949, Proc. Roy. Soc., London, vol.197A, p.396.

134. LAZAN, B.J. & WU, T., 1951, Proc. A.S.T.M., vol.51, p.649.

135. MORROW, J., 1965, Proc. A.S.T.M. STP 378, p.45.

136. TULER, F.R., 1962, M.S. Thesis, Dept.of Theo. & Appl. Mechanics, University of Illinois.

137. WADSWORTH, N.J., 1957, "Dislocations and Mechanical Properties of Crystals", J.Wiley & Son Inc., N.Y., p.489.

138. SNOWDEN, K.U., 1963, Acta. Met., vol.11, No.7, p.675.

139. SHINOZAKI, D. & EMBURY, J.D., 1969, Metal Science Journal, vol.3, p.147.

140. ALDEN, T.H., 1962, J. Metals (A.I.M.E.), vol.14, p.828.

141. ALDEN, T.H. & BACKOFEN, W.A., 1961, Acta. Met., vol.9, p.352.

142. FELTNER, C.E. & LAIRD, C., 1967, Acta. Met., vol.15, p.1621, 1633.

143. SEGALL, R.L., PARTRIDGE P.G. & HIRSCH, P.B., 1961, Phil. Mag., vol.6, p.1493.

144. SEGALL, R.L., 1963, "Electron Microscopy and Strength of Crystals", Interscience, N.Y., p.515.

145. FELTNER, C.E., 1965, Phil. Mag., vol.12, p.1229.

146. GROSSCREUTZ., J.C., 1971, Phys. Stat. Sol., vol. 47, p.11.

147. FINNEY, J.M. & LAIRD, C., 1975, Phil. Mag., vol.31, p.339.

148. PIQUERAS, J., GROSSCREUTZ, J.C. & FRANK, W., 1972, Phys. Stat. Sol., vol.11, p.567.

149. HELGELAND, O., 1965, J. Inst. Metals, vol.93, p.570.

150. ROBERTS, W.N., 1969, Phil. Mag., vol.20, p.275.

151. LUKAS,P., KLESNIL, M. & KREJCI, J., 1968, Phys. Stat. Sol., vol.27 p.545.

152. WOODS, P.J., 1973, Phil. Mag., vol.28, p.155.

153. McGRATH, J.T. & BRATINA, W.J., 1965, Phil. Mag, vol.11, p.429.

154. WEI, R.P. & BAKER, A.J., 1965, Phil. Mag., vol.11, p.1087.

155. LUTHER, R.G. & WILLIAMS, T.R.G., Metal Science, vol.10, p.367.

156. ABEL, A. & MUIR, H., 1973, Acta. Met., vol.21, p.93.

157. MACKOWIAK, J., 1965, "Physlical Chemistry for Metallurgists", Allen & Unwin, London.

158. DARKEN, L.S., SMITH, R.P. & FILER, E.W., 1951, Trans. A.I.M.M.E., vol.191, p.1174.

159. --------- 1961, "Standard Methods of Analysis", The United Steel Co. Ltd, Lund, Humphries & Co., London.

160. BEEGHLEY, H.F., 1949, Anal. Chem., vol.21, p.1513.

161. ERASMUS, L.A., 1964, J.I.S.I., vol.202, p.32.

162. ERASMUS, L.A., 1964, J.I.S.I., vol.202, p.1018.

163. ERASMUS, L.A., 1966, Iron and Steel, vol.40, p. 477.

164. LESLIE, W.O., RICKETT, R.L., DOTSON, C.L. & WALTON, C.S., 1954, Trans. Amer. Soc. Metals, vol.43, p.260.

165. CAHN, J.W. 1962, Acta. Met., vol.10, p. 789.

166. GLADMAN, T. & PICKERING, F.B., 1967, J.I.S.I., vol.205, p.653.

167. BAIN, E.C. & PAXTON, H.W., 1947, A.S.M., "Alloying Elements in Steels", p.117.

168. HALLEY, J.W., 1946, Trans. A.I.M.E., vol. 167, p.224.

169. CHATTERJEA, A.B. & NIJHAWAN, B.R., 1957, Metal Treatment, vol.24. p.3-6; 54-60.

170. RICKETT, R.L. & LESLIE, W.C., 1957, Metal Treatment, vol.24, p.59.

171. PHILIPS, R. & CHAPMAN, J.A., 1966, J.I.S.I., vol.204, p.615.

172. WHITELEY, J.H., 1943, J.I.S.I., vol. 148, p.513.

173. BROPHY, J.H., ROSE, R.M. & WULFF, J., 1964, "The Structure and Properties of Materials", Vol.II, J.Wiley & Son, p. 95.

174. ---------- 1963, A.S.T.M. Standard, E112-63, Part 3.

175. ERASMUS, L.A., 1970, Ph.D. Thesis, University of Cape Town, South Africa.

176. SETO, W.W., 1964, "Theory and Problems of Mechanical Vibrations", McGraw-Hill.

177. STEPHENS, R.I., 1968, Journal of Materials, vol.3, No.2, p.386.

178. LLOYD, D.J. & GREENOUGH, A.P., 1969, Metal Sci. Journal, Vol.3, p.134.

179. SHIH, C.H., AVERBACH, B.L.& COHEN, M., 1956, Trans. A.S.M., vol.48, p.86.

180. TETELMAN, A.S. & McEVILY, A.J., 1967, "Fractures of Structural Materials", Wiley, N.Y..

181. ROBERTS, W., KARLSSON, S. & BERGSTRÖM, Y., 1973, Metal Science and Engineering, vol.11, p.247.

182. KEH, A. & WEISSMAN, S., 1961, "Conf. on the Impact of Transmission Microscopy and Theories of the Strength of Crystals" Berkeley, California.

183. FOURIE, J.T. & MURPHY, R.J., 1962, Phil.Mag., vol.7, p.1617.

184. GILMAN, J.J., 1962, J. Appl. Physics, vol.33, p.2703.

185. BERGSTRÖM, Y., 1970, Mat. Sci. Eng, vol.5, p.193.

186. BECHTOLD, J.H., 1956, Trans. Amer. Inst. of Min. (Metall) Engrs, vol.206, p.142.

187. CARREKER Jr, R.P. & GUARD, R.W., 1956, Trans. Amer. Inst. of Min. (Metall.) Engrs, vol.206, p.178.

188. PUGH, J.W., 1955, Trans. Amer. Soc. Metals, vol.47, p.984.

189. BECHTOLD, J.H., 1953, Trans. Amer. Inst. Min.(Metall.) Engrs, vol. 197, p.1469.

190. KETTUNEN, P.O., 1967, Acta. Met., vol.15, p.1275.

191. LUKAS, P. & KLESNIL, M., 1973, Mat. Sci. Eng, vol.11, p.345.

192. LUKAS, P., KLESNIL, M. & POLAK, J., 1972, "High Cycle Fatigue Life of Metals", Inst. of Phys. Met., Brno.

193. MUGHRABI, H., unpublished result quoted in Ref. 194.

194. LAIRD, C., 1976, Mat. Sci. Eng., vol.22, p.231.

195. THOMPSON, N. & WADSWORTH, N.J., 1958, Adv. Physics, vol.7, p.72.

196. LAIRD, C. & DUQUETTE, D.J., 1972, "Corrosion Fatigue", Natl Assoc. Corrosion Engineers, Houston, p.88.

197. WINTER, A.T., 1970, Phil. Mag, vol.30, p.719.

198. KLESNIL, M. 1965, Metal Treatment and Drop Forging, February, p.55.

199. THOMAS, W.R. & LEAK, G.M., 1955, J.I.S.I., vol.180, p.155

APPENDIX A

DETERMINATION OF NITROGEN IN STEEL

The total nitrogen content in steel is considered to be made up of two parts:

(i) Acid-insoluble nitrides, and

(ii) Acid-soluble nitrides, which consist mainly of aluminium nitride and interstitial nitrogen.

It is assumed that

$$\%\ N_{\substack{\text{as free}\\\text{interstitial}}} = \%\ N_{\substack{\text{as soluble}\\\text{nitrides}}} - \%\ N_{\text{as AlN}}$$

The procedure is summarised diagrammatically in Figure A(1).

(a) METHOD FOR DETERMINING SOLUBLE AND INSOLUBLE NITRIDES

3.5 gm of steel sample (in the form of drillings) is dissolved in about 40-50 ml of 18% sulphuric acid. The mixture is heated over a steam bath to aid the decomposition of metal. After cooling, 2 ml of barium chloride is added, and separation of the soluble and insoluble parts is carried out by centrifuging. (Barium chloride is added to improve the separation.)

The soluble part is siphoned off and 10 ml of concentrated sulphuric acid is added to the insoluble nitrides. Heat is added until complete dissolution of the 'insoluble' nitrides.

The soluble and 'insoluble' solutions are then separately steam distilled with 40-50 ml of sodium hydroxide and about 40 ml of ammonia free distilled water. The distillation apparatus is as shown in Figure A(2). The distillate is collected in 10 ml of boric acid solution. 2 ml of Nessler reagent is added to the distillates and

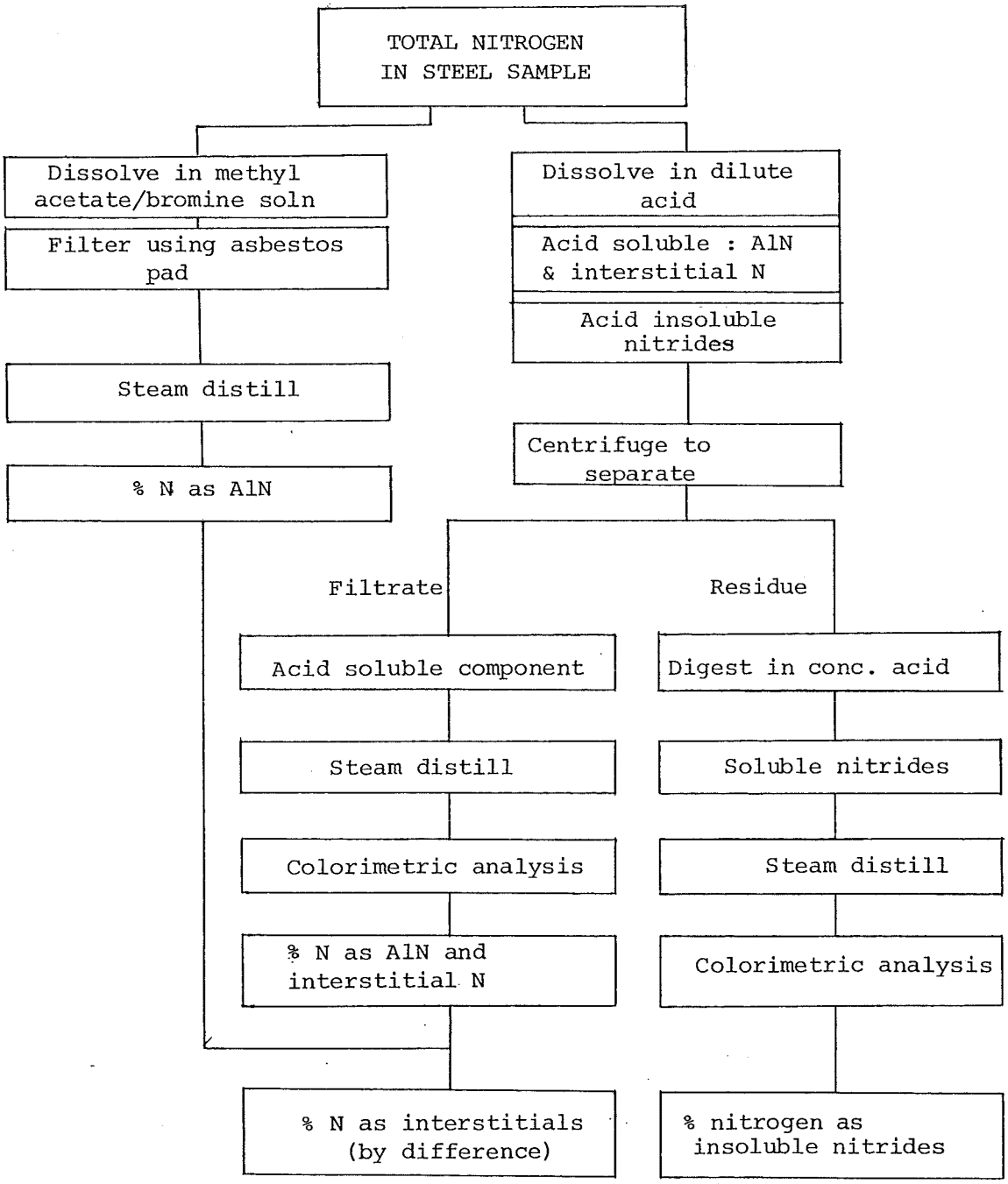

FIGURE A.1: Format for nitrogen analysis of steel

the solutions are adjusted to equal volume by adding ammonia-free water. The amount of nitrogen present in these solutions may then be determined using colorimetric examination, and the actual nitrogen level obtained from the calibration curve prepared using standard nitrogen solutions. The interstitial (or active) nitrogen is then given by the difference between the nitrogen in soluble nitrides and the nitrogen combined as aluminium nitride.

(b) METHOD OF DETERMINING THE ALUMINIUM NITRIDE

3.5 gm of steel sample (in the form of drillings) is dissolved in 50 ml of Methyl-Acetate plus 10 ml of Bromine. The mixture is dissolved with the aid of a small flame. Aluminium nitride, which is not soluble in these solutions, is filtered off using an asbestos pad. The pad is washed using Methyl-Acetate and then dried. The dried pad is then put into the distillation flask (E in Figure A(2)), and the nitrogen combined as AlN is obtained by steam distillation and determined using colorimetry.

The accuracy of these analyses is in the order of ±0.0005%.

(c) GENERAL PRECAUTION

(i) Care must be taken to ensure that decomposition of steel samples and the centrifuging separation process is complete.

(ii) Every precaution against contamination with extraneous ammonia must be taken.

(iii) Blank determination should be carried out with each batch of tests to ensure that nitrogen does not come from any other sources other than the steel sample.

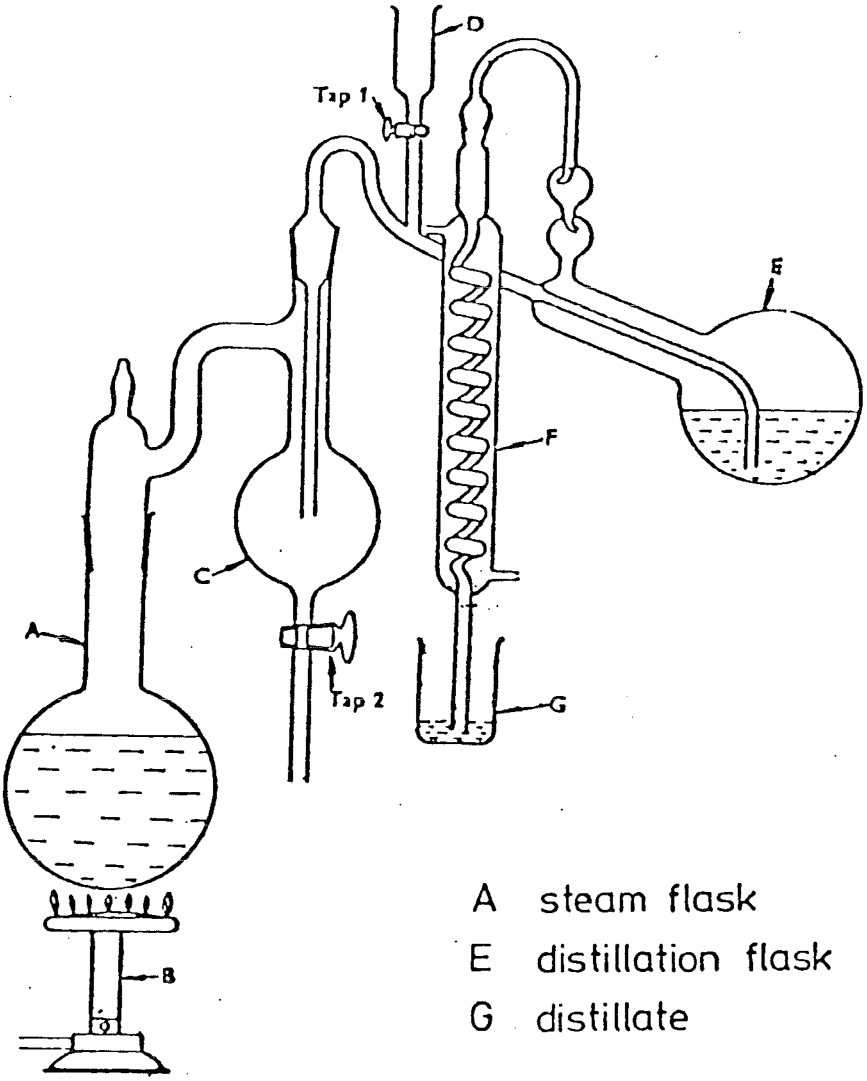

FIG. A.2 STEAM DISTILLATION APPARATUS

APPENDIX B

DETERMINATION OF FATIGUE LIMITS USING STAIRCASE METHOD

The most common test procedures used in determining the fatigue strength or fatigue limit of a material are the "Probit" method and the "Staircase" method. In the Probit method, one or more groups of specimens are tested for a fixed number of cycles at various stress levels close to the estimated fatigue strength (limit), a test being stopped if its endurance exceeds the required life. The percentage of failures at each stress level is then plotted against the stress level on a probability paper. The best line is then drawn through the points and the mean fatigue strength (limit) of the sample is the stress corresponding to 50% of failures.

The Probit method generally requires large numbers of specimens. The same results can be obtained more economically using the Staircase method, but the time required may be longer as the specimens have to be tested one at a time. In this investigation, as only one direct stress fatigue machine was available, the Staircase method was the obvious choice for the direct stress specimens.

The full details of the Staircase method are given in BS 3518, part 5, and will only be briefly summarised here. In the Staircase method, the first test piece is tested at an estimated mean value of fatigue strength (limit). If failure occurs before the required life, the next specimen is tested at one stress increment below the first stress

level. If, on the other hand, the first specimen survives the required life, then the next specimen is tested at one stress increment above the first stress level. This procedure is repeated for all the specimens to be tested. The results for the analysis in the Staircase method are taken from the first pair of opposite results. The analysis used the less frequent event, that is, if there are more failures than runouts, then the number of runouts is used, and vice versa.

The mean fatigue strength (limit) m is given by

$$m = S_0 + d\left(\frac{A}{n} \pm \frac{1}{2}\right) \qquad \text{Equation B.1.}$$

where S_0 = lowest stress

d = stress increment

n = total of less frequent events = $\sum_{i=0}^{z} n_i$

$A = \sum_{i=0}^{z} i n_i$

n_i = number of the less frequent events at i^{th} stress above S_0

i = coded stress level ($i = 0$ for S_0)

z = number of stress levels above S_0

$+\frac{1}{2}$ is used if the less frequent event is a runout, and

$-\frac{1}{2}$ is used if the less frequent event is a failure.

The estimated standard deviation S is given by

$$S = 1.62\, d \left[\frac{B \sum_{i=0}^{z} n_i - A^2}{n^2} + 0.029 \right] \qquad \text{Equation B.2}$$

where $B = \sum i^2 n_i$

The stress increment should be kept as small as possible, as the smaller the stress increment, the greater is the reliability of the results.

As only sixteen specimens were produced for each set of the experimental steels in this investigation, the mean fatigue limit m was calculated from the modified Staircase equation

$$m = \frac{C}{n} \qquad \text{Equation B.3}$$

where C = sum of stresses used on the last (n-1) tests, plus the stress that would have been used on the next test if it had been run

n = total number of specimens starting with the first pair of opposite results.

The Staircase results from the direct stress fatigue tests for the eight sets of experimental steels are shown in Figures B(1) - B(8).

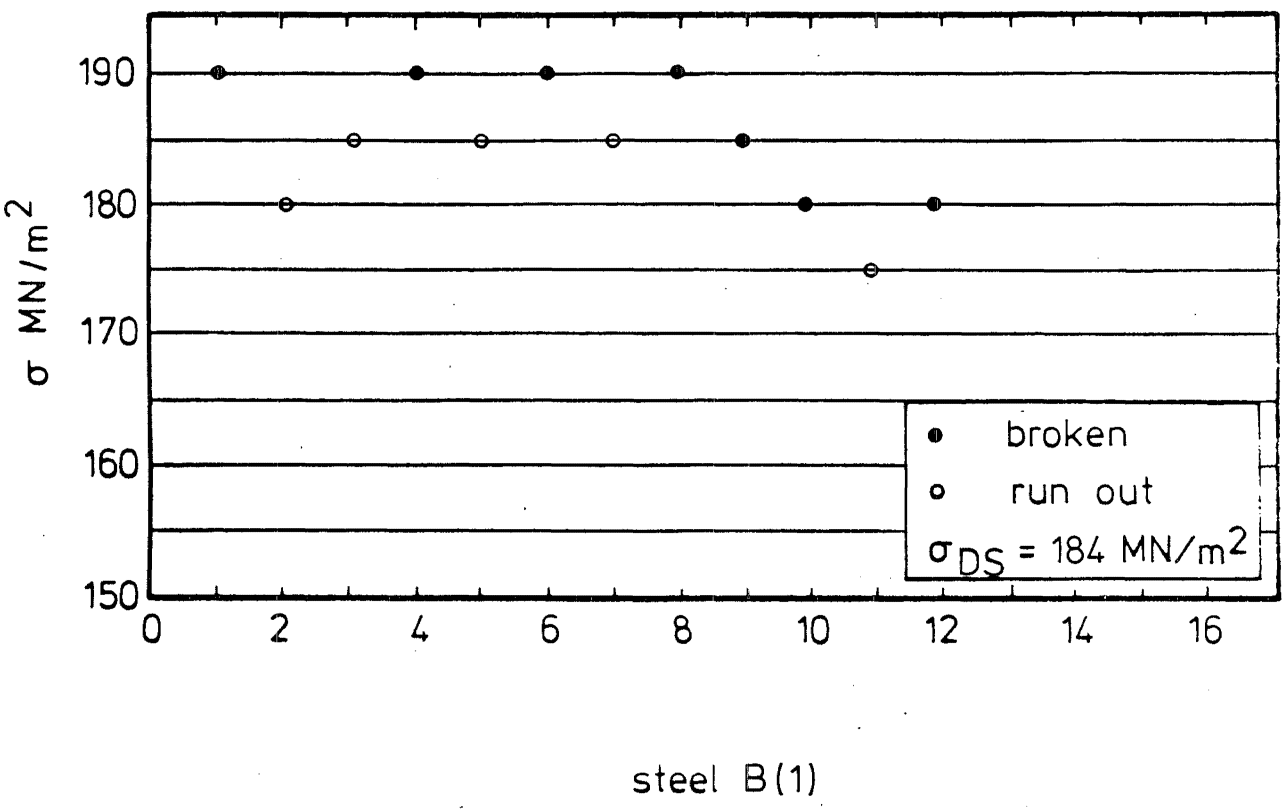

FIG. B.1 RESULTS OF FATIGUE TESTS USING THE STAIR-CASE METHOD

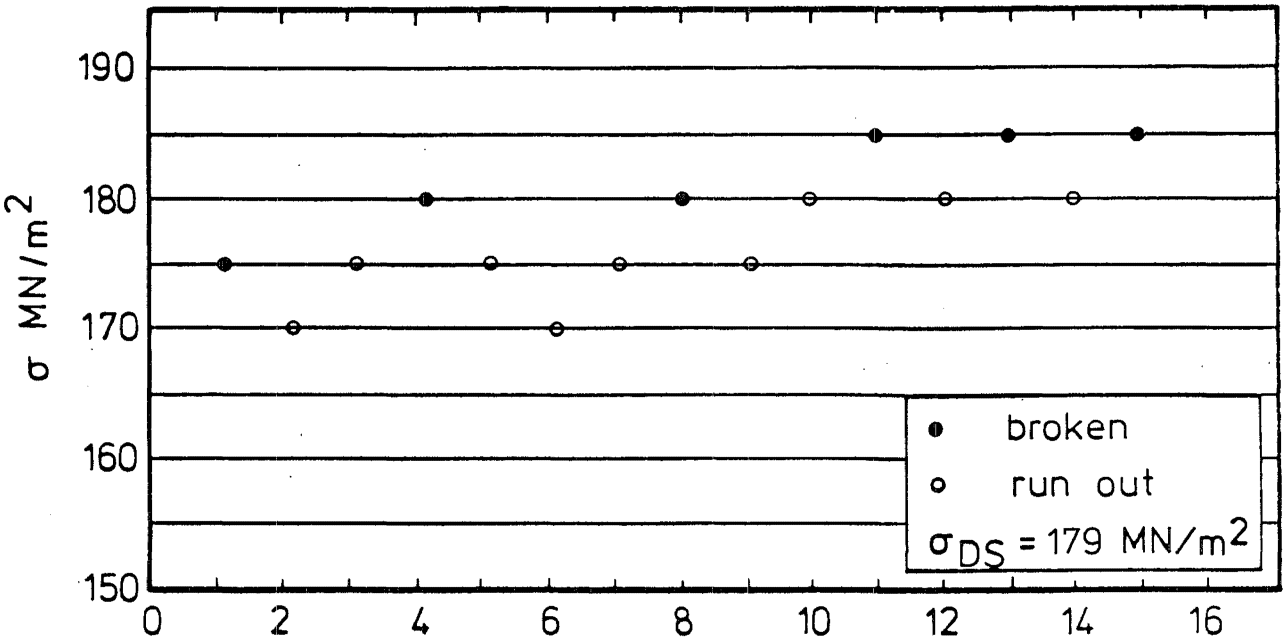

steel B(2)

FIG. B.2 RESULTS OF FATIGUE TESTS USING THE STAIR-CASE METHOD

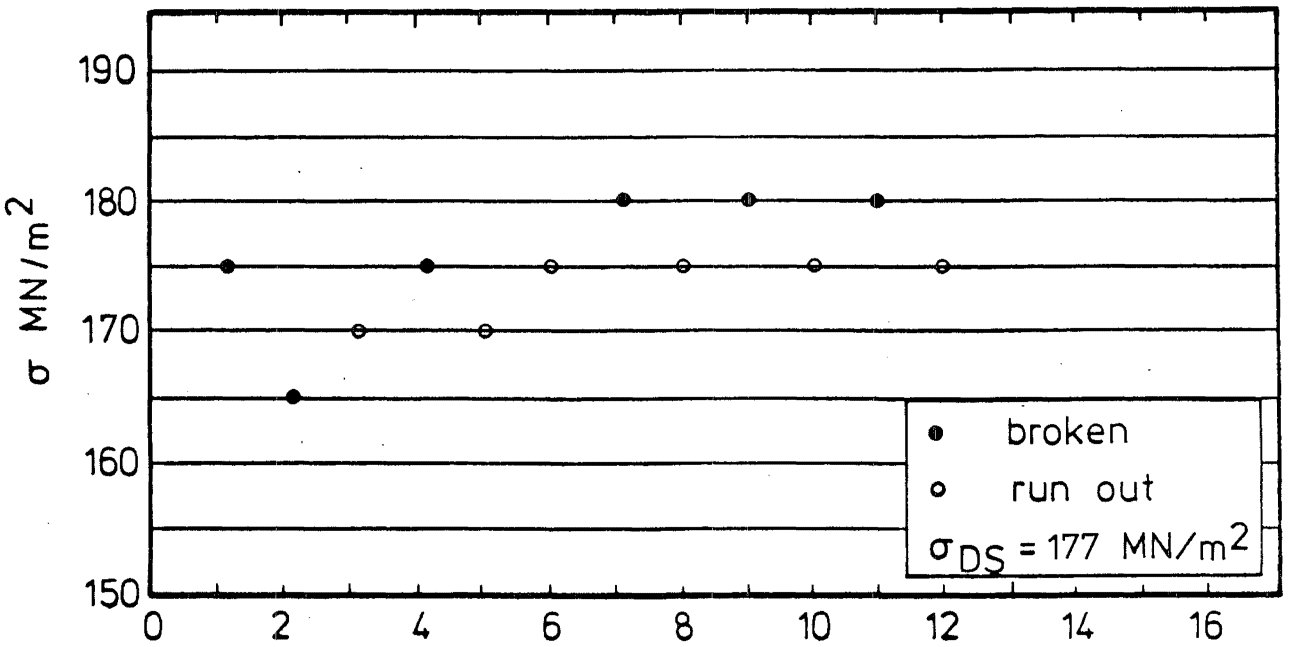

FIG. B.3 RESULTS OF FATIGUE TESTS USING THE STAIR-CASE METHOD

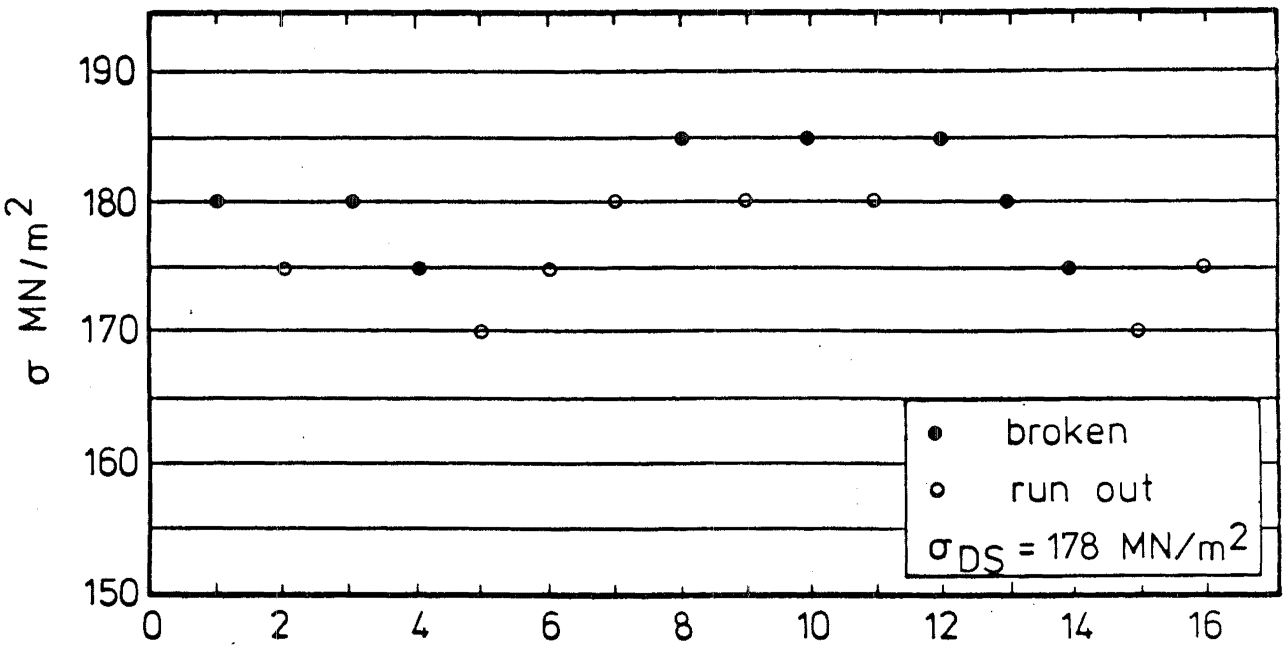

FIG. B.4 RESULTS OF FATIGUE TESTS USING THE STAIR-CASE METHOD

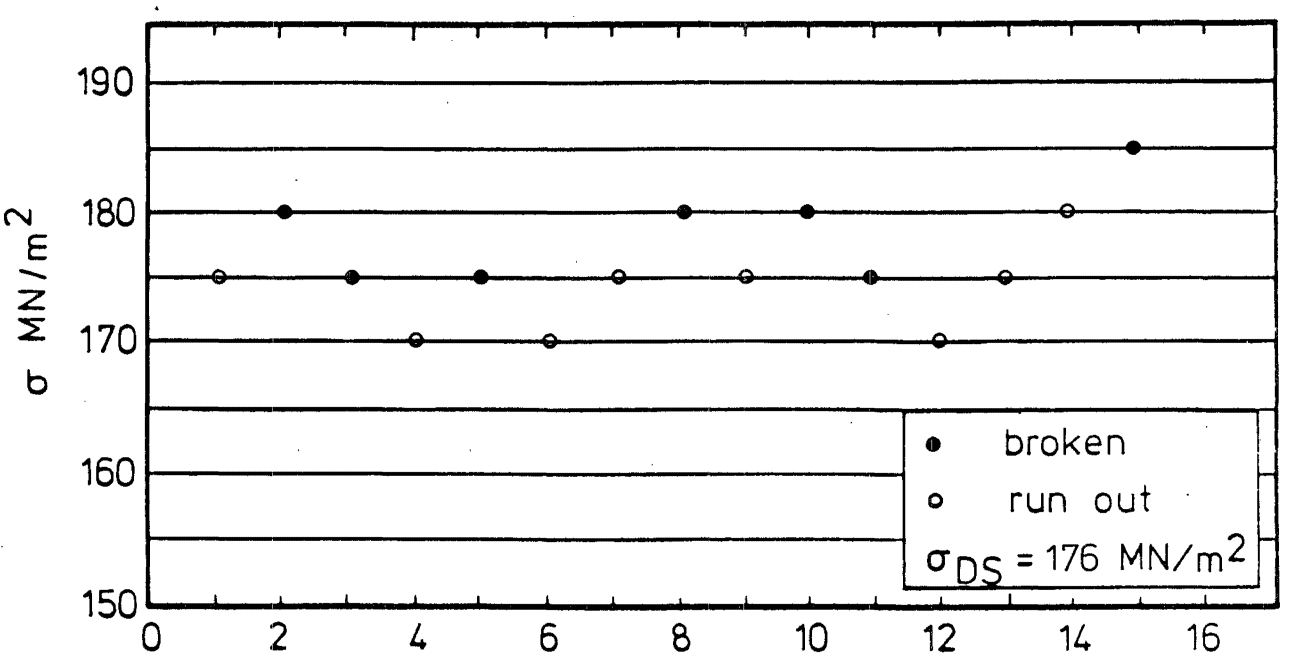

steel B (5)

FIG. B.5 RESULTS OF FATIGUE TESTS USING THE STAIR-CASE METHOD

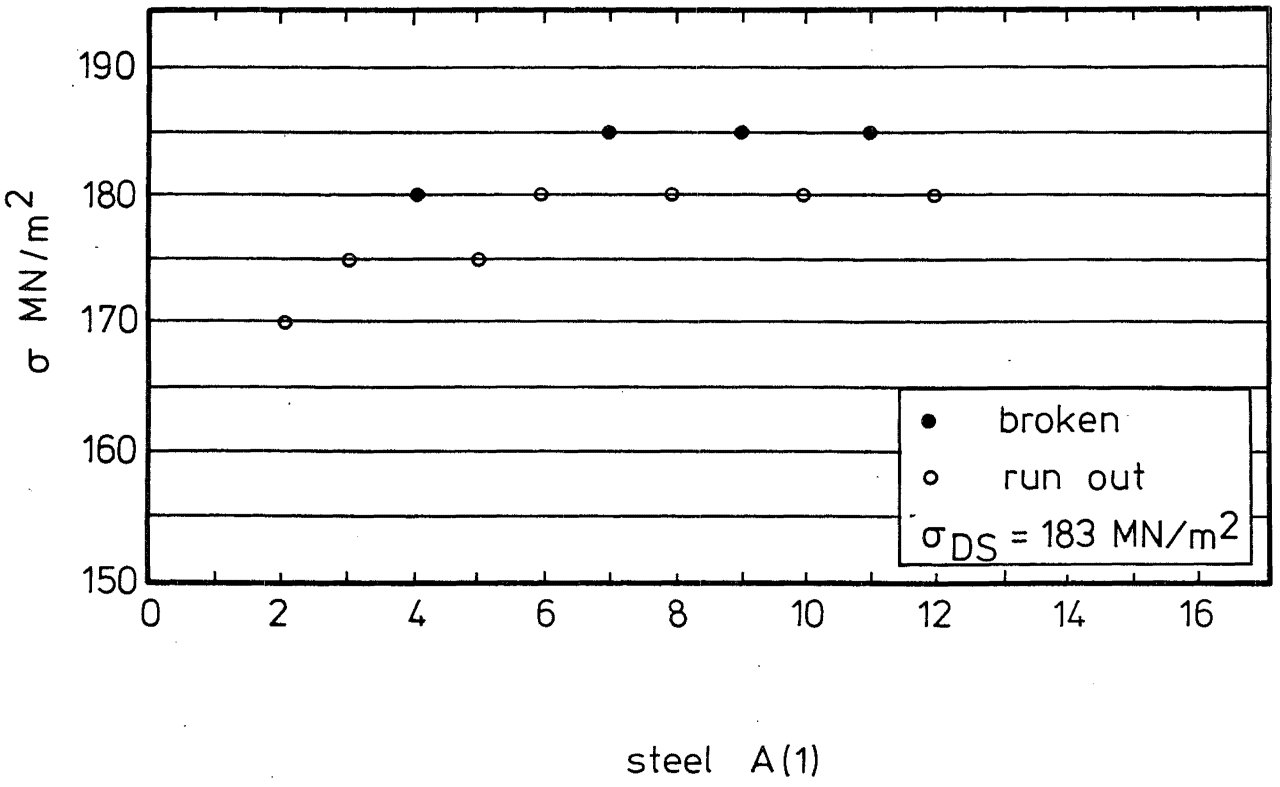

FIG. B.6 RESULTS OF FATIGUE TESTS USING THE STAIR-CASE METHOD

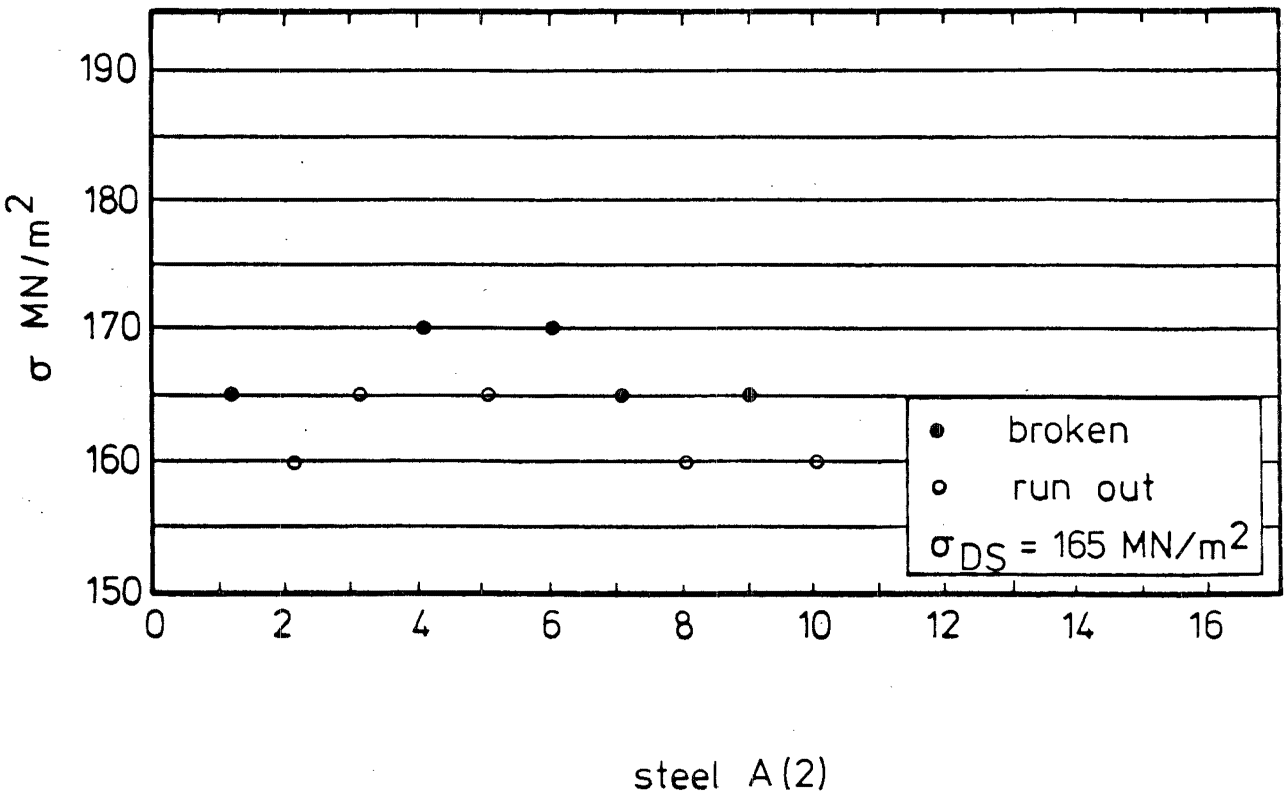

FIG. B .7 RESULTS OF FATIGUE TESTS USING THE STAIR-CASE METHOD

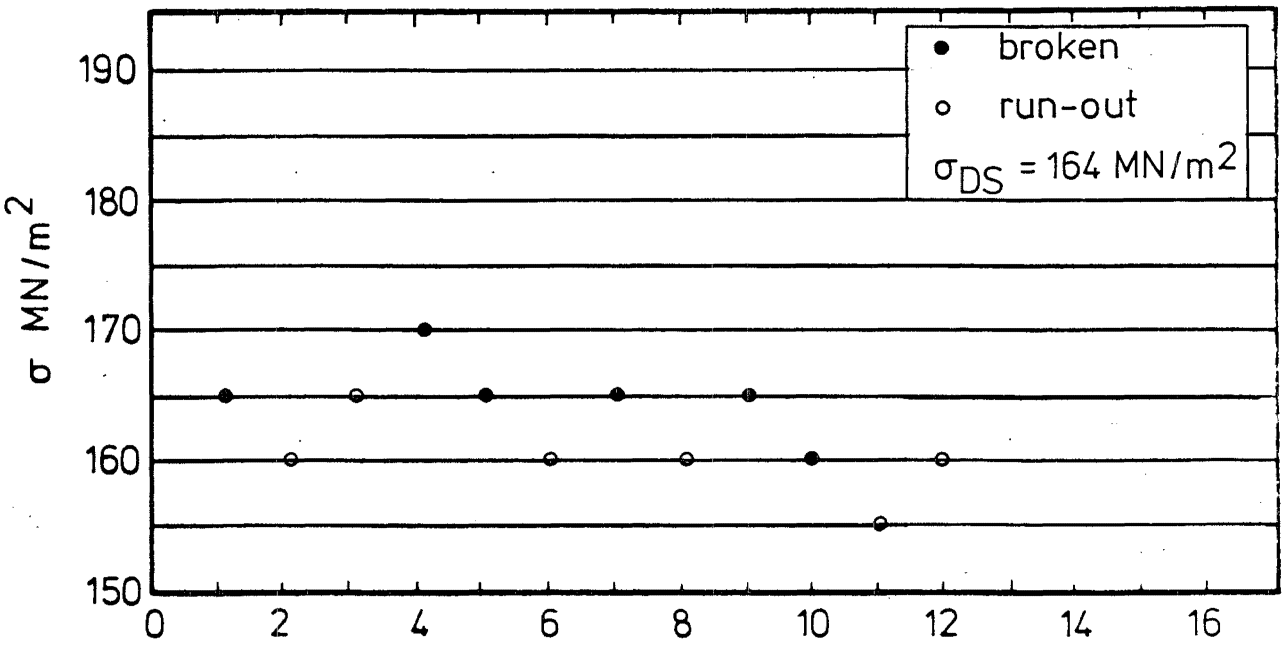

FIG. B.8 RESULTS OF FATIGUE TESTS USING THE STAIR-CASE METHOD

APPENDIX C

CALCULATION OF DISLOCATION DENSITY REQUIRED FOR COMPLETE AGEING OF EXPERIMENTAL STEELS

Strain ageing in α-iron has been shown to be caused by the migration of interstitial solute atoms (carbon and nitrogen) to dislocations to form anchoring atmospheres[48,49].

Using internal friction measurements, Thomas and Leak[199] estimated that the density of solute nitrogen atoms migrated to each dislocation per atom plane was 11·5. This figure was later confirmed by Wilson and Russell[75].

The results of Thomas and Leak show that for complete ageing of a steel containing 0.015% nitrogen, i.e., for all nitrogen atoms segregated to dislocation sites, the dislocation density has to be about 7.7×10^{10} lines/cm^2.

The experimental steel in this project contained 0.006%N. Hence for complete ageing, the dislocation density

$$\rho \approx \frac{0.006}{0.015} \times 7.7 \times 10^{10} \text{ lines/cm}^2$$

$$= 3.1 \times 10^{10} \text{ lines/cm}^2$$